

Potentials and Challenges of the Fuel Cell Technology
for Ship Applications

A Comprehensive Techno-economic and Environmental Assessment of Maritime
Power System Configurations

Von der Fakultät für Elektrotechnik und Informatik
der Gottfried Wilhelm Leibniz Universität Hannover
zur Erlangung des akademischen Grades
Doktor-Ingenieur
(abgekürzt: Dr.-Ing.)
genehmigte Dissertation

von Herrn
Lukas Kistner, M. Sc.

geboren am 17.03.1993
in Hannover, Deutschland

2023

1. Referent: Prof. Dr.-Ing. Richard Hanke-Rauschenbach
2. Referent: Prof. Dr.-Ing. Stephan Kabelac
Tag der Promotion: 23.05.2023

Abstract

The decarbonization of the global ship traffic is one of the industry's greatest challenges for the next decades and will likely only be achieved with new, energy-efficient power technologies. To evaluate the performances of such technologies, a system modeling and optimization approach is introduced and tested, covering three elementary topics: shipboard solid oxide fuel cells (SOFCs), the benefits of decentralizing ship power systems, and the assessment of potential future power technologies and synthetic fuels. In the following, the analyses' motivations, scopes, and derived conclusions are presented.

SOFCs are a much-discussed technology with promising efficiency, fuel versatility, and few operating emissions. However, complex processes and high temperature levels inhibit their stand-alone dynamic operation. Therefore, the operability in a hybrid system is investigated, focusing on component configurations and evaluation approach corrections. It is demonstrated that moderate storage support satisfies the requirements for an uninterrupted ship operation. Depending on the load characteristics, energy-intensive and power-intensive storage applications with diverging challenges are identified. The analysis also emphasizes to treat degradation modeling with particular care, since technically optimal and cost-optimal design solutions differ meaningfully when assessing annual expenses.

Decentralizing a power system with modular components in accordance with the load demand reduces both grid size and transmission losses, leading to a decrease of investment and operating costs. A cruise-ship-based case study considering variable installation locations and potential component failures is used to quantify these benefits. Transmission costs in a distributed system are reduced meaningfully with and without component failure consideration when compared to a central configuration. Also, minor modifications ensure the component redundancy requirements, resulting in comparably marginal extra expenses.

Nowadays, numerous synthetic fuels are seen as candidates for future ship applications in combination with either combustion engines or fuel cells. To drive an ongoing technology discussion, performance indicators for envisioned system configurations are assessed in dependence on mission characteristics and critical price trends. Even if gaseous hydrogen is often considered not suitable for ship applications due to its low volumetric energy density, resulting little operating costs are accountable for its superior performance on short passages. For extended missions, fuel cells operating on methanol or ammonia surpass hydrogen economically.

Keywords: Ship power systems; Hybrid ships; Fuel cells; Synthetic fuels; System design optimization; Environmental assessment; Decarbonization of the shipping sector

Zusammenfassung

Die Dekarbonisierung des globalen Schiffsverkehrs ist für die Industrie eine der größten Herausforderungen der nächsten Jahrzehnte und wird voraussichtlich nur mit neuen Antriebstechnologien erreicht werden können. Zur Bewertung solcher Technologien wird ein Systemmodellierungsansatz eingeführt und mit drei Analyse-themen erprobt: die Eignung von Festoxid-Brennstoffzellen (SOFCs) auf Schif-fen, die Vorteile einer Schiffsenergiesystem-Dezentralisierung und die Bewertung zukünftiger Antriebstechnologien und synthetischer Kraftstoffe. Im Folgenden werden Hintergründe und Schlussfolgerungen der Analysen präsentiert.

SOFCs weisen hohe Wirkungsgrade, Brennstoffflexibilität und geringe Emissio-nen im Betrieb auf. Hohe Betriebstemperaturen und komplexe Prozesse erschwe-ren jedoch einen dynamischen Solobetrieb. Daher wird ihr Einsatz in einem Hybridsystem untersucht, wobei das Hauptaugenmerk auf geeigneten Kompo-nentenkonfigurationen und Korrekturen des Bewertungsansatzes liegt. Es wird gezeigt, dass ein moderater Speichereinsatz die Schiffsbetriebsanforderungen er-füllt. Je nach Lastcharakteristik werden dabei energie- und leistungsintensive Speicheranwendungen mit unterschiedlichen Herausforderungen identifiziert. Die Analyse zeigt auch die Relevanz realitätsnäherer Alterungsmodelle, da technisch optimale und kostenoptimale Auslegungen voneinander abweichen.

Die Dezentralisierung der Stromversorgung mit modularen Komponenten unter Berücksichtigung des Lastbedarfs verringert sowohl Netzgröße als auch Übertra-gungsverluste und führt zu Investitions- und Betriebskostenreduzierungen. Zur Quantifizierung dieser Vorteile wird eine Kreuzfahrtschiff-Fallstudie mit variablen Installationsstandorten und Komponentenausfallberücksichtigung erstellt. Über-tragungskosten werden im verteilten System werden gegenüber einer zentralen Konfiguration mehr als halbiert. Außerdem genügen kostengünstige Anpassun-gen, um eine Komponentenredundanz gewährleisten zu können.

Derzeit werden zahlreiche synthetische Kraftstoffe und Antriebstechnologien für den zukünftigen Einsatz auf Schiffen diskutiert. Um die laufende Debatte voranzutreiben, wird die Performance für mögliche Lösungen in Abhängigkeit von Einsatzgebieten und kritischen Preistrends bewertet. Obwohl gasförmiger Wasser-stoff aufgrund seiner geringen volumetrischen Energiedichte als für Schiffsanwen-dungen ungeeignet scheint, sprechen niedrige Betriebskosten für die Überlegenheit des Energieträgers auf kurzen Strecken. Nur für längere Fahrten sind Methanol- oder Ammoniakbrennstoffzellen dem Wasserstoffansatz wirtschaftlich vorzuziehen.

Schlagworte: Schiffenergiesysteme; Hybride Schiffe; Brennstoffzell-Systeme; Synthetische Kraftstoffe; Ökologische Begleituntersuchungen; Defossilierung des Schiffsektors

Contents

Abstract	ii
Zusammenfassung	iv
List of Symbols	x
1 The Need for a Sustainable Shipping Industry	1
2 State of Research and Derived Research Issues	6
2.1 Designing Hybrid Ship Power Systems	6
2.2 Solid Oxide Fuel Cells for Marine Applications	8
2.3 Decentralized Ship Power Systems	10
2.4 Technologies for a Sustainable Future	12
2.5 Manuscript Structure and Segmentation of the Research Issues	15
3 Modeling and Designing a Hybrid Ship Power System	17
3.1 Central System Architecture	18
3.1.1 Solid Oxide Fuel Cells	18
3.1.2 Energy Storage	20
3.1.3 Electrical Load	21
3.2 System Component Models	21
3.2.1 Solid Oxide Fuel Cells	22
3.2.2 Energy Storage	25
3.2.3 Electrical Load	27
3.3 System Design Optimization	28
3.3.1 Optimization Task Formulation	28
3.3.2 Considerations on the Optimization Task	29
3.4 Heuristic Control Strategy for a Hybrid Power System	31
3.4.1 Energy Management Strategy	32
3.4.2 Component Management Strategies	35
3.5 Computational Framework	37

4	Exemplary Design Optimization of an SOFC-based Hybrid Power System	39
4.1	Case Studies	39
4.2	Results and Discussion	40
4.2.1	Case I: Motor Yacht	40
4.2.2	Case II: General Cargo Ship	41
4.3	Increasing the Storage Models' Levels of Detail	46
4.3.1	Li-ion Battery Model	46
4.3.2	Supercapacitor Model	52
4.4	Case Study Revision: Detailed Storage Models	56
4.4.1	Case I: Motor Yacht	57
4.4.2	Case II: General Cargo Ship	58
4.5	Extending the Objective Function by Fuel Expenses	60
4.6	Case Study Revision: Fuel Cost Inclusion	61
4.6.1	Case I: Motor Yacht	61
4.6.2	Case II: General Cargo Ship	63
4.7	Interim Conclusion	65
5	Distributed System Analysis with Consideration of Component Failures	70
5.1	Distributed System Architecture	70
5.2	Additionally Required Models	72
5.2.1	Electrical Grid	72
5.2.2	Multiple Stand-alone Fuel Cell Units	76
5.2.3	Multiple Stand-alone Battery Units	78
5.3	System Design Optimization	79
5.4	Control Strategy for a Distributed System	81
5.4.1	General Considerations	81
5.4.2	Rule-based Control Strategy	82
5.5	Case Study	86
5.6	Results and Discussion	88
5.6.1	Assessment without Malfunction Scenarios	88
5.6.2	Revised Assessment with Component Malfunction Scenarios	92
5.7	Interim Conclusion	95
6	Economic and Environmental Assessment of Power Technologies under Discussion for Future Ship Applications	98
6.1	State-of-the-art and Future Power Technologies	99
6.2	Additionally Required Models	104
6.2.1	Physical Models	104
6.2.2	Component Management	106
6.2.3	Economic Models	106

6.2.4	Environmental Models	111
6.3	System Design Optimization	116
6.4	Universal System Control Strategy	118
6.5	Results and Discussion	120
6.5.1	Benchmark Assessment: State-of-the-art Internal Combustion Engines	120
6.5.2	Future Assessment: Suitable Solutions for the Utilization of Synthetic Fuels	126
6.6	Interim Conclusion	142
7	Summary, Conclusion and Limitations	147
A	Operating Strategy Examples	151
A.1	SOFC-based Hybrid Power System	151
A.2	Distributed SOFC-based Power System	153
A.3	Universal System Control Strategy	156
B	Technology Performance Assumptions	158
B.1	Operation-specific Fuel Consumption	158
B.2	Operation-specific Emissions	159
C	Publication Contributor Roles	161
D	Curriculum Vitae	162
	List of Figures	164
	List of Tables	169
	Bibliography	172

List of Symbols

A	annuity factor	1 / a
\vec{a}	battery degradation parameters	
C_E	energy capacity	kWh
C_E^{BOL}	energy storage capacity at beginning of life	kWh
C_Q	battery charge capacity	Ah
C_S	capacitor displaying a supercapacitor's dynamic behavior	F
C_0	supercapacitor's storage capacitor	F
C_m	energy density	Wh / kg
c_{gen}^a	generator maintenance cost factor	1 / a
D_c	control parameter (placeholder)	-
$E_{\text{FC}}^{\text{exc}}$	modulation excess energy	kWh
F	storage's state of energy (SoE)	-
F^{high}	desired highest state of energy	-
F^{low}	desired lowest state of energy	-
F_{crit}	critical SoE for excess energy	-
F^{max}	maximum SoE	-
F^{min}	minimum SoE	-
$F_{\text{Q,B}}$	battery's state of charge (SoC)	-
F_S	averaged hybrid storage's SoE	-
$F_{\text{SC,des}}$	desired supercapacitor's SoE	-
F_{\emptyset}	average SoE for multiple components	-
g_{gen}	generator cost exponent	-
h^{LHV}	lower heating value	MJ / kg
I^{cell}	single storage cell current	A
$I_{\text{B,CV,cha}}^{\text{cell}}$	battery current (CV charging)	A
$I_{\text{B,CV,dis}}^{\text{cell}}$	battery current (CV discharging)	A
$I_{\text{B,cut}}^{\text{cell}}$	cut-off cell current	A
I_{C_S}	current of capacitor C_S	A
I_{C_0}	current of capacitor C_0	A

$I_{cha}^{cell,max}$	maximum cell charge current	A
$I_{dis}^{cell,max}$	maximum cell discharge current	A
$I_{RMS,0}$	baseline supercap RMS current	A
$I_{SC,RMS}$	average supercap RMS current	A
I_{str}	string current	A
I_{str}^{max}	maximum string current	A
$J_{E,B,deg}$	battery energy capacity fade rate	kWh / a
$J_{F,SC,deg}$	supercap capacitance fade rate	F / a
j	interest rate	-
k	ICE on/off control	-
k_{SD}	storage self discharge coefficient	1 / d
L	number of full storage cycles	-
l_{cable}	length of one cable	m
M	molar mass	kg / mol
m	mass	kg
m_{fuel}	consumed fuel mass	kg
\dot{m}^{spec}	operating-point-specific in-/output	g / kWh
N	number of modules	-
N_{FZ}	number of fire zones	-
\vec{N}	numbers of units among fire zones	-
N^*	number of units during malfunction	-
P	electric power	kW
P_{FC}^{input}	predefined fuel cell module power	kW
P^{min}	generator minimum power	kW
P^r	rated power	kW
$P_{B,set}^{tot}$	total set power for batteries	kW
P_{cha}^{max}	storage max. charge power	kW
P_{dis}^{max}	storage max. disch. power	kW
$P_{gen,rel}^{min}$	min. relative power output	-
$\dot{P}_{gen,rel}^{max}$	max. relative power gradient	1 / s
P_k	transformer copper losses	kW
P_{loss}	power losses	kW

P_{mod}^r	rated power of one module	kW
P_0	hysteresis, eddy-current losses	kW
P_{\rightarrow}	cable power flow	kW
P_{set}	desired power	kW
$P_{\text{m,gen}}$	generator power density	kW / m ³
p^a	annual costs	€ / a
$p_{\text{B}}^{\text{inv}}$	battery investment costs	€ / kWh
p_{c}	battery charge fit parameters	
p_{d}	battery discharge fit parameters	
p_{fuel}	fuel price	€ / MWh
$p_{\text{gen}}^{\text{inv}}$	generator investment costs	€ / kW
$p_{\text{LNG,loss}}^a$	annual fuel costs from transmission losses	€ / a
Q	electric charge	Ah
$R_{\text{B,i,cha}}^{\text{cell}}$	battery resistance (charging)	Ω
$R_{\text{B,i,dis}}^{\text{cell}}$	battery resistance (discharging)	Ω
R_{con}	connection resistance (supercapacitor)	Ω
$R_{\text{S,str}}$	specific string resistance	Ω
R_{s}	parallel resistor for dynamic behavior	Ω
R_{sa}	series resistor for dynamic behavior	Ω
R_{p}	supercapacitor's self discharge resistor	Ω
S	apparent power	VA
S_{trafo}^r	rated transformer apparent power	VA
t	time	s
t_{cal}	calendar lifetime	a
t_{op}	passage time	s
t_{L}	component lifetime	a
t_0	beginning of passage	s
U_{CS}	voltage over capacitor C_{S}	V
U_{C0}	voltage over capacitor C_0	V
U^{cell}	storage cell voltage	V
$U^{\text{cell,max}}$	maximal storage cell voltage	V

$U^{\text{cell,min}}$	minimal storage cell voltage	V
$U_{\text{B,cha}}^{\text{cell}}$	battery cell voltage (charge)	V
$U_{\text{B,dis}}^{\text{cell}}$	battery cell voltage (discharge)	V
$U_{\text{B}}^{\text{cell,r}}$	rated battery cell voltage	V
$U_{\text{B,0,cha}}^{\text{cell}}$	battery open circuit voltage (charge)	V
$U_{\text{B,0,dis}}^{\text{cell}}$	battery open circuit voltage (discharge)	V
U_{HV}	rated grid high voltage	V
U_{LV}	rated grid low voltage	V
$U_{\text{SC,0}}$	supercapacitor baseline voltage for life estimation	V
V	volume	m^3
$W_{\text{LNG,id}}$	chemical energy consumption	MWh
$W_{\text{LNG,loss}}$	extra energy consumption for grid losses	MWh
Y_{FC}	local state machine variable	-
Z	automaton state	-
ΔF	state machine buffer zone (SoE)	-
ΔP	power delta in one fire zone	kW
ΔP_{act}	power delta that requires action	kW
ΔP_{des}	desired power delta	kW
$\Delta P_{\text{L,FC}}$	power delta between load and fuel cells	kW
Δt	operating time	s
ΔU	state machine buffer zone (voltage)	V
η	energy efficiency	-
θ	ambient temperature	$^{\circ}\text{C}$
ζ	operating scenario	-
ζ_{emis}	global warming potential factor	$\text{kgCO}_2 / \text{kg}$
$\kappa_{\text{CO}_2}^{\text{eq}}$	specific CO_2 eq. footprint	$\text{kgCO}_2 / \text{kWh}$
ξ	mass fraction	$\text{kg} / \text{kg}_{\text{fuel}}$
ξ_{B}	battery balance power factor	-
ξ_{gen}	normalized generator operating point	-
Π_{cha}	specific maximum charge power	kW / kWh
Π_{dis}	specific maximum discharge power	kW / kWh

ρ	density	kg / m ³
ϕ	high voltage grid phase angle	-
φ_L	load scaling factor	-
φ_{vol}	volume cost scaling factor	-
τ_0	supercap base life expectancy	s
χ	specific environmental costs	€ / kg

List of Indices

a	annual values (extrapolation)	<i>k</i>	fire zone location
B	battery	L	electrical load
BC	black carbon	LE	local emissions
cable	high voltage power cable	LH2	liquid hydrogen
cell	single cell (battery/supercap)	LNG	liquefied natural gas
CGH2	compressed gaseous hydrogen	MeOH	methanol
CH4	methane	NH3	ammonia
CO	carbon monoxide	NOx	nitrogen oxides
CO2	carbon dioxide	PEM	proton exchange membrane FCs
CO2eq	carbon dioxide-equivalent unit	S	energy storage
emis	emissions placeholder	SC	supercapacitor
FC	Fuel cells	SNG	substitute natural gas
FTD	Fischer-Tropsch diesel	SOFC	solid oxide fuel cells
fuel	fuel placeholder	SOx	sulfur oxides
gen	power generator	tank	fuel tank
grid	electrical transmission grid	trafo	power transformer
H2	hydrogen	VLSFO	very low sulfur fuel oil
ICE	internal combustion engine	vol	volume
<i>i</i>	Storage technology placeholder		

1 The Need for a Sustainable Shipping Industry

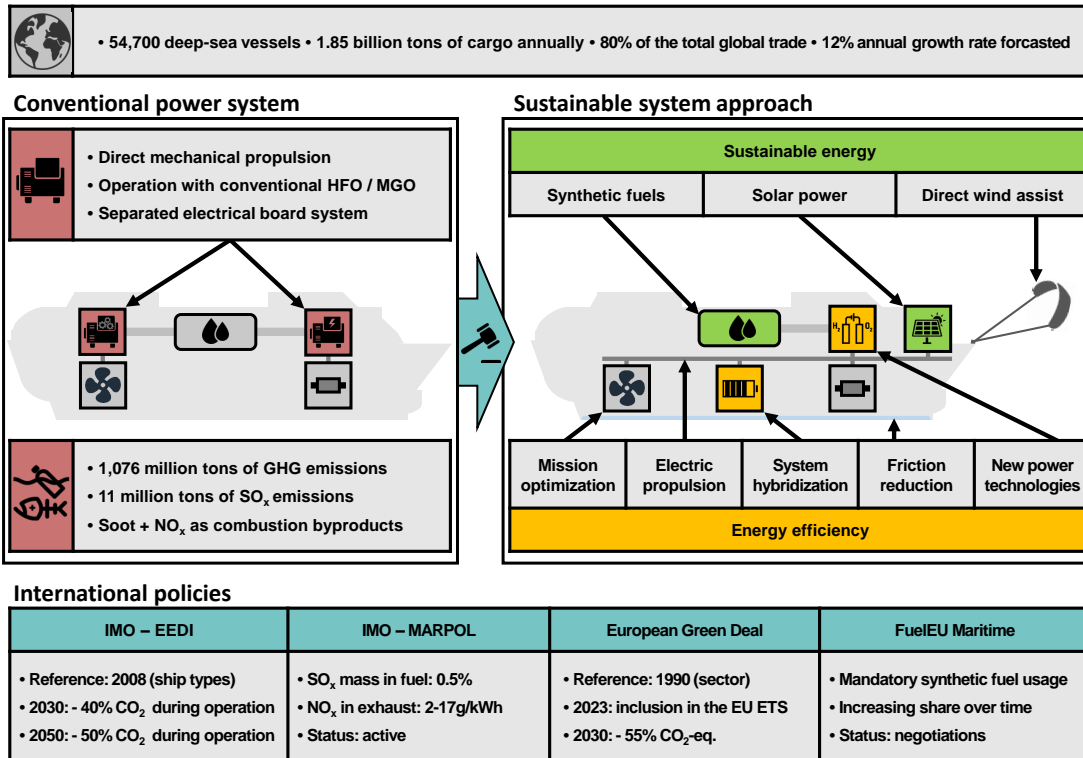
In the face of the climate and biodiversity crisis and the global defossilization efforts, the international shipping industry is concerned with developing near-future technological solutions for cleaner transportation. Contributing to this challenge, the present dissertation focuses on partial solutions regarding the ship power system to pave the way toward a more sustainable maritime sector.

To give a first overview of the shipping industry's defossilization challenge, its most relevant aspects are summarized in Fig. 1.1, including (1) the sector's economic and environmental key data, (2) the most relevant near-future legislations, and (3) the potential elements of environmental improvement. These three categories are outlined in the following.

Key data of the deep-sea shipping sector

The world merchant fleet consists of more than 54,700 vessels, including container and bulk carriers, tankers, and passenger ships, whereby general cargo ships constitute the largest share with over 15,000 vessels [1]. In 2020, these ships transported around 1.85 billion tons of cargo, which is estimated to be far over 80% of the total global trade [2]. However, the market is expected to expand at an annual growth rate of 12% in the current decade [3]. While very large container ships create a minuscule gravimetric carbon footprint for cargo compared to other transport vehicles (below 4% of a truck, below 0.7% of air freight [4]), their sheer number constitutes a significant share of the emissions with global warming potential: international shipping's carbon dioxide emissions in 2020 amount to 646 million tons CO₂ [5] and 1,076 million tonnes of total greenhouse gases (GHG), which accounts for 11% of emissions in transport [6] or close to 3% of the total anthropogenic emissions [7]. The sector is also one of the largest sulfur dioxide producers (11 million tons in 2019, or 4-9% of the anthropogenic emissions [8],[9]), emits combustion byproducts like soot or nitrogen oxides (up to 15% of the anthropogenic emissions [9]) and therefore massively harms the marine environment [9].

In view of the ongoing climate crisis and the threat to biodiversity, severe measures are required to shift the industry towards a sustainable future. However, the sector's overall emissions are increasing every year and projections are far off the envisaged two-degree target, as the sector still relies on heavy fuel oils [7],[10].



International policies

IMO – EEDI	IMO – MARPOL	European Green Deal	FuelEU Maritime
<ul style="list-style-type: none"> • Reference: 2008 (ship types) • 2030: - 40% CO₂ during operation • 2050: - 50% CO₂ during operation 	<ul style="list-style-type: none"> • SO_x mass in fuel: 0.5% • NO_x in exhaust: 2-17g/kWh • Status: active 	<ul style="list-style-type: none"> • Reference: 1990 (sector) • 2023: inclusion in the EU ETS • 2030: - 55% CO₂-eq. 	<ul style="list-style-type: none"> • Mandatory synthetic fuel usage • Increasing share over time • Status: negotiations

Fig. 1.1: Relevant aspects regarding the shipping industry’s defossilization challenge: economic and environmental key data, near-future legislations, and potentially utilizable sustainable technologies

International policies for the shipping sector

International policy makers certainly have recognized the negative environmental impact of the shipping industry. Unlike single nations, which virtually cannot control deep-sea shipping activities, several federations are able to meaningfully regulate this sector with binding directives. Here, a brief activity summary of two important organizations, the *International Maritime Organization (IMO)* and the *European Union (EU)*, is given.

IMO: Energy Efficiency Design Index – The *IMO* is a *United Nations* institution consisting of 175 member states. The agency holds the regulatory power for open-sea shipping, which is implemented in a variety of conventions. Its main objective is the prevention of marine and atmospheric pollution and the security of shipping. In 2018, the *Marine Environment Protection Committee (MEPC)* announced their new climate protection targets, which consider carbon dioxide emissions for the first time [11]. According to the directive, beginning in the year 2050 the *Energy Efficiency Design Index (EEDI)* [12] of a ship must not exceed 50%

of a defined reference from 2008. In 2020, *IMO* member countries also approved short-term measures to achieve the target of decreasing carbon intensity 40% by 2030 [13]. However, the *IMO* does not actively plan to fine remaining emissions or to determine legally binding reduction milestones prior to 2030. While several *IMO* member countries demand earlier and more strict measures [14], no majorities can be found at present. In this regard, the *International Energy Agency* states that the currently projected carbon intensity reduction measures are by far not concordant to global net-zero requirements. Calculated scenarios fall short of at least 15% decrease in 2030 and 83% in 2050 [5].

IMO: Convention for the Prevention of Pollution from Ships – Unlike the carbon dioxide regulations, which are not applied until the year 2030, the *IMO* today addresses sulfur oxide and nitrogen oxide emissions in the *International Convention for the Prevention of Pollution from Ships (MARPOL)*. In 2020, the maximum content of sulfur in fuel oils was reduced to a flat 0.5% from 3.5% (mass percentage) [15]. Nitrogen oxide emission limitations range from 2–17 g/kWh mechanical energy in dependence on the ship construction date and the rated engine speed and last have been modified in 2016 [16].

EU: European Green Deal – Recently, the *European Commission* adopted a proposal to cut GHG emissions of the transport sector by at least 55% by 2030 compared to a 1990 reference [17] as a part of the *European Green Deal*. Since international shipping falls far behind this objective, the *European Parliament* requested the integration of the shipping sector into the *European Emissions Trading System (ETS)* [18] to generate incentives for sustainable investments. The *European Commission* accepted the request and schedule the introduction of the law to the year 2023 [19].

EU: FuelEU Maritime – Further, in 2021 the *FuelEU Maritime* initiative launched by the *European Commission* [20] proposed to implement a regulatory obligation for the use of a sustainable fuel share to create a stable market introduction. Since the heavily disputed industry entirely relies on fossil fuels today and renewable fuels entail much higher operating costs, the sector would otherwise most likely delay to build the required infrastructure. As of yet, the proposal is subject of discussion in the *European Council* and a version of compromise has been sent to the member states.

While the *EU* is hereby placing a focus on the use of sustainable fuels, the *IMO* suggests a variety of design, operational, and economic solutions realizable both in the short and medium term [21]. An initial overview of the addressed potential technological solutions is given in the following.

Defossilization potentials of the shipping industry

On the basis that the international shipping industry is not going to reduce its overall transport capacities and decrease the economic globalization for the sake of the climate crisis, two fundamental elements of action remain to reduce its negative environmental impact: (1) the usage of less energy resulting from an increase of operating efficiency and (2) the utilization of cleaner energy in the form of renewable power sources (cf. Fig. 1.1).

Energy efficiency – Efficiency measures can be taken in the design phase, the ship maintenance, and the operating phase. Using a power generation technology with few conversion losses is one of the most impactful measures to increase the ship’s overall energy efficiency. For the power train, all-electric ships, which substitute direct with electric propulsion and an interposed electric power generator, offer advantages in terms of power system operation [22]. Electric propulsion also allows for hybrid ship configurations, where energy storage units support the power supply to improve their operating requirements [23]. Other design methods include the optimization of hull and propulsion system design [21], as well as friction reduction methods like the use of specific paint or air-filled hull bottoms [24]. To maintain small friction coefficients, the periodic removal of biofouling is also inevitable. The operating phase can be tailored to reduce fuel consumption with the help of speed reduction, appropriate energy management, and route/logistics optimization [21].

Sustainable energy – Renewable energy sources can be utilized directly or processed in the form of synthesized energy carriers. To harness wind energy, available solutions include (solid) sails [25], kites [26], and Flettner rotors [27]. Wind-assisted propulsion does not require any further conversion steps but to some extent demands flexible route adjustments. The maritime application of photovoltaic panels could cover shipboard power supply but can also support the propulsion of all-electric ships [28]. While container ships lack large installation spaces on deck, bulk carriers and tankers often provide deck installation possibilities. Still, both wind and solar energy can not guarantee the security of power supply for essential applications like propulsion, navigation, and communication at all times. According to the IMO’s *International Convention for the Safety of Life at Sea (SOLAS)*, lighting, freshwater production, and heating/ventilating/air conditioning (HVAC) are also vital functions, which must be operational at all times [29]. Therefore, additional secure power sources still are a necessity for deep-sea shipping. For a sustainable ship, this power source must include an energy converter with high efficiency and small operating emission production, as well as an energy carrier with a small environmental footprint.

Until today, however, not one single best technology emerged to ideally fit this task. Instead, many different fuels including hydrogen, ammonia, methanol, methane, and synthetic diesel are subject of discussion for usage in either internal combustion engines (ICEs), proton exchange membrane fuel cells (PEMFCs) or solid oxide fuel cells (SOFCs). Since neither the maritime industry nor the scientific consultation established a uniform or standardized approach regarding the design of a sustainable and secure shipboard power system, the addressed open issues lead to the overarching question:

**What does a well-designed, secure, sustainable
future marine power system look like?**

Prior to the outline of this dissertation's structural setup, a detailed review of the state of the literature and emerging research issues is given in the following.

2 State of Research and Derived Research Issues

As stated in Chapter 1, there exists a variety of meaningful methods to increase a ship’s sustainability. However, this dissertation solely focuses on potential improvements for the secure core ship power system. Specifically, three of the previously raised “energy efficiency” and “sustainable energy” measures are objects of investigation: (1) the power system hybridization with a storage unit support, (2) the energy-efficient SOFC power technology, and (3) the usage of synthetic fuels in future scenarios. In this respect, to conduct economic and environmental analyses concerning the three topics of interest, a comprehensive ship power system modeling method is aspired. Therefore, Section 2.1 addresses the methodical research issue of designing a multi-component ship power system on a model-and-optimization basis with a special focus on energy storage systems. Sections 2.2 and 2.3 focus on the SOFC technology, which also serves as a vivid example of power system design complexity. Here, both the challenge of operating limitations and the opportunities of a new power system build are raised. Section 2.4 covers the economic and environmental comparison of future power technologies and synthetic fuels. Finally in the Section 2.5, the raised research issues are assigned to the following chapters.

2.1 Designing Hybrid Ship Power Systems

In this section, a hybrid ship system structure is introduced, followed by a review of open literature concerning hybrid ship power system models. Subsequently, the state of research is critically discussed and the first emerging research issues are articulated.

Disclosure: The topic of optimally designing hybrid ships is already topic of previously published works. The following section is in part based on the publication: L. Kistner; A. Bensmann; R. Hanke-Rauschenbach, Optimal Design of Power Gradient Limited Solid Oxide Fuel Cell Systems with Hybrid Storage Support for Ship Applications, Energy Conversion and Management (2021) [30]. For a detailed description of the author contributions see Appendix C.

Today, many state-of-the-art ship power systems consist not only of electricity generators, but also include an energy storage for operational support. Most commonly, lithium-ion batteries are used in this application [31]. In general, hybrid power systems can be categorized into two groups, based on the recharge process of the energy storage: plug-in hybrids periodically charge at ports and are used as an extra power source in addition to the main engines [32]. By contrast, in conventional hybrid systems the energy storage is charged with shipboard the generators' residual power. For the sufficient operation of a hybrid power system, the storage design should be customized in dependence of the power generator characteristics and the underlying concept for its utilization. Therefore, supporting design decisions with ship energy system modeling is a topic of rising interest and is especially relevant for hybrid configurations.

Developing an optimized hybrid ship power system is a task that several scientific articles cover. For example, the authors of [33] devise a general design method for battery-hybrid ships. For the battery model, they declare minimum and maximum energy content limits and calculate the ideal change of stored energy step-wise. In [34], the charged and discharged battery energy equals the total excess or required system energy for discrete time steps, disregarding potential power limitations. Thereby, the model includes a fixed storage efficiency to consider operating losses. In [35], a system based on a combustion engine is hybridized with different storage technologies. Rated power and energy capacity are taken into account for the optimal configuration. In [36], the design optimization includes a battery state of charge calculation, energy efficiency and power limitations. Overall investment and operating costs are added up with predefined weight factors to minimize the consumed fuel. In [37], an assessment for the hybridization of PEMFCs, batteries, and supercapacitors is conducted. Here, the storage model is based on a discrete state of charge description and also considers power limitations. For the design optimization's objective, total investment costs are chosen.

What is striking is that the model approaches to some extent lack in detail regarding the following three categories:

1. The physical behavior of the system components is oversimplified. Not all presented system-level storage models consider power or current limitations, charge and discharge losses, and a time-dependent state of energy. Most also neglect self discharge or state-of-charge-dependent efficiencies.
2. As ship load profiles tend to have a very fluctuating character, a fixed time discretization approach is inferior to model approaches that include dynamic equation systems. Latter can cover short load peaks resulting from power-intensive maneuvers. A dynamic description is also of major importance to cover the load shift limitations of power generators like SOFCs.

3. Presented cost analyses ignore component lifetime and minimize investment costs or operating costs only. While maintenance costs are considered in some cases, non of the works listed above considers load-dependent storage degradation, which also influences real-life annual system costs.

Since the open literature does not provide adequate model approaches for hybrid ship power systems, the methodical framework for the envisaged analyses first must be developed. In detail, the following questions are addressed in the course of the power system modeling:

- 1 Research issue: Which aspects matter for the conceptual design of a hybrid ship power system?**
 - 1.1 Which performance indicators should be evaluated in the decision process to achieve a proficient design of a stand-alone marine power system?
 - 1.2 Which component properties should be considered and what model level of detail is sufficient for a power system simulation?

2.2 Solid Oxide Fuel Cells for Marine Applications

In this section the potential of marine fuel cells are outlined. Benefits and challenges compared to other power technologies are hinted, followed by a compilation of literature evaluating the performance of hydrocarbon-based fuel cell systems for ship applications. Thereupon, a second set of open research questions is formulated.

Disclosure: the performance of hydrocarbon-based SOFCs is already topic of previously published works. The following section is in part based on the publications: L. Kistner; A. Bentsmann; R. Hanke-Rauschenbach, Optimal Design of Power Gradient Limited Solid Oxide Fuel Cell Systems with Hybrid Storage Support for Ship Applications, Energy Conversion and Management (2021) [30] and L. Kistner; F.L. Schubert; C. Minke; A. Bentsmann; R. Hanke-Rauschenbach, Techno-economic and Environmental Comparison of Internal Combustion Engines and Solid Oxide Fuel Cells for Ship Applications, Journal of Power Sources (2021) [38]. For a detailed description of the author contributions see Appendix C.

Since the climate protection targets introduced in Chapter 1 can most likely only be achieved with upcoming new technologies, a special focus of this dissertation is placed on alternatives to internal combustion engines for open-sea operation. In contrast to onshore microgrids, shipboard components' size and weight constraints are critical and their reliability is even more essential [39]. Therefore, battery-only

solutions are evaluated not to be suitable for long voyages and heavy-weight vessels [40]. For mission characteristics that do not fit battery requirements, fuel cells are discussed as one of the most promising technologies to achieve a higher energy efficiency and a decisive reduction of emissions [41]. Even if their capital investment costs are currently larger than the costs of conventional ICEs, a higher energy efficiency will lead to the reduction of a ship's fuel costs, which represent one of the largest expenses for ship owners [42].

While more and more large-scale joint projects launch to investigate different fuel cell technologies [41], criticism from maritime industry participants persists based on three ideas: (1) fuel cell systems imply too high capital costs, (2) early investing in the wrong technology leads to a major disadvantage for the shipowner, and (3) hydrogen lacks in availability and volumetric energy density, thus rendering the application of fuel cells on ships impossible. To remedy the weak spots of hydrogen, several upcoming fuel cell system approaches focus on the usage of ammonia, methanol, and liquefied natural gas (LNG) [43]. While ammonia and methanol are mostly discussed to be introduced to the shipping sector in the medium-term future, LNG today is bunkered in 24 of the largest 25 ports and in 76% of all ports worldwide [44]. Hence, LNG-based fuel cell systems could likely be the first technologies suitable for broader application. Since high temperature SOFCs are compatible with carbon monoxide-contaminated hydrogen from steam reforming [45] and therefore allow the further use of carbon-based fuels like LNG without excessive interim process steps [46], the technology is frequently discussed by shipping sector participants. Arguably, while the operation with LNG will not lead to emission neutrality, byproducts of combustion like nitrogen oxides, carbon monoxide and particulate matter would be eliminated in addition to the reduction of carbon dioxide.

In the open literature, there already exist several assessments concerning the techno-economic assessment of fuel cells with non-hydrogen fueling for ship operation. For example, the authors of [47] conducted a life cycle analysis of a diesel-fed molten carbonate fuel cell system already in 2006. The authors integrated three different stationary ship operating modes for a defined energy system. The authors of [48] characterized the operation of a methanol-based SOFC in 2010. In the operating phase, their work builds upon fixed fuel cell efficiency. Recently in [49], an LNG-based SOFC system's energy, cost, and emission reduction potentials are analyzed on the basis of discrete daily load profiles with static operation. In [50], diesel combustion is compared to several fuel cell technologies economically and environmentally. Unlike the investigated combustion engine, fuel cell systems are supported by an energy storage system. Still, the assessment is based on constant efficiencies and staggered load scenarios. However, two major aspects have not been considered in these analyses:

1. Since the efficiency and emissions of the fuel cells are influenced by their operating point, examining their performance with averaged estimations or even full load specifications might be a misleading simplification. Consequently, load profiles with an appropriate time resolution and dynamic component models should be the basis for model-based investigations.
2. Due to the operative restrictions of steam reforming and fuel cell processes, load shifts of the power system are limited to a certain degree. Since ship load profiles tend to have a very fluctuating characteristic, which by far outpaces the capabilities of a hydrocarbon-based fuel cell system, a secondary power source of sufficient sizing is mandatory for uninterrupted operation. This hybridization with e.g. combustion engines [51] or an electrical energy storage unit [50] is already addressed in the methodical issue and should be included into a model-based system assessment.

Since the non-stationary operation of SOFCs or other high-temperature fuel cells is often discussed in theory but not reliably tested in a marine environment, a model-based verification is a useful first step towards the first real large-scale use case. The derived research questions take into account the SOFCs' operating limitations and the consequences for a hybrid system design:

- 2 Research issue: Are SOFCs suitable for marine applications?**
- 2.1 Are the load shift limitations of an SOFC system with onboard steam reforming inhibiting their use on ships with fluctuating power demand?
 - 2.2 If not, what additional support is required to ensure an uninterrupted supply of power on a ship?
 - 2.3 How does a cost-optimal hybrid power system including SOFCs look like?

2.3 Decentralized Ship Power Systems

Another highly interesting fuel cell-related topic is the option of a ship power system decentralization. To introduce this novel topic, general benefits of distributed power systems are addressed and investigations already covered in scientific articles are listed. Since the presented literature raises further questions, a third set of research issues is articulated.

Disclosure: Distributed ship power systems are already topic of previously published work. The following section is in part based on the publication: L. Kistner; A. Bensmann; R. Hanke-Rauschenbach, Optimal Design of a Distributed Ship

Power System with Solid Oxide Fuel Cells under the Consideration of Component Malfunctions, *Applied Energy* (2022) [52]. For a detailed description of the author contributions see Appendix C.

In the past, distribution approaches for ICEs have been dismissed in favor of large gensets with a lower specific waste heat flux. In contrast to ICEs, novel power system components like fuel cells or batteries can be sized for a specific power demand without substantial efficiency losses and therefore present an excellent opportunity for a system distribution. Benefits of such approaches include downsizing the shipboard power grid, a reduction of transmission losses, and creating a more reliable component redundancy. Since the restructuring of a ship's room arrangement is necessary for a successful implementation, system decentralization is mostly an important consideration for the design of future newbuilt ships. While shipboard distributed power systems are a newer trend that is almost exclusively discussed in a scientific context, ship builders today can already profit from the onshore system-focused research results of the last decade in terms of architecture [53],[54] and software solutions [55],[56].

In the literature, qualitative advantages and challenges of distributed ship energy systems have already been covered with regard to different power technologies. For example, in [57] PEMFCs, SOFCs and micro gas turbines are introduced as potential technology solutions for decentralization. General construction ideas, a potential ship grid topology, and peripheral components of the technologies are discussed here. In [58], shipboard microgrid structures, design potentials, and power control strategies are addressed qualitatively. Thereby, the authors place a focus on power supply quality and the advantages of direct-current approaches. In [59], the authors define and compare distributed designs with either PEMFCs, SOFCs, gas turbines, and energy storage support on the basis of load profiles. The assessment gives a general overview of technology performances but does not quantify benefits that a distribution includes in general. In [60], the same system components are compared for electrical and thermal cogeneration integration with an optimal-design and unit-commitment approach. While component costs are included in the objective function, transmission system requirements are neglected.

An issue that has not been covered in the open literature is a direct techno-economic comparison of centralized and distributed ship designs. Consequently, the derived research questions address both the power transmission component specifications and the overall system redundancy requirements:

- 3 Research issue: How can the advantage of a fuel cell’s modular characteristic be leveraged in large-scale ship power systems?**
- 3.1 What quantitative benefits can the transmission grid of a distributed power system have over a central approach?
- 3.2 Is the optimal decentralized system design solution modified when malfunction scenarios are considered?
- 3.3 To what extent does a ship power system benefit from the components’ modularity regarding component redundancy?


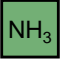
2.4 Technologies for a Sustainable Future


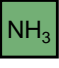





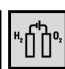


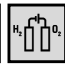
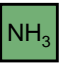
Finally, the techno-economic and environmental assessment of shipboard fuel cell systems’ and combustion engines’ key performance indicators is subject of discussion for the last thematic section. First, the latest literature in the field of future fuels and power technologies is reviewed extensively and relevant improvable aspects are given. Following, the last block of open research questions is formulated.


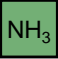



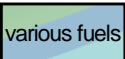
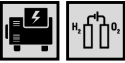

Disclosure: Synthetic fuels and future power technologies are already topic of previously published works. The following section is in part based on the publication: L. Kistner; A. Bensmann; C. Minke; R. Hanke-Rauschenbach, Comprehensive techno-economic assessment of power technologies and synthetic fuels under discussion for ship applications, Renewable and Sustainable Energy Reviews (submitted) [61]. For a detailed description of the author contributions see Appendix C.

Due to the exacerbated regulatory legislation [11],[62] and increasing social pressure, the shipping industry faces the challenge of developing sustainable power system solutions in the current decade. Currently, most decarbonization pathways count on the supply of synthetic fuels with small environmental footprints [62],[63]. However, the shipping industry does not agree on one single synthetic fuel or power technology approach but works on many different technological solutions.

Since the *IMO* released their future climate protection targets in the year 2018 [11], many comparison approaches concerning power technologies and synthetic fuels have been published in both a global and a ship-specific context. Comparative analyses are made for various biofuels, electrofuels and even carbon capture and storage solutions, as well as for PEMFCs, SOFCs, and ICEs. Discussion-driving examples including their focus of research and key findings are collected in Tab. 2.1.

Tab. 2.1: Literature overview: ship power technology and synthetic fuel discussions since the *IMO* released their climate reduction targets in 2018 [11]. Technology icons represent the study of internal combustion engines  and/or fuel cell systems , colored boxes constitute considered fuels

Authors	Techn.	Focus of research	Key findings
T&E [62]	 	<ul style="list-style-type: none"> regulatory advice for the European Union roadmaps for decarbonization with different scenarios 	<ul style="list-style-type: none"> efficiency measures facilitate transition mandating deployment for ships is required for a stable electrofuel supply
Center for Zero Carbon Shipping [63]	 	<ul style="list-style-type: none"> fuel supply chains transition paths required regulatory measures and market development global fleet perspective 	<ul style="list-style-type: none"> financial incentives, sustainable fuel production scale up, and global emission levy are key to the transition green ammonia is likely cheaper than other electrofuels
DNV [64]	 	<ul style="list-style-type: none"> total costs of ownership for a bulk carrier case study fuel transition preparation 	<ul style="list-style-type: none"> ammonia solutions indicate best financial performance in newbuilts alternatives include dual fuel engines
IRENA [65]	  	<ul style="list-style-type: none"> performance indicators of renewable fuels decarbonization pathways 	<ul style="list-style-type: none"> ammonia will be the backbone for decarbonising international shipping realistic carbon levies are required
Kim et al. [50]	  	<ul style="list-style-type: none"> technology comparison based on a case study ship predefined system designs battery support for ammonia systems 	<ul style="list-style-type: none"> conventional heavy fuel oil combustion economically outpaces ammonia SOFCs are the most environmentally friendly approach

Authors	Techn.	Focus of research	Key findings
de Vries et al. [66]	 	<ul style="list-style-type: none"> feasibility and risk assessment economic and qualitative environmental comparison 	<ul style="list-style-type: none"> ICEs are preferable over fuel cells due to their technology readiness levels
Horvath et al. [67]	 	<ul style="list-style-type: none"> three vessel types valuation of lost cargo space fuel price sensitivity analysis 	<ul style="list-style-type: none"> the combination of liquefied hydrogen and PEMFCs is more cost-efficient than concurring electrofuel approaches
McKinlay et al. [68]	 	<ul style="list-style-type: none"> comparison of system mass and volume including storage infrastructure 	<ul style="list-style-type: none"> hydrogen applications are viable despite low volumetric energy density
Korberg et al. [69]	 	<ul style="list-style-type: none"> economic assessment for different vessel types and voyage times focus on fuel production chains 	<ul style="list-style-type: none"> methanol engines are most cost-competitive for deep-sea operation fuel cells can substitute when reaching even higher efficiency levels

While many different angles are covered in the listed assessments and remarkable results are presented, at least one of the following three aspects emerges worthy of improvement:

1. The power technology descriptions require a clearer distinction and modeling with sufficient level of detail. Efficiencies and other generator specifications are often not described technology-specific and operating point-dependent but rather assumed to be constant or of linear characteristic. Time-dependent behavior and generator limitations are mostly not regarded.
2. The evaluation procedure needs to cover all relevant aspects for a decision-making process. Most of the assessments do not include all considerable technologies or fuels and thereby do not create a comprehensive picture. Also, the quantification of emissions including combustion byproducts or components' carbon footprints is still a relevant concern, which often is neglected for synthetic fuel discussions.

3. Study concepts should minimize any kind of bias. This includes avoiding a one-sided utilization of auxiliary components like storage units, preventing imbalanced assumptions regarding future trends with help of parameter studies, and circumvent prefixed configuration or manually created system designs.

Since non of the examined open-literature publications fulfills the outlined criteria, the last objective of this dissertation is to provide a clear and comprehensive comparison of ship power system technologies. To complete this task, the following research questions have to be addressed:

- 4 Research issue: Which is the most cost-efficient and sustainable ship power system configuration for the future?**
- 4.1 Which power technologies and fuels are eligible in the near future and how are they performing compared to state-of-the-art systems?
- 4.2 Which are the economic and environmental key performance indicators?
- 4.3 How can a configuration bias be prevented when comparing technologies?
- 4.4 Which relevant price developments are to be expected and how do they affect the economic performance of the technologies?
- 4.5 Are there mission profiles or operating scenarios for which certain approaches are particularly suited?

2.5 Manuscript Structure and Segmentation of the Research Issues

This dissertation is organized as follows: Chapter 3 offers an overview of the SOFC-based ship power system architecture and its components under consideration, the structure of component models, the fundamental objective of a system optimization, as well as the proposed system and component control strategy.

In Chapter 4 the economic optimization of a hybrid power system is demonstrated by means of two characteristic ship load profiles. Following, the optimization results are revised by adjusting of the storage models' levels of detail, as well as the optimization's scope of the objective function to answer the research issue [1]. Furthermore, research issue [2] is processed by interpreting the results of all conducted design optimization tasks.

Chapter 5 covers the potentials of a decentralized ship power system architecture. While the previous component models are taken as a basis and only modified

to represent distributed units, power transmission models and a restructured system optimization task are presented. The distribution approach is conducted for a cruise ship with a central design as benchmark. Further, component redundancy requirements are evaluated for both system structures and worst case assumptions, aiming to answer research issue [3].

Chapter 6 first gives an overview of today's and serviceable future ship power generation technologies and their operational readiness. Subsequently, additionally required component models are introduced. Finally, technology comparisons are presented with a special focus on the ship's mission characteristics, fuel price development and potentially increasing shipboard volume opportunity costs. In this chapter all questions regarding research issue [4] are addressed.

3 Modeling and Designing a Hybrid Ship Power System

In this chapter different aspects of the model-based system design optimization approach are discussed. In this regard, the SOFC technology is selected as an exemplary power generator. After a brief introduction of the power system components in Section 3.1, the integral elements of the investigation method displayed in Fig. 3.1 are examined: the system component models including the computation of relevant performance indicators and the ship’s time-dependent power demand (cf. Section 3.2), the utilized optimization approach (cf. Section 3.3), as well as the system control strategy (cf. Section 3.4). Finally, the underlying computational framework is presented in Section 3.5.

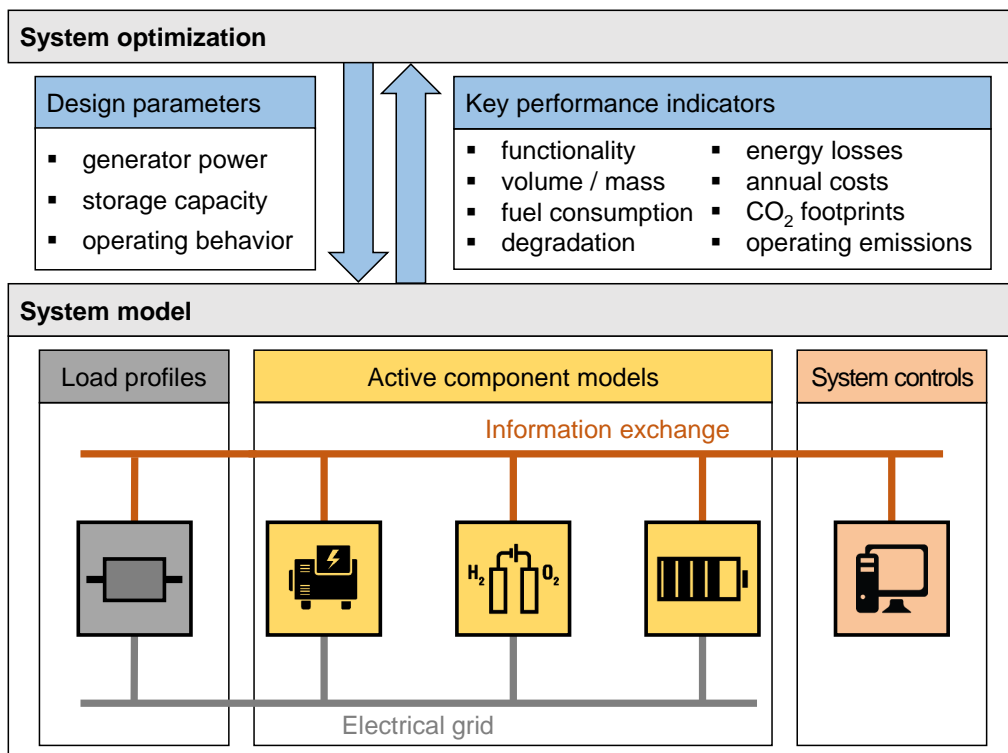


Fig. 3.1: Required elements for a system design optimization task: information input (degrees of freedom) and output (performance indicators) interfaces of a system model including power demand, active power system components, and a control strategy

Disclosure: The following chapter is in part based on the publications: L. Kistner; A. Bensmann; R. Hanke-Rauschenbach, Optimal Design of Power Gradient Limited Solid Oxide Fuel Cell Systems with Hybrid Storage Support for Ship Applications, Energy Conversion and Management (2021) [30] and L. Kistner; A. Bensmann; R. Hanke-Rauschenbach, Optimal Design of a Distributed Ship Power System with Solid Oxide Fuel Cells under the Consideration of Component Malfunctions, Applied Energy (2022) [52]. For a detailed description of the author contributions see Appendix C.

3.1 Central System Architecture

In the following, the ship’s power system components considered for the SOFC-based approach and displayed in Fig. 3.2 are introduced: the ship’s power demand (grey), a solid oxide fuel cell module (orange), as well as a hybridized storage unit containing batteries (yellow) and supercapacitors (blue). All components are directly connected to a busbar, forming a central system structure. For all ongoing investigations, the marked counting arrows constitute the direction of power flow.

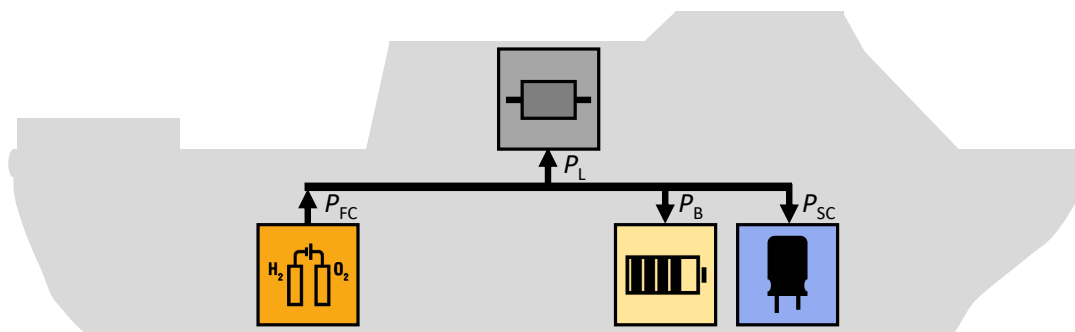


Fig. 3.2: Considered components and power flows of a ship energy system: electrical load (P_L), solid oxide fuel cell power output (P_{FC}), battery unit charge power (P_B), supercapacitor unit charge power (P_{SC})

3.1.1 Solid Oxide Fuel Cells

Core of the firstly assessed system is an SOFC module, which is characterized by a higher efficiency than state of the art combustion engines and most other applicable energy converters [43],[46]. The investigated module consists of an external steam reforming unit, creating a hydrogen-rich mixture from a methane-based natural gas input, and a downstream group of fuel cell stacks. The most relevant material and energy flows as well as the underlying chemical reactions occurring in the module are schematically given in Fig. 3.3. As displayed, the onboard steam

reforming process recuperates waste heat from the SOFCs for an endothermic reforming reaction [70]. While the external steam reforming chamber requires a rather complex heat transfer, it also enables a higher chemical conversion rate and better thermal management possibilities for dynamic operation compared to internal reforming processes. As opposed to PEMFCs [71],[72], SOFCs have a high tolerance towards carbon monoxide, which is an intermediate-product of steam reforming, resulting from an incomplete water-gas shift reaction [41]. Therefore, no extra gas cleaning steps apart from a sulfur oxide separator are required.

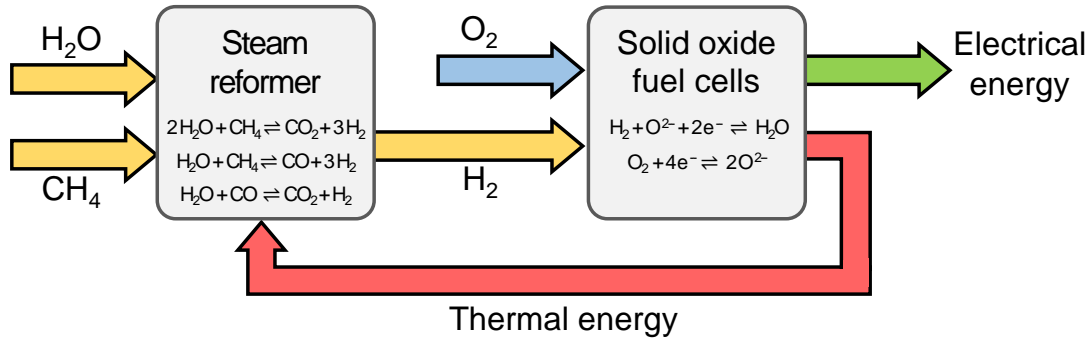


Fig. 3.3: Schematic material flows, energy flows, and chemical reactions occurring in the SOFC module with external steam reforming chamber

On top of the high energy efficiency, the investigated SOFC module entails four additional mentionable benefits:

1. Enabling the utilization of carbon-based fuels like liquefied natural gas (LNG) provides the accessibility to the existing fuel infrastructure in harbors [44].
2. The high volumetric energy density of LNG exceeds that of pressurized hydrogen at a pressure level of 70 MPa or liquid hydrogen at temperature levels around 20 Kelvin.
3. Further excess thermal energy has an ideal temperature level for general heating, freshwater generation, or laundry services and therefore allows for a beneficial cogeneration operation [73].
4. Not only does the usage of high-efficiency SOFCs equal fewer carbon dioxide emissions than ICE operation. Also, methane, particulate matter, nitrogen oxide, and carbon monoxide emissions are reduced to practically zero due to the electrochemical conversion method.

However, it must be taken into account that a high system temperature is a challenge with regard to the selection of construction materials, the need for sophisticated heat insulation, and several operating restrictions: load shift capabilities are limited to reduce thermal stress and also factor in inertia of the steam reformer. Also, a minimum power output is required to grant the desired fluid-dynamical behavior and to prevent the system from cooling down, which would otherwise impair the chemical reactions. Of course, the system must comply with the standards and guidelines for fuel cells in shipping [43]. Besides general equipment and component redundancy requirements, special regulations regarding the treatment of all gaseous and low-flash-point fuels are to be applied.

3.1.2 Energy Storage

Due to the limited operating flexibility of an SOFC module, another power source with fewer operating limitations must be utilized to meet the requirements of the mostly fluctuating ship load profile. While SOFCs are often discussed to be applied as a secondary power system to assist gas combustion engines [51],[74], this dissertation focuses on their stand-alone potentials with an electrical energy storage support. Since the ship grid is isolated and not capable of seamlessly disposing excess energy, the applied storage unit needs to fulfill the power balance while generators and load are not synchronized. In addition to the addressed load change support requirements, shipboard energy storage units are mainly used for one or more of the following objectives:

1. During peak shaving operation, a storage supports the generators for a period of high load demand (e.g. harbor thruster maneuvers). Consequently, the generator's rated power must not comply with the maximum power spike and can be selected according to more common operating events.
2. Low part load avoidance mainly increases a generators' energy efficiency and inhibits single engines from occasionally shutting off and on again [23]. Here, surplus energy is not wasted but charges the energy storage.
3. The exclusive operation of storage systems can be temporarily utilized in areas with very strict emission regulations like a fjord [75] or close to restricted ports close to metropolitan areas [76].

For the base storage, different battery technologies can be considered. While many (plugin-hybrid) short sea ferries with battery-electric propulsion settle on lithium-ion batteries with high gravimetric energy density and lower specific power like the lithium-nickel-manganese-cobalt (NMC) cells, batteries for open-sea hybrid systems likely need to feature different characteristics. Here, the lithium-iron-phosphate (LFP) battery technology with few safety concerns, high specific power,

and comparably long lifetime is chosen [77]. Depending on the load characteristics, an additional storage hybridization is conceivable. For the peak storage, electrostatic double-layer capacitors, also referred to as supercapacitors are chosen to support the battery system with their high specific power output, low degradation and immediate reaction time.

3.1.3 Electrical Load


The considered electrical load implies nautical equipment like radars and communication devices along with lighting, heating, ventilation, and fresh water generation. Depending on the ship type, freight cooling, crane structures, feed pumps or food preparation, laundry and entertainment applications also constitute a relevant energy demand. In addition, thruster maneuvers are investigated thoroughly. While propulsion represents another large power consumer, the focus of this dissertation is set to substitute the ship's auxiliary engines, whereas other measures are preferably applicable here (cf. Section 1).

3.2 System Component Models


In this section, the fuel cell system model, a technology-unspecific storage model approach, and considerations for the electrical load display are introduced. For the mathematical model description, no intentional formulation limitations are stipulated, as displaying the behavior of system operating points (eg. fuel consumption) appropriately is an essential element of the planned assessments. However, zero-dimensional models are preferably used and parameterized with manufacturers' data sheet parameters or already measured operating diagrams where applicable. Due to the identified importance of analyzing the time-dependent system behavior to investigate the relevance of the SOFC operating limitations and the derived energy storage capacity requirements, individual dynamic models are prepared.

Both the SOFC and the energy storage model description consist of a uniform four-part substructure, as is given in Fig. 3.4: (1) the physical model equations describe the dynamic behavior of the unit, including time-dependent states and energy efficiency. For the given model approach, system interfaces on the power level are provided. (2) The component management strategy (CMS) restricts the unit's operating behavior and prevents exceeding potentially hazardous or destructive limitations. (3) The economic model covers three kinds of expenses: the annuity payment equivalents of component investment costs, maintenance costs, and operating costs. (4) In the environmental model, different production and operating emissions are quantified and evaluated.


Physical model

	<p>Task: description of the dynamic component behavior</p> <p>Extent:</p> <ul style="list-style-type: none"> • Balance equations (energy, charge, fuel consumption) • Operating point dependencies (efficiency, addit. losses) • Utilization of data sheet and measurement information
---	---

Component management

	<p>Task: compliance with component limitations for safety concerns</p> <p>Extent:</p> <ul style="list-style-type: none"> • Power or current restrictions • State of energy, voltage limitations • Load change capability restrictions
---	--

Economic model

	<p>Task: determination of capital, maintenance and operating costs</p> <p>Extent:</p> <ul style="list-style-type: none"> • Literature and industry parameters/curves • Lifetime/degradation estimations • Annuity payment factor calculation
---	---

Environmental model


	<p>Task: determination of emissions during construction and operation</p> <p>Extent:</p> <ul style="list-style-type: none"> • Characteristic diagrams • Monetary emission assessment • Life cycle data (materials, production, operation, disposal)
---	--

Fig. 3.4: General substructure of the developed four-parted system component models

3.2.1 Solid Oxide Fuel Cells

Physical model –The physical description of one SOFC module is given with the operating-point-dependent fuel consumption in the form of an input mass flow

$$\dot{m}_{\text{fuel}} = \frac{P_{\text{FC}}(t)}{\eta_{\text{FC}}(\xi_{\text{FC}}) \cdot h_{\text{fuel}}^{\text{LHV}}}, \quad (3.1)$$

where

$$\xi_{\text{FC}} = \frac{P_{\text{FC}}}{P_{\text{FC}}^r} \quad (3.2)$$

is the normalized operating point with regard to the rated power P_{FC}^r , P_{FC} is the actual power output, η_{FC} is the fuel cell system efficiency, and $h_{\text{fuel}}^{\text{LHV}}$ is the lower heating value of the fuel. One equivalent notation of this description is given with

the specific fuel consumption (SFC) $\dot{m}_{\text{fuel}}^{\text{spec}}$, commonly used in a maritime context. The SFC specifies the fuel mass flow required to generate a certain amount of electrical power:

$$\dot{m}_{\text{fuel}} = P_{\text{FC}}(t) \cdot \dot{m}_{\text{fuel}}^{\text{spec}}(\xi_{\text{FC}}). \quad (3.3)$$

Both energy efficiency and SFC of the considered SOFC module are given in Fig. 3.5.

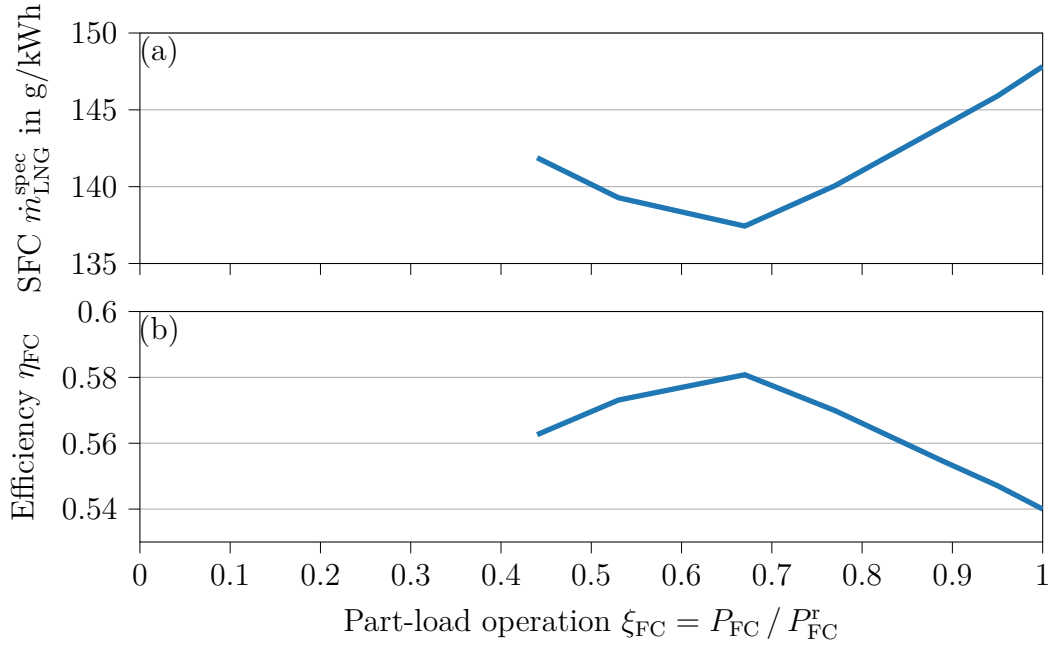


Fig. 3.5: (a) SOFC module's operating-point-specific fuel consumption (SFC) including power electronics based on [78]; (b) equivalent efficiency calculated with LNG's lower heating value (LHV), minor adaptations to display an upscaled system are included in consultation with the responsible research group

Component management – The fuel cell module operation must comply with two conditions, which already were discussed in Section 3.1. Firstly, the power output must not exceed the given operating limits:

$$P_{\text{FC}}^{\min} \leq P_{\text{FC}} \leq P_{\text{FC}}^r, \quad (3.4)$$

where P_{FC}^{\min} is the minimum power output. Secondly, too abrupt load alternations must be inhibited:

$$-\dot{P}_{\text{FC}}^{\max} \leq \frac{dP_{\text{FC}}}{dt} \leq \dot{P}_{\text{FC}}^{\max}, \quad (3.5)$$

where $\dot{P}_{\text{FC}}^{\text{max}}$ represents the product of a specific maximum power gradient and the rated power of the module. For simplicity reasons, the same limitation value for upshifts and downshifts is assumed. All required component management parameters are listed in Tab. 3.1.

Economic model – The converted annually accruing SOFC expenses

$$p_{\text{FC}}^{\text{a}} = p_{\text{FC}}^{\text{inv}} \cdot P_{\text{FC}}^{\text{max}} \cdot (c_{\text{FC}}^{\text{a}} + A_{\text{FC}}) \quad (3.6)$$

are calculated from a rated-power-specific investment cost term $p_{\text{FC}}^{\text{inv}}$, a maintenance cost factor c_{FC}^{a} (in %/year), and take into account the component lifetime with the annuity payment method:

$$A_{\text{FC}} = \frac{(1 + j)^{t_{\text{L,FC}}} \cdot j}{(1 + j)^{t_{\text{L,FC}}} - 1}, \quad (3.7)$$

where j is the given interest rate and $t_{\text{L,FC}}$ is the component's lifetime. In contrast to the well developed ICE systems for ship applications, the SOFC module price is highly dependent on material development and potential batch production in the near future. While market introduction prices of 2000 €/kW for complete systems are prognosticated, current prototype component costs amount to around 3500 €/kW. In the first assessment, the prototype price is assumed, while a low qualitative sensitivity of the results is assured for the conceivable SOFC cost range. Further information on SOFC cost estimation can be found in [79].

As the precise simulation of SOFC degradation would include a consideration of several effects [80], which are yet to be quantified for dynamic use, the service life prediction contains a constant module lifetime. Here, the chosen maintenance cost parameter includes cell replacement. The small influence of dynamic fuel cell operation on the cell's area-specific resistance [81] as well as the low probability of failure caused by thermomechanic stress at different temperatures [82] and for load changes [83] along with the introduction of a power-gradient-restrictive component management also support the assumption of operation-independent maintenance costs c_{FC}^{a} . All required economic parameters are listed in Tab. 3.1.

Environmental model – The environmental fuel cell operating characterization should include the investigation of three sections: (1) the fuel cell system production footprint, (2) the production resulting from fuel provision, and (3) the emissions occurring from the system's operation at sea. Since the environmental assessment is not part of the first analyses, but is at first covered for the direct comparison of different power technologies, an extensive model description is given in Chapter 6.

Tab. 3.1: SOFC system parameters

Management parameter		Value	Reference
Minimum system power	P_{FC}^{\min}	$0.5 \cdot P_{\text{FC}}^r$	manufacturer
Maximum power gradient	$\dot{P}_{\text{FC}}^{\max}$	$0.1 / \text{min} \cdot P_{\text{FC}}^r$	manufacturer
Economic parameter		Value	Reference
Specific investment costs	$p_{\text{FC}}^{\text{inv}}$	3500 € / kW	[79]
Maintenance costs	c_{FC}^a	0.04 a^{-1}	[84],[85]
System lifetime	$t_{\text{L,FC}}$	20 a	[41]
Interest rate	j	0.035	assumed

3.2.2 Energy Storage

Physical model – For the description of the battery and the supercapacitor units, a technology-unspecific storage model is used. The time evolution of the state of energy (SoE) F_i is determined from the energy balance

$$C_{\text{E},i} \frac{dF_i}{dt} = -k_{\text{SD},i} \cdot F_i \cdot C_{\text{E},i} + P_i \cdot \begin{cases} \eta_{\text{cha},i} & \text{if } P_i > 0 \\ \frac{1}{\eta_{\text{dis},i}} & \text{if } P_i < 0 \end{cases} \quad (3.8)$$

$$\forall i = \text{B, SC}$$

as a function of supplied or extracted power P_i , the average energy efficiency during charging $\eta_{\text{cha},i}$ and discharging $\eta_{\text{dis},i}$, and the self discharge factor $k_{\text{SD},i}$. While in reality the storage efficiency is current-and-voltage-dependent, this low-level model only considers an average value for all operating points and equal distribution of the turnover efficiency towards charging and discharging:

$$\eta_{\text{dis},i} = \eta_{\text{cha},i} \quad (3.9)$$

Each storage is composed of an amount of single cells N_i which together build the total energy capacity from single cell values $C_{\text{E},i}^{\text{cell}}$:

$$C_{\text{E},i} = C_{\text{E},i}^{\text{cell}} \cdot N_i \quad (3.10)$$

Since a hybrid storage application is investigated in this study, a substitute state of energy for the total unit is given with:

$$F_{\text{S}} = \frac{F_{\text{B}} \cdot C_{\text{E,B}} + F_{\text{SC}} \cdot C_{\text{E,SC}}}{C_{\text{E,B}} + C_{\text{E,SC}}} \quad (3.11)$$

Physical-model-related parameters are given in Tab. 3.2 for both battery and supercapacitor.

Component management – Two operating limitations are required to be controlled during storage operation: the charge/discharge power and the state of energy. Thereby, the state of energy is limited to prevent the storage from deep discharging and overcharging:

$$F_i^{\min} \leq F_i \leq F_i^{\max} . \quad (3.12)$$

In addition, restricting maximum charge or discharge power values are enforced:

$$P_{\text{dis},i}^{\max} \leq P_i \leq P_{\text{cha},i}^{\max} . \quad (3.13)$$

Maximum charge and discharge power values for the system are calculated from the number of single cells:

$$P_{\text{cha},i}^{\max} = P_{\text{cha},i}^{\max,\text{cell}} \cdot N_i , \quad (3.14a)$$

$$P_{\text{dis},i}^{\max} = P_{\text{dis},i}^{\max,\text{cell}} \cdot N_i . \quad (3.14b)$$

Further helpful for the investigation is the specific power parameter Π_i , which is equal for single cells as well as the system, and SoE-independent for this model:

$$\Pi_{\text{cha},i} = \frac{P_{\text{cha},i}^{\max}}{C_{E,i}} , \quad (3.15a)$$

$$\Pi_{\text{dis},i} = \frac{P_{\text{dis},i}^{\max}}{C_{E,i}} . \quad (3.15b)$$

All operating limitations for the battery and the supercapacitor unit are given in Tab. 3.2.

Economic model – For Li-ion and supercapacitor units, the investment costs are calculated with regard to their rated energy capacity:

$$p_i^{\text{a}} = p_i^{\text{inv}} \cdot C_{E,i} \cdot A_i(t_{L,i}) . \quad (3.16)$$

Note that the storage operability must be secured at end of life (EOL), which here is defined as a decrease of the rated energy capacity to 80% of the original capacity at the beginning of life (BOL). Consequently, capacity degradation effects must result in an intended oversizing of 25%. Chosen battery and supercapacitor costs also include extra specifications and certification for shipboard application. In analogy to the SOFC pricing, storage price modifications were investigated during the optimal design analysis. Although steady shifts of the cost optimum are identified, no qualitative different conclusions were found. In contrast to the

SOFC model, the storage lifetime is not estimated to be fixed but considers cycle aging and a maximum calendar lifetime:

$$t_{L,i} = \begin{cases} t_{\text{cal},i} & \text{if } t_{\text{cal},i} < \frac{C_{E,i} \cdot \Delta t}{E_{\text{dis},i}(\Delta t)} \cdot L_i \\ \frac{C_{E,i} \cdot \Delta t}{E_{\text{dis},i}(\Delta t)} \cdot L_i & \text{else,} \end{cases} \quad (3.17)$$

where Δt is the investigated operating time. The assumed number of maximum full charge-discharge cycles L_i is consulted and compared to the energy output in the simulated time frame $E_{\text{dis},i}$, normalized with the storage's energy capacity. The derived loss of lifetime then is extrapolated and compared to an absolute maximum value t_{cal} . Dependencies of degradation on state of energy and power are neglected for the moment. Parameters concerning the annual cost calculation and the lifetime estimation are given in Tab. 3.2 for both battery and supercapacitor.

Environmental model – In analogy to the SOFC model description, the environmental model for an energy storage unit is postponed to Chapter 6.

Tab. 3.2: LFP and supercapacitor parameters for the nonspecific storage model; values are derived from internal manufacturer data sheets if not marked otherwise

Physical parameter		LFP battery	Supercapacitor
Energy capacity	C_E^{cell}	92.3 Wh	2.29 Wh
Charging/discharging efficiency	$\eta_{\text{cha/dis}}$	0.97	0.949
Self discharge coefficient	k_{SD}	0.01 d ⁻¹	0.11 d ⁻¹
Management parameter		LFP battery	Supercapacitor
Maximum charge power	Π_{cha}	4.29 h ⁻¹	590 h ⁻¹
Maximum disch. power	Π_{dis}	-7.14 h ⁻¹	-590 h ⁻¹
Maximum SoE	F^{max}	1	1
Minimum SoE	F^{min}	0	0
Economic parameter		LFP battery	Supercapacitor
Specific investment costs	p^{inv}	1000 € / kWh [86]	30,000 € / kWh [87]
Calendar lifetime	t_{cal}	10 a [88]	16 a [88]
Number of full cycles	L	3500 [88]	10 ⁶ [88]

3.2.3 Electrical Load

Physical model – The shipboard electrical power demand is constituted with a time-dependent, power-referred load profile. The power demand is set to be a fixed model input and is not influenced by the system components' operations:

$$P_L = f(t) . \quad (3.18)$$

For further simplification, an immediate comply of the calculated demand and the active system components answers is assumed. A reaction delay due to real-time communication, inverter performance, and a grid voltage volatility are thereby neglected. Consequently, only simulation results without deviation between load and active components are approved to represent feasible design solutions.

Other submodels – Since the electrical load is declared to be a fixed information input, no component management is intended for the investigations. Also, the economic and environmental assessments focus on the active system components. The ship’s power consumption behavior is not further evaluated.

3.3 System Design Optimization

After the introduction of the system component models, the ship-power-system-specific optimization task including objective function, degrees of freedom, and constraints is formulated. Then, considerations regarding the task’s numerical feasibility are made with a focus on the previously prepared model equation characteristics.

3.3.1 Optimization Task Formulation

In this section a system-specific optimization task and associated constraints are presented. Design objective for the optimization is a minimization of the annual system expenses containing costs for fuel cells p_{FC}^a , batteries p_B^a and supercapacitors p_{SC}^a . To create a concise overview of the performance indicators influencing the design decision, a series of optimization tasks is conducted for different predefined fuel cell unit rated power output P_{FC}^r :

$$\underset{N_B, N_{SC}, F_B(t_0), F_{SC}(t_0), P_{FC}(t), P_B(t), P_{SC}(t)}{\text{minimize}} \quad p_{FC}^a + p_B^a + p_{SC}^a \quad (3.19a)$$

$$\text{subject to} \quad P_{FC}^r = P_{FC}^{\text{input}} , \quad (3.19b)$$

$$0 = P_{FC}(t) - P_L(t) - P_{SC}(t) - P_B(t) \forall t , \quad (3.19c)$$

$$F_B(t_0) \leq F_B(t_{op}) , \quad (3.19d)$$

$$F_{SC}(t_0) \leq F_{SC}(t_{op}) , \quad (3.19e)$$

where the degrees of freedom are the number of installed battery cells N_B and supercapacitor cells N_{SC} , and their state of energy (SoE) at the beginning of the

analyzed time period ($F_i(t_0); i = \text{B, SC}$), as well as the time-dependent power values of fuel cells and storage units. Apart from the fixed definition of the fuel cells' rated power $P_{\text{FC}}^{\text{input}}$ (cf. Eq. (3.19b)), the optimization constraints for a sufficient design approach are the power balance (cf. Eq. (3.19c)) and a cyclic boundary condition for the storage's SoE (cf. Eq. (3.19d)), which assures a continuous readiness for use and avoids a system failure after the simulated time frame. Finally, all introduced component models have to be complied with (cf. Eq. (3.19e)).

For the optimization task, cost-optimal energy capacities are firstly determined with a battery-only storage design and a cost optimum is located. Further, the storage lifetime as well as energy and power limitations are examined. Based on this analysis, potential use cases for the hybrid storage are indicated. For a continued economic review, the optimal supercapacitor sizes are computed as a function of fuel cell power and battery capacity. Note that optimized design points do not include factors for security of supply or emergency power generation [29].

3.3.2 Considerations on the Optimization Task

Now that the formulation of the objective function, the degrees of freedom and the constraints including component models is completed, the numerical optimization approach is discussed. As opposed to linear equation systems, which allow for a comparably small computational effort and fast solving times respectively due to a guaranteed convex objective function, several characteristics desired to adequately represent the system components (cf. Tab. 3.3) lead to a nonconvex solution space.

Tab. 3.3: Desired model attributes and programming requirements, resulting in a mixed-integer nonlinear programming (MINLP) problem

Desired model properties	Mathematical requirements
Fixed component unit sizes <ul style="list-style-type: none"> • Battery/supercapacitor cells • Fuel cell modules • Single component malfunctions 	Mixed-integer linear programming (MILP)
Operating-point-specific component behavior <ul style="list-style-type: none"> • Efficiency curves • Operating emissions • Component degradation 	Nonlinear programming (NLP)
Economic dependencies <ul style="list-style-type: none"> • Construction-size-dependent specific costs • Lifetime-dependent annuity payment factors • Operation-dependent expenses (e.g. volume costs) 	Nonlinear programming (NLP)

Still, two metaclasses of numerical design optimization methods are generally available for nonconvex equation systems: analytic optimization algorithms and heuristic algorithms. Their differentiation in terms of method and model requirements is briefly summarized in Tab. 3.4. Even if analytic optimization methods benefit from linear programming approaches, nonconvex model properties do not disallow their usage in general, but potentially demand for modifications of the solver algorithm [89]. To name a few options, a list of possible workaround approaches is given in the following:

MILP optimization – Localization methods also referred to as cutting-plane algorithms support finding feasible integer solutions in mixed-integer problems [90].

NLP optimization – Enhancing interior-point methods, which can only solve in convex solution spaces [91], with a primal-dual approach [92] solves continuous, nonlinear systems.

Computational effort reduction – Branch-and-bound algorithms, which consecutively exclude potential combinatorial solutions, reduce the optimization time for objective functions with several local optima [93].

Model workarounds – Sectional linear approximation as well as convexification by creating a subset of solution spaces with convex envelope functions resemble two approaches to address nonconvex solution spaces [94].

Note that this enumeration should by no means claim to be complete, as MINLP optimization is a very wide mathematical topic. Rather, the examples should showcase the variety of potentials to address analytic optimization issues.

Tab. 3.4: Potential numerical optimization methods applicable to (slightly) nonconvex equation systems

	Analytic optimization	Metaheuristic optimization
Method	Find optima by directly analyzing the objective function	Treat equation system as “black box” and find optima based on empirical testing
Prospect of success	Make use of the function’s gradients for guaranteed local optima findings	Do not guarantee finding optima but only approximate solutions
Requirements	Adequate formulation of objective function/constraints to solve with reasonable computational effort	Smaller number of degrees of freedom to solve with reasonable computational effort
Limitations	Exclude various model description methods	Exclude time-dependent objective variables for high-resolution profiles

Moreover, a vast number of algorithm options for analytic optimization exist, including open-source solutions [95],[96],[97] and commercially available toolboxes [98],[99] with different performances depending on the degree of nonlinearity [100]. Several hybrid-ship-related application scenarios can be found in the open literature [101],[102],[103],[104]. However, since the introduced model properties are (a) highly nonconvex and (b) evaluated to be of high importance for an adequate problem description, a heuristic optimization approach is favored at this point.

Heuristic optimization algorithms do not restrict model formulations but entail a different significant limitation: high-resolution load profiles combined with optimizing the system's operating behavior in every time step involves a massive number of degrees of freedom and therefore leads to a tremendously slow conversion process for heuristic optimization approaches [105]. Consequently, a rule-based control strategy is utilized to emulate the desired operating behavior and reduce the degrees of freedom. Certainly, this workaround creates potentially suboptimal results and requires for adequate rules, which support the overarching objective, but also guarantees a valid design result accurately representing all component characteristics. With the introduction of a rule-based control strategy requirement, a revised optimization function based on Eq. (3.19) is given:

$$\begin{aligned}
& \underset{N_B, N_{SC}, F_B(t_0), F_{SC}(t_0)}{\text{minimize}} && p_{FC}^a + p_B^a + p_{SC}^a \\
& \text{subject to} && P_{FC}^r = P_{FC}^{\text{input}} , \\
& && 0 = P_{FC}(t) - P_L(t) - P_{SC}(t) - P_B(t) \forall t , \\
& && F_B(t_0) \leq F_B(t_{op}) , \\
& && F_{SC}(t_0) \leq F_{SC}(t_{op}) , \\
& && \text{Eqn. (3.1) - (3.18) ,} \\
& && \text{Eqn. (3.21) - (3.30c) ,}
\end{aligned} \tag{3.20}$$

excluding all time-dependent power values from the degrees of freedom and adding another set of constraints discussed in the following section.

3.4 Heuristic Control Strategy for a Hybrid Power System

As already addressed in Section 3.3, a rule-based operation control strategy is chosen due to the limitations of the heuristic optimization algorithm class. In the following, both an overarching cooperation approach for the total system including a hybrid storage and a component-specific management strategy (CMS) to comply with previously addressed operating limitations are introduced.

3.4.1 Energy Management Strategy

Existing rule-based control methods for ships with fuel cell application focus mostly on PEMFC-hybrid ships. Worth mentioning are a multi-scheme energy management resulting from a performance comparison of different strategies [106] and a system approach including a supercapacitor-battery-hybrid storage [107]. However, a rule-based strategy for SOFC systems urgently requires considering the module's stringent operating limitations. Therefore, a fitting standalone strategy is developed.

Overarching objective of the control strategy is to maintain the ship's operability at all times. Since the ship constitutes an islanded grid, no power surplus or shortage is permitted, as is already considered in the optimization task (cf. Eq. (3.19c)). Certainly, a rule-based strategy implementation requires the understanding of the systems' bottlenecks and must rely on a well-designed system resulting from the optimization task. As opposed to more complex approaches utilizing artificial neural network training [108],[109], a straightforward variable priority ranking is applied, as is displayed for a basic example in Fig. 3.6: at first, the load-shift-limited SOFC module is queried, before either battery or supercapacitor unit are utilized to cover the otherwise arising power delta in compliance with their CMS limitations. The management strategy is further divided into a general system control strategy and a hybrid storage utilization scheme. Both controls consist of a long-time, state-dependent objective as well as a present-time decision logic. The derived rules are introduced in the following.

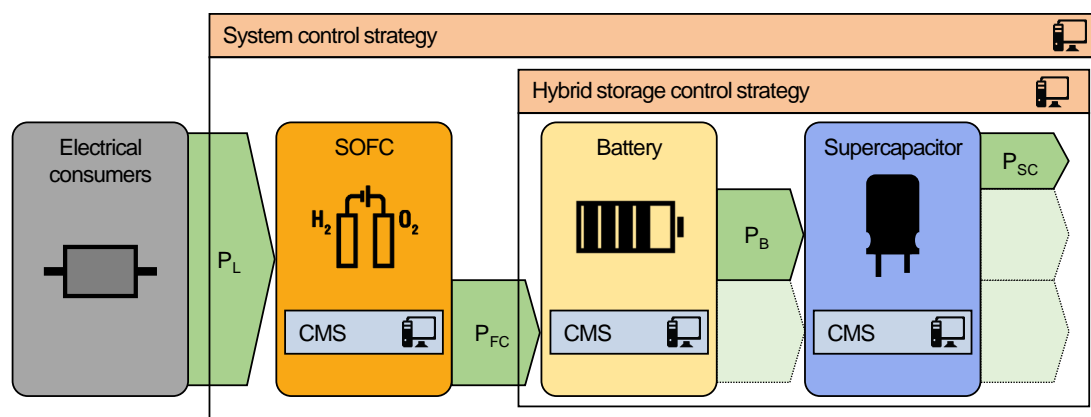


Fig. 3.6: Power flow diagram for a rule-based ranking: the SOFC module cannot cover the load demand on its own either due to already reaching its maximum power output or its gradient limitations; the hybrid storage system covers the power delta with help of both battery and supercapacitor (load peak).

System Control Strategy

The first task performed by the control strategy also referred to as energy management system (EMS) is to specify the SOFCs' desired power output. This demanded set value is regulated with help of a state machine given in Fig. 3.7. Here, state $Z_{\text{FC}} = 1$ represents the request of a steady operation at rated power, which is defined to be the default operation to prevent a shortage of electrical energy. On the other hand, state $Z_{\text{FC}} = 0$ permits dynamic load response operation:

$$P_{\text{FC, set}} = \begin{cases} P_{\text{FC}}^r & \text{if } Z_{\text{FC}} = 1 \\ P_L & \text{if } Z_{\text{FC}} = 0. \end{cases} \quad (3.21)$$

However, dynamic operation is only enabled when the storage's state of energy exceeds a defined critical value F_{crit} to prevent excess energy during operation. The added value ΔF acts as a buffer zone and prevents repetitive state changes.

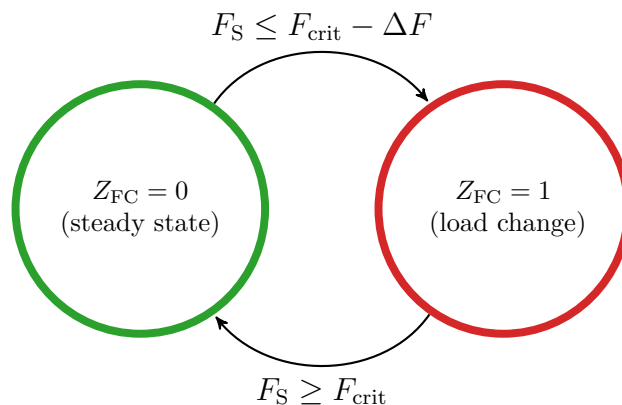


Fig. 3.7: State machine for the SOFC system operation

The next step is to determine logically critical state of energy F_{crit} . Since the SOFC operation at rated power likely charges the energy storage over time but a fully charged unit should be inhibited in order to maintain the system operable, the choice of this parameter is founded on the load shift capabilities of the SOFCs: for the time period of load change from maximal to minimal fuel cell power output, the potential energy excess

$$E_{\text{FC}}^{\text{exc}} = \frac{0.5 \cdot (P_{\text{FC}}^r - P_{\text{FC}}^{\text{min}})^2}{\dot{P}_{\text{FC}}^{\text{max}}} \quad (3.22)$$

must still be compensable by the storage, resulting in a minimum free capacity share at the critical SoE:

$$F_{\text{crit}} = F_{\text{S}}^{\text{max}} - \frac{E_{\text{FC}}^{\text{exc}}}{C_{\text{E,B}} + C_{\text{E,SC}}} . \quad (3.23)$$

In a second step, the EMS processes the deviation between set power value and fuel cell response. The delta between load demand and generated power is then passed to the energy storage:

$$P_{\text{S,set}} = P_{\text{FC}} - P_{\text{L}} . \quad (3.24)$$

Illustrative demonstration – For a better comprehensibility, the system control strategy is demonstrated for a minimal working example in Appendix A.1.

Hybrid Storage Control Strategy

The storage control's task is the best possible deployment of the supercapacitor's small energy capacity by keeping the unit at a desirable state of energy $F_{\text{SC,des}}$. For a load profile with characteristic demand peaks, excess energy should first be stored in the supercapacitor, which afterwards can provide a high-power output. However, the power distribution between the two storage technologies must be treated with care, as a suboptimal approach will invalidate the hybrid storage's scope of application. If in doubt, the desired SoE can be declared as a degree of freedom in the optimization.

Since the hybrid storage operation control strategy likewise follows a longterm SoE-related objective, another state machine is introduced. Here, three different states effect the set value determination: The supercapacitor's SoE is below ($Z_{\text{HY}} = -1$), at ($Z_{\text{HY}} = 0$), or above the desired value ($Z_{\text{HY}} = 1$). All transition criteria can be comprehended in Fig. 3.8.

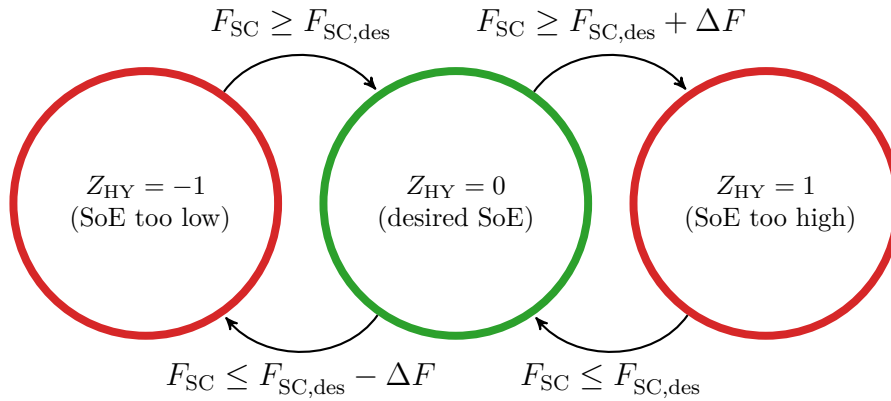


Fig. 3.8: State machine for comparing the supercap's state of energy with the desired value

The derived set values form a variable ranking, giving the supercapacitor priority over the battery whenever the desired power value $P_{S,\text{set}}$ declared by the EMS is useful for reaching the hybrid control's objective (cases 1 and 2):

$$P_{\text{SC},\text{set}} = \begin{cases} P_{S,\text{set}} & \text{if } Z_{\text{HY}} = -1 \wedge P_{S,\text{set}} > 0 \\ P_{S,\text{set}} & \text{if } Z_{\text{HY}} = 1 \wedge P_{S,\text{set}} < 0 \\ P_{S,\text{set}} - P_{\text{B}} & \text{else.} \end{cases} \quad (3.25)$$

Analogous, the battery unit is addressed first, if the power set value contradicts achieving the desired state of energy:

$$P_{\text{B},\text{set}} = \begin{cases} P_{S,\text{set}} & \text{if } Z_{\text{HY}} = -1 \wedge P_{S,\text{set}} < 0 \\ P_{S,\text{set}} & \text{if } Z_{\text{HY}} = 0 \\ P_{S,\text{set}} & \text{if } Z_{\text{HY}} = 1 \wedge P_{S,\text{set}} > 0 \\ P_{S,\text{set}} - P_{\text{SC}} & \text{else.} \end{cases} \quad (3.26)$$

If the hybrid storage is designed adequately, the total power output then corresponds to the set value $P_{S,\text{set}}$ given by the EMS:

$$P_{\text{S}} = P_{\text{B}} + P_{\text{SC}} \quad (3.27)$$

Illustrative demonstration – For a better comprehensibility, the hybrid storage control strategy is demonstrated for a minimal working example in Appendix A.1.

3.4.2 Component Management Strategies

The component-specific management strategies are required to ensure compliance with the previously formulated operational inequality constraints (e.g. Eq. 3.4). In the following, the handling of component set values given by the energy management strategy is explained for both SOFCs and storage units.

Solid Oxide Fuel Cells

In order to control the power output limitations (cf. Eq. (3.4)), an intermediate value $P_{\text{FC},\text{set}}^*$ is calculated from the fuel cell set power $P_{\text{FC},\text{set}}$ given by the EMS:

$$P_{\text{FC},\text{set}}^* = \begin{cases} P_{\text{FC}}^r & \text{if } P_{\text{FC},\text{set}} > P_{\text{FC}}^{\text{max}} \\ P_{\text{FC},\text{set}} & \text{if } P_{\text{FC}}^{\text{min}} \leq P_{\text{FC},\text{set}} \leq P_{\text{FC}}^{\text{max}} \\ P_{\text{FC}}^{\text{min}} & \text{if } P_{\text{FC},\text{set}} < P_{\text{FC}}^{\text{min}} \end{cases} \quad (3.28)$$

Then, the maximum power gradient of the fuel cell module (cf. Eq. (3.5)) is controlled with

$$\frac{dP_{\text{FC}}}{dt} = \dot{P}_{\text{FC}}^{\text{max}} \cdot \text{sgn}(P_{\text{FC, set}}^* - P_{\text{FC}}) , \quad (3.29)$$

where “sgn” is the signum function, which extracts the sign of a real value.

Energy Storage

In the following, a state-machine-based implementation of the control method is introduced. The state machine given in Fig. 3.9 distinguishes a fully operable state ($Z_{\text{CMS,S}} = 0$) from charged ($Z_{\text{CMS,S}} = 1$) or discharged states ($Z_{\text{CMS,S}} = -1$). These indicate if limitations of Eq. (3.12) are reached and lay the foundation to formulate an adequate component answer.

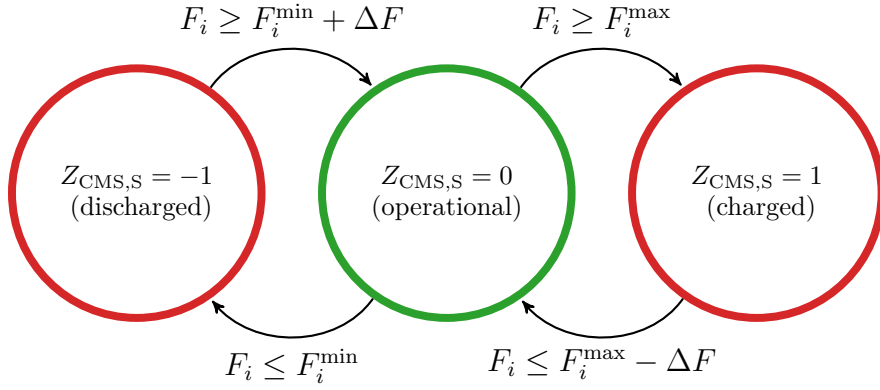


Fig. 3.9: State machine for the unified storage model

The storage’s characteristic state influences the power limitations in order to prevent overcharging or deep discharging. If the storage unit is completely operable ($Z_{\text{CMS,S}} = 0$), only the regular power limitations (cf. Eq. (3.13)) are applied:

$$P_i(Z_{\text{CMS,S}} = 0) = \begin{cases} P_{i, \text{set}} & \text{if } P_{i, \text{dis}}^{\text{max}} \leq P_{i, \text{set}} \leq P_{i, \text{cha}}^{\text{max}} \\ P_{i, \text{dis}}^{\text{max}} & \text{if } P_{i, \text{set}} < P_{i, \text{dis}}^{\text{max}} \\ P_{i, \text{cha}}^{\text{max}} & \text{if } P_{i, \text{set}} > P_{i, \text{cha}}^{\text{max}} . \end{cases} \quad (3.30a)$$

If the storage is fully charged ($Z_{\text{CMS,S}} = 1$), the maximum charge power is set to zero:

$$P_i(Z_{\text{CMS,S}} = 1) = \begin{cases} P_{i,\text{set}} & \text{if } P_{i,\text{dis}}^{\text{max}} \leq P_{i,\text{set}} \leq 0 \\ P_{i,\text{dis}}^{\text{max}} & \text{if } P_{i,\text{set}} < P_{i,\text{dis}}^{\text{max}} \\ 0 & \text{if } P_{i,\text{set}} > 0. \end{cases} \quad (3.30\text{b})$$

If the storage is fully discharged ($Z_{\text{CMS,S}} = -1$), the maximum discharge power is adjusted:

$$P_i(Z_{\text{CMS,S}} = -1) = \begin{cases} P_{i,\text{set}} & \text{if } 0 \leq P_{i,\text{set}} \leq P_{i,\text{cha}}^{\text{max}} \\ 0 & \text{if } P_{i,\text{set}} < 0 \\ P_{i,\text{cha}}^{\text{max}} & \text{if } P_{i,\text{set}} > P_{i,\text{cha}}^{\text{max}}. \end{cases} \quad (3.30\text{c})$$

3.5 Computational Framework

The computational process workflow established for the system design optimization tasks is displayed in Fig. 3.10. Here, the cooperation of optimization algorithm and model simulation is presented with specified intermediary steps and utilized open-access tools.

Simulation framework – Models and control strategies introduced in Sections 3.2 and 3.4 are created in the object-orientated programming language *Modelica* with help of the *OpenModelica* editor *OMEdit* [110]. The differential-algebraic equation systems are solved with either the *dassl* algorithm [111] or the *IDA* package [112], whereat both algorithms entail different computational advantages for specific mathematical problems. The algorithms contain a modified Newton method to solve implicit nonlinear equation systems, a flexible step width adjustment for integration, and an event-finding/step-back feature, which prohibits time-dependent inaccuracies beyond the requested tolerance.

Optimization framework – As was discussed in Section 3.3, a heuristic method is applied to solve the prepared optimization tasks. Thereby, optimizations are executed with help of the scientific *Python* library *pygmo* [113]. Instead of an ordinary differential-evolutionary optimization approach, the *Extended Ant Colony Optimization (gaco)* with readily prepared inclusion of integer degrees of freedom, the specification of constraints implemented with an oracle penalty method [114], as well as a utilizable computing parallelization is the heuristic of choice. For communication between the optimization algorithm and the simulation framework the *OMPpython* interface is used [110].

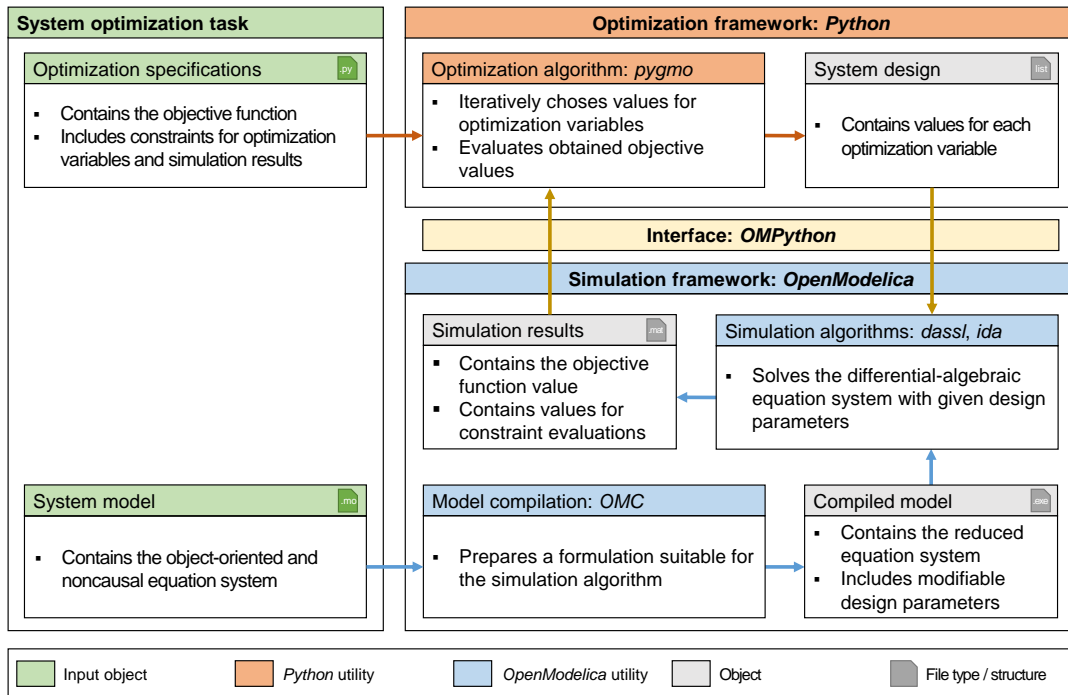


Fig. 3.10: Computational process workflow including input requirements, simulation framework, and optimization framework

4 Exemplary Design Optimization of an SOFC-based Hybrid Power System

In this chapter the first exemplary results of the model-based system design optimization approach are examined with the procedure introduced in Section 3.3. After the presentation of two distinctive case study load profiles in Section 4.1, a hybrid power system is designed cost-optimally for the first time in Section 4.2. Subsequent to the first analysis, technology-specific model descriptions are consulted in Section 4.3 to assess the reliability of a unified storage model. On this basis, in Section 4.4 new optimization results are discussed with a focus on the direct comparison with previously obtained configurations. The influence of including fuel expenses in the optimization's objective on the cost-optimal component configuration is investigated in Sections 4.5 and 4.6. Once more, immediate deviations are analyzed to evaluate if the addition of operating costs alter the results in a meaningful way. Finally, research issues [1] and [2] are addressed in Section 4.7.

Disclosure: The following chapter is in part based on the publication: L. Kistner; A. Bensmann; R. Hanke-Rauschenbach, Optimal Design of Power Gradient Limited Solid Oxide Fuel Cell Systems with Hybrid Storage Support for Ship Applications, Energy Conversion and Management (2021) [30]. For a detailed description of the author contributions see Appendix C.

4.1 Case Studies

For the system optimization, two load profiles with different characteristics are chosen: Case study I represents a motor yacht with a profile given in Fig. 4.1(a). Data for case study II were measured on a general cargo ship and is displayed in Fig. 4.1 (b). While both ships can be classified into the same category power-wise, the load profile for Case study I has a bulbous characteristic, whereas the profile for Case study II consists of a constant base with load spikes created by the breakaway starting current of the bow thruster induction motors. For the investigation, a power-intensive time frame is extracted from one month of records. Both profiles are assumed to represent characteristic operating behavior for the vessels.

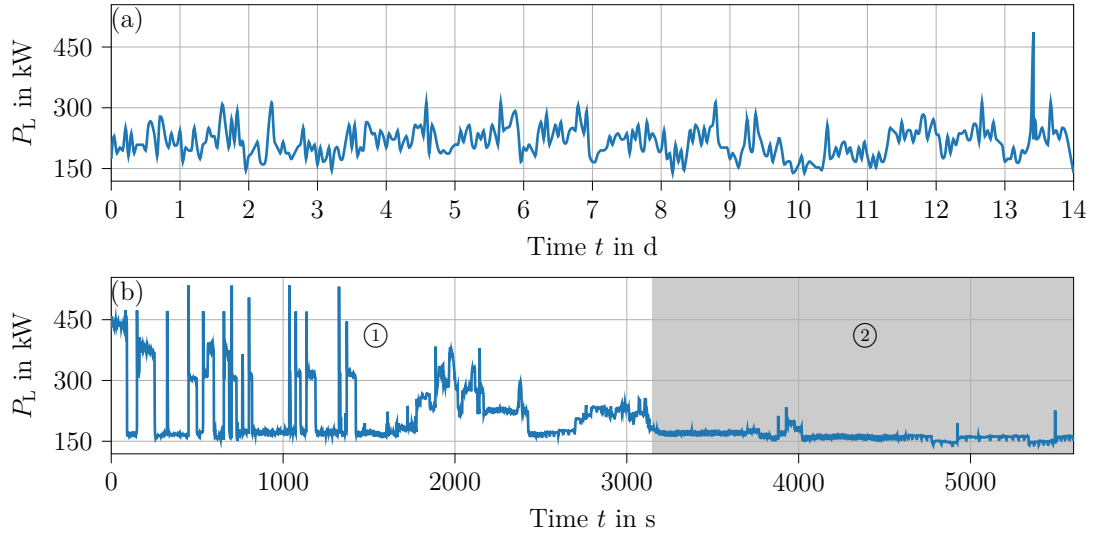


Fig. 4.1: Load profiles for (a) case study I; (b) case study II: ① bow thruster operation, ② open-sea operation.

4.2 Results and Discussion

The procedure to calculate a cost-optimized storage unit for a given fuel cell system power as previously described in Chapter 3 is now used for the two case studies. The first optimization is executed with a battery unit. Then, a potential hybridization with a supercapacitor unit is discussed. In this first part of the system design analysis, the straightforward storage model covered in Chapter 3 is used for both the battery and the supercapacitor.

4.2.1 Case I: Motor Yacht

The results of case study I are summarized in Fig. 4.2, which displays relevant technical and economic values as a function of the installed fuel cell rated power. In Fig. 4.2 (a) the total system power for the cost-optimized configurations including fuel cell module and battery unit is given. Thereby, the maximum discharge power is chosen to represent the battery. The figure indicates that a larger fuel cell system causes a first step then saturating reduction of the total installed power and therefore a reduction of the battery size.

Fig. 4.2 (b) displays the cost-optimal battery capacity and its maximally required charge and discharge power. As was already observable in the total power graph, increasing the fuel cell power results in a saturating reduction of storage capacity. Simultaneously, the power output requirements for the storage decline linearly due to the decreased difference between load peaks and stationary fuel cell power.

Meanwhile, the maximally required charge power increases slightly for larger fuel cell modules.

To better comprehend the opportunity for a continuous system power decrease, the specific battery power demand is depicted in Fig. 4.2 (c). While both values increase mostly due to the total capacity reduction, the demand can be fulfilled without particular difficulties. Therefore, the storage's energy capacity is identified to be the critical design bottleneck. With this information and the additional fact that the estimated battery lifetime continuously equals the assumed calendar limit of 10 years, the storage hybridization with a supercapacitor can be dismissed. This assumption is also verified with an extra hybrid storage optimization.

Finally, the component annuity payments and the total annual system costs are given in Fig. 4.2 (d). Despite the high fuel cell investment costs, a price optimum is not located at the minimally required fuel cell power. Instead, the cost analysis indicates an annual battery cost reduction by more than 80% to 21.000 €/a with a 10% fuel cell rated power increase. The cost-optimal configuration is a system with a rated fuel cell power of 249 kW and a rated battery capacity of 146 kWh.

4.2.2 Case II: General Cargo Ship

Analogous to Case study I, total system power, optimal battery capacity, specific power demand, and annual cost values are displayed in Fig. 4.3. In contrast to the previously investigated design case, Fig. 4.3 (a) indicates that the addition of fuel cell power does not influence the total system power for cost-optimal designs, but reduces the battery size proportionally. Concluding, an inversely proportional dependency between fuel cell power and battery capacity is observed (cf. Fig. 4.3 (b)).

Fig. 4.3 (c) provides the explanation for a linear capacity decrease: unlike in case I, the discharge demand equals the battery's maximum output. Thus, the battery capacity design is continuously limited by the specific output power, induced by the load spikes of the bow thruster maneuver. Battery capacity on the other hand is not a limiting factor for this system design task.

For the lifetime prediction, one month of load data was consulted. Thruster maneuvers occur roughly once a day and open-sea operation with less stress for the battery can be considered for the rest of the time, again leading to the assumption of ten years lifetime. Due to the high specific discharge power of the LFP technology, a vastly decreased energy storage dimension compared to case I is sufficient to achieve the power system operability. Since the battery size reduction potential is smaller than in Case study I, the cost minimum equals the smallest SOFC module (195 kW) with a battery capacity of 51.25 kWh (cf. Fig. 4.3 (d)).

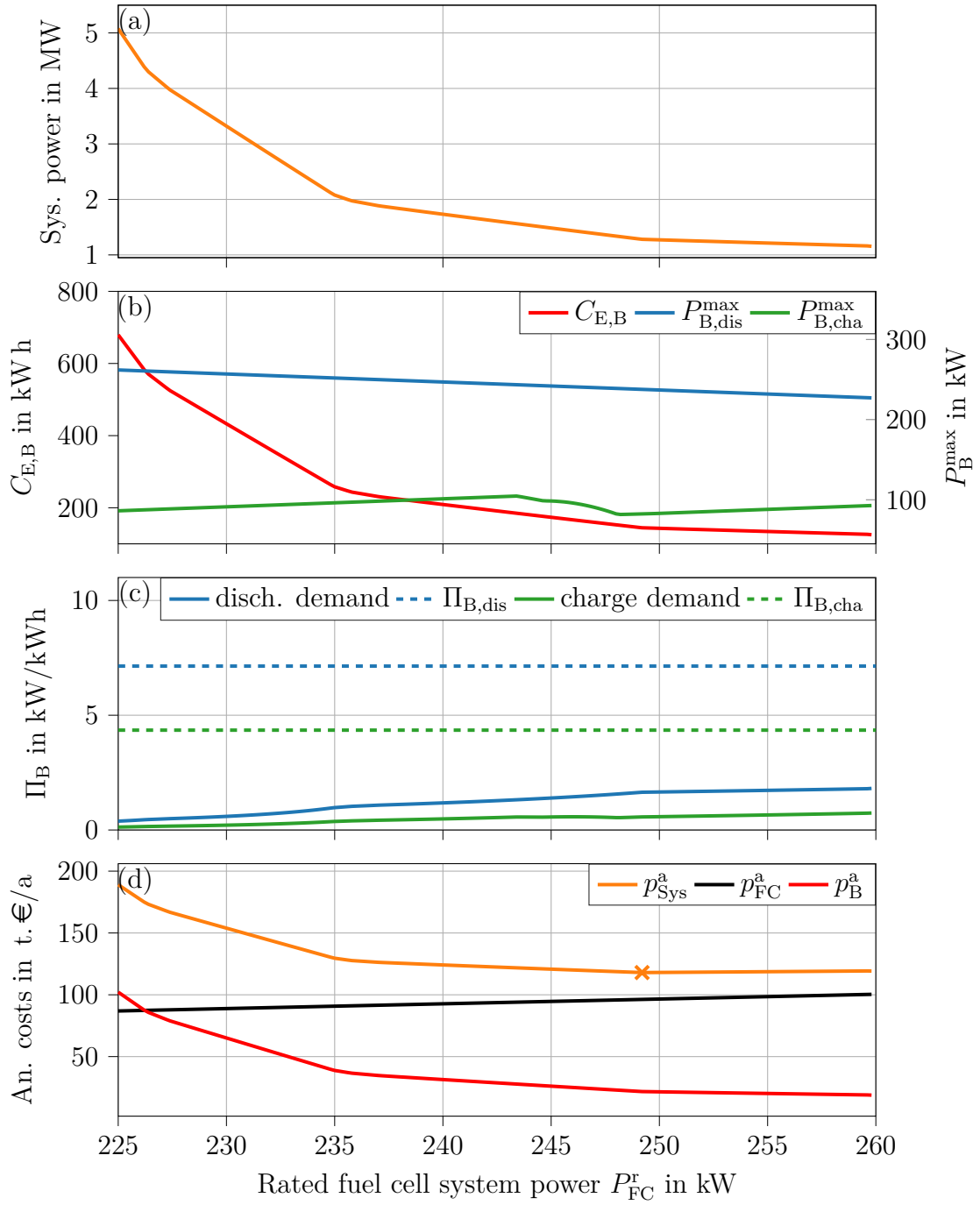


Fig. 4.2: Case study I: (a) total installed power, (b) rated battery capacity $C_{E,B}$, (c) specific power Π_B , and (d) annual system costs visualize the optimization results, \times marks the annual system cost minimum

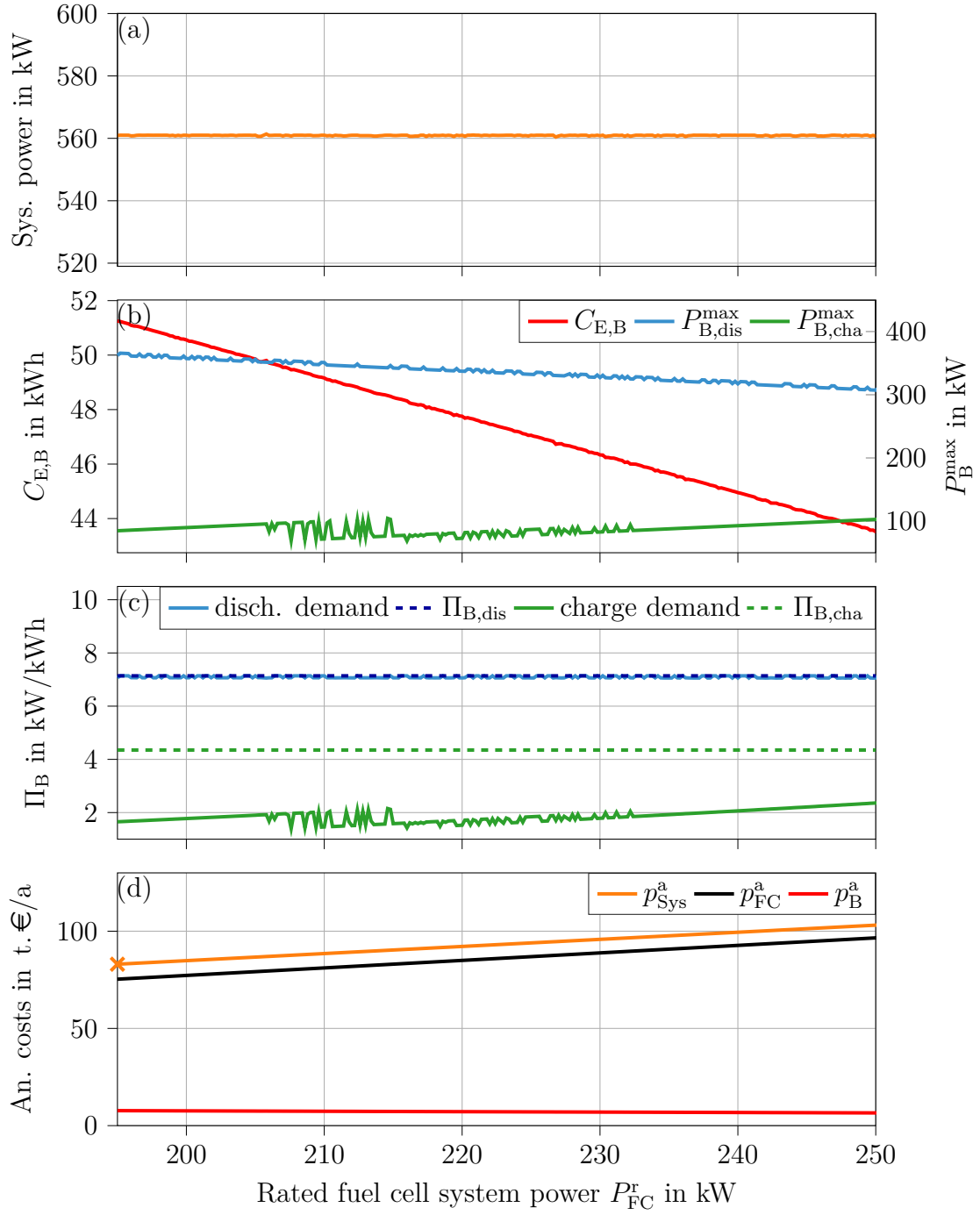


Fig. 4.3: Case study II: (a) total installed system power, (b) rated battery capacity $C_{E,B}$, (c) specific power Π_B , and (d) annual system costs visualize the optimization results, \times marks the annual system cost minimum

Since the battery's maximum power turns out to be the optimization bottleneck, a storage hybridization becomes appropriate and is examined in the following. For the hybrid storage power control, a supercapacitor's desired standby SoE of $F_{SC,des} = 1$ is chosen to provide energy for the thruster operation. The optimization results are depicted in Fig. 4.4 as a function of installed battery capacity and for different fuel cell rated powers.

In Fig. 4.4 (a) the total installed power of the cost optimized systems is given. Here, a minimum power plateau equals the constant value of the system with exclusive battery support. For small and large battery sizes, the total power increases to higher values. The plateau's location depends on the applied fuel cell system power. Both increases can be explained with the storage compositions, which vary in total power or energy capacity and are further discussed with help of the other graphs.

Fig. 4.4 (b) displays the supercapacitor's energy capacity. Analogous to the last two optimizations, higher fuel cell powers require less storage support. Independent of the power source dimensions, all graphs show two different gradients:

1. The steeper gradient on the left represents an exchange of capacity, where both technologies are valued equally and energy is the storage design's bottleneck.
2. The flat gradient represents an exchange of the storage powers, where roughly 80 battery cells replace one supercapacitor.

Consequently, the technical sizing optimum is located in the graph's kink, where neither capacity nor power are oversized. For very large batteries, no further supercapacitor support is required. Here, both capacity and rated power are not fully utilized.

An analysis of the annual system costs with help of Fig. 4.4 (c) shows that regardless of the chosen fuel cell power, a hybridization always is profitable. Most benefited are high SOFC power configurations, which demand less energy and more specific power support. However, the cost minima appear not to be resembled by the technical optimum, but are always located right of the graph's kink. Precisely, it is dependent on reaching the battery's maximal life expectancy, which again is the calendar limit (cf. Fig. 4.4 (d)). For smaller battery units an end of life resulting from reaching the number of maximum full cycles is estimated for the first time due to the higher specific load in a hybrid configuration. By contrast, the supercapacitor obtains the calendar maximum life of 16 years for every design in the considered range. Like in the single storage optimization, the cost optimum is found for the smallest applicable fuel cell rated power of 195 kW, a battery capacity of 47.5 kWh and a supercapacitor module of 45 Wh.

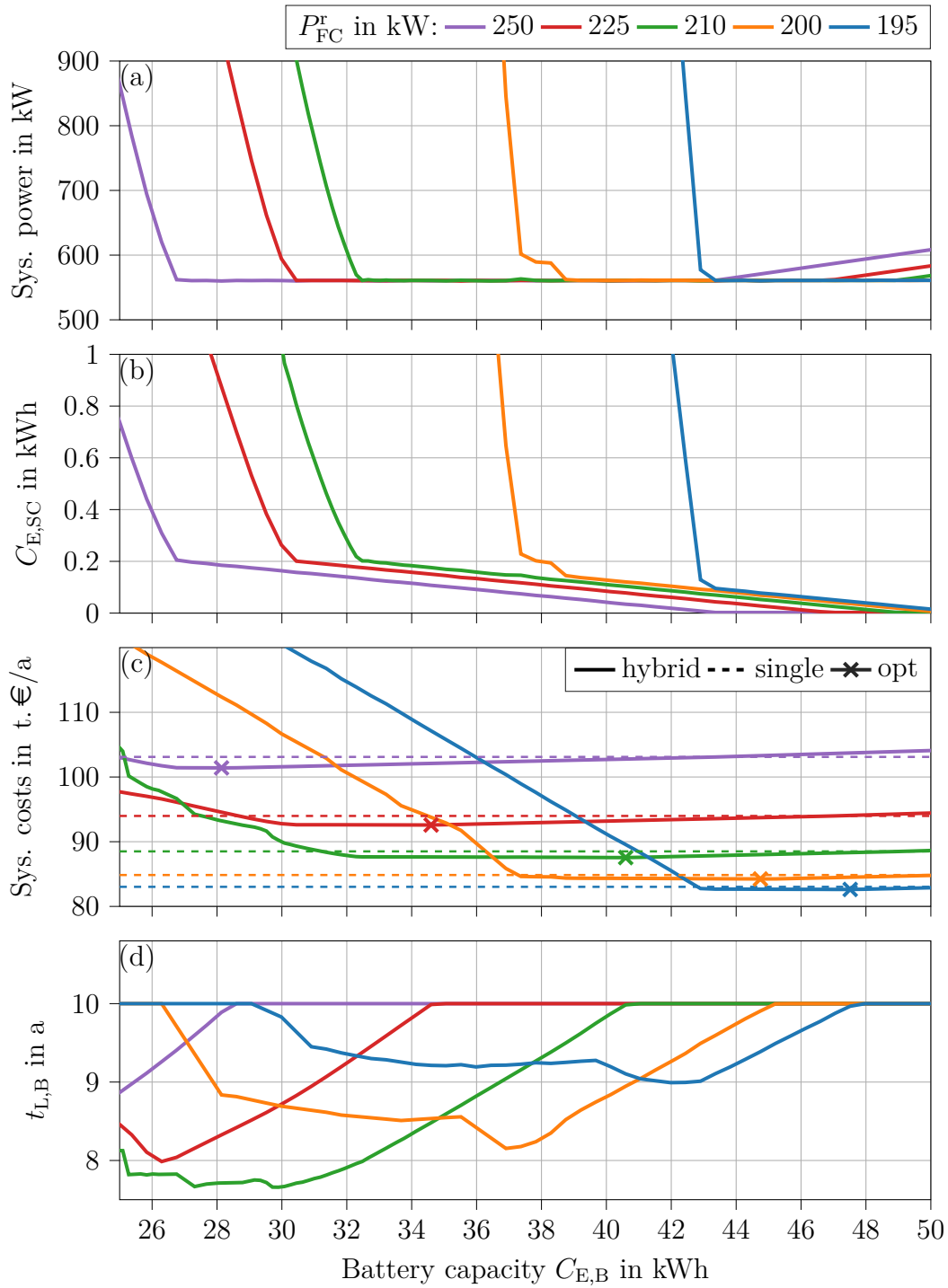


Fig. 4.4: Case study II: (a) cost-optimal installed system power, (b) storage configuration, (c) annual system costs, (d) battery lifetime, discontinuities can be traced back to different times of EMS state change for fuel cell modulation

4.3 Increasing the Storage Models' Levels of Detail

In a second analysis step, an investigation regarding the storage models' levels of detail is prepared to build a basis for a design optimization revision in Section 4.4. While the straightforward unified storage model is identical for battery and supercapacitor in terms of the equation system, two different model descriptions are chosen to consider the components' coulombic levels with voltage and current values. Component limitations are, in turn, revised. Further, for an intuitive direct comparison of the unified and the more detailed model behaviors, a method to assess energy-power relations is introduced. Here, the available energy is given as the function of a constant discharge power, considering internal losses and operating limitations. Alongside the changes in the physical models and the component management, the lifetime calculation is modified, too. SOFC component models and energy management system do not change for this analysis.

4.3.1 Li-ion Battery Model

Physical model – For the lithium-ion battery model, the state of charge (SoC) $F_{Q,B}$ replaces the previously used SoE. The state's time evolution equation is deployed with the battery's electric charge capacity $C_{Q,B}^{\text{cell}}$:

$$C_{Q,B}^{\text{cell}} \cdot \frac{dF_{Q,B}}{dt} = I_B^{\text{cell}}, \quad (4.1)$$

where I_B^{cell} is the single-cell current. Further, current-voltage dependencies are based on the Shepherd model [115] and extended by exponential functions to feature LFP characteristics. The model considers charge and discharge behavior, reflected in the voltage function

$$U_B^{\text{cell}} = 0.5 \cdot \left(U_{B,\text{cha}}^{\text{cell}} \cdot \left[1 + \tanh(I_B^{\text{cell}}) \right] + U_{B,\text{dis}}^{\text{cell}} \cdot \left[1 + \tanh(-I_B^{\text{cell}}) \right] \right). \quad (4.2)$$

Cell voltages are separated in open-circuit voltage and inner resistance voltage drop, as is presented in the equivalent circuit diagram in Fig. 4.5:

$$U_{B,\text{cha}}^{\text{cell}} = U_{B,0,\text{cha}}^{\text{cell}} + I_B^{\text{cell}} \cdot R_{B,i,\text{cha}}^{\text{cell}} \quad (4.3)$$

$$U_{B,\text{dis}}^{\text{cell}} = U_{B,0,\text{dis}}^{\text{cell}} + I_B^{\text{cell}} \cdot R_{B,i,\text{dis}}^{\text{cell}}, \quad (4.4)$$

where both the open-circuit voltages

$$U_{B,0,\text{cha}}^{\text{cell}} = p_{c,1} + p_{c,2} \cdot F_{Q,B} + p_{c,3} \cdot \exp\left[-p_{c,4} \cdot (1 - F_{Q,B})\right] - p_{c,5} \cdot \exp\left[p_{c,6} \cdot (-F_{Q,B})\right] \quad (4.5)$$

$$U_{B,0,\text{dis}}^{\text{cell}} = p_{d,1} + p_{d,2} \cdot F_{Q,B} + p_{d,3} \cdot \exp\left[-p_{d,4} \cdot (1 - F_{Q,B})\right] - p_{d,5} \cdot \exp\left[p_{d,6} \cdot (-F_{Q,B})\right] \quad (4.6)$$

and the inner resistances for charging and discharging operation

$$R_{B,i,\text{cha}}^{\text{cell}} = \frac{p_{c,7}}{C_{Q,B}^{\text{cell}}} \cdot \left(1 + p_{c,8} \cdot \frac{F_{Q,B}}{p_{c,9} - F_{Q,B}}\right) \quad (4.7)$$

$$R_{B,i,\text{dis}}^{\text{cell}} = \frac{p_{d,7}}{C_{Q,B}^{\text{cell}}} \cdot \left(1 + p_{d,8} \cdot \frac{1 - F_{Q,B}}{p_{d,9} + 1 - F_{Q,B}}\right) \quad (4.8)$$

are SoC-dependent. Thereby, both \vec{p}_c and \vec{p}_d are cell-chemistry, product-specific parameter vectors.

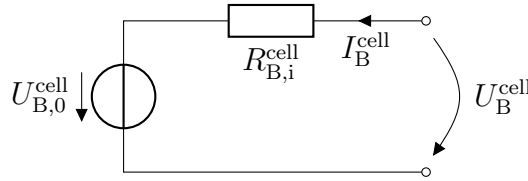


Fig. 4.5: Equivalent circuit diagram of a Li-ion battery

The battery's output power is calculated with

$$P_B = N_B \cdot U_B^{\text{cell}} \cdot I_B^{\text{cell}}. \quad (4.9)$$

Also, to keep all equations of the EMS unmodified, an approximation of the energetic capacity and the SoE is performed:

$$C_{E,B}^{\text{cell}} \approx C_{Q,B}^{\text{cell}} \cdot U_B^{\text{cell,r}}, \quad (4.10)$$

$$F_B \approx F_{Q,B}, \quad (4.11)$$

where $U_B^{\text{cell,r}}$ is the rated cell voltage.

Control strategy – Since the formulated EMS only provides a desired set power value, the derived desired current is given with

$$I_{B,\text{set}} = \frac{P_{B,\text{set}}}{U_B}. \quad (4.12)$$

Generally, the battery management system now maintains current and voltage limits instead of maximum power and state of energy:

$$N_B \cdot I_{B,\text{dis}}^{\text{cell,max}} \leq I_B \leq N_B \cdot I_{B,\text{cha}}^{\text{cell,max}}, \quad (4.13)$$

$$N_B \cdot U_B^{\text{cell,min}} \leq U_B \leq N_B \cdot U_B^{\text{cell,max}}. \quad (4.14)$$

However, after reaching one voltage limit, it is possible to further charge and discharge the cells without exceeding the component limitations by decreasing the applicable current in the so called constant voltage phase:

$$I_{B,\text{CV,cha}}^{\text{cell}} = I_{B,\text{cha}}^{\text{cell,max}}(F_{Q,B}), \quad (4.15)$$

$$I_{B,\text{CV,dis}}^{\text{cell}} = I_{B,\text{dis}}^{\text{cell,max}}(F_{Q,B}). \quad (4.16)$$

In the implemented heuristic control approach, the battery can be operated in five states $Z_{\text{CMS,B}}$, where the two additional states represent the constant voltage phases (cf. Fig. 4.6).

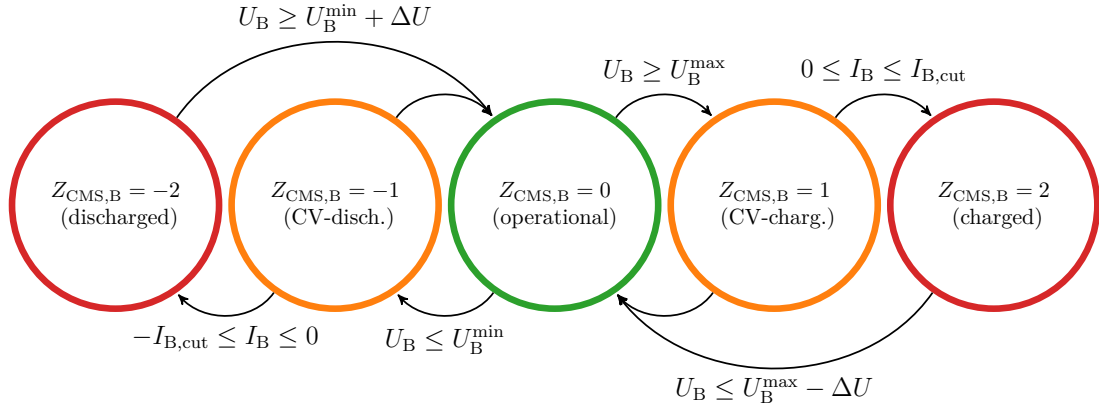


Fig. 4.6: State machine for Li-ion's voltage limitation control and CV phase initiation

The states influence the operability of the battery unit as follows: while $Z_B = -2$, all discharge requests are dismissed, since the unit is fully discharged. On the other hand, charging the battery is only limited by the maximum charge current:

$$I_B(Z_B = -2) = \begin{cases} I_{B,\text{cha}}^{\text{max}} & \text{if } I_{B,\text{set}} > I_{B,\text{cha}}^{\text{max}} \\ I_{B,\text{set}} & \text{if } 0 \leq I_{B,\text{set}} \leq I_{B,\text{cha}}^{\text{max}} \\ 0 & \text{if } I_{B,\text{set}} < 0. \end{cases} \quad (4.17a)$$

For state $Z_B = -1$ (discharge CV phase), a potential discharge current is a function of the battery's SoC to maintain the minimal voltage as long as the battery is not requested to charge:

$$I_B (Z_B = -1) = \begin{cases} I_{B,cha}^{\max} & \text{if } I_{B,set} > I_{B,cha}^{\max} \\ I_{B,set} & \text{if } 0 \leq I_{B,set} \leq I_{B,cha}^{\max} \\ f(F_{Q,B}) & \text{if } I_{B,set} < 0. \end{cases} \quad (4.17b)$$

Batteries in state $Z_B = 0$ are not constrained apart from maximal currents:

$$I_B (Z_B = 0) = \begin{cases} I_{B,cha}^{\max} & \text{if } I_{B,set} > I_{B,cha}^{\max} \\ I_{B,set} & \text{if } I_{B,dis}^{\max} \leq I_{B,set} \leq I_{B,cha}^{\max} \\ I_{B,dis}^{\max} & \text{if } I_{B,set} < I_{B,dis}^{\max}. \end{cases} \quad (4.17c)$$

State $Z_B = 1$ limits regarding charge requests analogous to state $Z_B = -1$:

$$I_B (Z_B = 1) = \begin{cases} f(F_{Q,B}) & \text{if } I_{B,set} > 0 \\ I_{B,set} & \text{if } I_{B,dis}^{\max} \leq I_{B,set} \leq 0 \\ I_{B,dis}^{\max} & \text{if } I_{B,set} < I_{B,dis}^{\max}. \end{cases} \quad (4.17d)$$

Finally, state $Z_B = 2$ indicates a fully charged unit and reflects limitations of state $Z_B = -2$:

$$I_B (Z_B = 2) = \begin{cases} 0 & \text{if } I_{B,set} > 0 \\ I_{B,set} & \text{if } I_{B,dis}^{\max} \leq I_{B,set} \leq 0 \\ I_{B,dis}^{\max} & \text{if } I_{B,set} < I_{B,dis}^{\max}. \end{cases} \quad (4.17e)$$

Energy-power relation – For the first comparison of the two different battery model approaches, an energy-power relation diagram is introduced in Fig. 4.7. Here, the available energy of a fully charged storage is plotted for a series of constant power outputs, displaying both physical behavior of the models and implementation of the operating limitations.

In the unified storage model, maximum discharge power and a specified available storage capacity are considered. Since discharge losses are not related to the cell's operating point, the resulting available energy is resembled by a constant value, which is cut off at the maximally operable cell power. Only for very small powers, the battery's self discharge effect becomes visible.

By contrast, the consideration of voltage and current limitations in the detailed model results in a slightly altered relation diagram. Here, a higher energy content is available for smaller powers due to the consideration of current-dependent discharge losses. Until the breakover point at around 0.6 kW, voltage limitations terminate the constant-power discharge operation. High power demands on the

other hand are cut off by the current limitations, which promptly become effective due to a rapidly decreasing battery voltage level. Still, the results overall resemble one another with the small exception of high-power operation, emphasizing an adequate component description with the unified model approach.

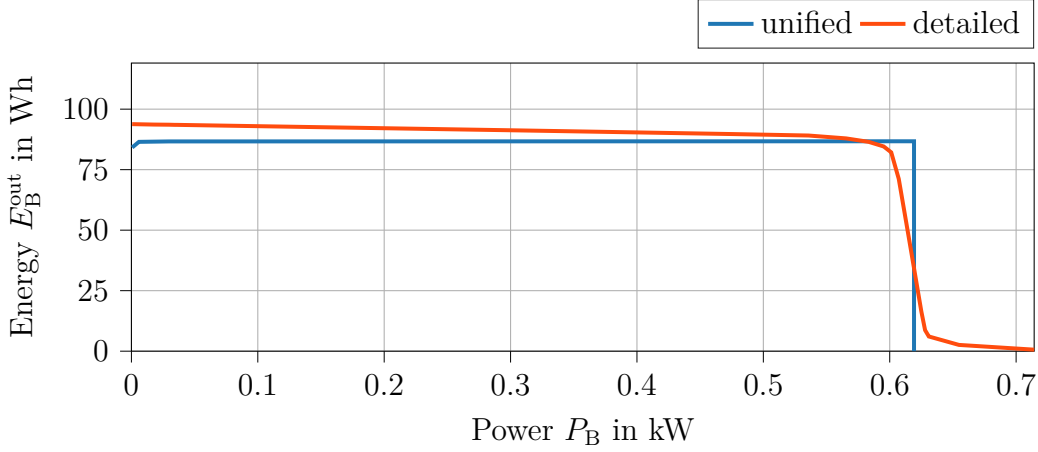


Fig. 4.7: Energy-power relations of one single battery cell, evaluated with the unified model and the technology-specific component description

Economic model – For the detailed battery model, capacity degradation now is described with a dynamic fade rate $J_{E,B,\text{deg}}$ that symbolizes the operation-dependent capacity loss per time unit. The battery system lifetime is reached when the energy capacity from the beginning of life $C_{E,B}^{\text{BOL}}$ is decreased by 20%. Extrapolating from the simulation period, this leads to a lifetime estimation in the following form:

$$t_{L,B} = \frac{0.2 \cdot C_{E,B}^{\text{BOL}}}{\frac{1}{t_{\text{end}} - t_0} \int_{t_0}^{t_{\text{end}}} J_{E,B,\text{deg}} d\tau}, \quad (4.18)$$

For the fade rate approximation, an approach from [116] is chosen, which displays LFP battery energy capacity degradation as a function of cell current and voltage. Unfortunately, in the original scientific article a degradation of an 1.1 Ah cell was examined. However, the results were remapped into the capacity-specific power-energy-dimension in [117] and therefore be applied for the 30 Ah cell that is used for the present investigations. Degradation is computed with

$$J_{E,B,\text{deg}} = C_{E,B}^{\text{BOL}} \cdot \max \left(\vec{a}_1 \frac{P_B}{C_{E,B}^{\text{BOL}}} + \vec{a}_2 F_B + \vec{a}_3 \right), \quad (4.19)$$

where $\vec{a}_1, \vec{a}_2, \vec{a}_3$ are parameter vectors listed in [117].

Model parameters – Model simulation is executed with operating limitations and generated fit parameters of an LFP battery cell given in Tab. 4.1. To compute the physical cell behavior, a parameter fit resulting from constant current charge and discharge measurements of a 15.5 kW SAFT battery cabinet is used. All underlying constant-current voltage-SoC curves are depicted in Fig. 4.8.

Tab. 4.1: Battery cell operation parameters for the analyzed LFP battery

Parameter	Value	Fit Parameters
Cell charge capacity	$C_{Q,B}^{\text{cell}}$ 30 Ah	$p_{c,1}$ 3.234 V $p_{d,1}$ 3.247 V
Maximum cell charge current	$I_{B,\text{cha}}^{\text{cell,max}}$ 120 A	$p_{c,2}$ 0.12 V $p_{d,2}$ 0.165 V
Maximum cell discharge current	$I_{B,\text{dis}}^{\text{cell,max}}$ -200 A	$p_{c,3}$ 0.599 V $p_{d,3}$ 0.581 V
Cut-off cell current	$I_{B,\text{cut}}^{\text{cell}}$ 1 A	$p_{c,4}$ 18.577 $p_{d,4}$ 20.261
Maximum cell voltage	$U_B^{\text{cell,max}}$ 3.8 V	$p_{c,5}$ 0.917 V $p_{d,5}$ 1.245 V
Minimum cell voltage	$U_B^{\text{cell,min}}$ 2.7 V	$p_{c,6}$ 44.094 $p_{d,6}$ 43.128
Rated cell voltage	$U_B^{\text{cell,r}}$ 3.3 V	$p_{c,7}$ 0.0516 Vh $p_{d,7}$ 0.0416 Vh
		$p_{c,8}$ -72.884 $p_{d,8}$ -0.50
		$p_{c,9}$ 233.179 $p_{d,9}$ 15.927

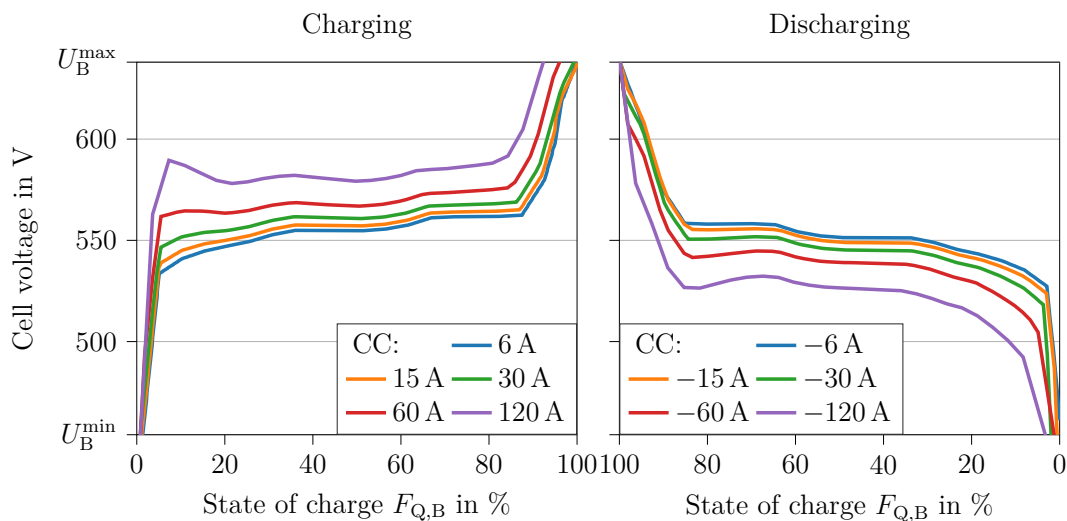


Fig. 4.8: SAFT Lithium-Ion Battery System BTR-0554V-VL30-SFP-012M (554 V / 15.5 kWh)

4.3.2 Supercapacitor Model

Physical model – The description of the supercapacitor is given by the electrical equivalent circuit in Fig. 4.9 [118]. Thereby, dependencies of the Faraday capacitance on the current, as well as the inductive nature of the conductors are neglected.

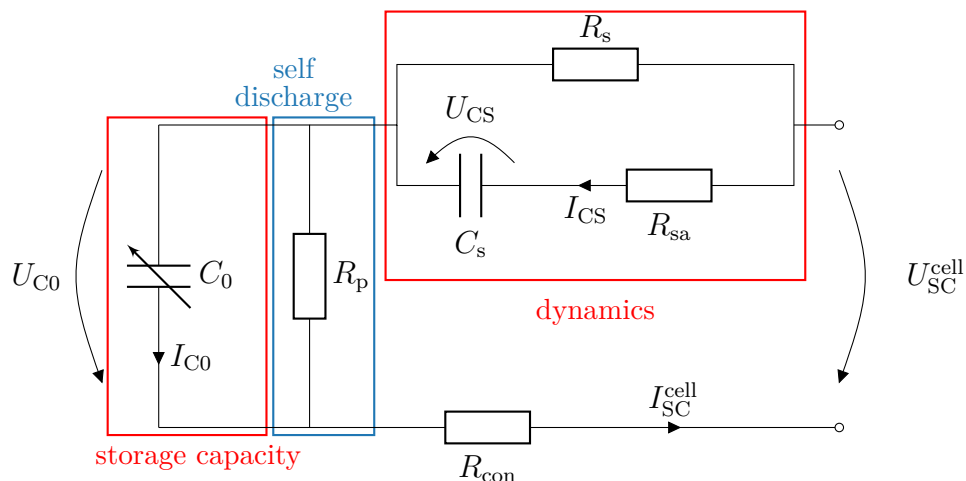


Fig. 4.9: Circuit diagram of a two-layer capacitor [118]

Two differential equations are used to describe the storage's dynamic behavior

$$I_{CS} = C_s \cdot \frac{dU_{CS}}{dt} \quad (4.20)$$

and its SoC/SoE equivalent open circuit voltage change

$$I_{C0} = C_0 \cdot \frac{dU_{C0}}{dt} , \quad (4.21)$$

where the typical non-linear capacitance for the chosen technology can be approximated with the hyperbolic function

$$C_0 = 2770 \text{ F} + 520 \text{ F} \cdot \tanh \left(\frac{U_{C0}}{0,9 \text{ V}} - 0.9 \right) . \quad (4.22)$$

Additionally, three more equations can be obtained with Kirchhoff's Voltage Law:

$$U_{SC}^{\text{cell}} = R_{\text{con}} \cdot I_{SC}^{\text{cell}} + R_s \cdot (I_{SC}^{\text{cell}} - I_{CS}) + R_P \cdot (I_{SC}^{\text{cell}} - I_{C0}) , \quad (4.23)$$

$$U_{CS} = R_s \cdot (I_{SC}^{\text{cell}} - I_{CS}) - R_{SA} \cdot I_{CS} , \quad (4.24)$$

$$U_{C0} = R_P \cdot (I_{SC}^{cell} - I_{C0}) . \quad (4.25)$$

The component's power is calculated as the sum of all cells powers outputs

$$P_{SC} = N_{SC} \cdot U_{SC}^{cell} \cdot I_{SC}^{cell} . \quad (4.26)$$

The more complex computation of the energy capacity

$$C_{E,SC} = \int_{Q(U_{SC}^{cell,min})}^{Q(U_{SC}^{cell,max})} U(Q) dQ \quad (4.27)$$

is approximated with the simplification of a linear dependence of voltage and charge:

$$C_{E,SC} \approx 0.5 \cdot N_{SC} \cdot C_{Q,SC}^{cell} \cdot (U_{SC}^{cell,max} + U_{SC}^{cell,min}) , \quad (4.28)$$

where the charge capacity equals

$$C_{Q,SC}^{cell} = U_{SC}^{cell,max} \cdot C_0 (U_{SC}^{cell,max}) - U_{SC}^{cell,min} \cdot C_0 (U_{SC}^{cell,min}) . \quad (4.29)$$

The SoE then can be derived with

$$F_{SC} \approx \frac{0.5 \cdot N_{SC}}{C_{E,SC}} \cdot \left[U_{C0} \cdot C_0 - U_{SC}^{cell,min} \cdot C_0 (U_{SC}^{cell,min}) \right] \cdot \left[U_{C0} + U_{SC}^{cell,min} \right] . \quad (4.30)$$

Control strategy – In analogy to the battery management system, a desired current value

$$I_{SC,set} = \frac{P_{SC,set}}{U_{SC}} \quad (4.31)$$

is monitored to not exceed voltage and current limitations unsuitable for safe operation:

$$N_{SC} \cdot U_{SC}^{cell,min} \leq U_{SC} \leq N_{SC} \cdot U_{SC}^{cell,max} , \quad (4.32)$$

$$N_{SC} \cdot I_{SC,dis}^{cell,max} \leq I_{SC} \leq N_{SC} \cdot I_{SC,cha}^{cell,max} . \quad (4.33)$$

Since the supercapacitor operation does not meaningfully benefit from the previously introduced constant voltage phases, only three states are considered in this state-machine-based control strategy (cf. Fig. 4.10).

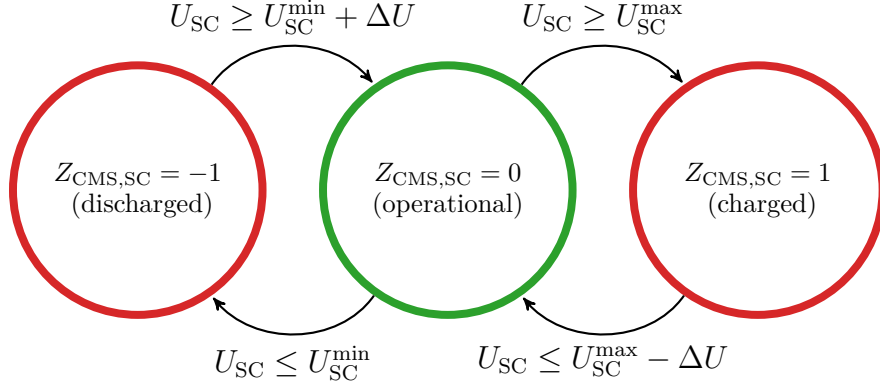


Fig. 4.10: State machine for the supercapacitor's voltage limitation control

The permitted current again follows the limitations depending on the units state:

$$I_{SC}(Z_{SC} = -1) = \begin{cases} I_{SC,cha}^{\max} & \text{if } I_{SC,set} > I_{SC,cha}^{\max} \\ I_{SC,set} & \text{if } 0 \leq I_{SC,set} \leq I_{SC,cha}^{\max} \\ 0 & \text{if } I_{SC,set} < 0, \end{cases} \quad (4.34a)$$

$$I_{SC}(Z_{SC} = 0) = \begin{cases} I_{SC,cha}^{\max} & \text{if } I_{SC,set} > I_{SC,cha}^{\max} \\ I_{SC,set} & \text{if } I_{SC,dis}^{\max} \leq I_{SC,set} \leq I_{SC,cha}^{\max} \\ I_{SC,dis}^{\max} & \text{if } I_{SC,set} < I_{SC,dis}^{\max}, \end{cases} \quad (4.34b)$$

$$I_{SC}(Z_{SC} = 1) = \begin{cases} 0 & \text{if } I_{SC,set} > 0 \\ I_{SC,set} & \text{if } I_{SC,dis}^{\max} \leq I_{SC,set} \leq 0 \\ I_{SC,dis}^{\max} & \text{if } I_{SC,set} < I_{SC,dis}^{\max}. \end{cases} \quad (4.34c)$$

Energy-power relation – In analogy to the first comparison of the two battery descriptions, both introduced supercapacitor model approaches are directly compared to each other by assessing the available energy of a fully charged cell for varied power outputs. Since the unified model does only consider a fixed discharge efficiency and a operation-unspecific maximum power, the expectable rectangle shape is displayed in Fig. 4.11.

In contrast to the detailed battery simulation results, the technology-specific supercapacitor model generates energy-power relations far off the results obtained from the unified model approach. Here, the hyperbolic behavior of the storage capacity is significantly influencing the outcome in addition to the operating-point-specific power loss description. Even if the resulting graph does not display an

abrupt breakover point as it is the case for the battery model, voltage limitations are stopping the constant-power discharge process below 0.1 kW, while current limitations are dominating the discharge termination for larger power demands. Conclusively, the combination of physical model and operating limitations used for the unified model approach does not resemble the supercapacitor behavior well due to several nonlinear characteristics. In addition, the parameters obtained from a manufacturer's data sheet likely overestimate the capabilities of one single cell, which could lead to non-functional design decisions.

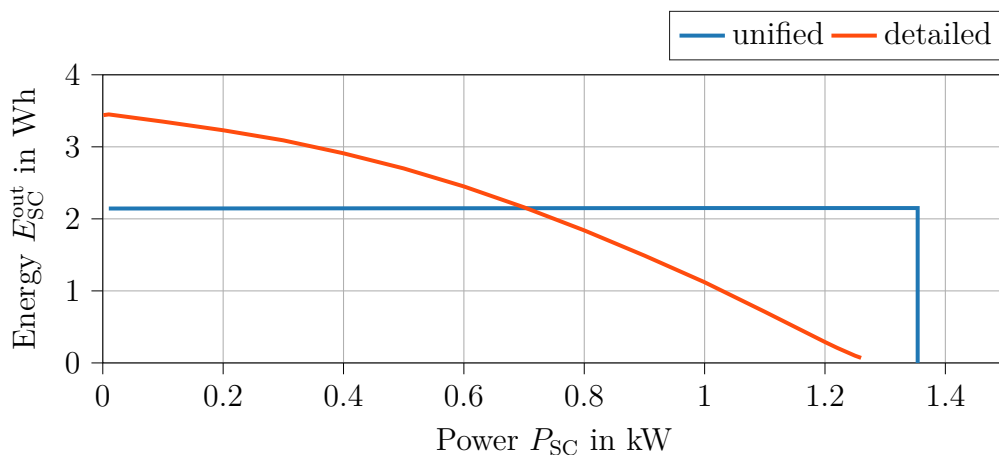


Fig. 4.11: Energy-power relations of one single supercapacitor cell, evaluated with the unified model and the technology-specific component description

Economic model – The newly chosen degradation model approach covers cells with the same brand and capacitance as selected for the physical modeling, so equations can be used without further modification [119]. The lifetime can be expressed in a form similar to Eqn. (4.18), where $J_{F,SC,deg}$ is the relative faded capacitance per time and τ_0 is the baseline life expectancy from [119]:

$$t_{L,SC} = \frac{\tau_0}{\frac{1}{t_{end} - t_0} \int_{t_0}^{t_{end}} J_{F,SC,deg} d\tau} . \quad (4.35)$$

Although this equation does not exactly flag the same end of life as announced for the battery (20% capacitance and 20% energy capacity slightly differ), the approximations from Eq. (4.28) and (4.29) allow an assumption of proportionality. The fade rate calculation expands the equivalent calendar degradation approach with a factor for current consideration, leading to the equation

$$J_{F,SC,deg} = \exp \left(\frac{U_{SC}^{cell}}{U_{SC,0}} + \frac{\theta}{\theta_0} + \frac{I_{SC,RMS}}{I_{RMS,0}} \right) , \quad (4.36)$$

where θ is the ambient temperature, $U_{SC,0}, \theta_0, I_{RMS,0}$ are parameters from [119], and

$$I_{SC,RMS} = \sqrt{\frac{1}{t_{end} - t_0} \int_{t_0}^{t_{end}} (I_{SC}^{cell})^2 d\tau} \quad (4.37)$$

is the root mean square (RMS) cell current.

Model parameters – All required operating parameters for a Maxwell supercapacitor with 3000 F rated capacity are given in Tab. 4.2.

Tab. 4.2: Simulation parameters for the 3000 F Maxwell supercapacitor [118], [119]

Parameter		Value
Maximum cell charge current	$I_{SC,cha}^{cell,max}$	500 A
Maximum cell discharge current	$I_{SC,dis}^{cell,max}$	-500 A
Maximum cell voltage	$U_{SC}^{cell,max}$	2.7 V
Minimum cell voltage	$U_{SC}^{cell,min}$	0.2 V
Series resistance	R_{sa}	0.6 m Ω
Connection resistance	R_{con}	70 $\mu\Omega$
Parallel resistance	R_s	0.3 m Ω
Capacitor for dynamics	C_S	504.444 F
Self discharge resistance	R_P	643.333 Ω
Ambient temperature	θ	25 $^{\circ}\text{C}$
Baseline life expectancy	τ_0	$1.4 \cdot 10^{13}$ s
Baseline voltage	$U_{SC,0}$	0.2/ $\ln(2)$ V
Baseline temperature	θ_0	10/ $\ln(2)$ $^{\circ}\text{C}$
Baseline RMS current	$I_{RMS,0}$	30/ $\ln(2)$ A

4.4 Case Study Revision: Detailed Storage Models

In the second part of the power system design analysis, the detailed storage models are used to display battery and supercapacitor, respectively. Thereby, potential deviation of storage performances and resulting system designs, as well as alterations of estimated annual costs due to diverging storage lifetimes are focus of the investigations.

4.4.1 Case I: Motor Yacht

The analysis is repeated with the revised battery storage model and the optimization results are shown in Fig. 4.12. It can be seen in Fig. 4.12 (a) that fewer cells are required for an operable energy system. As already indicated in the power-energy relation in Fig. 4.7, different calculations of the storage losses, the modified power limitations, and the possibility of CV operations play a role here. Still, the graphs are similar qualitatively and do not show a vast variance.

Even if fewer battery cells are required for the cost-optimal design, the annual system costs in Fig. 4.12 (b) display an increase of about 5% for the optimum, which now is found at a slightly bigger fuel cell system with 251 kW and a smaller battery unit with 1402 cells (a rated capacity of 129 kWh).

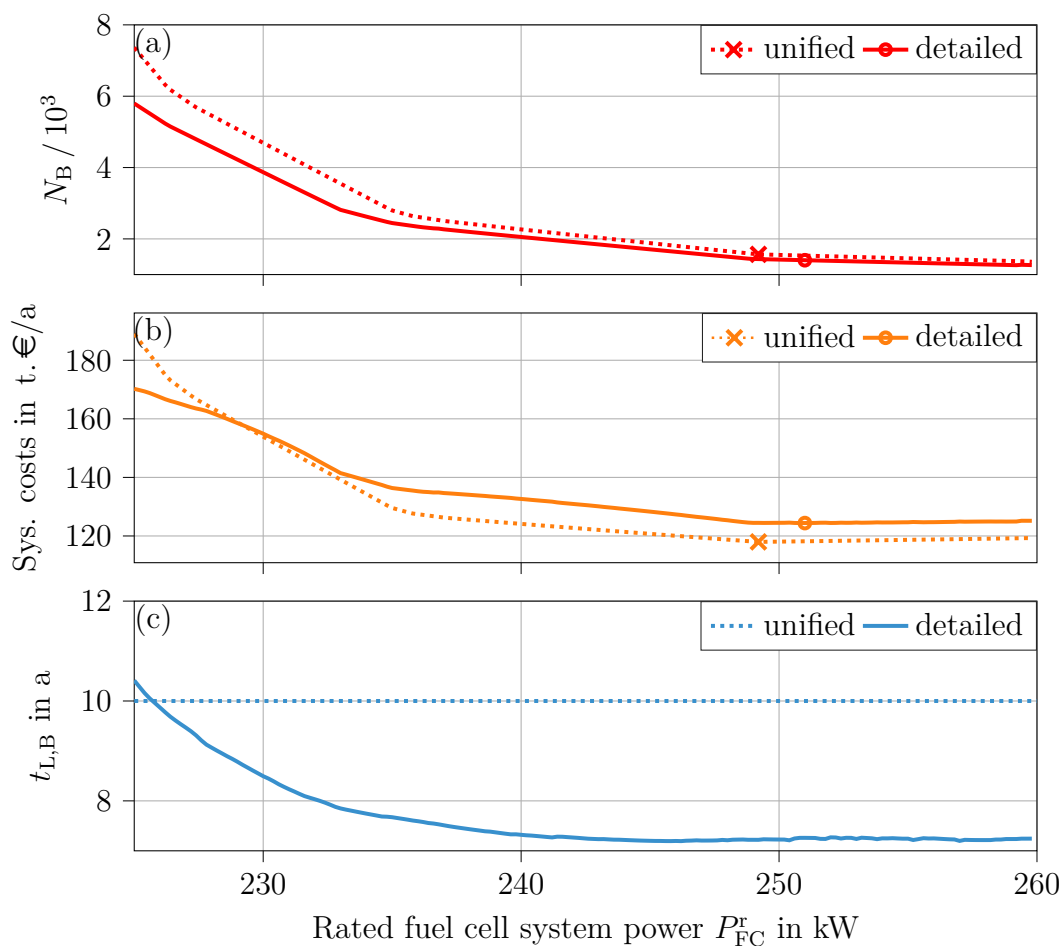


Fig. 4.12: Revision of case study I – detailed storage models: (a) number of battery cells N_B , (b) annual system costs, and (c) battery lifetime $t_{L,B}$, ● highlights the calculated cost optimum, × marks the reference cost minimum declared with the basic storage model

Apparent cost increases can be explained with the predicted battery lifetime, which falls to 7.2 years for smaller storage units (cf. Fig. 4.12 (c)). Here, smaller battery units equal a higher specific cell load and therefore lead to a more frequent cell replacement and higher annual costs.

Conclusively, the very close results for the optimal system parameters suggest that a design with help of the basic storage model is satisfactory, especially in the case of little technological battery data for parameterization. Only the basic degradation estimation proves to be oversimplified, since it mostly leads to reaching the calendar maximum value. Here, instead of using the full load cycle / calendar approximation, the more detailed fade rate integration can supplement the unified model, as it is remapped into the power and capacity level anyways.

4.4.2 Case II: General Cargo Ship

For the second load profile, a storage hybridization is already declared as advisable and a cost optimum is found for the lowest installed fuel cell power of 195 kW. In order to get a feeling about relative and absolute deviations, the hybridization is revised for the lower three fuel cell rated powers with both detailed storage models. The cost-optimal supercapacitor-battery pairings are depicted in Fig. 4.13 (a). They show a qualitatively similar behavior compared to the results created with the basic storage models. Quantitatively, the new graphs are shifted more to the right, which is caused by one relevant effect already demonstrated in Fig. 4.11: the unified storage model approach is not entirely able to present the nonlinear behavior of a supercapacitor. The different evaluation of the supercapacitor's maximum power and capacity generates a new exchange rate between the technologies, that also results in a flatter gradient left of the graphs' kinks. Storage compositions are also affected by the cost-and-degradation-orientated formulation of the optimization function. Minimizing the number of installed cells would lead to a different shape of the graphs, but is dismissed for the sake of higher storage lifetimes.

In addition to the alterations observed in the cell composition analysis, the system cost calculation results given in Fig. 4.13 (b) present an offset for the revised simulations. Like in case study I, this effect can be referred to the different degradation models. Now, technical and cost optimal designs diverge even further. The cost-optimal configuration is composed of a 195 kW SOFC, a 49.4 kWh battery and a 71 Wh supercapacitor.

Battery lifetime simulation results given in Fig. 4.13 (c) showcase an estimation difference of roughly three years between the chosen model approaches. Only the lifetime increase with the number of cells per unit can be assessed to be qualitatively similar. It reflects less stress for the individual cell during the open-see operation, that takes up 95% of the use time and mostly does not involve supercapacitor usage.

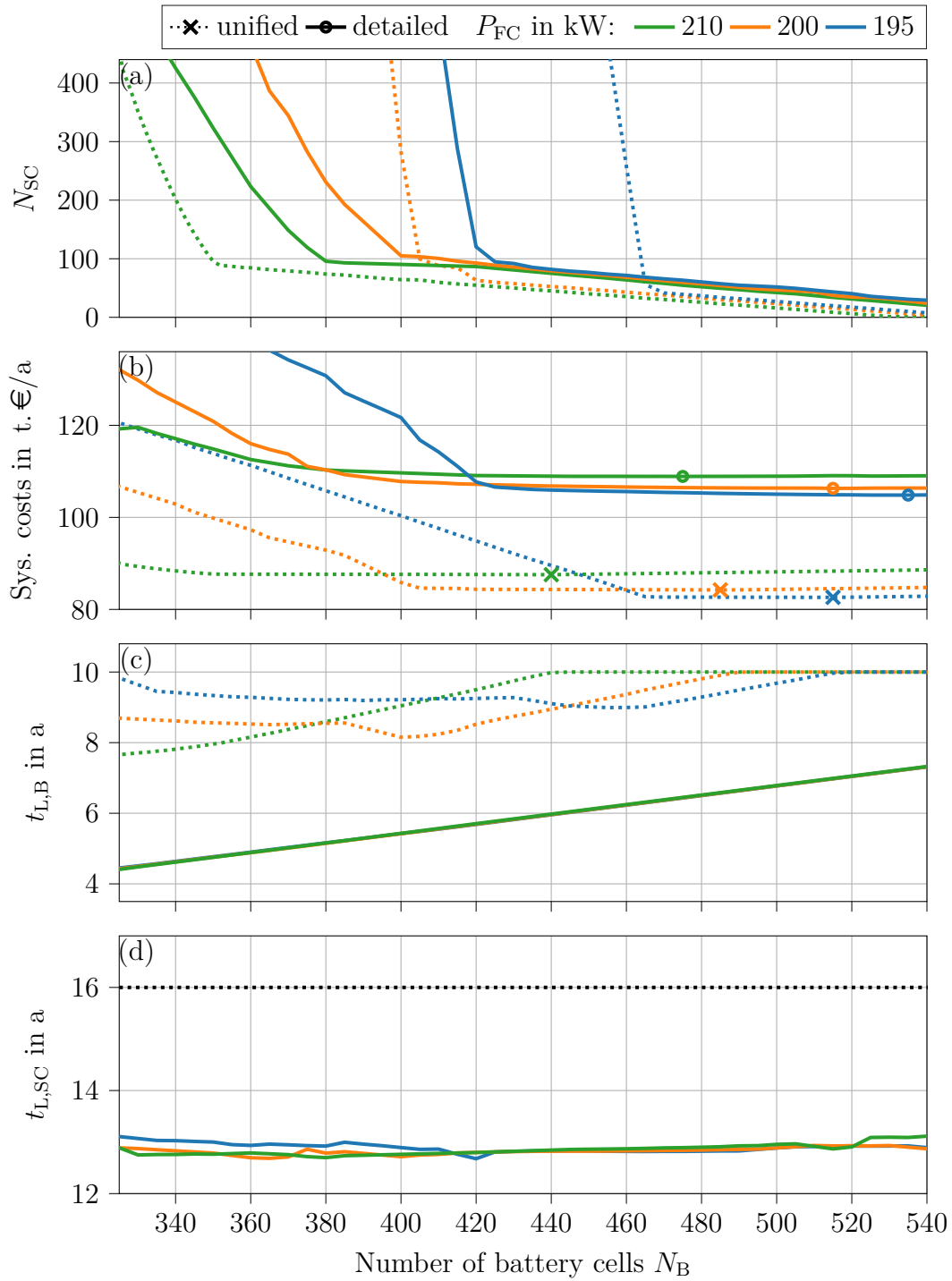


Fig. 4.13: Revision of case study II – detailed storage models: (a) number of supercapacitor cells N_{SC} , (b) annual system costs, (c) battery lifetime $t_{L,B}$, and (d) supercapacitor lifetime $t_{L,SC}$, • highlights the calculated cost optimum, × marks the reference cost minimum declared with the unified storage model

Fig. 4.13 (d) also shows a three years smaller life estimation for the supercapacitors, which is generally not affected by the storage composition. Overall, these factors again lead to a cost optimum located right from the technical optimum (kink) to increase the lifetime of the lithium-ion battery without risking higher supercapacitor degradation.

4.5 Extending the Objective Function by Fuel Expenses

In the previous analyses, solely component investment and maintenance costs are considered for the system design optimization. However, the operating behavior of the investigated power system certainly influences the fuel consumption, leading to considerable annual expenses. As already addressed in Chapter 3, fuel cell systems entail a higher energy efficiency when operated in part-load conditions and therefore benefit from larger design approaches. To visualize this tradeoff, for the lastly conducted configuration optimizations in this chapter, the objective function is extended by annually accruing fuel costs. In doing so, the initially introduced optimization function (cf. Eq. (3.20)) is modified:

$$\underset{N_B, F_B(t_0)}{\text{minimize}} \quad p_{\text{FC}}^{\text{a}} + p_{\text{B}}^{\text{a}} + p_{\text{LNG}}^{\text{a}} \quad (4.38\text{a})$$

$$\text{subject to} \quad 0 = P_{\text{FC}}(t) - P_{\text{L}}(t) - P_{\text{B}}(t) \forall t ,$$

$$F_{\text{B}}(t_0) \leq F_{\text{B}}(t_{\text{op}}) ,$$

$$\text{Eqn. (3.1) - (3.16), (3.18), (3.28) - (3.30c)} , \quad (4.38\text{b})$$

$$\text{Eqn. (3.21) - (3.24)} , \quad (4.38\text{c})$$

$$\text{Eqn. (4.18) - (4.19)} , \quad (4.38\text{d})$$

$$\text{Eq. (4.39)} , \quad (4.38\text{e})$$

where $p_{\text{LNG}}^{\text{a}}$ are the annually accruing fuel-related costs. The SOFC model descriptions as well as the unified storage model are reused for the component simulation (cf. Eq. (4.38b)). Also, the operating strategy is not changed (cf. Eq. (4.38c)). Since the previous results emphasize the use of a more complex battery degradation description, the only component model alteration is given with the more complex degradation calculation from [117] (cf. Eq. (4.38d)). Considering that the focus of this assessment is set on the fuel cell system sizing, the hybrid storage utilization is neglected and only battery support is provided for both revised case studies.

Fuel costs – The fuel-related costs include the fuel tank annuity payment $p_{\text{LNG,tank}}^{\text{a}}$ and the annual refueling expenses $p_{\text{LNG,refueling}}^{\text{a}}$. Latter are extrapolated from the investigated time frame:

$$\begin{aligned}
p_{\text{LNG}}^{\text{a}} &= p_{\text{LNG,refueling}}^{\text{a}} + p_{\text{LNG,tank}}^{\text{a}} \\
&= p_{\text{LNG}} \cdot \frac{t_{\text{op}}^{\text{a}}}{t_{\text{op}}} \int^{\text{t}_{\text{op}}} \dot{m}_{\text{LNG}}(P_{\text{FC}}, t) dt + p_{\text{LNG,tank}} \cdot A_{\text{LNG,tank}}(t_{\text{L,tank}}). \quad (4.39)
\end{aligned}$$

The energy-specific fuel price p_{fuel} , the LNG tank investment costs p_{LNG} , the annual ship operating time t_{op}^{a} , and the fuel tank lifetime $t_{\text{L,LNG,tank}}$ are given in Tab. 4.3.

Tab. 4.3: Parameters required to calculate annual occurring fuel costs of the investigated cases

Parameter		Value	Reference
Price for LNG including port fee	p_{LNG}	19.04 €/MWh	based on [120],[121]
Specific LNG tank price	$p_{\text{LNG,tank}}^{\text{inv}}$	144 €/MWh	[60]
Annual operating time	t_{op}^{a}	350 d	own analysis
LNG tank lifetime	$t_{\text{L,tank}}$	20 a	own analysis

4.6 Case Study Revision: Fuel Cost Inclusion

In the third and last part of the design analysis, cost-optimized power system configurations with and without fuel consumption consideration are directly compared to each other. Again, optimization results are given as a function of the installed fuel cell module's rated power for both case studies I and II.

4.6.1 Case I: Motor Yacht

The new optimization results and economic performance indicators for case study I are given in Fig. 4.14. Here all resulting graphs completely overlap, signaling that the optimal SOFC-battery combinations are not influenced by the new objective function. Consequently, Fig. 4.14 (a)–(c) represent shapes similar to the previous investigations. As expected, the fuel costs given in Fig. 4.14 (d) decrease with the rated power of the fuel cells, shifting the cost-optimal configuration towards higher fuel cell rated powers.

However, the fuel cost reduction achieved by operating under higher-efficiency conditions only makes up for around 500 €/a or 0.5% of the total annual costs. Therefore, while the cost-optimal configuration displayed in Fig. 4.14 (e) is now accomplished with a 3% larger generator unit, the overall cost reduction turns out comparatively small.

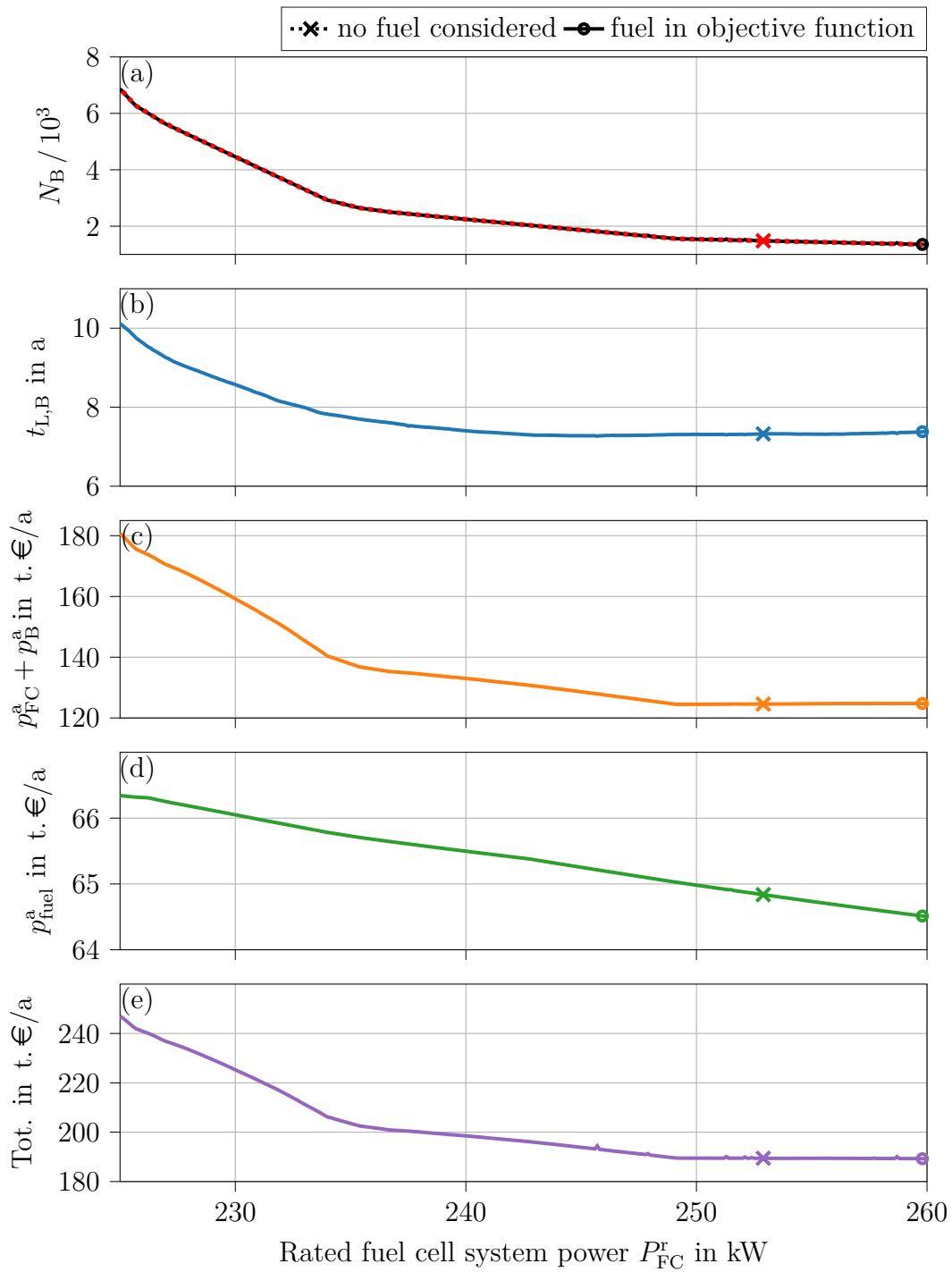


Fig. 4.14: Revision of case study I – fuel cost consideration: (a) number of battery cells N_B , (b) battery lifetime $t_{L,B}$, (c) component costs, (d) fuel costs, and (e) annual system costs; \bullet highlights the calculated cost optimum considering fuel expenses, \times marks the reference cost minimum declared without fuel costs consideration

4.6.2 Case II: General Cargo Ship

To support the results of the first fuel-related system analysis and obtain further qualitative findings, case study II is repeated with the new objective function. In analogy to Section 4.6.1, design results and economic performance indicators are given in Fig. 4.15. Contrarily to the first assessment of Case study II (cf. Section 4.2.2) no linear battery size decrease is recorded for an increase of the fuel cell system's rated power. Instead, Fig. 4.15 (a) displays two relatively evenly decreasing fractions separated by a steep drop around 206 kW rated SOFC power. This effect primarily results from the operation-dependent storage degradation estimation and a benefiting trade-off towards smaller specific loads for the single battery cells. Also to be observed is that optimization results with and without fuel consideration diverge for the first time. However, the battery size increase must be caused by a fuel-related effect, since the larger unit does not further reduce the battery annuity payments (cf. Fig. 4.15 (b),(c)). Instead, the reasoning for this is found in the EMS formulation: a system with larger battery is able to operate above the critical storage SoE (cf. Eq. (3.23)) for a longer time frame, resulting in a load-following (part load) operation with a higher energy efficiency. The initial increase of fuel costs displayed in Fig. 4.15 (d) is also in large parts owed to a combination of the load profile characteristics and the energy management strategy, which proposes fuel cell operation at maximum power by default. Here, the expected cost reduction is not identifiable within the investigated design range. Conclusively, it is advisable to consider fuel consumption characteristics while creating a control strategy for future tasks and not only concentrate on maximizing the operability of the power system.

Total system costs again minimize for the smallest applicable rated fuel cell system power, as is demonstrated in Fig. 4.15 (e). While the cost-optimal fuel cell system size equals the result of the first assessments, a more than double-sized battery unit is suggested here for the discussed control-strategy-associated reasoning.

In addition, monitoring the annual fuel expenses is of relevance for the following two reasons: (1) a higher relative influence of the fuel consumption on the total annual expenses can be expected for increasing fuel prices and decreasing fuel cell system costs, whereby both effects occur in the subsequent analyses. (2) In addition, when assessing different fuels, their economic impact must certainly be displayed within the conceptual design phase. Therefore, fuel costs are further on considered in the optimization procedure.

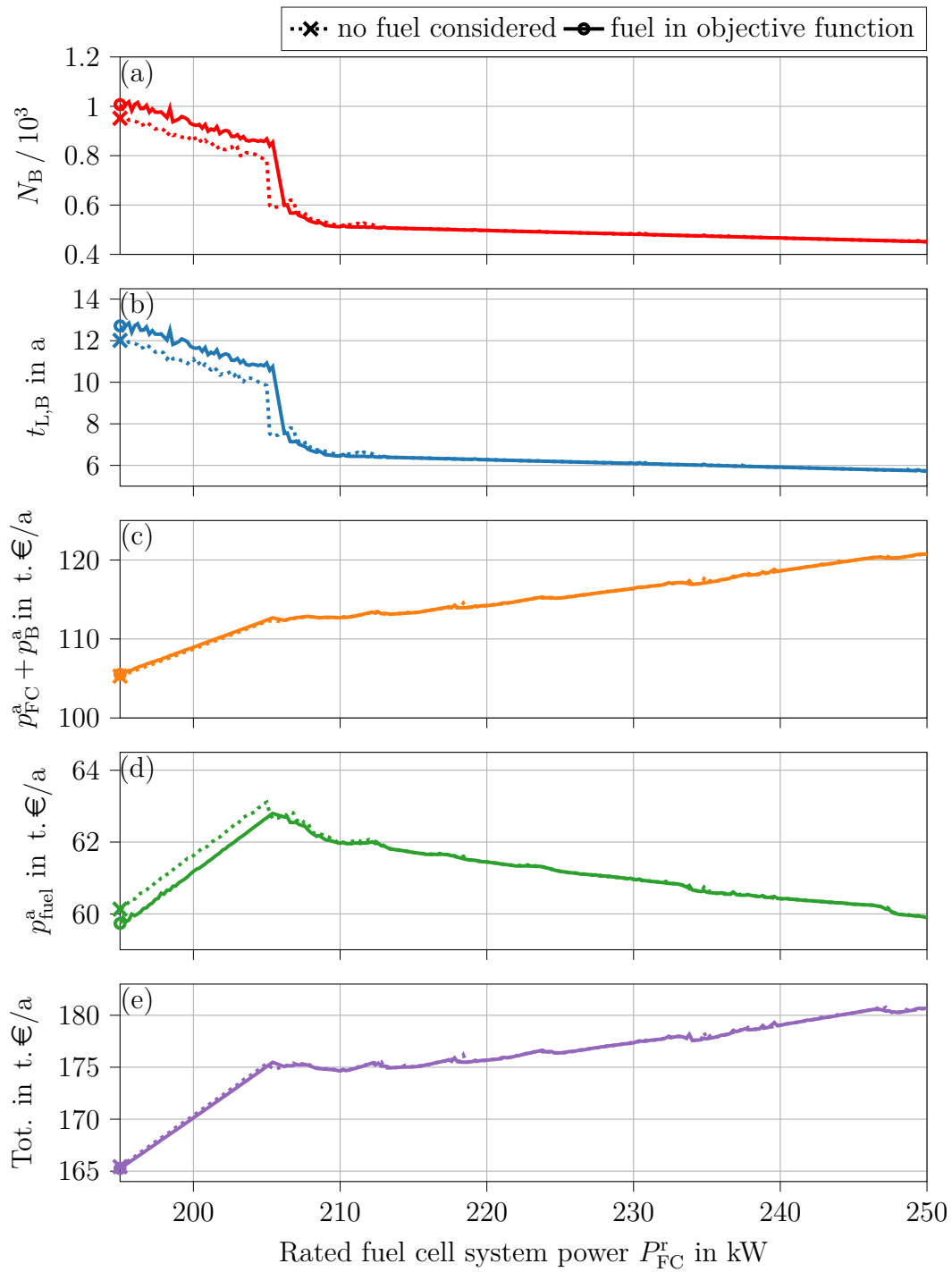


Fig. 4.15: Revision of case study II – fuel cost consideration: (a) number of battery cells N_B , (b) battery lifetime $t_{L,B}$, (c) component costs, (d) fuel costs, and (e) annual system costs; \bullet highlights the calculated cost optimum considering fuel expenses, \times marks the reference cost minimum declared without fuel costs consideration

4.7 Interim Conclusion

In this chapter the challenge of ensuring the uninterrupted power supply on a ship with a power-gradient-limited SOFC module and a hybrid energy storage was investigated. For this purpose, a design optimization was conducted based on the proposed energy management strategy to address both research issues [1] and [2] introduced in Chapter 2.

The system-model-based design optimization is a decent tool for conceptual-phase observations, but requires the proper preparation of component models, input data, and evaluation methods. Therefore, a comprehensive investigation of key performance indicators, model detail specifications, and simulation technique requirements is consulted to support the developed toolbox and to answer the first research issue (“[1] Which aspects matter for the conceptual design of a hybrid ship power system?”). In the following, the derived detailed questions regarding the research issue are answered:

[1.1] Which performance indicators should be evaluated in the decision process to achieve a proficient design of a stand-alone marine power system?

To evaluate the adequacy of a developed system design, two aspects are identified to be essential: (1) simulating the system operation to ensure application safety despite the components’ operating limitations and (2) assessing the economic reasonableness of the configuration by comparing it to alternative design approaches. The conclusions regarding these two aspects are once again summarized in the following.

Component limitations – The concern that many energy storage models neglect relevant operating limitations was already mentioned in the literature discussion of Section 2.1. This observation is strongly supported by the present investigation results. For the conducted case studies, two different design bottlenecks are identified and assigned to specific load profile characteristics.

The storage capacity is of high importance for energy-intensive profiles like in Case study I, with bulbous characteristics instead of a steady consumer demand. Here, the consideration of the SOFC load shift limitations is especially relevant, as the delta between load and generator specifies the storage requirements. Since the energy storage is not operating close to maximum power values, a hybridization with a supercapacitor is generally not advisable.

On the other hand, the retrievable power of the energy storage is identified to be a bottleneck in the power-intensive Case study II. Here, the storage hybridization with supercapacitors is applicable in order to create a configuration with less

capacity oversizing. Still, the energy capacity consideration is significant for the supercapacitors, since they can only be operated for the short time of the load peaks and therefore require an adequate design to function during one maneuver.

Annuity payments – calculating annual costs is a straightforward approach to compare payments for components with different lifetimes, as well as maintenance and operating expenses. The assessment of annual system costs instead of installed resource values also best reflects the shipowner’s incentive. It is demonstrated that cost-optimized system configurations do not necessarily resemble the smallest possible number of cells but involve the operation-dependent storage degradation. This influence becomes particularly clear when a cost-optimal hybrid storage is found not to resemble the technical optimum but an oversized solution in order to increase the battery unit’s lifetime. Therefore, the cost-optimal hybridization distribution between SOFC and energy storage should consider the component’s lifetime with an annuity payment method as opposed to pure investment cost optimization.

1.2 Which component properties should be considered and what model level of detail is sufficient for a power system simulation?

In the first optimization attempt, a straightforward model approach, which is able to display the operating limitations in a simple way, was chosen to create a benchmark result. On this basis, the two investigated case studies were repeatedly conducted with revised component models in order to identify reasonable model assumptions and oversimplifications. The abstracted results are summarized in the following.

Coloumbic storage models – To validate the firstly obtained results, the storage models’ levels of detail were increased to technology-specific voltage and current descriptions. In the revised assessments, overall similar system configurations were obtained for both case study ships. Specifically for an LFP battery, the unified energy storage model introduced in Chapter 3 represents a potentially usable application with decent results, if no detailed component data are available. Contrarily, the behavior of a supercapacitor does not fit this+ basic model, which in this analysis led to a performance overestimation when using data sheet parameters. Consequently, the parameterized model with nonlinear voltage and capacitance should be considered for future assessments.

Storage degradation – While the component configurations obtained from a second design optimization resemble the prior results qualitatively, the model modification generated different system costs and local configuration optima mostly due to the changed lifetime calculation. With the introduction of operation-related degradation, overall increased degradation rates are estimated due to the higher specific cell power demands, which were neglected by the simple lifetime model. Since the remapped degradation models are applicable in combination with the the unified physical description, especially the LFP battery should further on be modeled with a mixed composition of the two introduced approaches.

Fuel consumption – since the power generator’s operating behavior is dependent on its size and energy demand, the fuel consumption finally was added to the optimization decision process. Here, it is apparent that cost-optimal designs could shift towards larger fuel cell system sizes in order to decrease the relative operating point and increase the energy efficiency. It is also shown that a cost-optimal storage design does not relevantly diverge for a given fuel cell system rated power when including fuel expenses to the cost optimization. However, since the investigation of different fuel types is part of a subsequent assessment, annual fuel expenses are from now on included as part of the optimization’s objective function. In addition, one other deliberation should be to alter the energy management strategy in favor of a lower fuel consumption.

Now that research issue [1] is fully processed, all detailed questions regarding the SOFC operation at open sea introduced in Section 2.2 are answered individually.

[2.1] Are the load shift limitations of an SOFC system with onboard steam reforming inhibiting their use on ships with fluctuating power demand?

For each analyzed load profile, a fully functioning power system configuration was found. However, the introduced minimum output power limitation to prevent a too low cell/reformer temperature and maintain proper fluid-dynamical system behavior only allows for a rather small design range in the investigated vessel types. In addition, the load change limitations of the SOFCs do not permit an adequate autonomous load-following operation for the investigated profiles. Consequently, its ship application is feasible only in hybrid power systems, which include at least one power source with a fast reaction time and no significantly limited power gradient.

2.2 If not, what additional support is required to ensure an uninterrupted supply of power on a ship?

SOFC power generation with battery support proves to be a feasible system configuration approach, as is shown in the conducted ship case studies. However, the storage support can only be warranted if its energy content fits the planned operation. Consequently, the deployed power management strategy must ensure an appropriate cooperation of both system components. Since all optimally sized designs include moderately large battery and supercapacitor support, the assessment emphasizes the usability of the SOFC technology in marine applications. From an economic perspective, in the cost-optimal configuration an energy storage application only amounts to 18% of the annual component costs for the energy-intensive load profile and 9% of the power-intensive mission. On the other hand, the storage system allows for a 40–51% decreased power generator size due to its load peak shaving function.

2.3 How does a cost-optimal hybrid power system including SOFCs look like?

The cost-optimal hybrid configuration of the power system components is not only a function of the maximum required power or the amount of storage energy capacity, but is heavily dependent on the load profile characteristics. In the conducted assessment, the classification of two bottlenecks for the storage design are identified. Key findings for these cases are summarized individually:

Energy bottlenecks – An energy-intensive battery task is characterized with a frequently up-and-downshifting load profile, resulting in a larger divergence of the load-shift-limited fuel cell power output and the ship's electric demand. Increasing the rated power of the SOFCs to a value higher than the minimally applicable design immediately reduces the operating requirements for the energy storage. Here, two effects are found to be equally responsible: (1) the lower and higher operating point limitations of the SOFCs fit the load profile better for the conceivable design range, allowing for a reduced delta between generated and consumed energy. (2) The higher absolute load shift capability further reduces the time frames at which the batteries compensate high amounts of the power delta. Consequently, for the firstly analyzed case study a cost reduction potential higher than 20% compared to an approach that minimizes the fuel cells' rated power can be achieved by decreasing the battery unit requirements. However, since the total costs of ownership also are a function of degradation effects, this drawn profit entails a saturating be-

havior. Here, a trade-off between lower investment costs and higher degradation effects is mainly attributable to an increased specific battery load.

Larger fuel cell systems not only reduce the operating requirements for the battery unit but also benefit the overall fuel consumption due to a higher operating efficiency. Therefore, in an even larger SOFC module is found to be cost-optimal in the in the fuel-considering analysis.

Power bottlenecks – The observed trend of a minimized fuel cell system for a storage design case with power bottleneck can be explained with the following logic: consulting the investment costs only and neglecting maintenance or replacement, one fuel cell power unit costs twenty times the amount of a battery. Yet, it does not relax the storage system requirements in a way it would in a design case with energy bottleneck, where fuel cell power modulation decreases the needed capacity significantly and is therefore profitable. Consequently, this observation can be generalized at least for the assumed component investment costs relation.

In the second case study, the intensity of maneuver operations meaningfully affects the battery lifetime when considering a power-dependent degradation. Still, the annual battery costs do not encourage drastic unit oversizing. However, this must not be true for every power-intensive application: for example, a higher occurrence of thruster maneuvers could likely result in oversizing the battery.

Since a hybridization of the energy storage with supercapacitors leads to even higher specific loads for the battery, a cost-optimal design does not equal a technically optimal configuration, where neither power nor storage capacity are oversized. However, a general rule for the perfect configuration is not derivable due to a number of interdependencies.

Ultimately, one central message of this assessment is that proper storage modeling and dynamic system simulation improves the quality of power system designs and is an important tool to supplement a shipbuilder’s experience. Since an adequately sized energy storage is not only an optional feature but a necessity for a functioning SOFC-based power system, a simulation-based design optimization becomes even more urgent. Still, the research issue [2] “Are SOFCs suitable for marine applications?” can clearly be answered positively.

5 Distributed System Analysis with Consideration of Component Failures

The second SOFC-based assessment addresses the power system architecture of large ships and the potential benefits, which a modular-built power generator unit offers. To analyze the influence of restructuring such power systems, a direct comparison of central and distributed design approaches is conducted. Thereby, the consideration of component malfunctions and the achievement of component redundancy play a major role and are investigated in a two-step case study.

After the brief introduction of a typical large-vessel power transmission architecture in Section 5.1 and component models are given in Section 5.2. A revised design optimization task is addressed in Section 5.3. A specifically modified energy management strategy is formulated in Section 5.4. The conduct of the cruise ship case study is introduced in Section 5.5. Finally, the results of four design optimizations for both central and distributed power systems with and without component malfunction consideration are discussed comprehensively in Section 5.6. Finally, research issue [3] is addressed in Section 5.7.

Disclosure: The following chapter is in large parts based on the publication: L. Kistner; A. Bensmann; R. Hanke-Rauschenbach, Optimal Design of a Distributed Ship Power System with Solid Oxide Fuel Cells under the Consideration of Component Malfunctions, Applied Energy (2022) [52]. For a detailed description of the author contributions see Appendix C.

5.1 Distributed System Architecture

The investigated power system consists of electrical consumers, modular SOFCs, battery units, and a power transmission grid including high-voltage power cables and power transformers. The latter connect the ship's fire zones (encapsulated safety areas, also referred to as main vertical zones [29]) with a zone-connecting power backbone. A schematic overview of the designed and analyzed approach is given in Fig. 5.1. While the consumer locations are fixed for this assessment, every fire zone can be variably equipped with fuel cell and storage modules. Both the system components and the grid topology are discussed in the following. Then, qualitative advantages of a distributed power system are given.

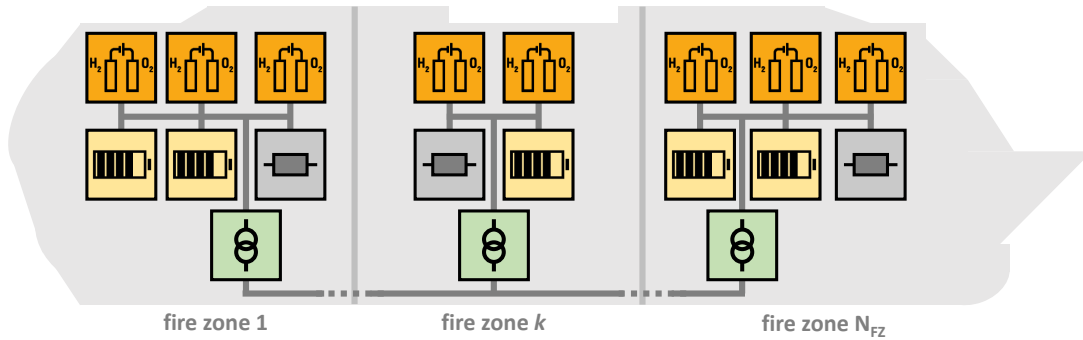


Fig. 5.1: SOFC (orange), battery (yellow), electrical load (gray) in each of the ship's N_{FZ} fire zones, connected via power transformers (green) and a high-voltage power backbone

System components – The considered electrical consumers cover navigation (radars, position tracking etc.), lights, hotel load, air conditioning, freshwater production, and maneuvering thrusters. However, a decentralized approach is not reasonable for the propulsion power system, since the propellers are located only in the stern of the ship. Therefore propulsion power demand is not included in the assessment.

The core components of the analyzed power system are modular SOFC units with integrated natural gas steam reforming, which are already introduced in Chapter 3. In analogy, additional electrical energy storage units support the fuel cell system in terms of load leveling. As stated before, SOFCs are limited in their load change capabilities to avoid high thermomechanical tension [122] and require a permanent operation higher than 50% part load to prevent cool down.

The transmission grid with a radial-forked topology consists of a low voltage and a high-voltage level, which are interconnected with power transformers in each fire zone. The low voltage 440 V grid connects the local consumers, SOFCs, and batteries, whereas the 11 kV grid connects all fire zones. This high-voltage level power backbone is typically chosen to reduce occurring currents and transport losses, respectively. Even though direct current grids are discussed for ship systems containing batteries and fuel cells [58] to reduce the number of power electronic components and to eliminate frequency deviation and harmonic problems [123], this work focuses on the optimal distribution of components under the assumption of a conventional alternating current set-up. Therefore, a possible grid topology transformation, which could further benefit the decentralization approach [59],[60] is not regarded.

Advantages of a distributed system – The advantages of distributing the introduced system components into the ship's fire zones can be categorized into two groups: (1) the electric grid requirements and (2) power-system-related emergency cases. In traditional ship power systems, the generators responsible for shipboard

electrical energy supply are typically located in the stern. Cables usually have to tolerate a high power flow between the engine rooms and thrusters in the vessel's bow. Also, power transformers distributed over the ship's fire zones are designed to transmit the peak power requirements of the local electrical consumers. With the right distribution of the system components, the high-voltage electric grid and the power transformer size can be decreased. Shorter distances for energy transportation also result in fewer transmission losses.

The second aspect concerns the preparation for emergency cases. The legally binding *Safety of Life at Sea (SOLAS)* convention [29] follows the so-called "safe return to port" strategy [124], which specifies requirements for component redundancy in case of a malfunction [125]. The convention states that a malfunction of one single component must be compensated by the remaining system without endangering the power supply. The system must then stay operable for at least 72 hours, even if the problem is not solved.

As both propulsion and electrical power supply must not be covered by only one single generator, a genset of four to six auxiliary 4-stroke engines provides electrical energy on large ships. Here, the requirements for component redundancy unavoidably lead to oversized ICEs. This effect is minimized with the introduction of modular fuel cells, because the malfunction of a smaller unit can be compensated more easily. While the conducted analysis only examines the N+1 component redundancy for fuel cells and batteries, other safety aspects can be listed for a distributed modular power system: a failure in one engine room could harm more than one component, whereas with distributed components more power sources remain operable in a locally occurring emergency scenario. With a high number of power generators that are not located in the same engine room, a separate emergency power supply might not be a requirement in future ship power systems as opposed to today's regulations [29]. Furthermore, the components could be arranged in a way, so that during any sort of grid failure, each fire zone would at least be partly operable.

5.2 Additionally Required Models

This section includes the formulation of additionally required mathematical models of the power transmission components under consideration (high-voltage power cables and power transformers), and the revised presentation of distributed fuel cell and battery modules.

5.2.1 Electrical Grid

Physical model – The physical model of the transmission system is limited to the description of the power backbone and the power transformers, whereas the

low voltage side of the grid is assumed to be mostly unchanged for different configurations. The power flow nomenclature can be obtained from Fig. 5.2.

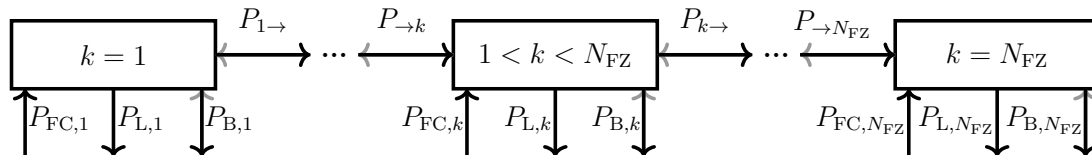


Fig. 5.2: Nomenclature of power flow and fire zone connections: fuel cell power P_{FC} , consumer power P_L , battery power P_B , and power transmission P_{\rightarrow}

For the subsequent equations, an overall power balance is assumed, whereas local power differences are defined as

$$\Delta P_k = P_{FC,k} - P_{L,k} - P_{B,k}, \quad (5.1)$$

where $P_{FC,k}$ is one time-dependent fuel cell system power, $P_{L,k}$ is one predefined local consumer, and $P_{B,k}$ is one battery power in- or output. The bidirectional power flow between fire zone k to zone $k+1$ is given with

$$P_{k \rightarrow} = \begin{cases} \Delta P_k & \text{if } k = 1 \\ 0 & \text{if } k = N_{FZ} \\ \Delta P_k + P_{\rightarrow k} & \text{else} \end{cases} \quad (5.2)$$

where

$$P_{k \rightarrow} = P_{\rightarrow(k+1)}. \quad (5.3)$$

To further describe power transformers and cables, transport-characteristic time-dependent values are calculated. For the cables, the electric current in one string is chosen under the assumption of small voltage and phase angle deviation:

$$I_{\text{str},k \rightarrow} \approx \frac{P_{k \rightarrow}}{\sqrt{3} \cdot U_{HV} \cdot \cos(\varphi)} \quad (5.4)$$

where U_{HV} is the phase-to-phase high voltage and $\cos(\varphi)$ is the power factor. For the power transformer, its apparent power is calculated:

$$S_{\text{trafo},k} = \frac{\Delta P_k}{\cos(\varphi)}. \quad (5.5)$$

Both grid current and transformer apparent power are used to estimate transmission losses. Three-phase cable losses are quantified with

$$P_{\text{loss,cable},k} = 3 \cdot l_{\text{cable},k} \cdot \frac{R_{S,\text{str}}}{N_{\text{cable},k}} \cdot (I_{\text{str},k \rightarrow})^2, \quad (5.6)$$

where $l_{\text{cable},k}$ is the high-voltage cable length between the transformers, $R_{\text{S, str}}$ is the specific resistance of one string, and N_{cable} is the number of three-phase cables per fire zone connection. Since energy loss effects of the power transformers are dependent on their geometry and construction size, an approximation least-square fit function is chosen based on discrete values from [126]. It is assumed that two power transformer units are located in each fire zone in order to achieve system redundancy. Hysteresis and eddy-current losses $P_{0,k}$ as well as load dependent copper losses $P_{k,k}$ are considered for the parallel operating transformers with symmetrical power distribution:

$$P_{\text{loss,trafo},k} = 2 \cdot \left(P_{0,k} + \left(\frac{S_{\text{trafo},k}/2}{S_{\text{trafo},k}^{\text{r}}} \right)^2 \cdot P_{k,k} \right), \quad (5.7)$$

$$P_{0,k} = 0.028 W^{0.218} \cdot (S_{\text{trafo},k}^{\text{r}})^{0.782}, \quad (5.8)$$

$$P_{k,k} = 0.303 W^{0.251} \cdot (S_{\text{trafo},k}^{\text{r}})^{0.749}, \quad (5.9)$$

Total grid losses then follow with

$$P_{\text{loss,grid}} \approx \sum_{k=1}^{N_{\text{FZ}}-1} P_{\text{loss,cable},k} + \sum_{k=1}^{N_{\text{FZ}}} P_{\text{loss,trafo},k}. \quad (5.10)$$

For simplification, the compensation of transmission losses by the SOFCs or batteries (which in turn increases the transmission losses) are not calculated in an implicit loop. Instead, losses are determined based on the ideal transmission values. Further, a minimal change of the SOFC efficiency caused by the marginally increasing SOFC power output is neglected. The power limitations of the installed SOFCs are secured not to be a relevant design bottleneck in the assessed scenario. This simplification benefits the chosen control approach described in Section 5.4, which otherwise could not calculate set values of the batteries based on SOFC operating specifications without considerable iterative extra work.

Component limitations – Both power transformers and high-voltage cables are passive components and not directly connected to an active component management. Still, power transmission is limited by the components' safety limitations. To adequately size the number of cables and the power transformer dimensions, their respective maximum load is determined. Note that the transformer and the cables are implemented in with the N+1 component redundancy in mind. The number of required cables for one fire zone connection is calculated from the maximum current occurring during the considered operating time:

$$N_{\text{cable},k} = 2 \cdot \left\lceil \frac{\max(|I_{\text{str},k \rightarrow}(t)|)}{I_{\text{str}}^{\text{max}}} \right\rceil, \quad (5.11)$$

where $I_{\text{str}}^{\text{max}}$ is the permitted current of a single string. One of the redundant power transformer's rated apparent power equals the maximum value within the investigated ship mission:

$$S_{\text{trafo},k}^{\text{r}} = \max(|S_{\text{trafo},k}(t)|) . \quad (5.12)$$

Economic model – Cable costs are calculated for the number of required cables and therefore include the already considered redundancy:

$$p_{\text{cable}}^{\text{a}} = 3 \cdot p_{\text{str}}^{\text{inv}} \cdot \left(\sum_{k=1}^{N_{\text{F}}-1} N_{\text{cable},k} \cdot l_{\text{cable},k} \right) \cdot A_{\text{grid}} , \quad (5.13)$$

where $p_{\text{cable}}^{\text{inv}}$ is the length-specific price for one string in the three-phase cable and A_{grid} is the annuity payment factor for the grid with the assumed lifetime $t_{\text{L,grid}}$ and interest rate j :

$$A_{\text{grid}} = \frac{(1+j)^{t_{\text{L,grid}}} \cdot j}{(1+j)^{t_{\text{L,grid}}} - 1} . \quad (5.14)$$

Transformer costs are calculated with a nonlinear power-to-price ratio analogous to [127], but fitted with results of an own market analysis as follows:

$$p_{\text{trafo}}^{\text{a}} \approx 2 \cdot p_{\text{trafo}}^{\text{inv}} \cdot \left(\sum_{k=1}^{N_{\text{FZ}}} (S_{\text{trafo},k}^{\text{r}})^{0.94} \cdot \text{kVA}^{0.06} \right) \cdot A_{\text{grid}} , \quad (5.15)$$

where $p_{\text{trafo}}^{\text{inv}}$ is the base price for a transformer and two redundant transformers are required. Total annual grid costs are given with

$$p_{\text{grid}}^{\text{a}} = p_{\text{trafo}}^{\text{a}} + p_{\text{cable}}^{\text{a}} . \quad (5.16)$$

Model parameters – All required cable, transformer, and grid topology parameters are listed in Tab. 5.1. For the power backbone, a 50 mm² single-core copper cable with ship certification is chosen. While the lifetime of a ship is estimated to be up to 25 or even 30 years, transformer isolation failures might very well occur earlier [128]. The lifetime of the grid components is therefore reduced to average estimations.

Tab. 5.1: Parameters for high-voltage cables and power transformers

Physical parameter		Value	Reference
High-voltage level	U_{HV}	11 kV	based on [57]
Low voltage level	U_{LV}	440 V	based on [57]
Cable length bow/rear	$l_{\text{cable},f=\{1,8\}}$	50 m	own analysis
Cable length central	$l_{\text{cable},f=\{2-7\}}$	60 m	own analysis
Cable specific resistance	$R_{\text{S, str}}$	0.386 Ω / km	[129]
Power factor	$\cos(\varphi)$	0.85	own analysis
Component limitation parameter		Value	Reference
Cable maximum current (string)	$I_{\text{str}}^{\text{max}}$	196 A	[130]
Economic parameter		Value	Reference
Specific cable price (string)	$p_{\text{str}}^{\text{inv}}$	30 € / m	manufacturer
Specific transformer price	$p_{\text{trafo}}^{\text{inv}}$	50.41 € / kVA	manufacturer
Grid lifetime	$t_{\text{L, grid}}$	20 a	[128]

5.2.2 Multiple Stand-alone Fuel Cell Units

Physical model – For the fuel cell system description, the model approach introduced in Chapter 3 is adopted. However, minor model adaptations are taken in order to display different fuel cell modules, which are distributed over the ship. One unit in fire zone k is described by its operating-point-dependent system efficiency $\eta_{\text{FC},k}$ (cf. Fig. 3.5), and the resulting chemical energy consumption:

$$W_{\text{LNG, id}} = \sum_{k=1}^{N_{\text{FZ}}} \int_0^{t_{\text{op}}} \frac{P_{\text{FC},k}(\tau)}{\eta_{\text{FC},k}(\xi_{\text{FC},k})} d\tau, \quad (5.17)$$

with the normalized operating point

$$\xi_{\text{FC},k} = \frac{P_{\text{FC},k}}{P_{\text{FC}}^{\text{max}} \cdot N_{\text{FC},k}} = \frac{P_{\text{FC},k}}{P_{\text{FC},k}^{\text{r}}}. \quad (5.18)$$

For one SOFC unit a net rated power output of $P_{\text{FC}}^{\text{max}} = 300$ kW in form of an alternating current is chosen, since the resulting size ideally fits container solutions. The modules combine to the rated SOFC power of one fire zone $P_{\text{FC},k}^{\text{r}}$. As stated before, the costs resulting from transport losses are estimated without influencing the fuel cells' operating points. Instead, fuel expenses are calculated with the

time-dependent average efficiency $\eta_{\text{FC,av}}$:

$$W_{\text{LNG,loss}} = \int_0^{t_{\text{op}}} \frac{P_{\text{loss,grid}}(\tau)}{\eta_{\text{FC,av}}(\tau)} d\tau, \quad (5.19)$$

assuming the evenly distributed compensation of losses.

Component management – The SOFC units entail the two already discussed limitations of operating above a minimum power (in this case 50% part load)

$$P_{\text{FC}}^{\min} \cdot N_{\text{FC},k} \leq P_{\text{FC},k} \leq P_{\text{FC}}^{\max} \cdot N_{\text{FC},k} \quad (5.20)$$

and load shifting with a maximum power gradient

$$\left| \frac{dP_{\text{FC},k}}{dt} \right| \leq \dot{P}_{\text{FC}}^{\max} \cdot N_{\text{FC},k}. \quad (5.21)$$

Both limitations are monitored as described in Section 3.4.2.

Economic model – Annual costs for the installed fuel cell units are calculated with power-specific investment costs for each module:

$$p_{\text{FC}}^{\text{a}} = p_{\text{FC}}^{\text{inv}} \cdot P_{\text{FC}}^{\max} \cdot (A_{\text{FC}}(t_{\text{L,FC}}) + c_{\text{FC}}^{\text{a}}) \cdot \sum_{k=1}^{N_{\text{FZ}}} N_{\text{FC},k}. \quad (5.22)$$

Annual fuel costs (cf. Section 4.6) are, in turn, extrapolated from the investigated passage and include the annual costs of a gas tank according to the fuel consumption during the passage:

$$p_{\text{LNG,id}}^{\text{a}} = W_{\text{LNG,id}} \cdot \left(\frac{t_{\text{op,eq}}^{\text{a}}}{t_{\text{op}}} \cdot p_{\text{LNG}} + p_{\text{tank}}^{\text{inv}} \cdot A_{\text{tank}}(t_{\text{L,tank}}) \right). \quad (5.23)$$

The annual costs of the LNG caused by grid losses are estimated equivalent to Eq. (5.23):

$$p_{\text{LNG,loss}}^{\text{a}} = W_{\text{LNG,loss}} \cdot \left(\frac{t_{\text{op,eq}}^{\text{a}}}{t_{\text{op}}} \cdot p_{\text{LNG}} + p_{\text{tank}}^{\text{inv}} \cdot A_{\text{tank}} \right). \quad (5.24)$$

Model parameters – Parameters for the SOFC modules are listed in Tab. 5.2. As opposed to the previously assumed values, specific costs now include the prognoses of advanced cell lifetimes and reduced investment costs with increasing production in the near future [131],[132]. Maintenance costs include replacement of stacks and active materials for the desulfurization. The applied specific estimation from [84]

and [85] still is accurate for newer stack cost and degradation estimations [132]. The annual operating time assumption is based on the time schedule of a vessel with similar operating characteristics [133].

Tab. 5.2: Additional or altered parameters for one SOFC module

Management parameter		Value	Reference
Maximum operating point	$P_{\text{FC}}^{\text{max}}$	300 kW	manufacturer
Minimum operating point	$P_{\text{FC}}^{\text{min}}$	150 kW	manufacturer
Maximum power gradient	$\dot{P}_{\text{FC}}^{\text{max}}$	30 kW / min	manufacturer
Economic parameter		Value	Reference
Specific system price	$p_{\text{FC}}^{\text{inv}}$	2000 € / kW	own analysis
An. operating time	$t_{\text{op,eq}}^{\text{a}}$	8400 h	[133]

5.2.3 Multiple Stand-alone Battery Units

Physical model – Analogous to the SOFC system, the storage model introduced in Chapter 3 is used and revised to display multiple distributed units. The energy balance of a battery unit in one fire zone is given with

$$C_{\text{E},\text{B},k} \cdot \frac{dF_{\text{B},k}}{dt} = -k_{\text{SD},\text{B}} \cdot F_{\text{B},k} \cdot C_{\text{E},\text{B},k} + P_{\text{B},k} \cdot \begin{cases} \eta_{\text{B},\text{cha}} & \text{if } P_{\text{B},k} \geq 0 \\ \frac{1}{\eta_{\text{B},\text{dis}}} & \text{if } P_{\text{B},k} < 0 \end{cases}, \quad (5.25)$$

where

$$C_{\text{E},\text{B},k} = N_{\text{B},k} \cdot C_{\text{E},\text{B}}^{\text{cell}} \quad (5.26)$$

is the unit's energy capacity built from single cells with the cell capacity $C_{\text{E},\text{B}}^{\text{cell}}$.

Component management – Battery operating limitations include k individual state of energy F_{B} controls

$$0\% \leq F_{\text{B},k} \leq 100\% \quad (5.27)$$

and maximum power boundaries

$$N_{\text{B},k} \cdot P_{\text{B},\text{dis}}^{\text{cell},\text{min}} \leq P_{\text{B},k} \leq N_{\text{B},k} \cdot P_{\text{B},\text{cha}}^{\text{cell},\text{max}}. \quad (5.28)$$

The implementation is conducted with a state machine logic analogous to Section 3.4.2.

Economic model – Again, annual costs are derived from specific investment costs p_B^{inv} , number of battery cells, and lifetime:

$$p_B^a = p_B^{\text{inv}} \cdot C_{E,B}^{\text{cell}} \cdot \sum_{k=1}^{N_{\text{FZ}}} N_{B,k} \cdot A_{B,k}(t_{L,B,k}) . \quad (5.29)$$

The lifetime calculation based on a capacity fade rate approximation from [117], which has been introduced in Section 4.4 is adopted. Here, the storage’s end of life capacity equals 80% of the rated value. The lifetime is extrapolated from the capacity losses calculated from the operation analysis:

$$t_{L,B,k} = \frac{0.2}{\frac{1}{t_{\text{op}}} \cdot \int^{t_{\text{op}}} \max \left(\vec{a}_1 \frac{P_{B,k}(\tau)}{C_{E,B,k}} + \vec{a}_2 F_{B,k}(\tau) + \vec{a}_3 \right) d\tau} . \quad (5.30)$$

Model parameters – Parameters for the lithium iron phosphate battery cells and systems are derived from a 30 Ah cell and a 15.5 kW cabinet including an inverter and listed in Tab. 5.3. Since a near-future scenario is investigated, battery unit prices are decreased in accordance with manufacturer statements.

Tab. 5.3: Additional or altered parameters for lithium iron phosphate batteries

Management parameter		Value	Reference
Cell max. charge power	$P_{B,\text{cha}}^{\text{cell,max}}$	0.396 kW	manufacturer
Cell max. disch. power	$P_{B,\text{dis}}^{\text{cell,min}}$	-0.658 kW	manufacturer
Economic parameter		Value	Reference
Specific battery costs	p_B^{inv}	800 € / kWh	manufacturer

5.3 System Design Optimization

Objective of the design optimization is the minimization of the annual system costs containing fuel cell system costs p_{FC}^a , battery storage costs p_B^a , cable and power transformer costs p_{grid}^a , LNG expenses $p_{\text{LNG,id}}^a$, and extra costs for LNG caused by electrical losses $p_{\text{LNG,loss}}^a$. In the assessment, three scenarios for ship operation are covered: the regular scenario without component failure consideration (case $\zeta = 1$), which is consulted for cost calculation, a second that includes a fuel cell unit failure ($\zeta = 2$), and a third that includes a battery failure ($\zeta = 3$). The given optimization function is explained step by step in the following:

$$\begin{aligned} & \text{minimize} && p_{\text{FC}}^{\text{a}} + p_{\text{B}}^{\text{a}} + p_{\text{grid}}^{\text{a}} + p_{\text{LNG,id}}^{\text{a}} + p_{\text{LNG,loss}}^{\text{a}} \text{ for } \zeta = 1 && (5.31) \\ & \vec{N}_{\text{FC}}, \vec{N}_{\text{B}}, && && \\ & \vec{F}_{\text{B}}(t_0), \vec{F}_{\text{FC}}(t_0), \vec{D}_{\text{F}} && && \end{aligned}$$

$$\text{subject to} \quad \text{if } \zeta = 1 \rightarrow \sum_{k=1}^{N_{\text{FZ}}} F_{\text{B},k}(t_0) \leq \sum_{k=1}^{N_{\text{FZ}}} F_{\text{B},k}(t_{\text{op}}) \quad (5.32 \text{ a})$$

$$\text{if } \zeta = 2 \rightarrow \exists! k \in \{1, \dots, N_{\text{FZ}}\} \Rightarrow N_{\text{FC},k}^* := (N_{\text{FC},k} - 1) \quad (5.32 \text{ b})$$

$$\text{if } \zeta = 3 \rightarrow \exists k : N_{\text{B},k} = \max(\vec{N}_{\text{B}}) \Rightarrow N_{\text{B},k}^* := 0 \quad (5.32 \text{ c})$$

$$\sum_{k=1}^{N_{\text{FZ}}} \Delta P_k(t) = 0 \forall \zeta \in \{1, 2, 3\}, t \in \{t_0, \dots, t_{\text{op}}\} \quad (5.33)$$

Eqn. (5.1) – (5.30),

Eqn. (5.34) – (5.40).

The optimization's degrees of freedom are the number of fuel cell units \vec{N}_{FC} , battery cells \vec{N}_{B} , and their position on the ship. Here, each vector contains one entry per fire zone where the index k indicates the fire zone location (eg. $N_{\text{FC},k}$). Additionally, the starting states of energy (SoE) $\vec{F}_{\text{B},0}$ of the batteries, operating points of the SOFCs $\vec{F}_{\text{FC},0}$ and several parameters included in the control strategy \vec{D}_{F} (cf. Section 5.4) are adjustable during the optimization process.

There are six constraints to consider: Eq. (5.32 a) states that the batteries' SoE at end of operation ($t = t_{\text{op}}$) must at least equal the level at beginning of operation ($t = t_0$). This cyclic boundary was already used in the previous assessment and ensures that the ship is operable after the analyzed time period and must only be applied for regular operation ($\zeta = 1$). Eq. (5.32 b) represents the emergency case of a fuel cell system malfunction ($\zeta = 2$). The scenario is defined as follows: one single SOFC unit disconnects from the grid and $N_{\text{FC},k}^*$ units remain active, provided that all modules can operate individually. Here, the malfunction location is randomized, as it does not influence the operability of the total system or the assessed system costs. Eq. (5.32 c) represents a battery unit malfunction ($\zeta = 3$) and states that the largest of all storages among the fire zones disconnects from the grid. While the malfunction extent could be reduced by further spatial separation of the battery unit into different rooms, this straightforward procedure is chosen as worst case scenario. Eq. (5.33) states that the sum of all power differences in the fire zones must be equal to zero at all times and for all operating scenarios. Finally, compliance with the system component models and energy management strategy introduced in the following must be given.

5.4 Control Strategy for a Distributed System

Next, a general discussion about system control strategies for microgrids and the control strategy formulated for the fuel cell ship system approach are covered.

5.4.1 General Considerations

There are three different principles to approach an energy management strategy in a decentralized power system: droop control, agent-based control and global control. They differ in terms of information exchange and set value allocation. In Fig. 5.3 required communication paths are visualized for the example of one fire zone including an SOFC and a battery unit. For a conventional droop control approach (cf. Fig. 5.3 (a)), decision making is based on local information of the grid's state (e.g. voltage, frequency). Typically, this approach is found for shipboard synchronous generators driven by internal combustion engines [58]. An example for a decentralized system approach is given in [134]: here, proton exchange membrane fuel cells are supported by ICEs for primary control.

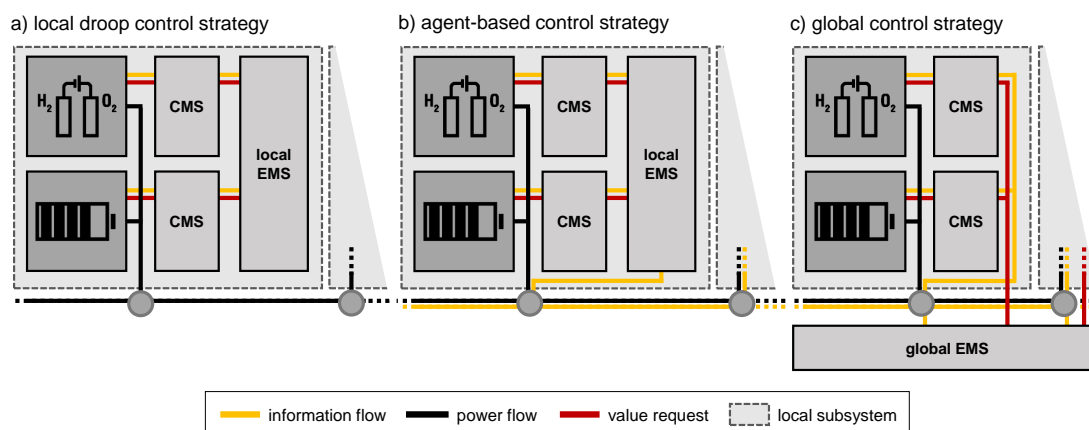


Fig. 5.3: Different approaches to control a decentralized energy system with regard to the amount of information exchanged: black connectors represent the electrical grid, yellow connectors represent fire zone state information, red connectors represent set values calculated by the energy management system (EMS) and approved components' responses processed by the component management system (CMS).

In an agent-based energy management (cf. Fig. 5.3 (b)), an unidirectional communication flow that could incorporate behavior of other system components is included in a decentralized decision-making process [135],[136]. Usually, the existence of different decision makers or the absence of real-time communication possibilities are the reasoning for this. In a global control strategy (cf. Fig. 5.3 (c)),

set values for all system components are calculated based on real-time data [137]. As the confined space on a ship allows for extended communication between components and a centralized EMS, a global strategy is evaluated to be practical and therefore chosen instead of droop control or agent-based methods.

5.4.2 Rule-based Control Strategy

As already stated, a rule-based strategy can only be effective if the rules are formulated appropriately. Therefore, power system operability and the positive influence of the control strategy on the objective function are prioritized. During the development of the control strategy it turned out that SOFC investment costs and fuel expenses are the largest cost factors, followed by battery investment costs. Therefore, the main objectives are A high SOFC energy efficiency and a low battery degradation. In contrast, the grid cost reduction is mainly influenced by a suitable design approach and is only considered as secondary objective for the control strategy. The resulting heuristic is split into fuel cell and battery management. A comprehensive model description is given in the following, whereas a visual example is given in Appendix A.2.

Fuel cell system control strategy – Four priorities are covered with the derived control approach for the SOFCs:

1. To increase battery lifetime, a low specific power demand is targeted, which can be achieved with the overall reduction of the power delta between fuel cells and load.
2. To reduce fuel consumption, SOFCs should be operating in the 60-80% part load area, because this corridor provides the highest conversion efficiency.
3. The EMS prioritizes dynamic operation of SOFCs with the largest relevant local supply-demand difference to reduce power transport between fire zones.
4. Finally, the strategy also considers that batteries should not be fully charged or discharged, but ready to operate at all times.

For the SOFC control strategy, the set values are calculated as a function of a global state description variable Z_{FC} and the local state variables $Y_{FC,k}$, as well as the distributed load demand $P_{L,k}$. The first state machine (cf. Fig. 5.4) is designed to prevent fully charged or discharged battery units by monitoring the average SoE

$$F_{\emptyset} = \frac{\sum_k F_{B,k} \cdot C_{E,S,k}}{\sum_k C_{E,S,k}}. \quad (5.34)$$

Thereby, critical SoEs F_{high} and F_{low} are adjusted within the optimization process (represented by \vec{D}_F in Eq. (5.31)). The global state machine includes three mutually exclusive states:

- $Z_{\text{FC}} = 1$ represents highly charged batteries and demands a decreasing the power output.
- $Z_{\text{FC}} = -1$ represents highly discharged batteries and demands a power increase.
- $Z_{\text{FC}} = 0$ represents uncritical battery charge and results in dynamic or steady state operation specified in the following.

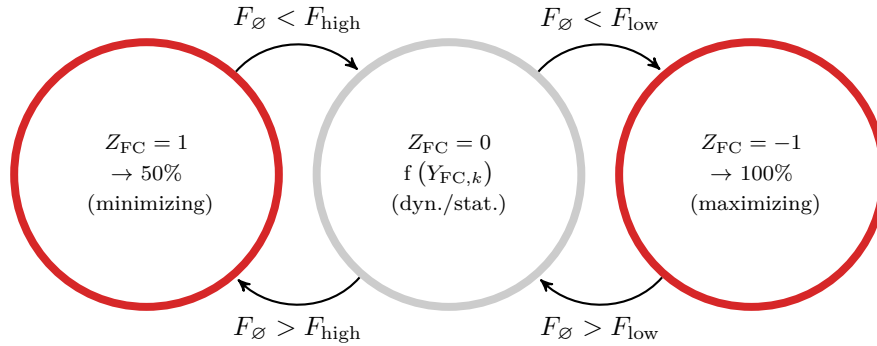


Fig. 5.4: State machine for the fuel cell system control to prevent fully charged or discharged battery units

Objective of the second state machine (cf. Fig. 5.5) is the synchronization of load and fuel cell modules' total power output. Here, three states display steady-state operation:

- $Y_{\text{FC},k} = 1$ indicates steady state in desired 60-80% part load area,
- $Y_{\text{FC},k} = -2$ indicates steady state operation up to 100%,
- $Y_{\text{FC},k} = 2$ indicates steady state operation down to 50%

and additional three states allow dynamic operation:

- $Y_{\text{FC},k} = 0$ allows dynamic operation in the desired 60-80% part load area,
- $Y_{\text{FC},k} = -3$ allows dynamic operation operation up to 100%,
- $Y_{\text{FC},k} = 3$ allows dynamic operation operation down to 50%.

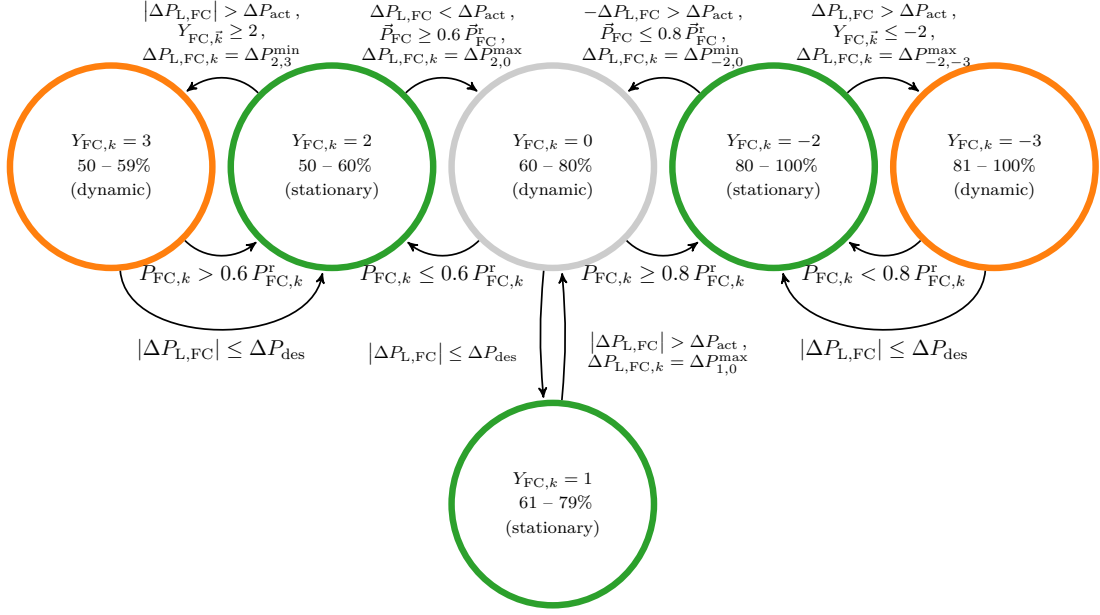


Fig. 5.5: Additional state machine for the fuel cell control if $Z_{FC} = 0$

The strategy aims for operating points between 60 and 80% to increase the energy efficiency. When a dynamically operating unit reaches one corridor limit, steady state operation is initiated ($Y_{FC,k} = -2$ for 80%, $Y_{FC,k} = 2$ for the 60% border). Another unit begins dynamic operation until all components reach the checkpoint. Other state changes between dynamic and steady state operation are dependent on the global delta $\Delta P_{L,FC}$ and all local deltas $\Delta P_{L,FC,k}$ between fuel cell output power and consumer demand:

$$\Delta P_{L,FC} = \sum_f P_{L,k} - P_{FC,k}, \quad (5.35)$$

$$\Delta P_{L,FC,k} = P_{L,k} - P_{FC,k}. \quad (5.36)$$

Control parameters ΔP_{des} and ΔP_{act} are used to describe a requirement for SOFC load change: When the value ΔP_{act} is exceeded by the difference between SOFCs and load, a state change from a stationary state i to a dynamic state j is initiated. The fuel cell units in the fire zone with the largest local delta towards the direction of modulation ($\Delta P_{i,j}^{max}$ or $\Delta P_{i,j}^{min}$) start a dynamic operation. Steady-state operation is initiated for every SOFC unit as soon as the delta reaches the desired value ΔP_{des} . If the desired value is not reached within a certain time, the energy management changes the state $Y_{FC,f}$ in an additional fire zone.

The exact formulations for delta-concerning state change conditions are listed below. They take into account the most convenient local delta between load and SOFC power $\Delta P_{L,FC,k}$ and include the fire zone states for decision:

$$\Delta P_{2,0}^{\max} = \max \left(\Delta P_{L,FC,k} (Y_{FZ,k} \neq \{-2, 0\}) \right), \quad (5.37a)$$

$$\Delta P_{-2,0}^{\min} = \min \left(\Delta P_{L,FC,k} (Y_{FZ,k} \neq \{2, 0\}) \right), \quad (5.37b)$$

$$\Delta P_{1,0}^{\max} = \begin{cases} \max \left(\Delta P_{L,FC,k} (Y_{FZ,k} \neq \{-2, 0\}) \right) & \text{if } \Delta P_{L,FC} > 0 \\ \min \left(\Delta P_{L,FC,k} (Y_{FZ,k} \neq \{2, 0\}) \right) & \text{else,} \end{cases} \quad (5.37c)$$

$$\Delta P_{2,3}^{\min} = \begin{cases} \max \left(\Delta P_{L,FC,k} (Y_{FZ,k} \neq 3) \right) & \text{if } \Delta P_{L,FC} > 0 \\ \min \left(\Delta P_{L,FC,k} (Y_{FZ,k} \neq 3) \right) & \text{else,} \end{cases} \quad (5.37d)$$

$$\Delta P_{-2,-3}^{\max} = \begin{cases} \max \left(\Delta P_{L,FC,k} (Y_{FZ,k} \neq -3) \right) & \text{if } \Delta P_{L,FC} > 0 \\ \min \left(\Delta P_{L,FC,k} (Y_{FZ,k} \neq -3) \right) & \text{else.} \end{cases} \quad (5.37e)$$

SOFC units in steady-state operation receive a set value equally to their current power output. All actively modulating cells share the demanded adjustment depending on their module's number of units:

$$P_{FC, \text{set}, k} = \begin{cases} N_{FC,k} \cdot P_{FC}^{\min} & \text{if } Z_{FC} = 1 \\ N_{FC,k} \cdot P_{FC}^{\max} & \text{if } Z_{FC} = -1 \\ P_{FC,k} + \frac{\Delta P_{L,FC} \cdot P_{FC,k}^r}{\sum_k P_{FC,k}^r (Y_{FC,k} = -3)} & \text{if } Z_{FC} = 0, Y_{FC,k} = -3 \\ P_{FC,k} & \text{if } Z_{FC} = 0, Y_{FC,k} = -2 \\ P_{FC,k} + \frac{\Delta P_{L,FC} \cdot P_{FC,k}^r}{\sum_k P_{FC,k}^r (Y_{FC,k} = 0)} & \text{if } Z_{FC} = 0, Y_{FC,k} = 0 \\ P_{FC,k} & \text{if } Z_{FC} = 0, Y_{FC,k} = 1 \\ P_{FC,k} & \text{if } Z_{FC} = 0, Y_{FC,k} = 2 \\ P_{FC,k} + \frac{\Delta P_{L,FC} \cdot P_{FC,k}^r}{\sum_k P_{FC,k}^r (Y_{FC,k} = 3)} & \text{if } Z_{FC} = 0, Y_{FC,k} = 3. \end{cases} \quad (5.38)$$

Storage control strategy – Three priorities are covered with the desired battery power calculation:

1. The main objective of the battery system is to ensure the power balance, which cannot be achieved with the SOFCs at all times. The total set power

for storage systems includes the opportunity for load peak shaving and is calculated as

$$P_{\text{B,set}}^{\text{tot}} = \sum_{k=1}^{N_{\text{FZ}}} P_{\text{FC},k} - P_{\text{L},k} , \quad (5.39)$$

2. To increase battery lifetime, a low specific power demand is targeted. Therefore, the set value is distributed evenly among the battery units to decrease degradation (cf. Eq. (5.40)).
3. One addition to priority 2 considers the deviation of the batteries' SoEs. Since fully charging or discharging one battery unit leads to potentially losing required balancing power, battery SoEs should ideally be at the same level. Consequently, during a power shortage emptier units provide less power, whereas for charging operation less power is assigned to higher charged units. A desired set value distribution is calculated with the case distinction

$$P_{\text{B,set},k} = P_{\text{B,set,tot}} \cdot \begin{cases} \frac{F_{\text{B},k} \cdot C_{\text{E,B},k}}{\sum_k F_{\text{B},k} \cdot C_{\text{E,B},k}} & \text{if } P_{\text{B,set,tot}} < 0 \\ \frac{(1 - F_{\text{B},k}) \cdot C_{\text{E,B},k}}{\sum_k (1 - F_{\text{B},k}) \cdot C_{\text{E,B},k}} & \text{else.} \end{cases} \quad (5.40)$$

Illustrative demonstration – For a better comprehensibility, the control strategy characteristics are demonstrated for a minimal working example in Appendix A.2 for both the fuel cells and the battery units.

5.5 Case Study

In this section, the case study ship and the investigated load profile are introduced, followed by a brief description of the conducted assessments with and without failure considerations.

Case study origin – The investigated case study is adapted from a measured load profile from [138]. The authors describe the electrical consumer behavior of a 330 m cruise ship with a tonnage of 156,000 GT. Total electrical energy demand, consisting of 65% navigation, lights, fans, air compressors, various pumps, and hotel load, 31% heating, ventilation, and air conditioning, 2% fresh water production, and 2% thrusters for harbor maneuvers, is presented in Fig. 5.6 (a).

Load data adjustment – Since the investigated load profile originally has a 10 minute time resolution, the data are superimposed with normalized typical fluctuating profiles in the seconds range. In this respect, two separate profiles for sea

operation and thruster maneuver operation are chosen to imitate more representative conditions. For the decentralization analysis, the combined load profile is divided into shares for each fire zone, based on the expected consumer positions (cf. Fig. 5.6 (b)). Nine fire zones are assumed, as one zone must not exceed the length of 40 meters [29]. Thrusters are located in fire zones 1 and 9.

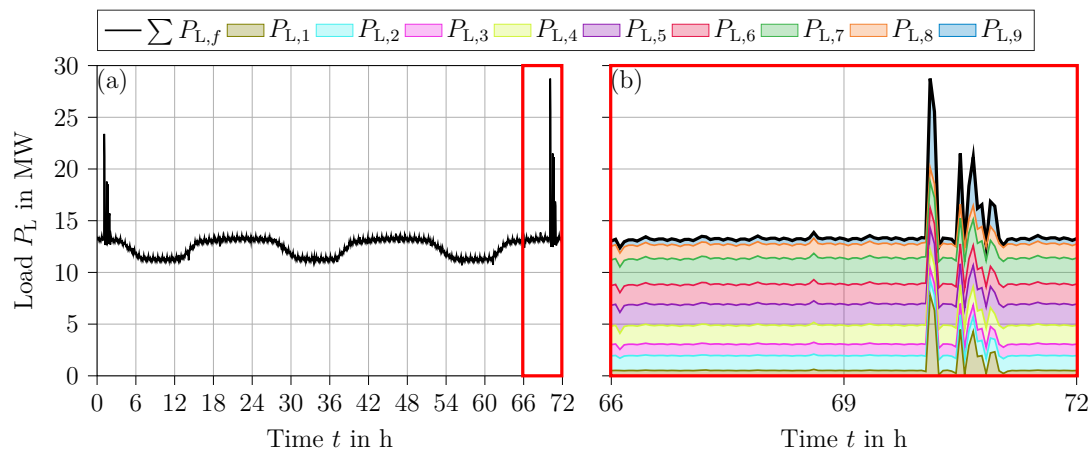


Fig. 5.6: (a) 72 h passage with total hotel load day-night rhythm and two harbor maneuvers, (b) second harbor maneuver load profile with separate and added up fire zone profiles.

Assessment description – The four different cases investigated in the analysis are summarized in Tab. 5.4 and described in the following:

- Case (1a) describes a central power system without SOFC or battery failure considerations ($\zeta = 1$, cf. Eq. (5.31)). This case functions as a benchmark to quantify the effects of component distribution on the reduction of the energy transmission system. It is assumed that all power units and batteries are installed in the stern of the vessel (fire zone $k = 1$), whereas the load distribution and the EMS strategy remain identical.
- Case (1b) allows a distribution of SOFC and battery units onto all nine fire zones but does still not consider component failures.
- Case (2a) considers component failures and the required redundancies with the additional scenarios $\zeta = 2$ and $\zeta = 3$ for a central configuration. For the battery failure scenario (since only one battery unit exists), one ninth of the capacity is defined to be unavailable, inspired by the number of fire zones in this case study.
- Case (2b) considers the possibility of distributed power system components and the requirements for component redundancy as explained in Section 5.3.

Tab. 5.4: Summary of the conducted assessments and their location in the following sections

	System approach	
	central	distributed
Without failure consideration (Section 5.6.1)	①a	①b
With failure consideration (Section 5.6.2)	②a	②b

5.6 Results and Discussion

Finally, system optimization results are discussed for a central benchmark case and a distributed configuration. With the described equation system and input values, cost optimal system designs are compiled for the presented four cases.

5.6.1 Assessment without Malfunction Scenarios

The first part of the analysis covers cases ①a and ①b to directly compare a central and a distributed configuration. The assessment results indicate an annual cost reduction of 206,000 € resp. 2.77% of the total system costs achieved by decentralization. Decreasing costs can be explained by the optimal system designs presented in Fig. 5.7: 47 SOFC units with a total rated power of 14.1 MW are installed in both cost-optimal configurations. The spatial power separation is given in Fig. 5.7 (a). For case ①b, the fuel cells are distributed to fit the local load profile’s average power or demand peaks.

Fig. 5.7 (b) displays the battery capacity distribution. In the central case ①a 37,499 cells with a total energy capacity of 3,460 kWh are implemented. For case ①b a 20% larger overall battery capacity is found to be cost-optimal. Hereby, the largest units are located in the first and the last fire zone to reduce peak transmission values during thruster maneuvers. Battery “gaps” in every second fire zone and larger storage units inbetween create the possibility of one zone supporting two neighboring fire zones.

Fig. 5.7 (c) displays an overall decrease of the power transformer sizes in case ①b compared to case ①a without an apparent pattern. As expected, the largest size reduction is located in fire zone 1. An exception for fire zone 3 can be explained with the continuous support of fire zones 2 and 4, which both have a larger consumer demand (cf. Fig. 5.6 (b)). The smaller sizing accounts for the first of three cost reduction shares.

In Fig. 5.7 (d) the configuration for central case ①a mostly resembles the second thruster maneuver, where a large amount of power is required in the ship’s bow (fire

zone $k = 9$) and transported through all other zones. As the other zones demand power as well, a stepwise decrease is recognizable. For case (1b) a reduction to only two installed cables per connection is achieved. As two parallel cables are required to comply with the provided grid redundancy, the cost minimum is reached. The reduction from 4960 to 920 meters cable represents the second share to reduce annual costs.

Decreasing transmission losses result in the third cost reduction share. To display the effects of system decentralization, average power flows in transformers and cables are displayed in Fig. 5.8 for both the central and the distributed system.

Fig. 5.8 (a) shows the average power transmission between fire zones. While the fixed configuration for central case (1a) again results in a monotonous decrease, the distributed approach (2a) shows a general power flow reduction with especially small values for connections 1, 5, 6, and 7. Fire zone 4 receives the most support from its neighbors due to minimized dimensions of storage and a comparatively small fuel cell system. Fire zone 9 supports other zones due to its oversized components except for the bow thruster maneuvers, where it receives additional support.

Fig. 5.8 (b) shows the average power delta in each fire zone: in the central case (1a) the bars mostly resemble the characteristics of the load profile, as no other system components are placed in fire zones 2 to 9. As expected, in the distributed case (1b) the smaller utilization of power transformers on average and massive reduction in fire zone 1 is recognizable.

Now that component designs and operating behavior are covered, resulting annual costs for the central and the distributed approach are broken down in Fig. 5.9 (a). SOFC system and fuel consumption account for the largest cost shares, which come out nearly identical for both central and distributed approaches due to the component design and energy management strategy. The 20% larger battery selected for case (1b) only accounts for a cost increase of 2.3%. This can be explained with reduced degradation resulting from smaller specific loads for the battery cells: while the average battery lifetime is estimated as 8.1 years for case (1a), the distributed units reach their end of life after 9.9 years. The small cost increase for larger battery units in case (1b) pays off by reducing the transmission infrastructure significantly.

A detailed description of power transmission expenses is given in Fig. 5.9 (b). Costs for grid components and extra fuel consumption are reduced by more than 76% compared to a central approach. Here, decreased transformer sizes make up the largest cost share. As long as no failure scenarios are considered, the achieved annual cost reduction accounts for 5.3% of the capital investment or 2.77% of the total considered power system costs.

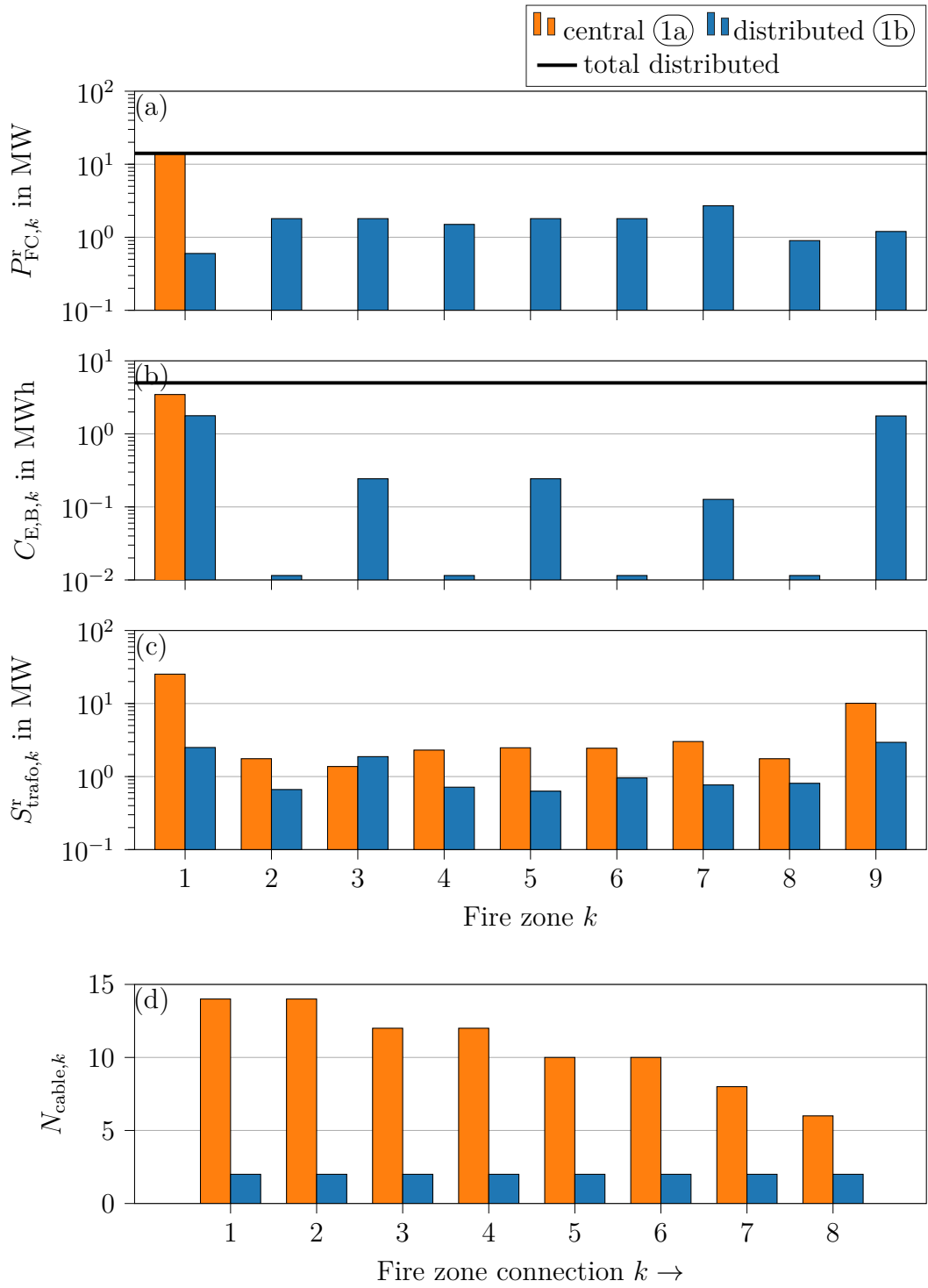


Fig. 5.7: Cost-optimal SOFC and battery unit distribution, resulting power transformer and cable design for a central and a distributed system without component failure consideration ($\zeta = 1$)

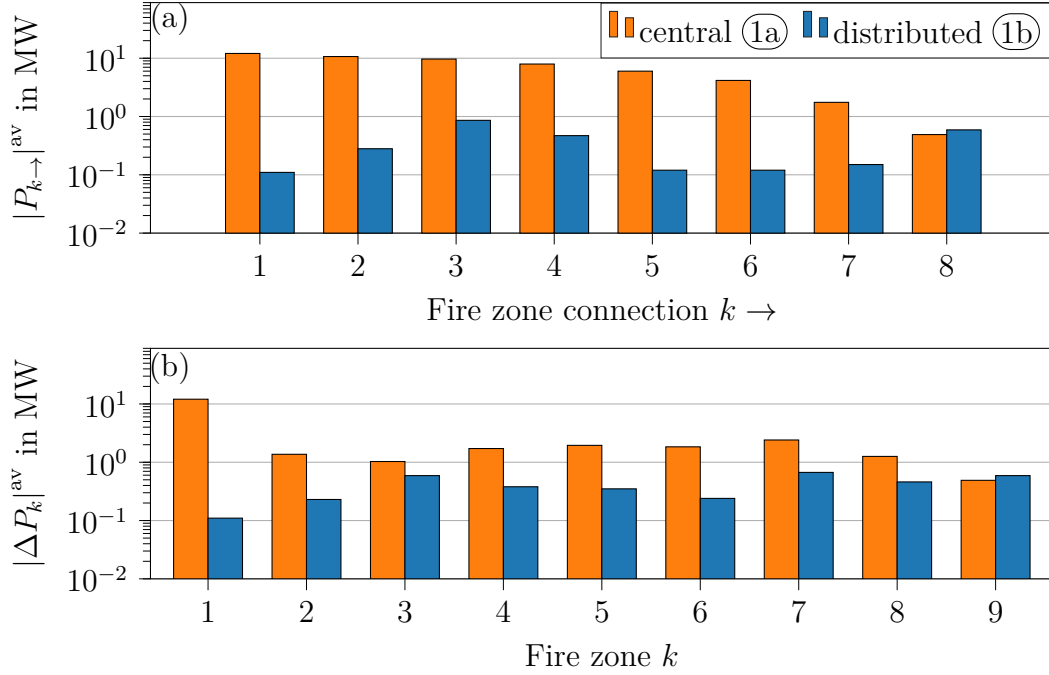


Fig. 5.8: Average grid power flow $|P_{k \rightarrow}|^{\text{av}}$ and average transformer power transmission $|\Delta P_k|^{\text{av}}$ for a central and a distributed system without component failure consideration

Of course, the cost reduction percentage is influenced by model and parameter inaccuracies: it rises with increasing fuel prices and transmission system investment costs, as it decreases with higher specific battery and fuel cell prices. However, throughout several sensitivity analyses concerning the assumed cost parameters (SOFC: 1500–3000 €/kW, battery: 600–1000 €/kWh, power transformer: 50–150 €/kVA, LNG price: 10–50 €/MWh, interest rate: 0.01–0.05) neither a tipping point regarding the qualitative results, nor a disproportionate impact of one single parameter on the quantitative results is found. Higher LNG prices and lower SOFC investment costs induce an increase of fuel cell rated power up to 16.2 MW to optimize the specific operating point and thereby minimize fuel consumption. Smaller battery costs imply a cost-optimized design with only marginally larger storage units to further reduce power transformer sizing. Nevertheless, the observed component distribution arrangement remains unaffected qualitatively.

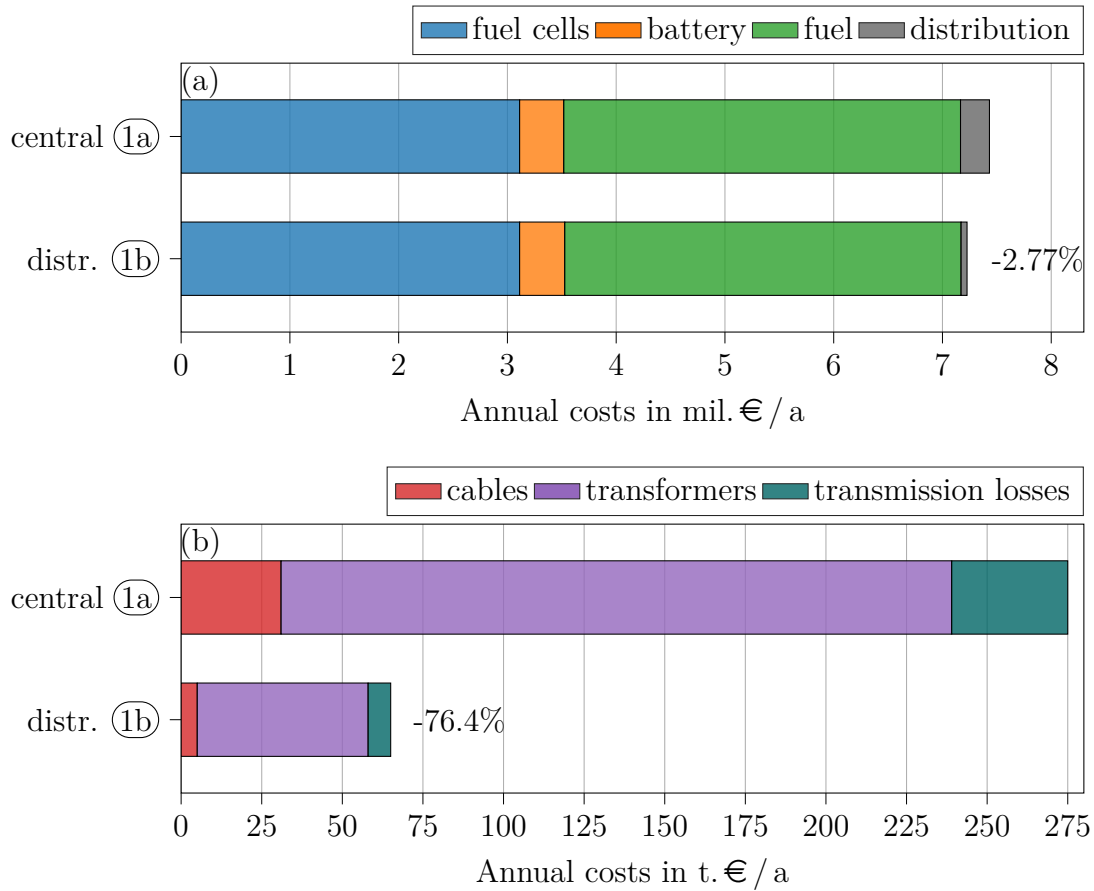


Fig. 5.9: (a) Annual costs for a central and a distributed system without component failure consideration; (b) detailed presentation of the power-distribution-related costs

5.6.2 Revised Assessment with Component Malfunction Scenarios

The second part of the assessment covers the cases (2a) and (2b) with the goal of quantifying additional costs to achieve component redundancy. To examine how the optimal distribution is affected when including component malfunction scenarios $\zeta = 2$ and $\zeta = 3$, the revised optimal configuration given in Fig. 5.10 is compared with the previous design (cf. Fig. 5.7). Fig. 5.10 (a) displays the revised fuel cell unit distribution. The total numbers of installed fuel cells remain identical for both the central case (2a) and the distributed case (2b), even though a unit failure is required to be compensated. The distribution for case (2b) changes along with a major battery unit restructuring, to lower the transmission components. Still, the division is influenced by the load profiles' average and peak powers.

While a storage size increase of 11% would be sufficient to compensate the malfunction for the central case (2a), the battery is designed larger to also com-

pensate an SOFC unit failure (cf. Fig. 5.10 (b)). For case (2b) a surprising overall decrease of battery capacity is observable compared to case (1b) without failure consideration. This can be explained on the one hand with the now reduced synergy achievability for the reduction of the transmission components. On the other hand, the tradeoff between higher investment costs for larger batteries and their resulting longer lifetime is reduced due to the increased power compensation demand. Therefore, a stronger intent to reduce the capacity exists. Larger battery systems for the bow thruster operations are now avoided to reduce the number of malfunctioning cells in the failure scenario. Instead, the optimization results in a relatively even distribution. As a result, 19.4% of the total battery capacity is lost in case (2b) during worst-case unit malfunction.

While Fig. 5.10 (c) and (d) display no design change for the central case (2a) compared to (1a), the power transformer sizing for distributed case (2b) must be increased in all fire zones but zone 3 compared to case (1b). Additional cables towards the outer fire zones are also required for thruster maneuver support. Still, the power transmission components of the distributed system remain smaller compared to the central approach. As expected, the redundant grid designs allow operation during component malfunction scenarios without further measures.

The costs resulting from the revised design and deviations from the previous analysis are given in Fig. 5.11 (a). The consistent SOFC and fuel costs between cases are linked to the identical fuel cells' sizing. For case (2a) a larger battery equals less stress in regular operation, which results in a longer lifetime compared to case (1a). Therefore, no proportional cost increase is registered. To achieve redundancy of the central system, less than 0.5% higher cost effort is required with the modular component approach.

For the distributed case (2b) a battery cost increase is calculated despite the smaller capacity compared to case (1b). Since the distribution of the components is conducted with the two malfunction boundaries, the specific load demand from the storage units increases due to a suboptimal distribution. This effect results in a smaller battery lifetime of 9.39 years in this case and therefore increases annual costs. Nevertheless, redundancy is achieved with a cost increase of 1.57% compared to the annual costs of a distributed system without failure consideration. However, total system savings from decentralization are further reduced to 3.3% of the capital investment costs and 1.7% of the total annual costs due to an 76.9% increase of the transmission component costs (cf. Fig. 5.11 (b)).

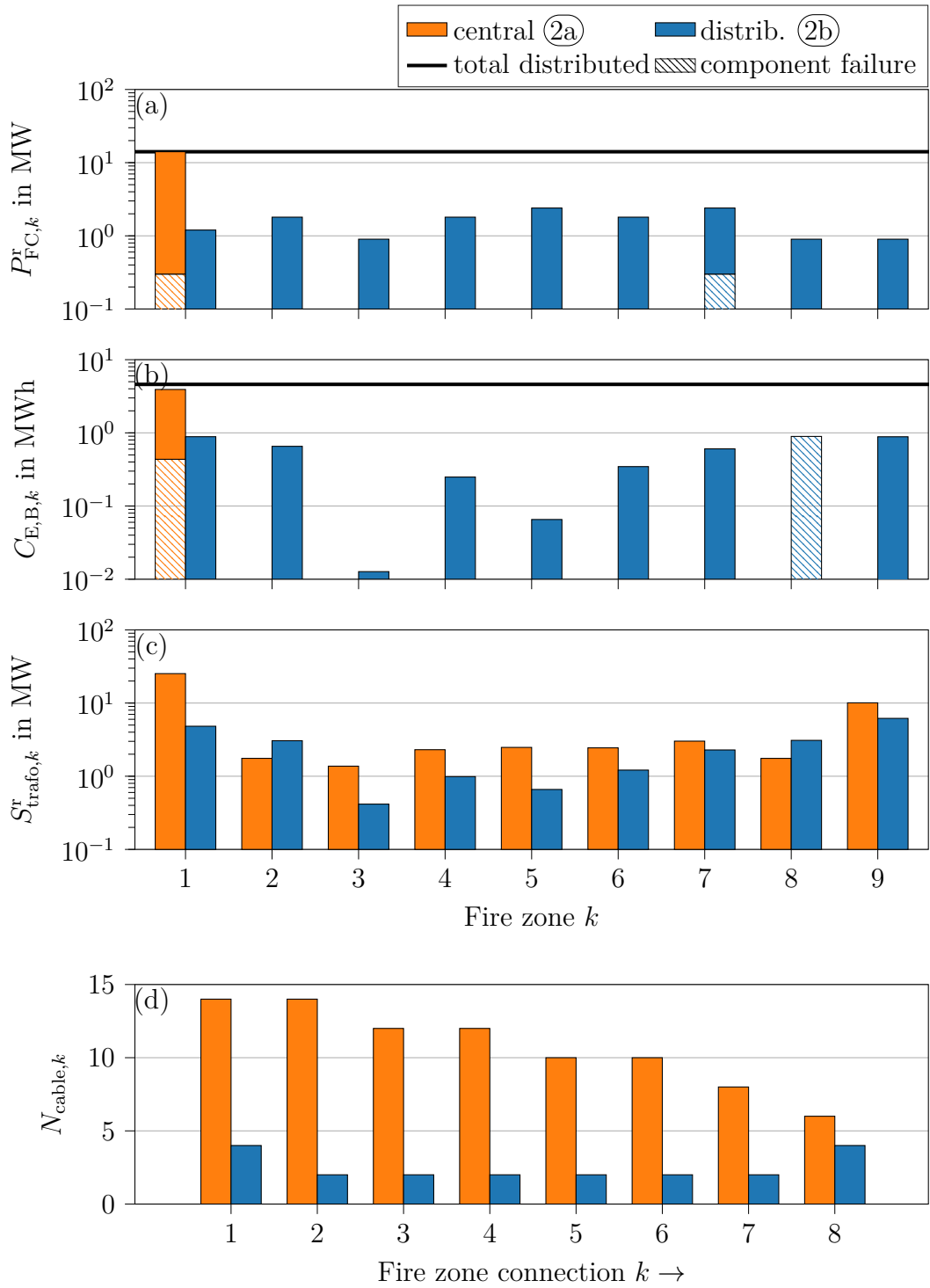


Fig. 5.10: Cost-optimal distribution of the central and distributed power system units and resulting power transmission component design when considering malfunction scenarios: shaded bars resembles the failing components for the two emergency scenarios ($\zeta = 2$ and $\zeta = 3$)

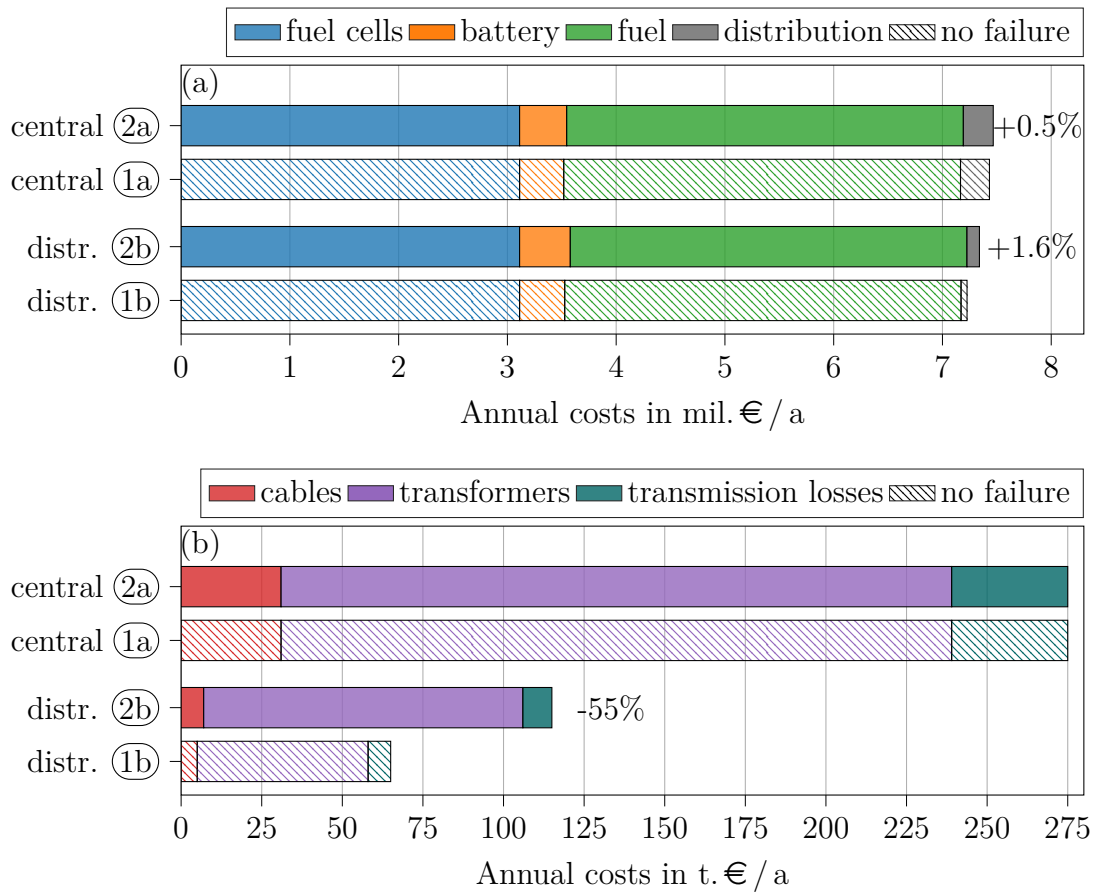


Fig. 5.11: (a) Annual costs for systems with central and distributed components with failure consideration and comparison with previous design in parentheses (cf. Fig. 5.9); (b) detailed presentation of the power-distribution-related costs

5.7 Interim Conclusion

The presented cruise ship case study with model-based design optimization and rule-based energy management strategy outlines the advantages of a distributed ship power system with SOFC and battery units over a central system configuration. In the following, all detailed questions regarding research issue [3] introduced in Section 2.3 are answered individually.

[3.1] What quantitative benefits can the transmission grid of a distributed power system have over a central approach?

Grid perspective – The conducted cruise ship case study demonstrates that a system distribution approach vastly reduces both the required high-voltage cable

and power transformer dimensions, as well as transmission losses. The redesigning thereby obtains a notable annual grid cost reduction. Additionally, no interfering impact on components' behaviors regarding SOFC fuel consumption and battery degradation are projected.

System perspective – However, cost savings appear small compared to other investigated matters of expense and might be outweighed by ship construction stipulations. It is questionable if the cost savings of a power system decentralization justify the complete ship built restructuring effort, even though cost reduction effects are demonstrated. Extra costs arise from potentially required mechanical reinforcements, electrical protective mechanisms or explosion prevention equipment in the numerous engine rooms.

Supplemental arguments – Still, four other qualitative arguments for the distributed approach remain:

1. For current fuel prices it is shown that transmission loss reduction makes up the by far smallest share of operating costs. This statement is not maintained with heavily increased fuel prices resulting from environmental fees or the introduction of synthetic fuels to significantly lower CO₂ emissions. Here, the savings rise proportionally with larger fuel expenses.
2. SOFC operation under cogeneration mode to fulfill the ship's thermal energy demand for heating, freshwater production, and laundry service would result in another opportunity for transport loss reduction through distribution. As heat transport entails significantly larger specific losses, system decentralization would have a high impact here.
3. No zonal malfunctions but only component failures were analyzed. While a central engine room failure would have fatal consequences in a worst-case scenario, the spatially distributed configuration would still be partly operable.
4. The redundancy aspects of the distribution approach still are another argument to be exempted from emergency power generators and thus significantly reduce additional costs. Admittedly, while this argumentation seems reasonable for now, the idea first requires formal examination by the *International Maritime Organization*.

While three of the given four reasons for system distribution again can be quantified, at this point a holistic expenditure for mechanical restructuring also is required for a clear comparison at this stage of planning.

3.2 Is the optimal decentralized system design solution modified when malfunction scenarios are considered?

Fuel cells – From the SOFC perspective, neither the distribution approach nor the consideration of malfunction changes the numeral outcome of the system design optimization. Here, the failure of one unit is compensated by the supporting batteries without a larger effort. The unit distribution is mainly aimed at the load demand but a reciprocal orientation with the battery unit configuration is identified as well.

Batteries – By contrast, the battery decentralization results are vastly dependent on the assessed scenario: while large storage modules are located at the ship’s stern and bow to massively support thruster operation, an uneven distribution is later on discarded to prevent a large capacity breakdown. Instead, a relatively even unit distribution is aspired, increasing transmission losses and grid sizing.

Economic results – The conducted scenarios with and without failures show that configuration synergy and therefore cost reduction effects resulting from the distribution approach decrease when considering potential component malfunctions. In the case study, the reduction potentials of 76% without failure consideration decrease to 55% when considering battery failures, resulting in an overall annual power system cost reduction of 1.7% when including fuel expenses.

3.3 To what extent does a ship power system benefit from the components’ modularity regarding component redundancy?

Results of the four case studies certainly indicate that both central and distributed modular configurations allow for an easily achievable component redundancy. Here, marginal modifications resulting in less than 2% annual cost increase are sufficient to create component redundancy for both the central and the distributed system. Due to the case study design, which only addresses component malfunctions but no zonal emergencies, investigated benefits are mostly attributed to the modular component characteristics and not the decentralization.

Quantifying the cost savings from the distribution approach and the additional costs incurred for a redundant system should at this point suffice to answer the third research issue “[3] How can the advantage of a fuel cell’s modular characteristic be leveraged in large-scale ship power systems?”.

6 Economic and Environmental Assessment of Power Technologies under Discussion for Future Ship Applications

The third analysis addresses a direct comparison of the most envisaged power technologies and fuels under consideration for today's and future ship applications. Thereby, an assessment of their economic and environmental performances is conducted to support an ongoing decision making process of the industry's participants, of which the completion is of major importance for the sector. Currently, a hen-and-egg problem must be solved: Early investments into specific power generation technologies require the safety of fuel supply in particular ports. On the other hand, establishing a fuel infrastructure calls for the security of customers. Therefore, only when the number of discussed future fuel approaches is reduced significantly, much required large-scale fuel supply chains can be established with a reasonable investment security [64], [65]. Concurrently, ship owners then can start to modify their fleets accordingly, as they receive reliability of supply.

This chapter is organized as follows: Section 6.1 offers an overview of the investigated technologies including their technology readiness. In Section 6.2 the system models for investigated technologies including economic and environmental descriptions are given. In Section 6.3 the optimization task is again revised to fit the assessment goals. In Section 6.4 a universal system control strategy is introduced. In Section 6.5 technology comparisons are presented starting with a benchmark scenario of state-of-the-art combustion engines. Then, for a comprehensive future scenario, a focus is set on the ship's mission characteristics, fuel price development and potentially increasing shipboard volume opportunity costs. Finally, research issue [4] is addressed in Section 6.6.

Disclosure: The following chapter is based on the publications: L. Kistner; F.L. Schubert; C. Minke; A. Bensmann; R. Hanke-Rauschenbach, Techno-economic and Environmental Comparison of Internal Combustion Engines and Solid Oxide Fuel Cells for Ship Applications, *Journal of Power Sources* (2021) [38] and L. Kistner; A. Bensmann; C. Minke; R. Hanke-Rauschenbach, Comprehensive techno-economic assessment of power technologies and synthetic fuels under discussion for ship applications, *Renewable and Sustainable Energy Reviews* (submitted) [61]. For a detailed description of the author contributions see Appendix C.

6.1 State-of-the-art and Future Power Technologies

In order to create a basis for the conducted analysis, this section will introduce selected fuels and power technologies and support this with examples of industry or research projects. The present assessment covers the two most widespread conventional power technologies, the compression-ignition and the spark-ignition combustion engine, for a year-2020 analysis, as well as several ICE, SOFC, and PEMFC technologies for the year-2030 assessment. Thereby, the following electro-fuels are investigated: Fischer-Tropsch diesel (FTD), liquefied substitute natural gas (SNG), ammonia (NH₃), methanol (MeOH), liquified hydrogen (LH₂), and compressed gaseous hydrogen (CGH₂). Further, a potential system hybridization with battery units is considered for each investigated technology. Fig. 6.1 gives an overview of today's and theoretically conceivable future configurations of technologies and fuels in a matrix. While all matrix combinations are briefly discussed in the following, only serviceable solutions are marked with a ship pictogram. Note that the assessment excludes fuels recovered from biomass since their production capacity is limited and will nowhere near cover the demand of the shipping industry [63],[139]. This stance is even more valid when considering that biofuel capacities are contested by other sectors due to their comparably small prices [140]. Moreover, the authors of [62] state that the emerging orientation towards biofuels will harm the overall required supply capacity of sustainable fuels by impeding the up-scaling of the electrofuel production. Therefore, solely fossil fuels and electrofuels are assessed in this study, as they are evaluated to be the only sector-overarching fuel solutions. In the following, the assessed power technologies are introduced in detail, grouped in four categories: state-of-the-art ICEs, potential future ICEs, SOFCs, and PEMFCs.

Internal combustion engines in 2020 – Today, diesel combustion engines are by far the most commonly used ship power technology with a market share of 98%. 73% of them were operated on marine heavy fuel oils (HFO) with a sulfur share of up to 3.5% in 2018, followed by marine gas oils (MGO) at 25% [141]. However, since the year 2020 heavy fuel oil combustion is only permitted in combination with an exhaust gas cleaning system also called sulfur scrubber [8]. An alternative to installing a scrubber is the use of very low sulphur fuel oils (VLSFO) with a sulfur content of up to 0.5% to comply with *MARPOL* (cf. Chapter 1). While this allows operation in open sea, special zones with a 0.1% limitation already exist [142]. Since VLSFO is predicted to heavily increase in relevance due to the sulfur regulations, it is chosen as a default fuel for the conducted benchmark assessment.

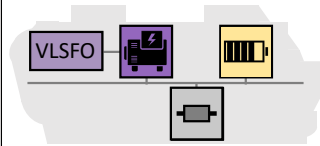
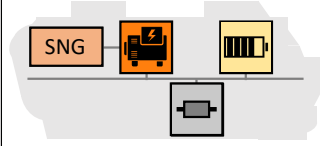
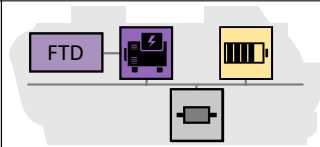
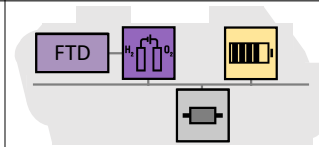
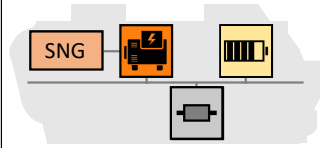
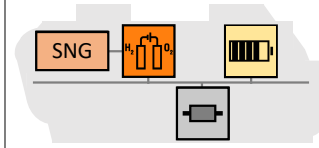
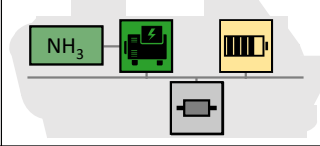
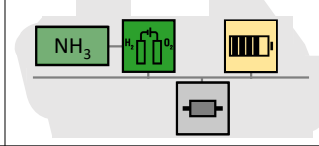
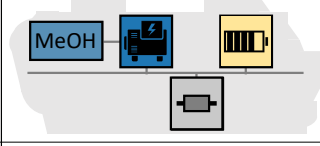
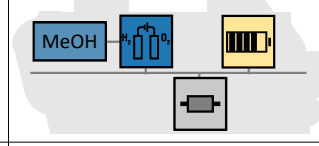
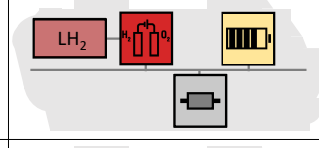
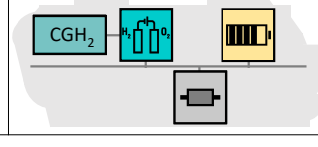
Benchmark assessment (2020)			
	ICE	SOFC	PEM
VLSFO			
LNG			
Future assessment (2030)			
	ICE	SOFC	PEM
FTD			
SNG			
NH3			
MeOH			
LH2			
CGH2			

Fig. 6.1: Considered hybrid system configurations for the benchmark study (year 2020) and the future assessment (year 2030) – ship pictograms represent practical/investigated applications. The chosen color scheme is reused in the assessment.

For ICEs in the investigated dimensions, 4-stroke engines are selected over 2-strokes with lower rotation speed and comparably lower friction losses, since latter are utilized only for the largest power outputs and are designed mainly for propulsion instead of auxiliary power [143], [144].

The tightening of sulfur limitations and the greenhouse gas emission reduction targets also result in a growing interest in LNG as ship fuel. LNG contains close to no sulfur and is also less expensive than low-sulfur diesel fuels [145],[120]. Standard natural gas consists of 87-96% methane. During its combustion, approximately 25% less carbon dioxide is emitted per energy unit compared to heavy fuel oils [146],[147]. LNG-based ship power system numbers are growing by up to 40% per year, and while not many ships are retrofitted with gas engines, more than 10% of newly built deep-sea orders are LNG-fueled [148]. For LNG-ICE ship applications, lean burn spark ignition engines are considered over dual fuel engines for rated powers from 0.5 to 8 MW due to their lower fuel slip [146].

Internal combustion engines in 2030 – For ICEs in the 2030 scenario, the analogous application of FTD and SNG requires only minor effort in state-of-the-art technologies. Proof of concepts for operation with synthetic fuels exist (e.g. the vessel *ElbBlue* [149]).

Ammonia is already occasionally utilized in dual-fuel engines combined with diesel to reduce operating emissions [150]. However, for single-fuel operation in either spark- or compression-ignition engines, the flame stabilization requirements and the high compression ratio are identified weaknesses of the fuel. While pure NH₃ combustion is a topic of research [151], dual-fuel approaches with an upstream ammonia cracker and the combustion of a hydrogen-ammonia mixture [66] are a promising workaround for the remarked issues. Already today, marine engine manufacturers put high effort into solving these mentioned difficulties (e.g. *Wärtsilä* [152], *MAN Energy Solutions* [153]).

Methanol has a high knock resistance, making it suitable for spark ignition engines. Conversely, its small cetane number complicates the combustion in compression ignition engines and proper usability is given only for mixtures with ignition improvers (e.g. diesel dual-fuel engines), air heaters, and glow-plugs [154]. However, today's use cases show a trend toward compression ignition as the preferred technology in the shipping industry to achieve fuel flexibility and not create a reliance on MeOH. For future applications of single-fuel methanol compression ignition engines, partially-premix processes with high efficiency are indicated to be the go-to solution [155]. In contrast to ammonia combustion, the possibility to partially create hydrogen via steam reforming is not highly followed recently [156]. Industrial MeOH applications include recent efforts of engine manufacturers (e.g. *Caterpillar* [157]), as well as applications on methanol ocean tankers (e.g. *Waterfront Shipping* [158]), the large-scale ferry *Stena Germanica* with dual

fuel engines [159], and several cargo vessels (e.g. operated by *A.P. Moller-Maersk* [160], *X-Press Feeders* [161]).

Hydrogen combustion is a topic of interest for dual-fuel engines with a fuel share of up to 20% [162],[163] and represents a possibility to reduce operating emissions of existing engines. While hydrogen-only combustion engines are discussed to be introduced into the shipping sector at the end of this decade, transient operation and fuel injection controls still are a vast concern for the manufacturers [164]. However, at this point it is very questionable if a future H2-ICE concept will outclass a hydrogen fuel cell for the following reasoning: the PEMFC technology entails a high conversion efficiency in full and part load, high power density, no operating nitrogen oxide emissions, and a very fast load shift time, while implying mainly one restriction: the supply of clean hydrogen. If a shipboard hydrogen storage is provided anyway, fuel cells are most definitely the superior power technology over combustion engines today and in the future. Therefore, H2-ICEs are neglected in this case study.

Solid oxide fuel cells – The dynamic operation of SOFCs with FTD or SNG requires an upstream steam reforming process, which utilizes the fuel cells' waste heat for hydrogen generation [165],[78]. Since SOFCs are resilient to carbon monoxide, no complex purifying process is required. The shipboard steam reforming SOFC combination is arguably still in its research phase and not commercially available today. However, research projects (e.g. *MultiSchIBZ* [166], *Nautilus* [167], *HelenuS* [168]) and commercial product development (e.g. by *Bloomenergy* [169]) concentrate on advancing this technology.

Ammonia is also of high interest for SOFC applications. In contrast to the carbon-based fuels, NH₃ represents the possibility of unproblematic internal thermal fuel cracking to provide hydrogen [170]. Still, the advantages of a better unit control and increased cell lifetimes persist for a plant with external reforming. Here, faster load shifts (up to 1.26%/s with hydrogen [171] vs. 0.003%/s with ammonia [66]) can be achieved with higher investment costs for peripheral components but entail potentially worse heat utilization rates. Since input fuel mixtures of hydrogen and nitrogen do not massively influence the system efficiency [172], a larger focus is set on the direct use of ammonia with an off-gas afterburner for heat supply. While there exists no manufacturer for commercial shipboard modules known to the authors, the *ShipFC* joint research project is investigating the technology's potentials [173].

As opposed to FTD and SNG, methanol does not require temperature on the SOFCs' level for steam reforming [174]. This leads to a smaller advantage of the excess heat and simultaneously makes high temperature PEMFCs a direct competitor. One example for this application is the *METHAPU* research project, which closed in 2010 [175]. However, since no active research and thereby no state-

of-the-art data exists known to the author, this combination is not assessed in this study.

Better performance indicators of the PEMFC are also the reason why hydrogen is not considered as potential fuel for SOFCs in this study. Here, the slightly higher efficiency of SOFCs compared to PEMFCs is surpassed by the PEMFC's higher power density and smaller investment costs.

Proton exchange membrane fuel cells – The potential selection of fuels for the PEMFC technology is noticeably reduced compared to ICEs and SOFCs. Ship-board hydrogen production from FTD, SNG, and NH₃ involves temperature levels exceeding the values of today's PEMFC systems. On the other hand, supplementary heat sources and the technology requirements for purified hydrogen [71] massively reduce the achievable system efficiency of these combinations compared to other configurations. Even if examples of external ammonia cracking are theoretically given in the literature [50], [66] no large-scale projects are known to the author. Therefore, these three options are not considered in the study.

Due to a smaller temperature requirement of MeOH steam reforming, a high-temperature PEMFC can be operated with an upstream steam reformer and fuel cell heat extraction. While the recirculated thermal energy can likely cover the heat demand, internal calculations suggest an autothermal reforming process for lower part load operation. Here, a small share of the methanol reacts chemically with oxygen to generate the required heat for the steam reforming process. Electrical preheating features a less complex alternative, although impairing the system efficiency to a higher degree. Several commercial projects (e.g. the vessel *Hydrogen One* [176], tests by *Alfa Laval* [177]) and academic research efforts (e.g. *Pa-X-ell2* [178], *Rivercell* [179]) can be reported in the last years.

The PEMFC-hydrogen combination is an advanced technology already introduced to the shipping sector. Compared to SOFCs, the technology's main advantage is its realizable higher maximum cell current, which results in a vastly increased power density. While hydrogen fell out of favor in the discussion for open-sea shipping due to the small volumetric energy density, ship owners announced to utilize H₂-PEMFCs to operate in restricted areas (e.g. *Royal Caribbean Group* [180], *MSC Cruises* [181]). As opposed to other fuel cells with additional conversion steps, H₂-PEMFC units are already successfully sold (e.g. by *Proton Motor* [182]), and first type-approved modules for ship applications (e.g. by *Ballard* [183]) are already available for order. The transport of hydrogen is realized in either cryogenic form with the advantage of a higher gravimetric (fuel tank) and volumetric energy density, or in compressed form, with smaller energy commitment and preferable distribution attributes [184]. For LH₂, few examples of use exist (e.g. the ferry *MF Hydra* [185]), whereas more small vessels are planned to operate on CGH₂ (e.g. the cargo ship *Zulu* [186], the project *HySeas III* [187]).

6.2 Additionally Required Models

In this section, the equation systems for the component models (cf. Fig. 3.4: physical model, component management, economic model, environmental model) and a unified system control strategy are introduced. To recall the system model approach discussed in Chapter 3, the required model elements and the overall scope of the analysis are depicted in Fig. 6.2.

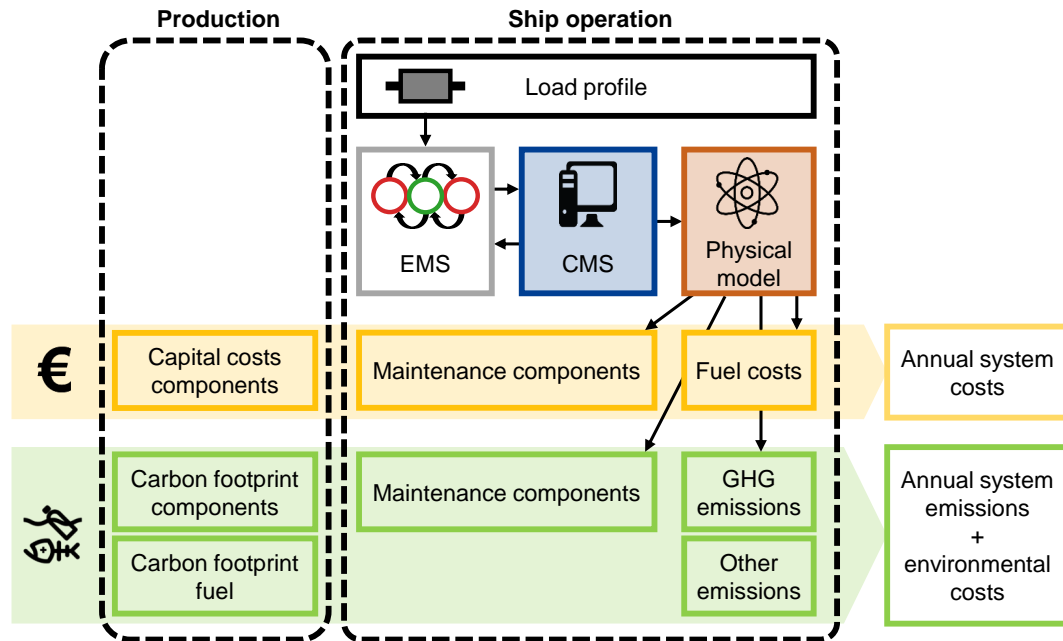


Fig. 6.2: Scope of the economic (yellow) and environmental (green) assessments, influenced by the production phase (cradle-to-gate, well-to-tank) and the system behavior (gate-to-grave, tank-to-wake), modeled in analogy to the concept introduced in Chapter 3.

The key economic elements (yellow) include the component investment costs as well as maintenance and fuel expenses for the ship operation segment. The latter are influenced by the ship's load profile and resulting system responses (top). The system behavior is also taken into account for the environmental assessment (bottom, green). Analogous to the economic analysis, components and fuels are investigated for the preparation and operation phases. Total systems costs and emissions are then evaluated for the technology comparison.

6.2.1 Physical Models

Power Generation Units – As already described in Section 3.2.1, the physical model of a power generator mainly consists of the fuel mass consumption descrip-

tion for a specific voyage m_{fuel} . Again, this is calculated for the time-dependent generator power and the relative operating point:

$$m_{\text{fuel}} = \int^{t_{\text{op}}} \dot{m}_{\text{gen-fuel}}^{\text{spec}}(P_{\text{gen}}, t) \cdot P_{\text{gen}}(t) dt, \quad (6.1)$$

where the index “gen” is a placeholder for either ICE or one fuel cell (FC) type, and $\dot{m}_{\text{gen,fuel}}^{\text{spec}}$ is the specific fuel consumption (SFC) given in Fig. 6.3 (a). For a better comparability of the technologies, the respective operating-point-dependent efficiencies are also shown in Fig. 6.3 (b). Assumed values for future technologies hereby include prognoses for technical advances until the year 2030. A detailed literature-reference-based description of the fuel consumption is given in Appendix B.1.

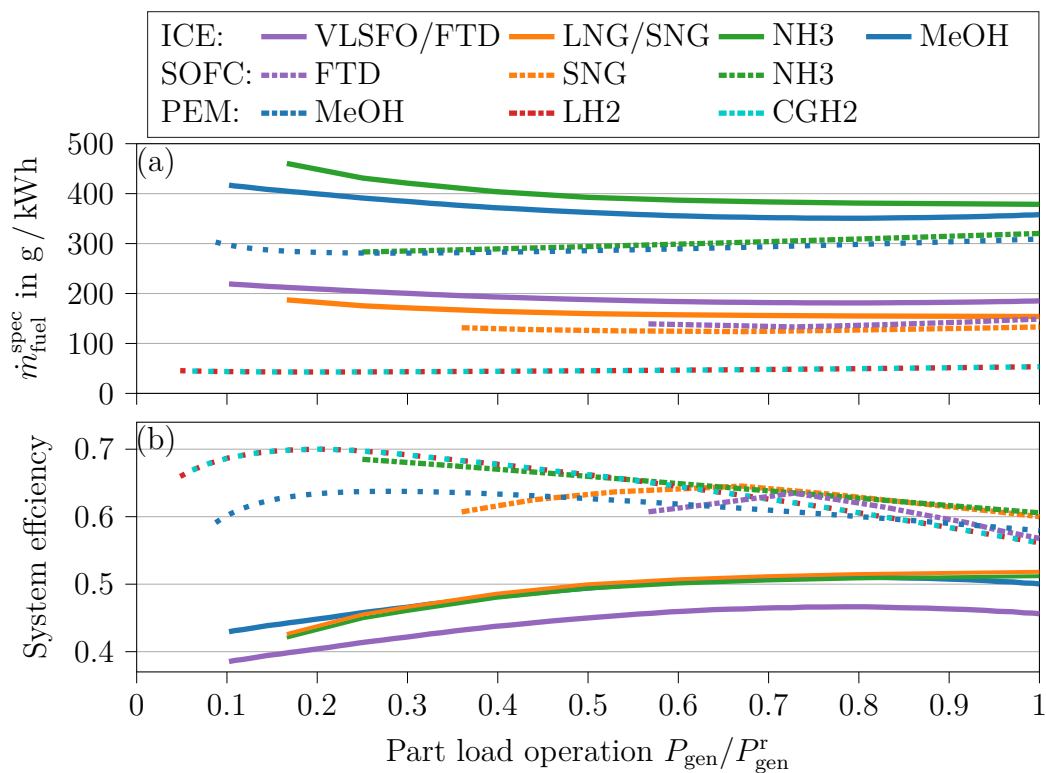


Fig. 6.3: (a) Operation-specific fuel consumption (SFC) of the investigated fuel-technology combinations, (b) resulting fuel efficiencies based on lower heating values.

Battery Units – For the assessment, the straightforward unified storage model is utilized to describe the physical behavior of the battery unit (cf. Section 3.2.2). As demonstrated in Chapter 4, no relevant oversimplifications are indicated for this part of the battery model.

6.2.2 Component Management

Power Generation Units – Analogous to the description of the SOFC’s operating limitations in Section 3.4.2, a general version describing minimal and maximal power output, as well as load change limitation is given to cover all investigated power technologies:

$$P_{\text{gen},j} \leq P_{\text{gen}}^r \quad (6.2a)$$

$$P_{\text{gen}} \geq P_{\text{gen,rel}}^{\text{min}} \cdot P_{\text{gen}}^r, \quad (6.2b)$$

where $P_{\text{gen,spec}}^{\text{min}}$ is the relative minimum operating point given (cf. Tab. 6.1) and

$$\left| \frac{dP_{\text{gen}}}{dt} \right| \leq \dot{P}_{\text{gen,rel}}^{\text{max}} \cdot P_{\text{gen}}^r, \quad (6.3)$$

where $\dot{P}_{\text{gen,spec}}^{\text{max}}$ is the maximum power gradient of a technology (cf. Tab. 6.1). For fast-reacting power sources like ICEs without prereforming processes and the H₂-PEM combination [188], a relative maximum power gradient of 100%/s is assumed, which is theoretically sufficient to cover the analyzed load profiles without support.

Tab. 6.1: Operating limitation parameters for the power generator-fuel-combinations (parameters without source are obtained by manufacturers or internal calculations)

	VLSFO ICE	LNG ICE	FTD ICE	FTD SOFC	SNG ICE	SNG SOFC
$P_{\text{gen,rel}}^{\text{min}}$ in -	0	0	0	0.567	0	0.5
$\dot{P}_{\text{gen,rel}}^{\text{max}}$ in s ⁻¹	1	1	1	1.67·10 ⁻³	0.008 [66]	3·10 ⁻⁴ [66]
	NH3 ICE	NH3 SOFC	MeOH ICE	MeOH PEM	LH2 PEM	CGH2 PEM
$P_{\text{gen,rel}}^{\text{min}}$ in -	0.05 [66]	0.25	0	0.11	0.06 [66]	0.06 [66]
$\dot{P}_{\text{gen,rel}}^{\text{max}}$ in s ⁻¹	1	1	1	0.03 [189]	1	1

Battery Units – For the battery units, the introduced heuristic approach again is utilized to describe the operating limitations of the battery unit (cf. Section 3.2.2)

6.2.3 Economic Models

In the following, economic models for power generation units, fuel consumption, battery units, and the newly introduced volume opportunity costs are listed.

Power Generation Units – The economic description of the power generation units is generalized to cover all assessed technologies. In addition, system volume

information is given here to lay the foundation for the volume opportunity cost calculation. The annuity payments of ICEs and FCs are calculated with

$$p_{\text{gen}}^{\text{a}} = p_{\text{gen}}^{\text{inv}} \cdot N_{\text{gen}} \cdot (P_{\text{gen,mod}}^{\text{r}})^{g_{\text{gen}}} \cdot (A_{\text{gen}} + c_{\text{gen}}^{\text{a}}) , \quad (6.4)$$

where $p_{\text{gen}}^{\text{inv}}$ are the power-specific investment costs including a possibly required fuel reformer unit, g_{gen} describes the potential nonlinear power-cost relation, $c_{\text{gen}}^{\text{a}}$ are the annually accruing specific maintenance costs, and A_{gen} is the annuity payment factor depending on the generator's lifetime $t_{\text{L,gen}}$:

$$A_{\text{gen}} = \frac{(1 + j)^{t_{\text{L,gen}}} \cdot j}{(1 + j)^{t_{\text{L,gen}}} - 1} . \quad (6.5)$$

Since the study aims to forecast the year 2030, technology cost advances are predicted: while the main investigations for ICEs are to estimate additional costs to achieve fuel accessibility, fuel cell system prices are predicted to fall tremendously with increasing production capacities and advanced material usage. However, not all system solutions will be priced identically, as production scaling effects and requirements differ from case to case [190]. Modules for ships will most likely be more expensive than for automotive applications due to smaller scaling effects and manufacturer requirements for class certification. Therefore, not the lowest prices [191], [192], [193] but a more conservative value including power electronics and other peripheral components is chosen in analogy to [66], [69]. SOFCs play a much smaller role in the automotive sector. Their potential range of application includes stationary and emergency power supply of partly-isolated grids, as well as heavy-duty transport. For ships and with the inclusion of complex onboard steam reforming and larger material expenditure they are expected to be more expensive than PEMFCs [131]. Specific investment costs, maintenance factors, and other economically-relevant parameters are given in Tab. 6.2.

The power generators' volumes are another relevant indicator for the conducted assessment. Their size is calculated with

$$V_{\text{gen}} = \frac{P_{\text{gen}}^{\text{r}}}{P_{\text{V,fuel-gen}}} , \quad (6.6)$$

where $P_{\text{V,fuel-gen}}$ is the specific power density of a technology specified for the operation with one investigated fuel. While the power density of combustion engines will most likely not increase significantly over the next decade, fuel cell technologies are still evolving rapidly: today, PEMFC stacks reach power densities much higher than large-scale combustion engines for ship applications [194],[195] and predictions give a hint of a continuous technology development in the near future [196]. This comparison is not only true for stacks but persists when peripheral

components like feed pumps and power electronics are included into the calculation [197]. For SOFC units, the lowest power density among the competitors is assumed. Selected parameters consider onboard reforming and restricted cell currents. The derived volumetric power densities are listed in Tab. 6.2.

Tab. 6.2: Physical and economic simulation parameters for the investigated power technologies

Specific investment costs		Value	Reference
VLSFO-ICE	$p_{\text{VLSFO-ICE}}^{\text{inv}}$	251.2 €/kW	based on [198]
LNG-ICE	$p_{\text{LNG-ICE}}^{\text{inv}}$	301.4 €/kW	based on [198],[199]
FTD-ICE	$p_{\text{FTD-ICE}}^{\text{inv}}$	251.2 €/kW	based on [198]
SNG-ICE	$p_{\text{SNG-ICE}}^{\text{inv}}$	301.4 €/kW	based on [198],[199]
NH3-ICE	$p_{\text{NH3-ICE}}^{\text{inv}}$	482.2 €/kW	based on [66],[199]
MeOH-ICE	$p_{\text{MeOH-ICE}}^{\text{inv}}$	276.1 €/kW	based on [69],[198]
FTD-SOFC	$p_{\text{FTD-SOFC}}^{\text{inv}}$	1200 €/kW	[131]
SNG-SOFC	$p_{\text{SNG-SOFC}}^{\text{inv}}$	1200 €/kW	[131]
NH3-SOFC	$p_{\text{NH3-SOFC}}^{\text{inv}}$	947.9 €/kW	[200]
MeOH-PEM	$p_{\text{MeOH-PEM}}^{\text{inv}}$	1070 €/kW	based on [69],[201]
H2-PEM	$p_{\text{H2-PEM}}^{\text{inv}}$	700 €/kW	[69]
Interest rate	j	0.035	-
Cost exponent		Value	Reference
ICE	g_{ICE}	1.1	[198]
FC	g_{FC}	1	-
Maintenance factor		Value	Reference
ICE	$c_{\text{ICE}}^{\text{a}}$	0.0045 a ⁻¹	[202]
SOFC	$c_{\text{SOFC}}^{\text{a}}$	0.019 a ⁻¹	[131]
PEM	$c_{\text{PEM}}^{\text{a}}$	0.06 a ⁻¹	[191]
Lifetime	$t_{\text{L,gen}}$	20 a	[41]
Power density		Value	Reference
ICE	$P_{\text{V,ICE}}$	37.05 kW/m ³	based on [194],[47]
FTD-SOFC	$P_{\text{V,FTD-SOFC}}$	6.67 kW/m ³	manufacturer
SNG-SOFC	$P_{\text{V,SNG-SOFC}}$	6.67 kW/m ³	manufacturer
NH3-SOFC	$P_{\text{V,NH3-SOFC}}$	10.2 kW/m ³	own analysis
MeOH-PEM	$P_{\text{V,MeOH-PEM}}$	40.8 kW/m ³	own analysis
H2-PEM	$P_{\text{V,H2-PEM}}$	850 kW/m ³	[197]

Fuels – It is already discussed in Section 4.6 that the consideration of fuel expenses is not negligible during a conceptual design process. Certainly, annual fuel costs play an even larger role when discussing potential future power system solutions. To better display the challenges of upcoming fuels like hydrogen or ammonia, costs here include fuel expenses and the annuity payment for the fuel tank. They are

extrapolated from the consumed fuel mass on one passage (cf. Eq. (6.1)):

$$p_{\text{fuel}}^{\text{a}} = \frac{t_{\text{op}}^{\text{a}}}{t_{\text{op}}} \cdot m_{\text{fuel}} \cdot p_{\text{fuel}} + p_{\text{fuel,tank}}^{\text{a}}, \quad (6.7)$$

where t_{op}^{a} is the annual ship operating time set to 350 days [133], p_{fuel} is the specific fuel price and

$$p_{\text{fuel,tank}}^{\text{a}} = p_{\text{fuel,tank}}^{\text{inv}} \cdot m_{\text{gen,fuel}} \cdot A_{\text{tank}}(t_{\text{L,tank}}) \quad (6.8)$$

are the annual costs for the fuel tank considering its annuity payment factor A_{tank} . To grant unified cost assumptions for the electrofuels, fuel costs are adopted from [69]. While the assumed liquid hydrogen tank price diverges severely from today's prices given for typical 40ft containers, costs are estimated for 2030 onward and include size and production scale factors discussed in [203]. The estimation is also supported by other assessments with similar topics [67],[140]. Since compressed hydrogen is not discussed in [69], additional information for infrastructure and compression are obtained from [204] but electrical energy price and electrolysis assumptions are not changed to maintain comparability. According to manufacturers, CGH2 tank costs are calculated with an estimated 35% price increase compared to LH2 tanks.

The consumed fuel volume is used to calculate the required tanks' volumes:

$$V_{\text{fuel}} = \frac{m_{\text{fuel}}}{\rho_{\text{fuel}}}, \quad (6.9)$$

where ρ_{fuel} is the fuel density. Note, that in reality a ship's fuel tank is not usually designed to last for exactly one passage but includes a manually determined reserve. Since the assessment covers continuous passage times, all oversizing effects can in theory be discussed by analyzing the given results. Fuel and tank prizes, as well as fuel densities are given in Tab. 6.3.

Tab. 6.3: Physical and economic simulation parameters for the considered fuels

Specific fuel price		Value	Reference
VLSFO	p_{VLSFO}	47.86 €/MWh	based on [205],[206]
LNG	p_{LNG}	19.04 €/MWh	based on [120],[121]
FTD	p_{FTD}	158 €/MWh	[69]
SNG	p_{SNG}	142 €/MWh	[69]
NH3	p_{NH3}	120 €/MWh	[69]
MeOH	p_{MeOH}	119 €/MWh	[69]
LH2	p_{LH2}	153 €/MWh	[69]
CGH2	p_{CGH2}	101 €/MWh	based on [69][204]
Specific tank price		Value	Reference
VLSFO/FTD	$p_{\text{FTD,tank}}$	70 €/MWh	[69]
LNG/SNG	$p_{\text{SNG,tank}}$	720 €/MWh	[69]
NH3	$p_{\text{NH3,tank}}$	230 €/MWh	[69]
MeOH	$p_{\text{MeOH,tank}}$	120 €/MWh	[69]
LH2	$p_{\text{LH2,tank}}$	1290 €/MWh	[69]
CGH2	$p_{\text{CGH2,tank}}$	1742 €/MWh	manufacturer
Lifetime	$t_{\text{L,tank}}$	20 a	[41]
Fuel density		Value	Reference
VLSFO/FTD	ρ_{FTD}	940 kg/m ³	[207]
LNG/SNG	ρ_{SNG}	450 kg/m ³	[208]
NH3	ρ_{NH3}	600 kg/m ³	[209]
MeOH	ρ_{MeOH}	792 kg/m ³	[209]
LH2	ρ_{LH2}	70.8 kg/m ³	[209]
CGH2	ρ_{CGH2}	39 kg/m ³	[209]

Battery Units – As already introduced in Section 3.2.2, annual battery costs are calculated with capacity-specific investment costs $p_{\text{B}}^{\text{inv}}$:

$$p_{\text{B}}^{\text{a}} = p_{\text{B}}^{\text{inv}} \cdot C_{\text{E,B}} \cdot A_{\text{B}}(t_{\text{L,B}}) . \quad (6.10)$$

Here, specific battery prices for large installations are given for the years 2020 and 2030 (cf. Tab. 6.4), since a price drop is considered highly probable. While single cell costs of lithium-ion batteries are predicted to be halved within the next years [210], the costs of peripheral components like inverters, housing, cooling, and controllers will most likely not change drastically. Therefore a price of 600 €/kWh is assumed for the year 2030, taking into account current market prices of ship-certified systems.

As it is demonstrated in Section 4.3 that the unified storage model approach is overestimating lifetimes $t_{\text{L,B}}$ for battery applications with high specific power demand, the degradation model from [117] for the lithium-iron-phosphate technol-

ogy and the end of life definition of 20% capacity loss is adopted here. Finally, the battery’s volume to calculate incurring opportunity costs is given with:

$$V_B = \frac{C_{E,B}}{C_{V,B}} \quad (6.11)$$

where $C_{V,B}$ is the specific volumetric energy density of the battery system.

Tab. 6.4: General physical and economic parameters for the LFP battery unit

Parameter		Value	Reference
Specific investment costs (2020)	$p_{B,2020}^{inv}$	800 €/kWh	manufacturer
Specific investment costs (2030)	$p_{B,2030}^{inv}$	600 €/kWh	based on [210]
Energy density	$C_{V,B}$	16.77 kWh/m ³	manufacturer

Volume Opportunity Costs – With few exceptions, the net usable volume on a ship is essential for the owner’s business case, weather it is provided to passengers, bulk, or cargo. Therefore, volume opportunity costs are introduced to quantify the loss of income resulting from a large shipboard power system. In this study, the volume occupied by the power system including generators, fuel tanks, and batteries is evaluated for the annual operating time:

$$p_{vol}^a = \frac{t_{op}^a}{t_{op}} \cdot p_{vol}(t_{op}) \cdot \sum_i V_i \quad (6.12)$$

$i = \text{gen, B, fuel},$

where p_{vol} are the specific volume opportunity costs. Transport prices are often a function of the ship’s scheduled passage time. For example, in [69], specific costs of 600 to 1100 € per 20-foot container are assumed for passages between 240 and 720 hours. These discrete estimations are generalized with a polynomial fit based to symbol the nonlinear voyage time-cost dependency:

$$p_{vol} = \left(5.23 + \frac{0.049}{h} \cdot t_{op} - \frac{2.27 \cdot 10^{-5}}{h^2} \cdot (t_{op})^2 \right) \cdot \frac{\text{€}}{\text{m}^3}. \quad (6.13)$$

6.2.4 Environmental Models

Unlike the previously introduced investment, operating and opportunity costs, the indirect environmental costs are not considered in the objective function (cf. Eq. (6.18)) but solely evaluated post optimization. In this section, the investigated ship-sector-related emissions and their negative effects are introduced. Then, emission quantification models for component productions (cradle-to-gate), fuel provision (well-to-tank), and ship operation (tank-to-wake) are given separately. Last,

the monetary valuation of occurring emissions is discussed.

Investigated emissions – The most relevant emissions coming from today’s ship traffic are sulfur oxides (SO_x), nitrogen oxides (NO_x), carbon monoxide (CO), particulate matter including black carbon (BC), methane (CH₄), and carbon dioxide (CO₂) [147],[211]. In the following, a brief summary of the emissions’ negative impacts is given: CO₂, CH₄ and BC are all classified to contribute to the greenhouse effect and therefore involve a global warming potential (GWP) [212]. CO₂ and BC, the most relevant component of particulate matter regarding global warming [213], are products of carbon-based fuel combustion. Methane emissions result from an incomplete combustion reaction and a resulting fuel slip in spark-ignited gas motors [214]. Sulfur oxides are the leading cause of marine ecosystem acidification and the reduction of biodiversity [9]. Diesel fuels are the main sulfur source, whereas LNG contains only a share of around 3.5 ppm [215]. Nitrogen oxides are a combustion byproduct and cause the formation of tropospheric ozone and the eutrophication of the waters. Also, the generation of acid rain is directly relatable to NO_x emissions [216],[217],[218]. While carbon monoxide is a respiratory poison in higher concentrations, long-term damages in an open environment are harder to determine [219]. Nevertheless, CO takes part in the formation of tropospheric ozone like nitrogen oxides. When adding potential future fuels to the assessment, ammonia slip emissions must also be addressed. NH₃ contributes to the acid deposition and threatens biodiversity with an impact factor of 2.5–3.2 compared to nitrogen oxides [220].

Supply of components and fuels – In order to conduct an environmental assessment, raw material extraction, production and emissions occurring during operation are considered. For the comparison of emissions with global warming potential, a 100 year reference period (GWP₁₀₀) is used [221]. Annual CO₂-equivalent emissions of generators $m_{\text{gen,CO2eq}}^{\text{prod,a}}$, batteries $m_{\text{B,CO2eq}}^{\text{prod,a}}$ and fuels $m_{\text{fuel,CO2eq}}^{\text{prod,a}}$ are calculated with help of a specific deployment factor κ_{CO2eq} :

$$m_{\text{gen,CO2eq}}^{\text{prod,a}} = \frac{1}{t_{\text{L,gen}}} \cdot P_{\text{gen}}^{\text{r}} \cdot \kappa_{\text{gen,CO2eq}} \quad (6.14\text{a})$$

$$m_{\text{B,CO2eq}}^{\text{prod,a}} = \frac{1}{t_{\text{L,B}}} \cdot C_{\text{E,B}} \cdot \kappa_{\text{B,CO2eq}} \quad (6.14\text{b})$$

$$m_{\text{fuel,CO2eq}}^{\text{prod,a}} = \frac{t_{\text{op}}^{\text{a}}}{t_{\text{op}}} \cdot m_{\text{fuel}} \cdot \kappa_{\text{fuel,CO2eq}} , \quad (6.14\text{c})$$

where component footprints are symmetrically divided over their lifetime t_{L} and fuel consumption is extrapolated to the annual operating time from the assessed voyage time.

For conventional fuels, extraction losses, refinery waste, gas flaring, fuel distribution, and leakage during transportation are causing the biggest shares of their carbon footprints. For hydrogen production, the specific carbon footprint emerges mostly from the electricity demand and not the water electrolyzer construction [222]. While it is stated by the authors of [222] that no information is publicly available for supplementary chemical plants, their inclusion would most likely not influence the quantitative carbon footprint of the fuels tremendously. Anyways, while a complete plant’s carbon footprint would further impair longer fuel production chains, the qualitative coherence between electrofuels is already given with their diverging demand of electrical energy.

In this study, an electrical energy carbon footprint forecast calculation for the European power grid mix in the year 2030 is initially selected to quantify the environmental impact of fuel supply [223]. Note that this is a more conservative estimation compared to evaluations of low-carbon power sources [224]. The environmental footprints for each fuel result from their energy demand described in [69]. Parameters for fuels and components are listed in Tab. 6.5.

Tab. 6.5: CO₂-equivalent emissions for supply of components and fuels including maintenance and stack replacements, carbon mass shares of the fossil fuels

Specific CO₂-eq. footprint		Value	Reference
ICE	$\kappa_{\text{ICE,CO2eq}}$	84.7 kg _{CO2eq} /kW	based on [47],[225]
SOFC	$\kappa_{\text{SOFC,CO2eq}}$	703.8 kg _{CO2eq} /kW	[226]
PEM	$\kappa_{\text{PEM,CO2eq}}$	112 kg _{CO2eq} /kW	[227]
Battery	$\kappa_{\text{B,CO2eq}}$	216 kg _{CO2eq} /kWh	[228]
VLSFO	$\kappa_{\text{VLSFO,CO2eq}}$	0.5907 kg _{CO2eq} /kg	[229]
LNG	$\kappa_{\text{LNG,CO2eq}}$	0.8344 kg _{CO2eq} /kg	[229]
FTD	$\kappa_{\text{FTD,CO2eq}}$	308 kg _{CO2eq} /MWh	based on [69],[223]
SNG	$\kappa_{\text{SNG,CO2eq}}$	270 kg _{CO2eq} /MWh	based on [69],[223]
NH ₃	$\kappa_{\text{NH3,CO2eq}}$	261 kg _{CO2eq} /MWh	based on [69],[223]
MeOH	$\kappa_{\text{MeOH,CO2eq}}$	270 kg _{CO2eq} /MWh	based on [69],[223]
LH ₂	$\kappa_{\text{LH2,CO2eq}}$	261 kg _{CO2eq} /MWh	based on [69],[223]
CGH ₂	$\kappa_{\text{CGH2,CO2eq}}$	215 kg _{CO2eq} /MWh	based on [69],[223]
Carbon Mass Share		Value	Reference
VLSFO	$\xi_{\text{C,VLSFO}}$	85.44%	[211]
LNG	$\xi_{\text{C,LNG}}$	75.68%	[208]

Production emissions with negative local effects but without global warming potential are not quantified here. Still, the petrochemical and the steel industry are among the largest industrial emitters of nitrogen oxides, and oil refineries also

produce an abundance of sulfur oxides [230],[231]. However, this part of the assessment focuses on local emissions that affect the open sea and coastal ecosystem caused by maritime traffic. Unlike the greenhouse gas emissions, adding up all emission sources distorts the analysis, as different environments cannot easily be compared to each other. Analyzing average effects of industry in different ecosystems is out of the investigation's scope.

Operation – For the analysis of today's power systems, the annually emitted carbon dioxide mass during ship operation is calculated with the combustion stoichiometry and considers other carbon-based emissions (CO,BC,CH₄):

$$m_{\text{gen,CO}_2}^{\text{a}} = \left(m_{\text{gen,fuel}}^{\text{a}} - m_{\text{gen,CH}_4}^{\text{a}} \right) \cdot \frac{M_{\text{CO}_2}}{M_{\text{C}}} \cdot \left(\xi_{\text{C,fuel}} - m_{\text{gen,BC}}^{\text{a}} - \frac{M_{\text{CO}}}{M_{\text{C}}} \cdot m_{\text{gen,CO}}^{\text{a}} \right), \quad (6.15)$$

where $m_{\text{gen,CH}_4}^{\text{a}}$, $m_{\text{gen,BC}}^{\text{a}}$, $m_{\text{gen,CO}}^{\text{a}}$ are the annual methane, black carbon, and carbon monoxide emissions, $\xi_{\text{C,fuel}}$ is the fuel's carbon mass share, and M_{C} , M_{CO} , M_{CO_2} are the substances' molar masses. Main incentive of a future synthetic fuel utilization is the reduction of an application's carbon footprint. Yet, the usage of carbon-based fuels (FTD, SNG, MeOH) still causes CO₂ emissions during ship operation. For simplicity reasons, however, a fully functioning carbon cycle is assumed. This assumption is supported by the carbon capture energy demand considered for fuel production. Operating CO₂ emissions resulting from electrofuel consumption are therefore neglected in this study.

Emissions other than CO₂ occur almost exclusively during combustion processes. The quantification of annually emitted masses is implemented in analogy to the fuel consumption calculation (cf. Eq. (6.1)):

$$m_{\text{emis}}^{\text{a}} = \frac{t_{\text{op}}^{\text{a}}}{t_{\text{op}}} \int^{t_{\text{op}}} \dot{m}_{\text{emis}}^{\text{spec}}(P_{\text{gen}}, t) \cdot P_{\text{gen}}(t) dt, \quad (6.16)$$

where “emis” is a placeholder for one of the considered emissions. Again, characteristics of the components are displayed with the operating-point-dependent specific mass flow $\dot{m}_{\text{emis}}^{\text{spec}}$. While specific emissions are straightforwardly displayed in Fig. 6.4, a more in-depth overview of all power technologies is given in Appendix B.2.

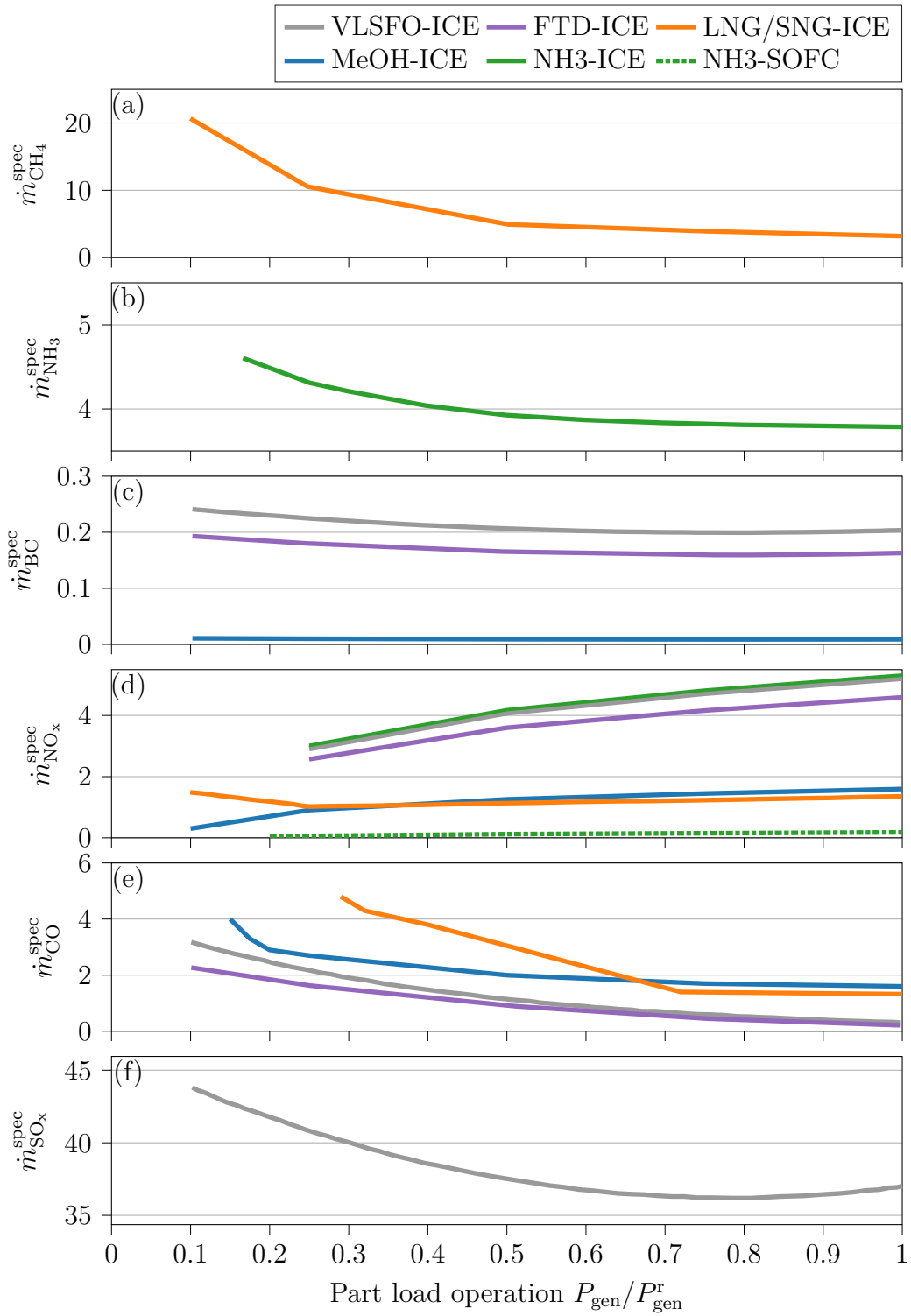


Fig. 6.4: Operating-point-dependent generator emissions displayed in g/kWh (electrical power)

Emission Valuation – To demonstrate the negative environmental effects of CO₂-equivalent emissions, it is not unusual to estimate a price χ_{CO_2} for the implicitly caused damage [232]. Here, the global warming potential over 100 years (GWP₁₀₀) ζ_{carb} is used to assess greenhouse gases other than CO₂. In analogy, emissions with negative local effects can be evaluated with specific social or environmental costs χ_k . Chosen literature values include the type and sensitivity of the ecosystem, population density, and overall pollution burden. Their respective sources are given in Tab. 6.6. Resulting social costs from production emissions $p_{\text{CO}_2\text{eq}}^{\text{prod,a}}$, CO₂ emissions during operation $p_{\text{CO}_2}^{\text{op,a}}$, other operating emissions with global warming potential $p_{\text{CO}_2\text{eq}}^{\text{op,a}}$, and emissions with local effects $p_{\text{LE}}^{\text{op,a}}$ are calculated as follows:

$$\begin{aligned}
 p_{\text{emis}}^{\text{a}} &= p_{\text{CO}_2\text{eq}}^{\text{prod,a}} + p_{\text{CO}_2}^{\text{op,a}} + p_{\text{CO}_2\text{eq}}^{\text{op,a}} + p_{\text{LE}}^{\text{op,a}} \\
 &= \sum_i m_{i,\text{CO}_2\text{eq}}^{\text{prod,a}} \cdot \chi_{\text{CO}_2} + \underbrace{m_{\text{gen,CO}_2}^{\text{a}} \cdot \chi_{\text{CO}_2}}_{\text{only fossil fuels}} + \sum_j m_j^{\text{a}} \cdot \zeta_{\text{carb}} \cdot \chi_{\text{CO}_2} + \sum_k m_k^{\text{a}} \cdot \chi_k \\
 i &= \text{gen, B, fuel}; j = \text{CH}_4, \text{BC}; k = \text{NH}_3, \text{NO}_x, \text{CO}, \text{SO}_x.
 \end{aligned} \tag{6.17}$$

Tab. 6.6: GWP₁₀₀ values and emission cost grading for the environmental investigation

Global warming potential (GWP ₁₀₀)		Value	Reference
CH ₄	ζ_{CH_4}	30 kg _{CO₂eq} /kg _{CH₄}	[233]
BC	ζ_{BC}	680 kg _{CO₂eq} /kg _{BC}	[234]
Specific social costs		Value	Reference
NO _x	χ_{NO_x}	9.29 €/kg _{NO_x}	[216]
NH ₃	χ_{NH_3}	23.23 €/kg _{NH₃}	based on [216],[220]
CO	χ_{CO}	0.997 €/kg _{CO}	[216]
SO _x	χ_{SO_x}	10.72 €/kg _{SO_x}	[216]
CO ₂	χ_{CO_2}	106.25 €/t _{CO₂eq}	[232]

6.3 System Design Optimization

Now that the technologies of consideration are introduced and modeled, the power system evaluation approach is discussed. The goal of the assessment is a direct comparison of the technologies' economic and environmental key performance indicators. For this purpose, expedient system designs ought to serve as a basis, emphasizing the technologies' qualities and eliminating the configuration bias. Therefore, a system optimization task with the objective of reducing the shipowner's costs is presented in Analogy to Section 3.3. In analogy to the previous analyses,

the objective function for the cost optimization consists of the annuity payments for the generator $p_{\text{gen}}^{\text{a}}$ and for the battery storage p_{B}^{a} , the annual fuel costs $p_{\text{fuel}}^{\text{a}}$, and an additional price for the totally required shipboard power system volume $p_{\text{vol}}^{\text{a}}$:

$$\begin{aligned}
& \underset{P_{\text{gen}}^{\text{r}}, C_{\text{E,B}}, F_{\text{B}}(t_0), D_{\text{c}}}{\text{minimize}} && p_{\text{gen}}^{\text{a}} + p_{\text{B}}^{\text{a}} + p_{\text{fuel}}^{\text{a}} + p_{\text{vol}}^{\text{a}} \\
& \text{subject to} && 0 = P_{\text{gen}}(t) - P_{\text{L}}(t) - P_{\text{B}}(t) \forall t, \\
& && F_{\text{B}}(t_0) \leq F_{\text{B}}(t_{\text{op}}), \\
& && \text{Eqn. (3.8) - (3.16), (3.30a) - (3.30c),} \\
& && \text{Eqn. (4.18) - (4.19),} \\
& && \text{Eqn. (6.1) - (6.17),} \\
& && \text{Eqn. (6.19) - (6.20),} \\
& && \text{Eqn. (6.21) - (6.27).}
\end{aligned} \tag{6.18}$$

Optimization degrees of freedom are the generator's rated power $P_{\text{gen}}^{\text{r}}$, the battery's energy capacity $C_{\text{E,B}}$ and its state of energy (SoE) F_{B} at the start time of the passage t_0 , as well as several parameters for the control strategy D_{c} . The first constraint covers the required power balance where generator power P_{gen} and battery power P_{B} must exactly compensate the load demand P_{L} at any time. The second constraint states that the battery's state of energy at beginning of operation must not exceed the value at end of operation. This guarantees operational functionality past the operating voyage time t_{op} . The third to seventh constraints represent the descriptions of the power system components with battery models adopted from Chapters 3 and 4, design requirements, and the developed control strategy. For the generators, two additional design constraints for FCs and ICEs are defined. While the number of installed combustion engines in the genset N_{ICE} is fixed and the rated power of one single unit $P_{\text{ICE,mod}}^{\text{r}}$ can be varied

$$P_{\text{ICE}}^{\text{r}} = \underbrace{P_{\text{ICE,mod}}^{\text{r}}}_{\text{variable}} \cdot N_{\text{ICE}}, \tag{6.19}$$

the opposite holds true for fuel cells, where the number of units N_{FC} is object of optimization:

$$P_{\text{FC}}^{\text{r}} = P_{\text{FC,mod}}^{\text{r}} \cdot \underbrace{N_{\text{FC}}}_{\text{variable}}. \tag{6.20}$$

Here, a fixed rated power of one unit is chosen to demonstrate the viable approach of modular installation.

6.4 Universal System Control Strategy

Control strategies specifically designed for the SOFC application are already discussed in Chapters 3 and 5. However, these strategies are not necessarily in accordance with the operating objectives of non-SOFC technologies. Since the creation of energy management strategies for every unique technology would lead to an undesirable bias, a general strategy suitable for all technologies is introduced. This unified management strategy is developed to control a hybrid system with either fuel cells or combustion engines, and a supporting battery unit. Its objective is to maintain the operability of a well-designed system under consideration of component behaviors and limitations. The strategy consisting of the interaction of generator and battery, as well as the interworking of the single power generation modules is first introduced generally and is demonstrated exemplarily in Appendix A.3 for better comprehension.

Generator and battery interaction – During the entire operating time, generators mostly target to follow the consumer demand, while the battery fulfills the role of compensating differences between power source and load:

$$P_{B,\text{set}} = P_{\text{gen}} - P_L, \quad (6.21)$$

where $P_{B,\text{set}}$ is the desired battery power output. Here, the load-following operation aims to reduce the required battery compensation power. However, a secondary objective is to prevent the battery from fully charging or discharging. Therefore, the desired behavior of the generators is influenced by the battery's SoE, which is monitored with help of the state machine displayed in Fig. 6.5.

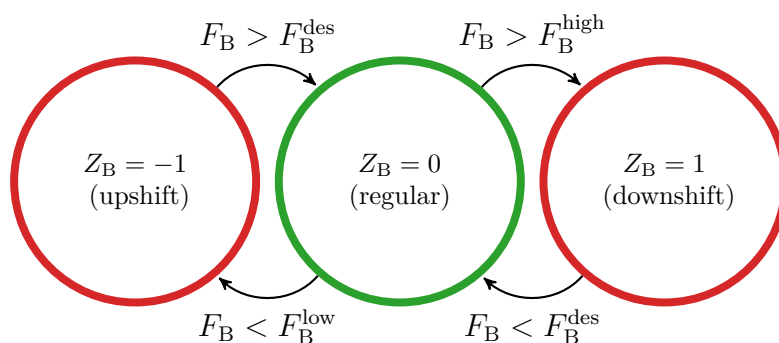


Fig. 6.5: State machine that monitors the battery state of energy F_B with help of the indicating state Z_B

Resulting, an increased or decreased generator output is aspired to counteract critical battery SoEs above F_B^{high} (state $Z_B = 1$) or below F_B^{low} ($Z_B = -1$). This

counteracting operation is conducted until a desired state of energy F_B^{des} is reached (state $Z_B = 0$). With the given state Z_B , the desired generator power output $P_{\text{gen,set}}$ is calculated. Thereby, a designable specific power factor ξ_B is introduced, which prevents the batteries from charging/discharging with maximum values if not required:

$$P_{\text{gen,set}} = \begin{cases} P_L & \text{if } Z_B = 0 \\ P_L + \xi_B \cdot P_{B,\text{dis}}^{\text{max}} & \text{if } Z_B = 1 \\ P_L + \xi_B \cdot P_{B,\text{cha}}^{\text{max}} & \text{if } Z_B = -1. \end{cases} \quad (6.22)$$

The introduced four degrees of freedom D_C can be optimized with regard to the power technology, the battery size, and the load profile characteristics (cf. Eq. (6.18)):

$$D_C = \left\{ F_B^{\text{high}}, F_B^{\text{low}}, F_B^{\text{des}}, \xi_B \right\}. \quad (6.23)$$

Allocation on power modules – The overall desired generator power is split further into demand values for each individual module. Here, fuel cell and combustion technologies are treated separately due to their diverging operating behavior. For the fuel cell modules, an equal distribution among all installed units is chosen to reach lower operating points with higher energy efficiency and prevent a shutdown with problematic cooldowns, water management or fluiddynamic behaviors:

$$P_{\text{FC,set},j} = \frac{P_{\text{gen,set}}}{N_{\text{FC}}}. \quad (6.24)$$

For ICEs, an on-off logic is implemented for the six engines to grant high-power operating points with better energy efficiency and smaller specific fuel slips. A minimization function ensures the provision of the desired power demand:

$$\begin{aligned} & \underset{k_j}{\text{minimize}} \quad \sum_{j=1}^{N_{\text{ICE}}} k_j \cdot P_{\text{ICE},j}^r \\ & \text{subject to} \quad P_{\text{gen,set}} \leq \sum_{j=1}^{N_{\text{ICE}}} k_j \cdot P_{\text{ICE},j}^r, k_j = \{0, 1\}, \end{aligned} \quad (6.25)$$

where k_j is an on/off switch for each of the engines. The total power is equally distributed across all active engines:

$$P_{\text{ICE,set},j} = P_{\text{gen,set}} \cdot \frac{k_j \cdot P_{\text{ICE},j}^r}{\sum_{g=1}^{N_{\text{ICE}}} k_g \cdot P_{\text{ICE},g}^r}. \quad (6.26)$$

Finally, the combined power generators' answer required for the battery set value calculation (cf. Eq. (6.21)) is given with

$$P_{\text{gen}} = \sum_{j=1}^{N_{\text{gen}}} P_{\text{gen},j}, \quad (6.27)$$

where $P_{\text{gen},j}$ is the actual power output of one single combustion engine or fuel cell unit.

Illustrative demonstration – For better comprehensibility, the control strategy characteristics are demonstrated for a minimal working example in Appendix A.3.

6.5 Results and Discussion

After the introduction of all required model equations, the two conventional combustion engines and the ten potential future combinations of power technologies and synthetic fuels are compared with one another on the basis of cost-optimized system designs. First, a benchmark study is conducted, in which the performance of today’s combustion engines is evaluated and the need for model-based design optimization is demonstrated. In the subsequent section, a comprehensive technology comparison is presented. Here, the scope of assessment is extended to examine the most relevant uncertainty factors and the influence of vessel specifications.

6.5.1 Benchmark Assessment: State-of-the-art Internal Combustion Engines

As introduced in Section 6.1, the benchmark assessment covers two state-of-the-art combustion technologies: the most conventional compressed-ignition diesel engine operated with VLSFO and the upcoming lean-burn-spark-ignition gas engine combined with liquefied natural gas. While many participants of the shipping sector promote liquefied natural gas for its better environmental characteristics and even call gas combustion an interim technology toward a sustainable industry [235],[236], most nongovernmental environmental associations doubt a positive influence of LNG-based operation [237],[238]. Therefore, the direct comparison of the present fossil fuels is not only an important first step to ranking potential future power technologies, but also aims to answer open questions regarding LNG as a marine fuel. The assessment also addresses typical analysis flaws leading to unfair technology comparisons, which have been introduced with the term “configuration bias”. After the introduction of the case study design for the year 2020, economic and environmental results are presented and discussed extensively.

Case Study

The firstly conducted case study is based on the 330 m long cruise ship built for 4100 passengers and a crew of 1700, which is already introduced in Chapter 5. For the sake of completeness, the observed load profile is given in Fig. 6.6. The profile functions as a basis for both the benchmark assessment for the year 2020 and the first analyses for the future scenario.

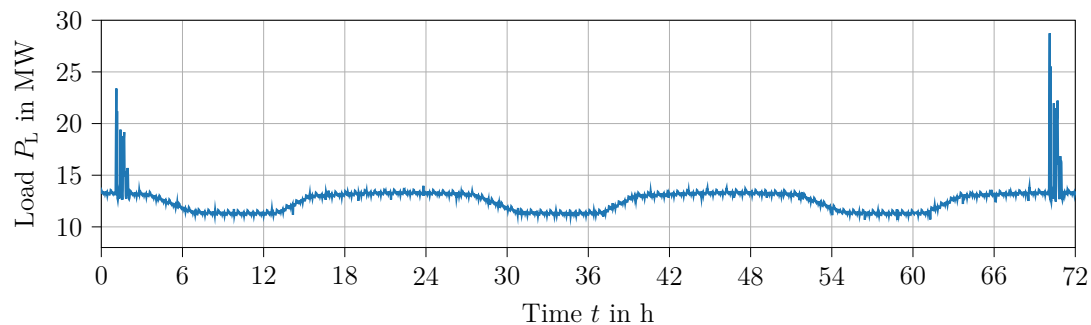


Fig. 6.6: 72 h passage with day-night rhythm hotel load and two harbor maneuvers [138]

In the benchmark assessment, four power systems with different generator configurations are designed to comply with the load demand of the cruise ship. As indicated, the main objectives of this first analysis can be categorized into two subtasks:

1. the demonstration of preventing a configuration bias in a scientific study design
2. the evaluation of the combustion engines' key performance indicators when operated with VLSFO or LNG.

The assessed configurations are summarized in Fig. 6.7 and explained in the following:

ORIGINAL – This configuration replicates the original system configuration. Three small and three large engines combine for more than 59 MW rated power.

MANUAL SIZE – This configuration is built from six identical diesel engines, which together are precisely able to fulfill the load peak power demand on their own. Battery support is not a design option here.

VLSFO-ICE – This configuration is built from six diesel engines with cost-optimal size. For a fair comparison to other technologies, which require an energy storage support, the optimization approach includes the possibility to select a battery unit of variable size to form a hybrid configuration.

LNG-ICE – This configuration is composed of six optimal-sized gas combustion engines with an additional battery unit.

Note that the ORIGINAL and the MANUAL SIZE design are not used for technology evaluation, but should signal that the comparison of prefixed and optimized systems distorts the results meaningfully.

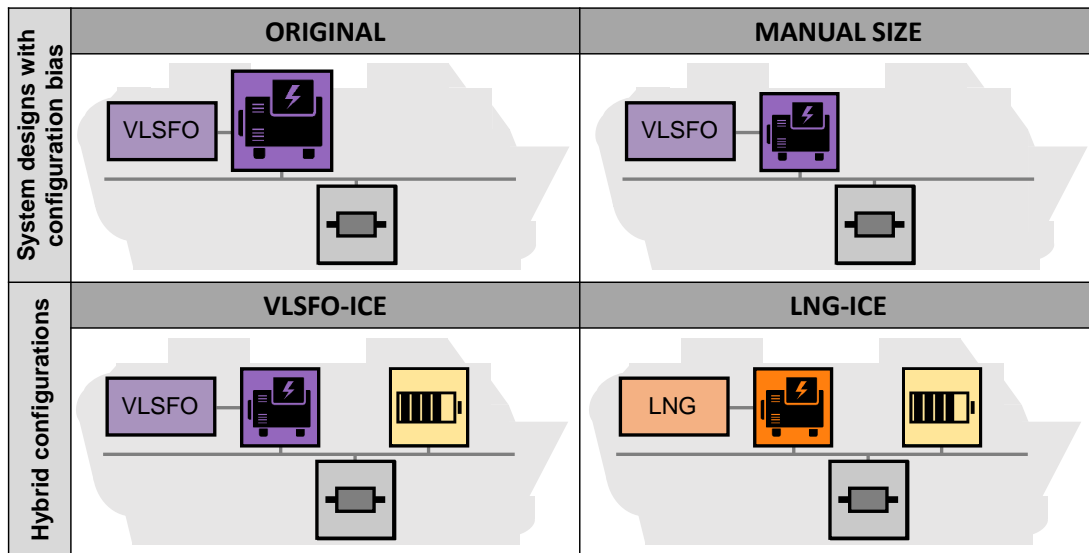


Fig. 6.7: Considered system configurations for the benchmark assessment, including two design examples with configuration bias and two optimally designed hybrid configurations

Economic and Environmental Results

In the following, key performance indicators of the manually created and the cost-optimized system designs (cf. Eq. (6.18)) are presented. The system configurations, total system volumes, emissions, and the resulting direct and environmental costs are summarized in Fig. 6.8.

In Fig. 6.8 (a) the generators' total rated power and the maximum discharge power of the supporting battery are displayed. As a reference, the maximal demand of the load profile (cf. Fig. 6.6) is plotted. The ORIGINAL design stands out as the largest system with close to 60 MW installed power. By contrast, the MANUAL SIZE and the cost-optimal hybrid configurations show a 45% decrease of totally installed power. For the VLSFO-ICE case, the generator power even is reduced by 74%. Certainly, the ORIGINAL power system was not designed for this specific route, and other passages might involve higher load demands. Most likely however, the design resulted from simultaneity factor calculation or estimations based on knowledge plus added safety factors. Here, it is already evident that

a fair technology comparison between the power generators could not have been made with only the ORIGINAL design case.

The two cost-optimized system configurations (VLSFO-ICE and LNG-ICE) indicate similarities, but do not present identical total rated power outputs. To reduce operating costs, the engine design aims for an optimal average energy efficiency without oversizing the components. While active, the VLSFO-ICE average relative operating point is 0.91, whereas the LNG-ICE average operating point is 0.96. These average operating points represent a level close to the SFC optima (cf. Fig. 6.3). In addition to the design incentive of high energy efficiency, the component investment costs also influence the design decision: as the specific LNG-ICE costs are higher than the VLSFO-ICE costs, slightly larger batteries are utilized for peak shaving during thruster maneuvers.

In Fig. 6.8 (b) the total system sizes consisting of generator, battery and fuel volumes are compared to each other. As expected, the ORIGINAL system design demands a much larger installation space than the systems optimized for the load profile. Certainly, also the fuel tank volume is not designed specifically for the investigated route. Here, the extra tank volume is indicated with a shaded bar but not included in the further assessment. Battery support reduces the optimal generators' rated power and thereby lowers the system's overall volume requirements compared to the MANUAL SIZE approach. Since LNG has a lower volumetric energy density, the fuel tank volume exceeds the diesel applications' values. Certainly, for a holistic consideration, maintenance space, installation flexibility, realistic tank volume, or other peripheral components like fuel inflow, cooling, exhaust pipes, required scrubbers, and even maintenance crew cabins could also be investigated. However, these investigations are not in the scope of this conceptual assessment.

In Fig. 6.8 (c) all quantified annual emissions with global warming potential are summarized. Here, components, fuel production and ship operation are differentiated. For all cases, operational emissions have the highest impact on the overall value, followed by the emissions resulting from the fuel production. The consideration of components' production does not meaningfully change the outcome of the comparison. Despite the methane slip, the LNG-ICE system saves one fifth of the VLSFO-ICE annual greenhouse gases. Since the operating behavior of the diesel-based systems does not highly deviate, the environmental performance of the optimally-sized power systems resembles the ORIGINAL results.

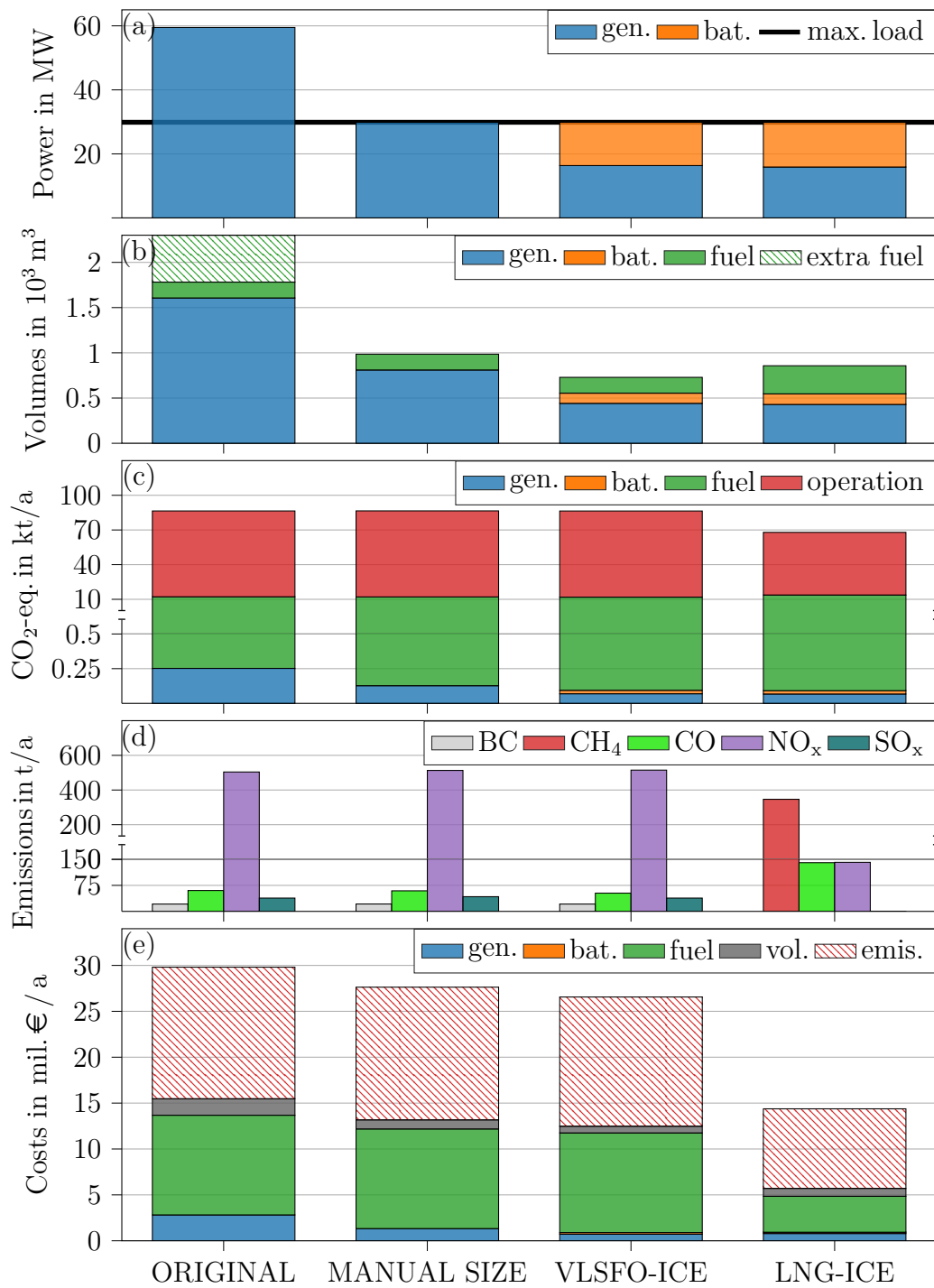


Fig. 6.8: State-of-the-art combustion engines in different configurations: (a) system designs, (b) resulting space requirements, (c) production and operating emissions with GWP, (d) non-CO₂ operating emissions, (e) annual direct and indirect costs.

In Fig. 6.8 (d) all non-CO₂ emissions with and without global warming potential resulting from the ship operation are presented. In analogy to the CO₂-equivalent emissions assessment, different designs of the diesel-based systems do not meaningfully influence the outcome of the non-CO₂ emissions. Nitrogen oxide and black carbon emissions are massively reduced when operating with LNG instead of VLSFO. Here, reduction potentials of over 99% and 72.5% are computed, respectively. In addition, the low sulfur content of the LNG implies an SO_x decrease of 99.9%. However, the lean-burn-spark-ignition engines annually emit close to 350 tons of methane.

The discussed designs result in annual system costs are summarized in Fig. 6.8 (e). It can be seen that fuel costs are by far the largest annual direct investments for all systems. Installing a battery on the other hand is not costly compared to its numerous benefits, even if the component has a comparably small lifetime. This is especially evident when comparing the MANUAL SIZE genset and the VLSFO-ICE approach: both capital investment costs and volume opportunity costs are decreased when hybridizing the power system. Only the fuel consumption cannot be reduced significantly here. While all assessed systems function without ship-board batteries in theory, the performance evaluation of generators with load shift limitations can only be conducted when considering supporting components. The comparison of the MANUAL SIZE and the VLSFO-ICE design therefore indicate that a fair technology comparison requires an equal opportunity of support to maximize the systems' performance potentials.

For this comparably short voyage time, volume opportunity costs do not represent a dominating share of the occurring annual costs. The smaller volumetric energy density of LNG therefore does not meaningfully influence the technology comparison. The LNG-ICE approach clearly is superior from an economic point of view despite larger capital investments, because LNG prices were far below VLSFO in the year 2020. Of course, the price trends of the two different fuels influence this assessment considerably. Still, when investigating other price ratios from the past, the results do not change qualitatively, as diesel and gas prices tend to interact strongly [120].

LNG also benefits the ship's environmental appearance: lower operating carbon-dioxide-equivalent emissions and higher energy efficiency of the gas engine clearly make up for a larger carbon footprint of the fuel and the methane slip. Still, a remarkable environmental damage of over 8.6 million € per year is computed. Therefore, the substitution of marine fuel oils with LNG is evaluated not to be a sustainable solution for the medium-term future.

6.5.2 Future Assessment: Suitable Solutions for the Utilization of Synthetic Fuels

The conducted analysis for the year 2030 is divided into five thematic sections: in the benchmark comparison, key performance indicators of the future fuel-technology combinations are illustrated analogous to Section 6.5.1. In addition, CO₂ avoidance costs are determined and graded. Then, longer voyage times are addressed to create a more generalized vision on the technology ranking and investigate the importance of energy density. The electrofuel cost and volume opportunity cost parameters are discussed in two extra sections, since they are identified to involve the largest assessment uncertainties. Finally, the analysis is repeated for different ship types.

Comparison of Today's and Future Power Technologies

In analogy to Fig. 6.8, system configurations, total system volumes, emissions, and the resulting direct and environmental costs of the year 2030 configurations are given in Fig. 6.9. For a better comparison with the previously assessed fossil-fuel-based combustion engines, the performance indicators of VLSFO-ICE and LNG-ICE are added to the figure as well.

Fig. 6.9 (a) gives an overview of the maximum load demand and the optimized system designs. For each application, rated generator power and maximum discharge battery power are displayed. The design results can be divided into three general categories:

1. The rated output power equals the maximum consumer demand and the battery fully supports during the maneuver load peaks. This design prevents generator oversizing, allows the generators to operate in favorable conditions and has been observed in the fossil-fuel-based engines, too. To give an example, the SNG-ICE engines on average operate at 92.3% part load with an close-to-optimal median fuel efficiency of 51.7% (cf. Fig. 6.3). Analogous results can be observed for all carbon-based ICEs and MeOH-PEM.
2. The total deployable power exceeds the load demand. Here, load-shift-limited generators require a supporting battery larger than beneficial for peak load shaving. As expected, the three assessed SOFC systems fall into this category. The NH₃-ICE application utilizes an even larger battery for efficiency matters: due to the on-off genset control strategy, engines averagely operate at 94.3% part load with a median fuel efficiency of 51.1%.
3. Battery units of hydrogen-based systems turn out significantly smaller than in other configurations. Here, the superior part load efficiency is utilized

by deliberately oversizing the generators instead (LH2 average efficiency = 67.4%, at an average 0.423 part load). However, the smaller price of gaseous hydrogen allows for a supporting storage to reduce capital investment costs in the CGH2-PEM configuration (average efficiency = 66.4%, at an average 0.487 part load).

Fig. 6.9 (b) compares the system volumes, which are consulted for the calculation of the volume opportunity costs. For the power generators, all SOFCs with small power densities have the highest disadvantage over other technologies, especially on this evaluated short mission. While fuels with smaller volumetric energy densities increase the required volume to a higher margin, the small tank volumes mostly do not outweigh component space requirements yet. As expected, generators' efficiencies apparently influence the overall volumes (e.g. MeOH-ICE requires a 19% larger tank than MeOH-PEM).

Fig. 6.9 (c) displays the annual carbon footprints of fuels and components. Here, fuel processing chains and power conversion efficiencies cause diverging results. Concerning components, SOFCs have the by far highest footprint but fall far behind the impact of the consumed electrofuels. Overall, the CGH2-PEM approach represents the best performance concerning the global warming potential. A striking example is the FTD-ICE approach, which reaches levels of a conventional VLSFO utilization. Note, that prognoses for CO₂-equivalent emissions are mostly owed to the conservative carbon footprint of the electrical energy used. However, since emissions are not included in the objective function of the optimization, results can be scaled linearly with a reduced carbon footprint for electricity generation. Therefore, a small revision is conducted subsequently to the discussion of Fig. 6.9.

Fig. 6.9 (d) quantifies emissions annually occurring during the ship operation. In analogy to assessments of conventional combustion engines, nitrogen oxide emissions and fuel slips dominate in terms of emitted mass per year. What stands out in the results is that NH₃-ICEs produce a significant amount of nitrogen-related gases, which are often not regarded in a carbon-dioxide-focused debate. The impact becomes even more lucid when solely comparing environmental costs resulting from emissions with negative local effects (cf. Fig. 6.10). Here, ammonia combustion entails a negative local impact of factor three compared to conventional diesel combustion. Therefore, exhaust gas treatments are an obligatorily measure and will inevitably increase investment and maintenance costs. In this respect, SNG-ICE and MeOH-ICE can be evaluated to be the most competitive of the combustion approaches. As stated, fuels cells do not emit relevant amounts of emissions during operation except nitrogen oxides from the NH₃-SOFC after-burner.

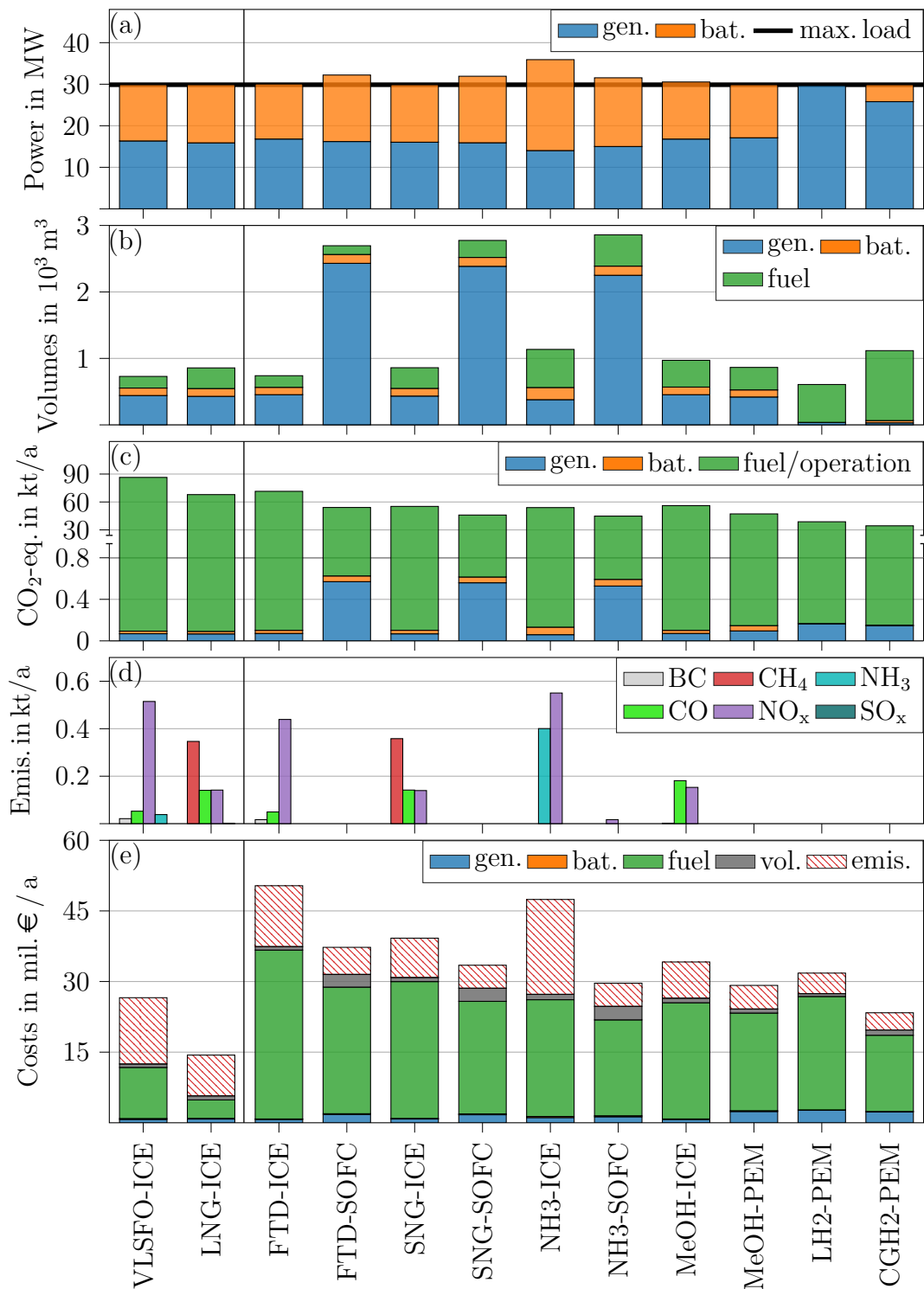


Fig. 6.9: Fuel-generator configurations in the assessment for the year 2030, comparison with results from Section 6.5.1: (a) system designs, (b) resulting space requirements, (c) production and operating emissions with GWP, (d) non-CO₂ emissions, (e) annual direct and indirect costs

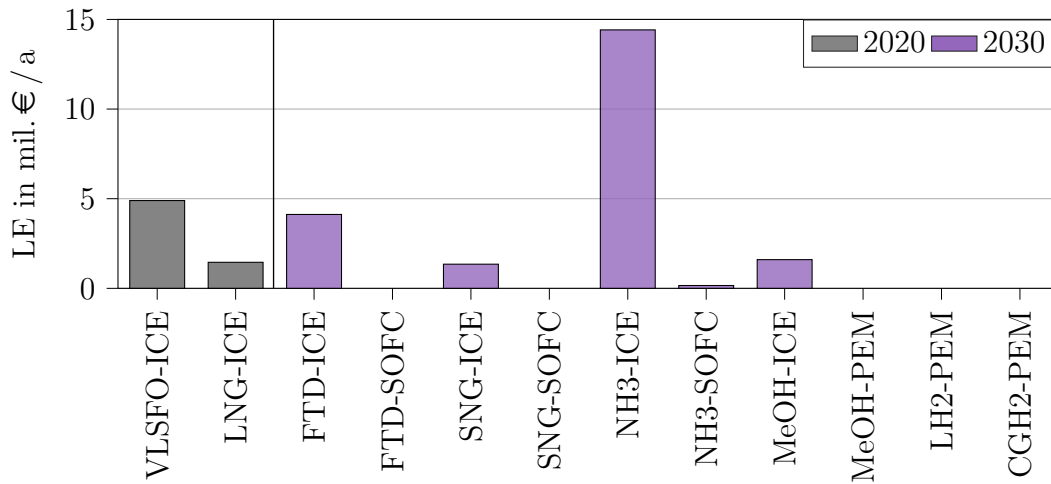


Fig. 6.10: Comparison of environmental costs resulting from emissions with negative local effects (LE) during fossil fuel and electrofuel operation.

Finally, Fig. 6.9 (e) compares the annual direct and additional environmental costs of the ten assessed approaches. Here, two trends can be identified:

1. The dominating cost drivers of the potential future applications are the annual fuel expenses, whereas capital investment costs and volume opportunity costs fall far behind. Therefore, applications with the smallest specific fuel costs, most notably the CGH2-PEM system, are ranked above fuel alternatives with high volumetric energy densities.
2. Since component investment costs are not largely influencing the total annual expenses, fuel cell solutions are economically superior over ICEs for each electrofuel due to their higher efficiency.

As expected, the switch from fossil to synthetic fuels entails a major increase of the ship's operating costs. Therefore, it is advisable to not only count on the market introduction of electrofuels but rather regard them as one necessary share of the full picture. Certainly, other efficiency measures and wind-assisted propulsion play a very important role to mitigate the cost increase. In the overall environmental ranking, the NH3-ICE approach takes the last place, followed by VLSFO-ICE and FTD-ICE when assuming the conservative electrical energy carbon footprint. Again, fuel cell solutions surpass combustion engines as expected. Therefore, in this first comparison CGH2-PEM is identified to be the best future technology regarding the defined indicators.

To give a more optimistic scenario regarding environmental cost reduction, a reduced electrical energy carbon footprint is assumed and revised results are displayed in Fig. 6.11. Now, the desired massive reduction of the ship's carbon in-

tensity becomes clearer, whereat gaseous hydrogen still offers the largest reduction potentials. A key takeaway certainly is that only fuels produced from renewable sources with the lowest carbon footprints lead to the desired results of a decarbonized shipping sector, whereas a grid mix in the year 2030 will likely not improve the ship traffic emissions. Note that a complete switch to low-carbon-footprint electrical energy sources within the next decade is evaluated to be unlikely.

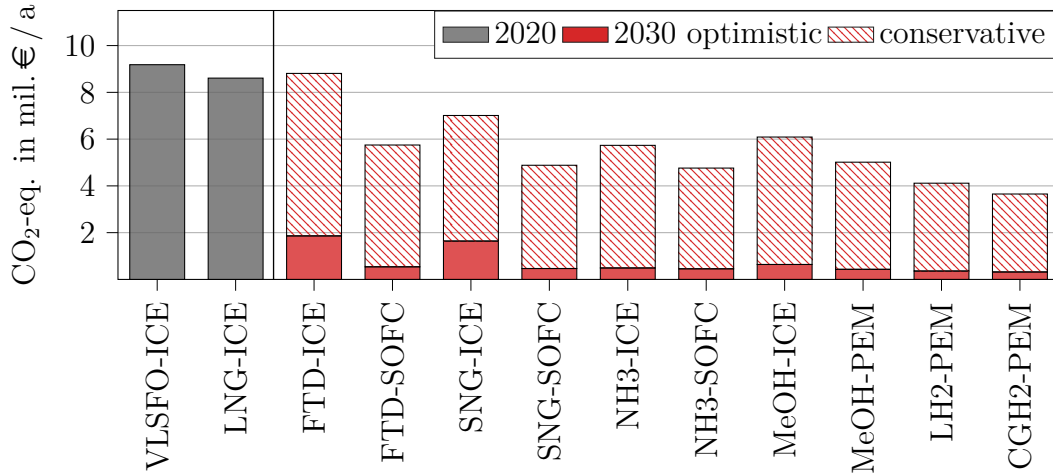


Fig. 6.11: Comparison of environmental costs resulting from emissions with global warming potential: conservative future scenario [223] and optimistic scenario [224].

In order to compare the application of electrofuels in the shipping sector with other environmental measures, specific CO₂ avoidance costs are calculated with the VLSFO-ICE benchmark. For the CGH₂-PEM example, avoidance costs amount to 0.086–0.14 €/kg_{CO₂eq}, depending on the assumed electrical energy carbon footprint. In contrast, the FTD-ICE configuration totals comparably high avoidance costs of 0.35–1.66 €/kg_{CO₂eq}, when compared to literature values regarding the maritime transport sector (0.11 €/kg_{CO₂eq} [232], 0.068–0.119 €/kg_{CO₂eq} [239]). Directly contrasting these values with carbon capture utilization and storage (CCUS) at fossil energy generation plants or for the non-power generation industry suggests that incurred costs for shipping are at the upper end of the spectrum (CCUS: up to 0.114 €/kg_{CO₂eq} [240]; industry: 0.083 €/kg_{CO₂eq} [241]). However, while in [242] exhaust-gas CCUS is evaluated as even less expensive (0.05–0.1 €/kg_{CO₂eq}), direct air carbon capture is estimated to be vastly higher-costed (up to 0.342 €/kg_{CO₂eq}). Hence, at least hydrogen-based ship applications are classified to be a reasonable environmental investment.

Influence of the Voyage Time

While a comparatively small influence of the volume opportunity costs is observed for a short mission, it is apparent that fuel tank volumes are becoming more important for longer passages. Here, gaseous hydrogen becomes more disadvantaged, since it has only 11.7% volumetric energy density compared to FTD, whereas storage costs amount to 2488% of an FTD tank. Therefore, the previously assessed load profile is extended to longer voyage times in the following. An example for the conducted profile extension is given in Fig. 6.12 for seven open-sea days. In total, missions from 2 to 31 days are investigated now. For each passage length, the power system is designed with an individual cost optimization task (cf. Eq. (6.18)).

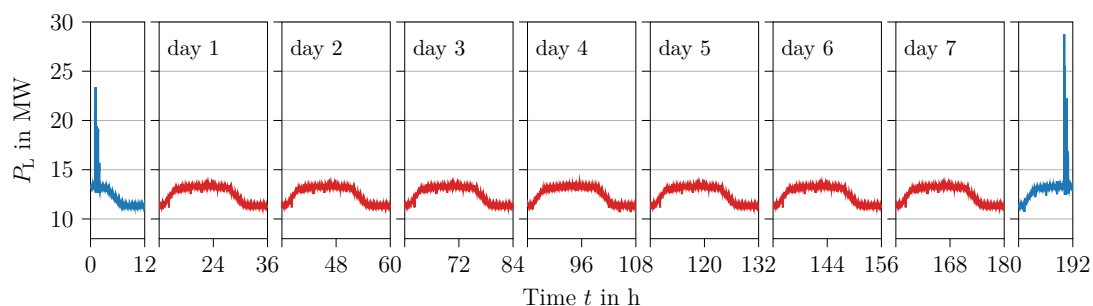


Fig. 6.12: Exemplary 192 h passage with seven open-sea days

The newly obtained annual direct and environmental system costs are displayed in Fig. 6.13 as a function of the ship's days on sea. The data at $t = 2$ days equal the results of the previously discussed detailed analysis (cf. Fig. 6.9 (e)). As can be seen in Fig. 6.13 (a), direct costs mostly increase over the length of the passage with a saturation behavior. This leads back to the nonlinear calculation of the volume opportunity costs (cf. Eq. (6.13)) on the one hand, and a reduced annual number of energy-intensive harbor maneuvers on the other hand. An exception are the FTD-SOFC, NH₃-SOFC, and the MeOH-PEM approaches with a low generator power density and high fuel energy density. Here, longer passages reduce the annual costs, since the generator volumes become less relevant over time. Even if steeper increases are visible for fuels with lower energy densities, CGH₂-PEM remains the most cost-efficient approach for passages shorter than 21 days. Only for longer missions, a trend reversal towards the NH₃-SOFC and the MeOH-PEM technology is visible. While hydrogen is categorically excluded from long missions in other investigations due to large volume requirements (eg. [41],[69]), the outcome of this assessment contradicts this assumption. To underline the feasibility, system volumes are in turn consulted: the cost-optimized CGH₂-PEM power systems require a total volume of 5,230 m³ for a 14 days passage and 10,990 m³ for a 31

day passage, whereas the investigated ship has a total gross volume of more than 440,000 m³.

In Fig. 6.13 (b) environmental costs are added to the optimized direct costs. A high cost increase for voyage times below seven days is displayed in addition to a general elevation of the graphs. Here, a higher average energy consumption per day is resulting from the accumulation of total maneuver operations. As expected, combustion engines fall further behind the respective fuel cell solutions in the ranking. CGH2-PEM now is uncontested over the whole assessment range due to the smallest environmental fuel footprint.

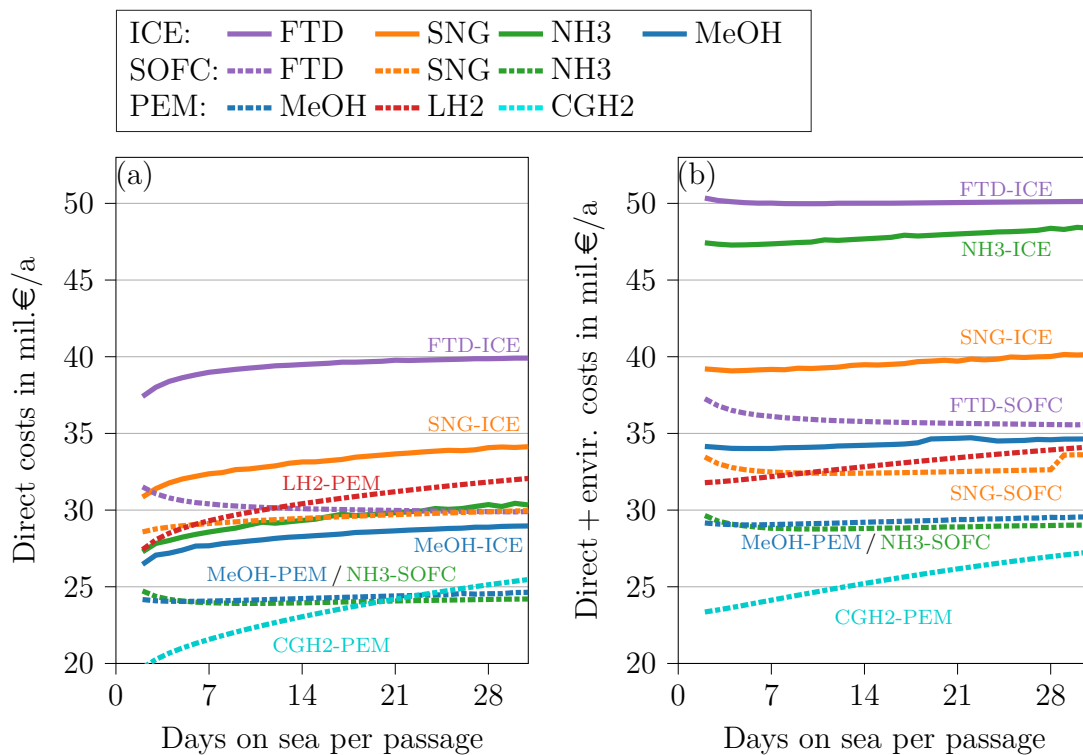


Fig. 6.13: (a) Annual direct system costs of the ten configurations as a function of the ship operating passage; (b) annual direct plus environmental costs

Influence of a Electrofuel Supply Cost Reduction

In the previous section, the assumed disparity of the specific fuel prices clearly overshadows the potential influence of component investment costs and volume opportunity costs regardless of the ship's mission length. However, since electrofuel prices have a large uncertainty range the longer a process chain is, a parameter study is conducted now. With previous results in mind, only a fuel cost reduction could theoretically change the qualitative outcome of the technology ranking.

Therefore, three scenarios including a decrease of the assumed electricity prices, an increased production efficiency, and a decrease of plant investment costs are set up to quantify effects on the results. Note that even if higher-costed fuels are benefited from the discounts to a larger degree, the relation between electrofuel prices will to some extent remain, as all rely on electrolysis and therefore electricity prices and plant investment costs.

Scenario 1: reduced electricity prices – Future electricity price prediction implies several large uncertainty factors. On the one hand, in [243] higher electricity prices are estimated for central European countries on the day-ahead market compared to the base fuel cost calculation in [69]. On the other hand, prices in potential electrofuel production locations like facilities in northern Africa will likely be lower: for an optimistic electrical cost reduction scenario, the specific energy price is reduced from a value of 30 to a value of 18 €/MWh which is congruent with estimations in the literature [244],[245]. Since resulting savings depend on the electricity cost share, both original cost percentages and new fuel prices are given in Tab. 6.7.

Scenario 2: increased production efficiency – The second scenario retains the assumptions of Scenario 1 and further adds cost reduction resulting from conversion efficiency increases. A higher electrolysis efficiency benefits all synthetic fuels analogous to the electricity cost reduction scenario. Here, an increase from 67% to 74% is chosen in analogy to [69]. The efficiency of different follow-up processes (Fischer-Tropsch, methanation, Haber-Bosch etc.) is estimated to not improve fundamentally but is determined on a flat 5% increase. Efficiencies and resulting specific fuel costs are again given in Tab. 6.7.

Scenario 3: decreased plant investment costs – The third scenario retains the cost reduction effects of Scenario 1 and Scenario 2. In addition, an electrolyzer capital cost reduction of 26.3% is chosen in analogy to the optimistic scenario from [244] for the year 2030. Analogously, specific cost reduction potentials for other required plant components are based on the predicted costs from [244] for SNG. As intended, the resulting prices given in Tab. 6.7 now correspond to other optimistic literature estimations. For example, in [244] a potential synthetic methane price below 100 €/MWh is assumed.

Fig. 6.14 presents the results of the revised assessment with the three different cost reduction scenarios. Again, annual costs are given as a function of the ship's voyage time. While the graphs' shapes appear very similar to the base assessment, it is immediately recognizable that the ordinate axis intercepts in all three scenarios are now decreased disparately. As a result, the trend reversal between CGH₂-PEM and NH₃-SOFC or MeOH-PEM as best technology-fuel combination shifts to 9–15 days. For the most optimistic Scenario 3, MeOH-ICE claims a third

place for passages longer than 24 days. Still, gaseous hydrogen remains the most competitive for short missions, whereas liquid hydrogen falls further behind other alternatives. While FTD and SNG approaches benefit the most from the assessed cost reduction, they still cannot compete with potential fuel alternatives economically.

Tab. 6.7: Revised specific fuel prices based on three cost reduction scenarios, percentage values originate from [69]

Scenario 1: electrical energy cost reduction (33 → 18 €/MWh _{el} [245])			
fuel	originating energy cost percentage		fuel price p_{fuel}
FTD	45.6%		125.3€/MWh
SNG	43.6%		113.9€/MWh
NH3	49.8%		92.8€/MWh
MeOH	52.0%		90.9€/MWh
LH2	39.1%		125.8€/MWh
CGH2	48.8%		78.6€/MWh
Scenario 2: Scenario 1 plus efficiency increase (+7% el. energy→H ₂ [69]; + 5% H ₂ → X)			
fuel	power→H ₂ efficiency	H ₂ → X efficiency	fuel price p_{fuel}
FTD	74%	78%	121.1€/MWh
SNG	74%	82%	109.9€/MWh
NH3	74%	92%	89.1€/MWh
MeOH	74%	84%	86.9€/MWh
LH2	74%	-	123.2€/MWh
CGH2	74%	-	76.0€/MWh
Scenario 3: Scenario 2 plus cost reduction (26.3% electrolyzer / 26.0% addit. plant [244])			
fuel	orig. electrolyzer cost	orig. addit. plant cost	fuel price p_{fuel}
FTD	20.9%	32.8%	98.9€/MWh
SNG	23.2%	23.3%	92.6€/MWh
NH3	27.5%	20.2%	74.2€/MWh
MeOH	27.7%	18.6%	72.5€/MWh
LH2	21.5%	17.1%	107.7€/MWh
CGH2	32.6%	9.6%	64.8€/MWh

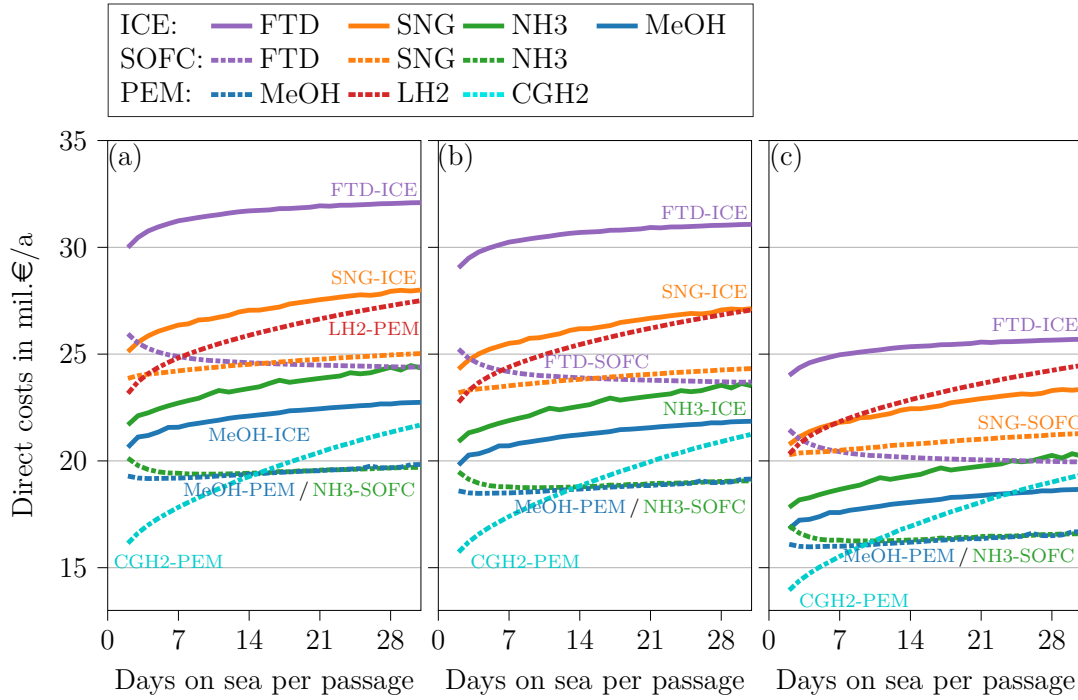


Fig. 6.14: Annual direct power system costs for the different fuel price scenarios: (a) electricity price reduction, (b) additional production efficiency increase, (c) additional reduction of plant investment costs

Influence of Rising Volume Opportunity Costs

Since direct fossil fuel replacements (FTD and SNG) do not profit from dropping fuel prices, their high volumetric energy density remains to be their only significant qualitative advantage. This upside could become especially relevant if service offering prices rise in the future due to higher operating expenses. Prices for transportation volumes are already heavily fluctuating today and certainly vary between passenger, cargo and bulk transport. For example, the price ranges of 553–2074 € per twenty-foot equivalent unit are reported in [67]. To cover potential market movements, in this section volume opportunity costs are increased. Here, higher prices are imitated with a linear scaling factor ϕ_{vol} :

$$p_{\text{vol, revised}} = \phi_{\text{vol}} \cdot p_{\text{vol}} \cdot \quad (6.28)$$

While market developments are hard to predict, the comparison of past and future fuel prices, which stipulate the ship service fees, are consulted to get a feeling about the potential opportunity costs increase: heavy fuel oil prices amount to around 25 €/MWh in 2020 [120], whereas FTD from [69] is 6.3 times as expensive. Here, scaled costs of 300%, 500%, and 700% are investigated.

Resulting annual costs are displayed in Fig. 6.15 as a function of the voyage time. As expected, cost functions now show a more sensitive behavior regarding passage lengths, depending on the utilized fuel and power technology. Still, ships with short mission profiles at best are operated on compressed hydrogen. Contrary, operating longer passages with hydrogen becomes vastly uneconomic. Here, a trend reversal towards MeOH-PEM is visible for eight or fewer days. Unlike in the previous assessments, the NH3-SOFC is clearly surpassed by the MeOH-PEM application for the first time, traced back to the smaller generator power density. Due to their worse energy efficiency, MeOH-ICE and NH3-ICE fall further behind the respective fuel cell solutions for longer voyage times. While costs for SOFC solutions are massively increased during short trip operations due to the small power density, they outpace ICEs with identical fuels for long passages. In particular, the FTD-SOFC application shows overall promising results for operating times over 28 days.

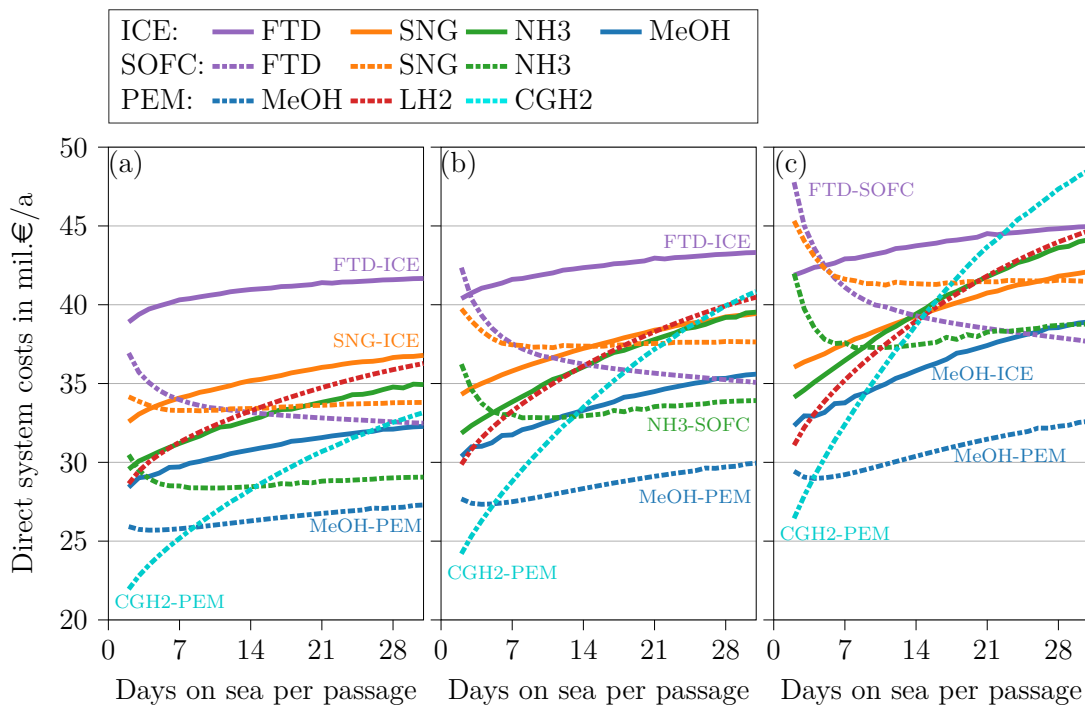


Fig. 6.15: Annual direct power system costs with varied volume opportunity costs: (a) 300% , (b) 500%, (c) 700% increased volume opportunity costs

Influence of the Vessel Size and Mission Characteristics

For the previously assessed load profile, CGH2-PEM and MeOH-PEM clearly are indicated to be economically superior over the other eight applications. Here, the choice of technology is not a question of future cost trends, but rather of passage

lengths the ship is operated on. Admittedly, the presented results are only valid for this specific use case and cannot be directly extrapolated on other ship sizes or types. Therefore, to further examine a potential influence of the load profile on the cost comparison, other mission characteristics are assessed (cf. Fig. 6.16).

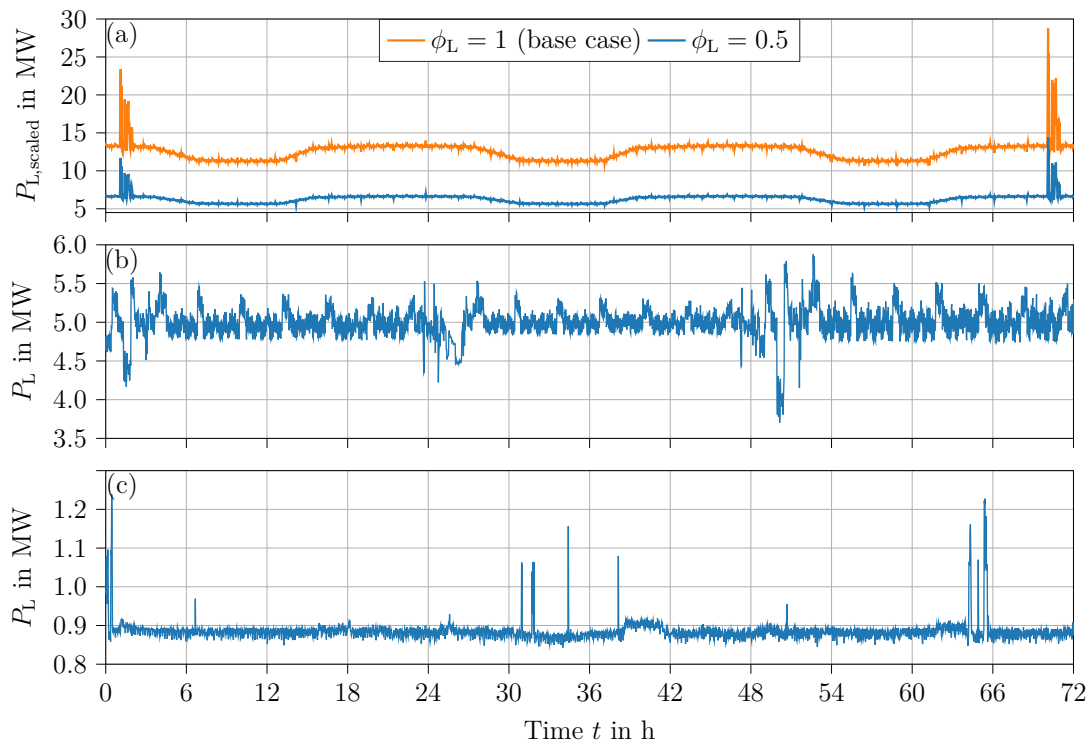


Fig. 6.16: Alternative load profiles: (a) 72 h cruise ship passage with linear scaling factor ϕ_L , (b) multi-purpose vessel, (c) general cargo ship

Two types of load variation are investigated: (1) the ship size and (2) the influence of specific load profile characteristics. Generally, a smaller ship equals less flexibility for the modular fuel cell system but also influences ICEs with nonlinear specific capital investment costs. Diverging system designs, in turn, affect the average energy efficiency of the power generators. To quantify these influences, the base case from Fig. 6.6 is modified with a scaling factor ϕ_L in a reasonable range:

$$P_{L,\text{scaled}} = P_L \cdot \phi_L \quad \forall \phi_L = \{0.1, \dots, 1.5\} . \quad (6.29)$$

An example for the factor $\phi_L = 0.5$ is displayed in Fig. 6.16 (a). Linearly scaling a load profile however neither changes the ratio between power and energy demand, nor does it represent different dynamic challenges for the hybrid system configurations. Hence, two additional profiles are analyzed. Fig. 6.16 (b) represents the

propulsion and board power demand of a multi-purpose ship with a highly fluctuating load. Fig. 6.16 (c) displays the load profile of a smaller cargo ship with a relatively constant base and comparably high peaks during maneuvers.

Again, a design optimization (cf. Eq. (6.18)) is conducted for voyage times between 2 and 31 days with each new case. Since the dimensions of the combustion engines are aspired to not change fundamentally, the number of units in the multi-purpose ship genset is reduced to two (cf. Eq. (6.19)). For the cargo ship, two combustion engines and fuel cell modules with a rated power of 100 kW (cf. Eq. (6.20)) are chosen as design constraints.

Neither for the scaled load profiles nor for the full-scale profiles with new characteristics a significant qualitative change of the results is recorded. Therefore, resulting annual costs for the technology-fuel configurations are not discussed in depth, but only displayed in Figs. 6.17, 6.18, and 6.19. In analogy to the last sections, eight total scenarios (base assessment, environmental cost consideration, 3x fuel cost reduction, 3x volume opportunity cost increase) are evaluated as a function of the voyage time.

Nevertheless, small qualitative assertions can be formulated from the assessments for the multi-purpose vessel and the general cargo ship: for a higher ratio between the load's peak power and the total energy demand, the power density of the generators becomes more relevant. This especially is apparent for SOFC technologies used on short passage lengths. In analogy, the fuel energy density becomes less important, leading to a shift of technology trend reversals between CGH2-PEM and MeOH-PEM. However, the general segmentation of best technologies for the operation still holds true. Last but not least, high load shift limitations can be compensated even for highly fluctuating profiles without large effort. Even contrary, the optimally supporting battery unit design here solely is adjusted for peak load shaving instead of load shift compensation. Hence, generator oversizing to establish adequate load-following operation is not recognizable for a single cost-optimized system. Concluding, the obtained results support a generalization of the elaborated key messages on the whole open-sea traffic sector.

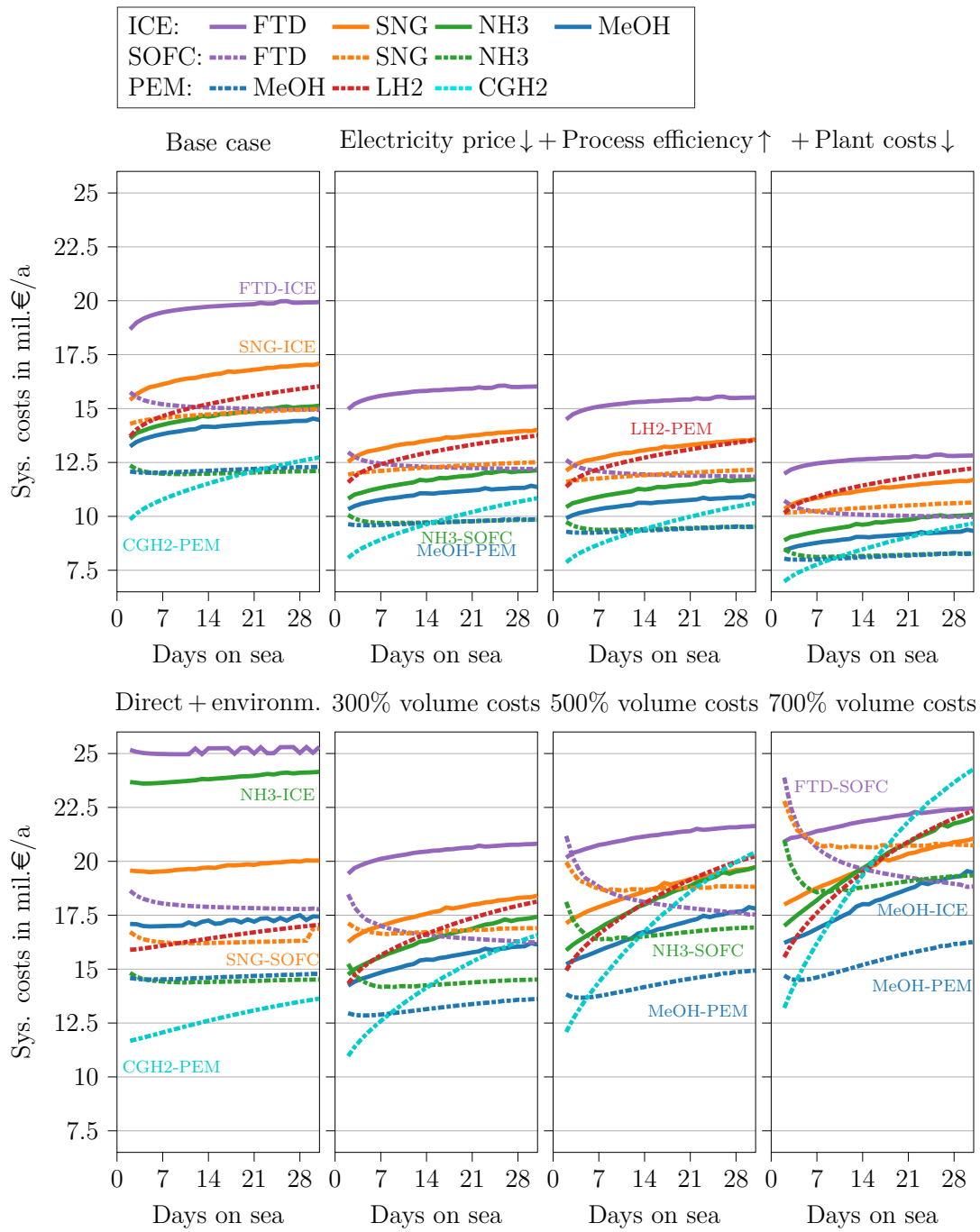


Fig. 6.17: Annual system costs for a cruise ship with the investigated base load profile scaled with the factor $\phi_L = 0.5$ (cf. Fig. 6.16 (a))

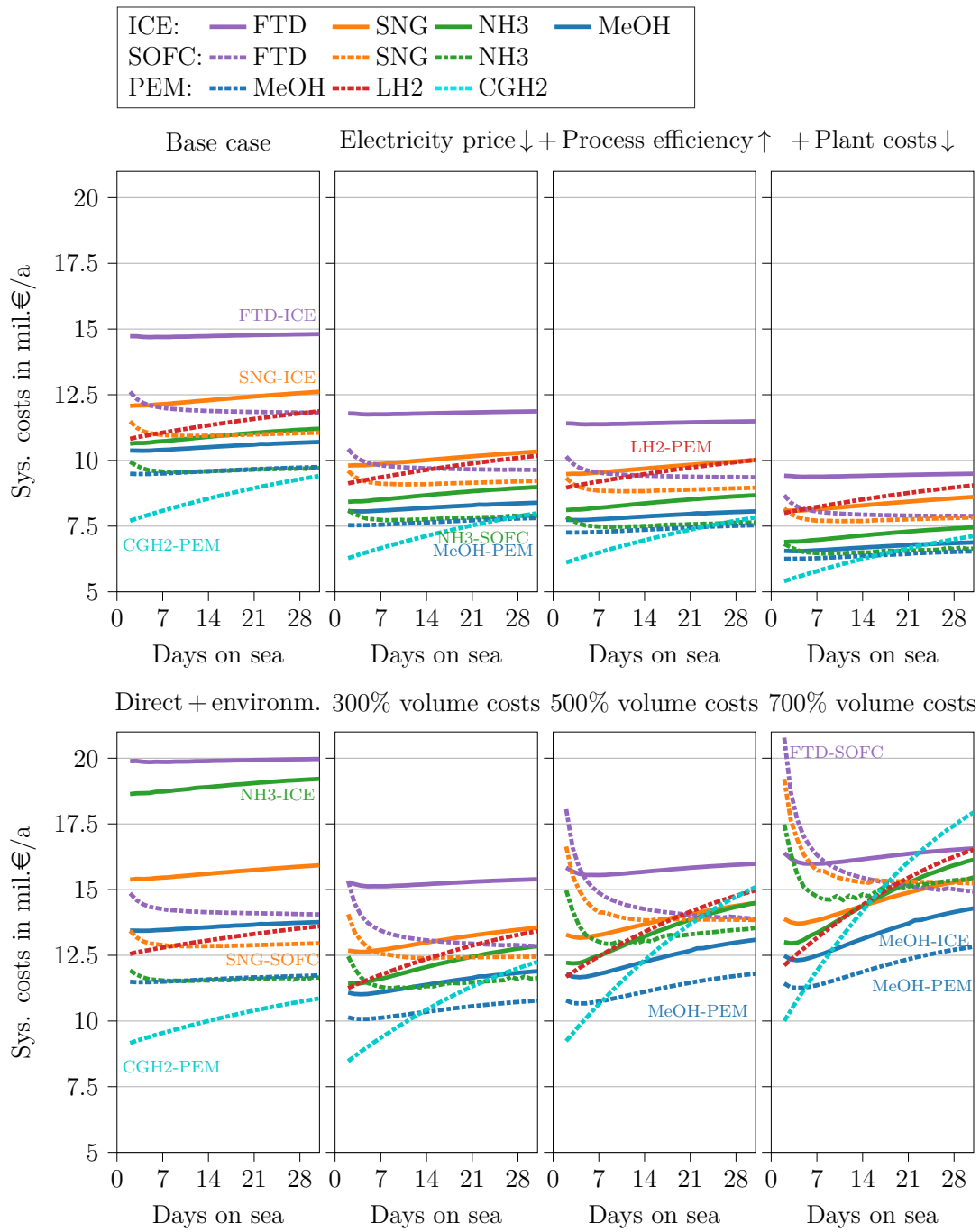


Fig. 6.18: Annual system costs for a ship with the multi-purpose vessel load profile (cf. Fig. 6.16 (b))

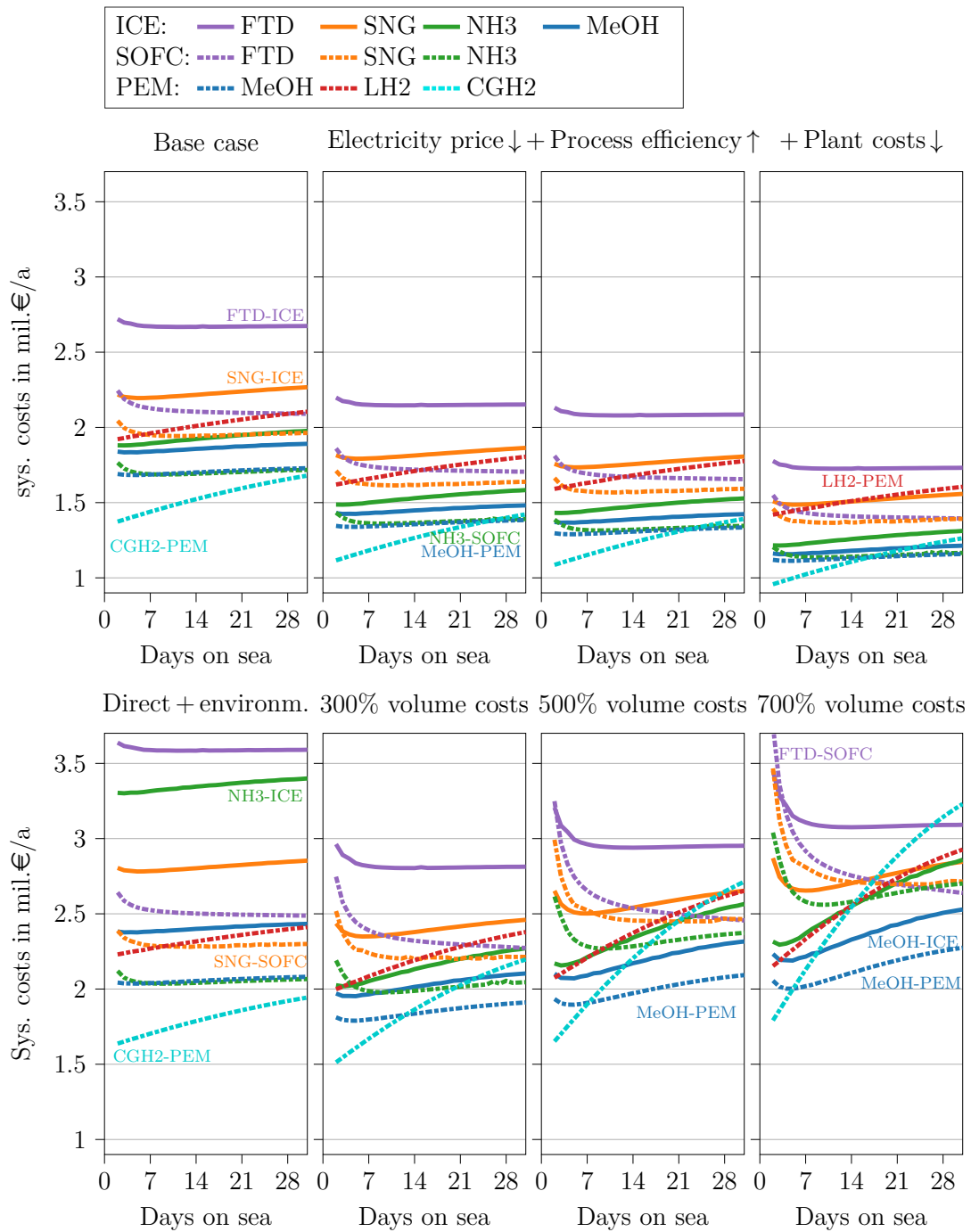


Fig. 6.19: Annual system costs for a ship with the cargo vessel load profile (cf. Fig. 6.16 (c))

6.6 Interim Conclusion

In the presented case studies, direct investment and operating costs, power system volume opportunity costs, as well as environmental costs are quantified for two state-of-the-art combustion engines and ten potential future power technology-electrofuel configurations. In doing so, an influence of the operating passage length, future fuel prices, and ship service fees are investigated for different ship types and sizes. In the following, all detailed questions regarding research issue [4] introduced in Section 2.4 are answered individually.

[4.1] Which power technologies and fuels are eligible in the near future and how are they performing compared to state-of-the-art systems?

In the shipping industry, several future fuel approaches are discussed to support a transformation towards sustainability. In this thesis, five different electrofuels based on the generation of hydrogen are selected to be the most reasonable energy carriers to cover the total demand of the shipping sector. On the other hand, bio-fuel capacities are identified to not closely suffice the sector's demand, but rather inhibit building the required electrofuel infrastructure due to their cheaper prices. For the sector transformation, three power generation technologies are aspired by the industry's participants: the continuance of internal combustion engines and the introduction of solid oxide or proton exchange membrane fuel cells. Ten reasonable future combinations of electrofuels and power generation technologies are identified and substantiated with real-life examples.

Economic assessment – In the case study comparison for the years 2020 and 2030, it is demonstrated that the introduction of electrofuels will massively increase the operating costs of a ship. Even the economically most profitable future electrofuel application does not match the costs of a conventional diesel system fueled with VLSFO. Natural gas however proved to reduce the ship's operating costs significantly. From a pure economic perspective, LNG combustion emerges as the most preferable configuration. Due to the potential massive increase of fuel costs, one takeaway should be to shift the main focus away from a purely fuel-centered debate. Here, other energy efficiency measures and the utilization of wind and solar power should be at least considered of equal value or even favored over a fast fuel transition.

Environmental assessment – The conducted analysis confirms the claimed emission reduction potentials of LNG over conventional marine fuel oils resulting in substantially smaller environmental costs. However, the overall damage

caused by gas motors still is determined to be in an unacceptable range. Thus, LNG combustion is rated not to function as a sufficient interim technology for the shipping sector.

Concerning the overall environmental impact of electrofuels, the electrical energy footprint is key to achieving desired reduction objectives. If fuel production relies on a 2030 grid mix and no low-carbon green power sources are established beforehand, reduction effects are not reaching the desired order of magnitude. With the introduction of green electricity, hydrogen fuel cells offer the smallest CO₂ avoidance costs down to 86 €/ton_{CO₂eq}.

In contrast to the analyzed fuel cell system approaches, the much-discussed ammonia combustion entails high nitrogen oxide and fuel slip emissions, which often is neglected in a CO₂-centered debate. The application involves the highest environmental costs and is even surpassing the conventional diesel engine. In general, all assessed future combustion engines require a massive exhaust gas treatment to be considered as a sustainable solution, even if they rely on electrofuels with small carbon footprints.

4.2 Which are the economic and environmental key performance indicators?

Economic assessment – Relevant economic indicators include component investment costs, operation expenses, and indirect costs caused by space requirements. As already introduced in Chapter 3, the calculation of annual system costs with an annuity cost method is ideally used to weigh long-term investments. Maintenance cycles and component degradation, especially important for energy storage units, are also part of a comprehensive technology evaluation. Fuel expenses make up for the by far largest share of the annual power system costs.

Environmental assessment – The environmental perspective should cover preparation and operating processes for both components and fuels. Here, not exclusively emissions with global warming potentials but also emissions with negative local effects including nitrogen oxides, ammonia, sulfur oxides, and carbon monoxide should be investigated. This is especially evident when investigating the ammonia combustion engine approach. Monetizing the annually occurring emissions with specific environmental costs allows for a direct comparison of the different emission types and indicates the relation to a shipowner's direct expenses.

4.3 How can a configuration bias be prevented when comparing technologies?

In order to avoid unfair study designs, four key elements should be considered:

1. It is required to not only analyze rated operating points, but reconstruct application-driven scenarios, which include part-load conditions and time-dependent load adjustments.
2. Only a comparison of optimized system designs enables a fair technology evaluation. If not all assessed systems are treated equally, results could be distorted significantly, as has been visualized with help of the cruise ship's original energy system design.
3. In this context, energy storage support should be assessed for all system approaches, as most applications benefit from it economically. This was shown for the conventional diesel-based system in the year-2020 assessment.
4. For a comprehensive study, a direct comparison should consider all key performance indicators and not solely focus on capital investment costs or system volume. In this context, it is helpful to find ways of performance comparability. Given examples include the monetization of system volumes with the introduction of opportunity costs, or the pricing of environmental damage caused by component production chains or operating emissions.

4.4 Which relevant price developments are to be expected and how do they affect the economic performance of the technologies?

System components – Both power generators and battery systems are evaluated not to be the biggest cost drivers in today's and in the future scenario. Therefore, higher investment costs for fuel cells after their large-scale market introduction should be accepted for the sake of better conversion efficiencies.

Fuel costs – On the other hand, annual fuel costs are identified to be the largest share of the total power system expenses. This becomes even more apparent with the application of costly electrofuels. Since a high dependence of the annual costs on the fuel expenses was identified, different cost trends were pursued in a revised study. However, due to the coupling of electrofuel cost reduction opportunities (electricity price, hydrogen generation efficiency, cost reduction of the electrolyzers) no decisive result deviations were identified.

Volume opportunity costs – Large system volumes are economically disadvantaged in particular for long voyage times. Nevertheless, resulting volume opportunity costs lack significance for the assumed base parameters. However, since energy costs constitute one of the largest overall expenses for a shipowner, more expensive fuels will likely increase the market price for shipping activities. In turn, volume opportunity costs will inevitably rise and change the outcome of the technology ranking in favor of energy-dense fuels and power-dense generators for long mission profiles. Still, the following addressed key messages regarding technology selection remain persistent.

4.5 Are there mission profiles or operating scenarios for which certain approaches are particularly suited?

Vessel type – The economic advantage of fuel cell applications and fuels with lower energy density compared to today’s fuel oils is not only seen for the cruise ship case study, but also for alternative vessel types. It has been shown, that a technology trend reversal occurs in dependency of the ship’s voyage time, but regardless of the assessed load profile characteristics. Since the generated technology ranking is reproducible for several ship load profile characteristics, the extrapolation of obtained results on the open-sea traffic sector suggests itself.

Short trip – Hydrogen-fed PEMFCs come out as the economically best solution for voyage times of at least one week in all analyses. At this point, the exclusion of gaseous hydrogen for open-sea traffic by reason of its small energy density often found in the open literature is proven to be wrong.

Long trip – The approach of fuel cells with shipboard methanol steam reforming is identified to be a promising technology for longer missions in terms of economic and environmental indicators. Alternatively, SOFCs operating on ammonia represent a similar performance but require a larger installation space and therefore imply higher volume opportunity costs. Concluding, a two-parted future fuel supply infrastructure containing hydrogen and methanol is recommended to cover presented advantages for short and long missions.

Certainly, fuel availability in ports will massively influence the shipowners’ choices of technology. Therefore methane or diesel-based applications have the advantage of not completely relying on synthetic fuels. In addition, the production output of electrofuels will not solely be decided by the shipping industry. Here, production and port locations, as well as decision making of states with a potentially high renewable energy surplus play an important role on the actual fuel supply capacities and prices. However, the presented results urge to conduct the suggested fuel

transition sooner rather than later to enhance early technology improvements and give starting directions to the fuel industry.

With the discussion of all five detailed questions, the fourth and last research issue (“[4](#) Which is the most cost-efficient and sustainable ship power system configuration for the future?”) is finally answered. While there is not one clear winner, power technologies and fuels suiting specific ship mission profiles are identified with help of the conducted case studies.

7 Summary, Conclusion and Limitations

The focus of the present dissertation is the development of a model-based ship power system assessment approach. Thereby, two overarching application tasks are addressed: finding criteria for a well-designed hybrid system configuration and evaluating potential future power technologies regarding their economic and environmental performances. In the following, the four research issues are readdressed and the formulated interim conclusions are summarized. Then, assessment method limitations are raised and linked to potential further research tasks.

Answers to the Research Issues

In this section, the most relevant aspects of the interim conclusion sections are outlined with allocation to the four thematic fields developed in Chapter 2.

1] Which aspects matter for the conceptual design of a hybrid ship power system?

Three key elements for modeling an isolated power system with fluctuating load profiles are showcased in the present dissertation: (1) the appropriate consideration of component's operating limitations, (2) the understanding of implications when using model assumptions and the recognition of oversimplifying complex correlations, and (3) the consulting of annual expenses by the help of annuity payment factors and operation-dependent component lifetime calculations to compare investment and operating costs. Examples found for these three elements include: (1) the explicit distinction between power and energy bottlenecks for storage designs depending on load profile and fuel cell system response, (2) the diverging optimal component configuration when first establishing a power-dependent storage degradation model, and (3) the deviation between technically optimal and cost-optimal but oversized configurations due to the lifetime-dependent annuity payment improvements. While the inclusion of operation-dependent fuel consumption only marginally influences the system design choice for the investigated LNG-SOFC combination, the assessment of operating costs becomes more important when comparing different technology and fuel solutions.

2] Are SOFCs suitable for marine applications?

While solid oxide fuel cells entail the much-discussed advantages of a high energy efficiency, the absence of combustion-typical emissions like nitrogen oxides, and beneficial flexibility towards carbon-based fuels, dynamic operating limitations inhibit their standalone application in marine power systems. However, it is demonstrated that moderate energy storage support suffices to grant an uninterrupted power supply for a fluctuating load demand, even if the high-temperature process requirements significantly limit the system's load shift capabilities. However, the potential design range for the hybrid system configuration turns out to be comparatively small, emphasizing the usage of the introduced design optimization approach to finding a suitable solution. In doing so, peak shaving conducted by the storage unit meaningfully reduces the power generator sizing requirements, irrespective of whether the energy capacity or power provision demands are identified to be the storage design bottleneck.

3] How can the advantage of a fuel cell's modular characteristic be leveraged in large-scale ship power systems?

Modular components potentially enable a system decentralization according to the shipboard power demand without meaningfully decreasing the power generation efficiency. Thereby, a distributed configuration has a positive effect on the power transmission system requirements along with reduced transport losses. While the accompanying built restructuring implies great effort, cost-saving potentials are identified for different calculated scenarios. The modularity of all power system components allows for achieving the legally binding redundancy requirements without a larger monetary effort. However, from a regulatory perspective the system decentralization is not a necessary measure but rather involves an intricate certification by a classification society. Apart from the assessment-related findings, several additional qualitative benefits are collected. These include a more easily integrable cogeneration operation of the fuel cells with fewer transport losses, the partial protection from a total blackout due to a zonal malfunction, and the theoretical abolition of emergency power generators.

4] Which is the most cost-efficient and sustainable ship power system configuration for the future?

While many ship owners speculate on maintaining their existing fleets, future synthetic fuel expenses will most likely massively outweigh the capital investment costs of new power technologies, clearly indicating the profitability of ship

retrofitting approaches. In a synthetic-fuel-centered future, ICEs generally succumb fuel cell solutions due to their worse energy efficiency not even including emission levies or environmental costs. Specifically, compressed gaseous hydrogen for shorter missions and ammonia or methanol with a higher volumetric energy density for extended voyage times are assessed to be the most economically competitive fuels. From an environmental perspective, it is confirmed that utilizing LNG to substitute diesel oils reduces a ship's environmental impact regardless of the denounced methane slip. However, such efforts do by far not suffice to reach the aspired environmental performance indicators. Still, synthetic fuels provide the requested results only if produced from low-carbon-footprint energy sources. Overall, the introduction of electrofuels is a cost-intensive emission reduction measure. Where applicable, priority should be given to alternative solutions like wind-assisted propulsion and friction reduction measures. Still, for a holistic approach, synthetic fuels from sustainable energy sources play a decisive role to guarantee a shipboard power supply security.

Assessment Limitations and Further Research Demand

Model-based system optimization constitutes a proficient tool for the conceptual design phase of a ship power system, However, the presented approach certainly implies an inaccuracy range that should be considered before coming to a final conclusion for construction. The following six topics are identified to be critical if steps beyond a conceptual thought process are aspired:

1. During the investigations it became apparent that participants in the shipping sector frequently lack high-quality operating data. In addition, since many large-scale ships are unique builds, shipbuilders can only obtain measured load profiles from similar vessels. Here, time-dependent load modeling could be a solution here and will see growing interest with a now quickly increasing number of vessels with hybrid power system.
2. While the power technologies' fuel consumption behaviors are modeled to be operating-point-dependent, efficiency drops during load shifts are not considered in the component description. However, depending on the investigated technology, a steady-state generator operation combined with a larger supporting energy storage could very well represent a more cost-efficient design solution. Although there exist few openly available publications on this topic, including this characteristic in the component model, is believed to be the next relevant refinement step.
3. Likewise, component lifetime assumptions neglect dynamic load shift effects as well as external ship-related influences like extraordinary temperatures,

vibration and high inclination angles. Since the annuity payment factors relevantly influence the design optimization, further investigations with measured cell degradation maps are of high interest to create an enhanced economic perspective.

4. For the assessment of a decentralized system structure, purely modular builds are assumed, neglecting plant scaling effects for peripheral components. In reality, larger modules might be more cost-efficient and therefore could influence a cost-optimal design. Analogously, fewer engine rooms would most likely result in lower safety equipment costs. As already stated in the respective interim conclusion, at this point a holistic ship construction assessment is required for a clearer picture.
5. Another practical challenge for a real-world installation is the component oversizing for extreme operating conditions that are not resembled in the analyzed load profile. While modular fuel cells with favorable part-load characteristics definitely mitigate this issue, a reasonable strategy must be applied to this subject to not forfeit the optimization process benefits. Further, component malfunctions can be hard to predict in advance but should be taken into account according to the assessed ship build to present adequate scenarios. Potential changes could be caused by shared fuel supplies or the spatial separation of battery units.
6. Finally, while the different energy management strategies function for the conceptual design phase, most aspects likely can be improved due to the large number of degrees of freedom and possibilities for component interaction.

A Operating Strategy Examples

A.1 SOFC-based Hybrid Power System

System Control Strategy – A straightforward example including one state change is given in Fig. A.1. Fig. A.1 (a) displays the load demand, the resulting fuel cell system set value and the limited system response. In Fig. A.1 (b) the battery power, which equals the delta between fuel cell output and load profile is given. Fig. A.1 (c) shows the resulting change of the storage’s energy content. At first, the SOFCs operate at rated power and therefore produce excess energy, which in turn is used to charge the storage (cf. Fig. A.1 ①) until the critical SoE is reached (cf. Fig. A.1 (c)). The defined state change then influences the SOFCs’ operating mode and a power downshift is conducted, followed by a delayed load-following operation (cf. Fig. A.1 (a) ②). The state of energy therefore does not reach a maximum and the system remains operable.

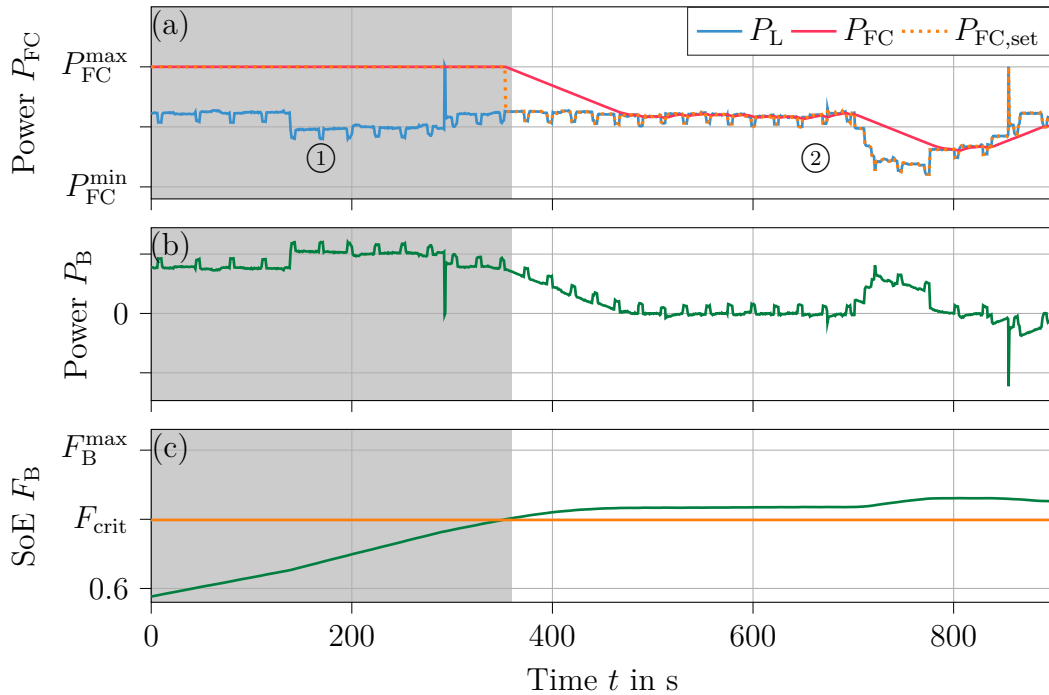


Fig. A.1: EMS strategy: fuel cells in full load operation (period ①) and part load operation after reaching the critical SoE (period ②).

Hybrid Storage Control Strategy – An example for the control strategy is given in Fig. A.2. The requested storage power first benefits reaching the desired SoE, resulting in a full transposition until achieving the target (Fig. A.2 ①). Battery charging is enabled, maintaining the supercapacitor SoE (Fig. A.2 ②). While discharging, battery power still requested first is limited by the maximum power. Consequently, the battery is supported by the supercapacitor, which in turn leaves the desired standby SoE (Fig. A.2 ③).

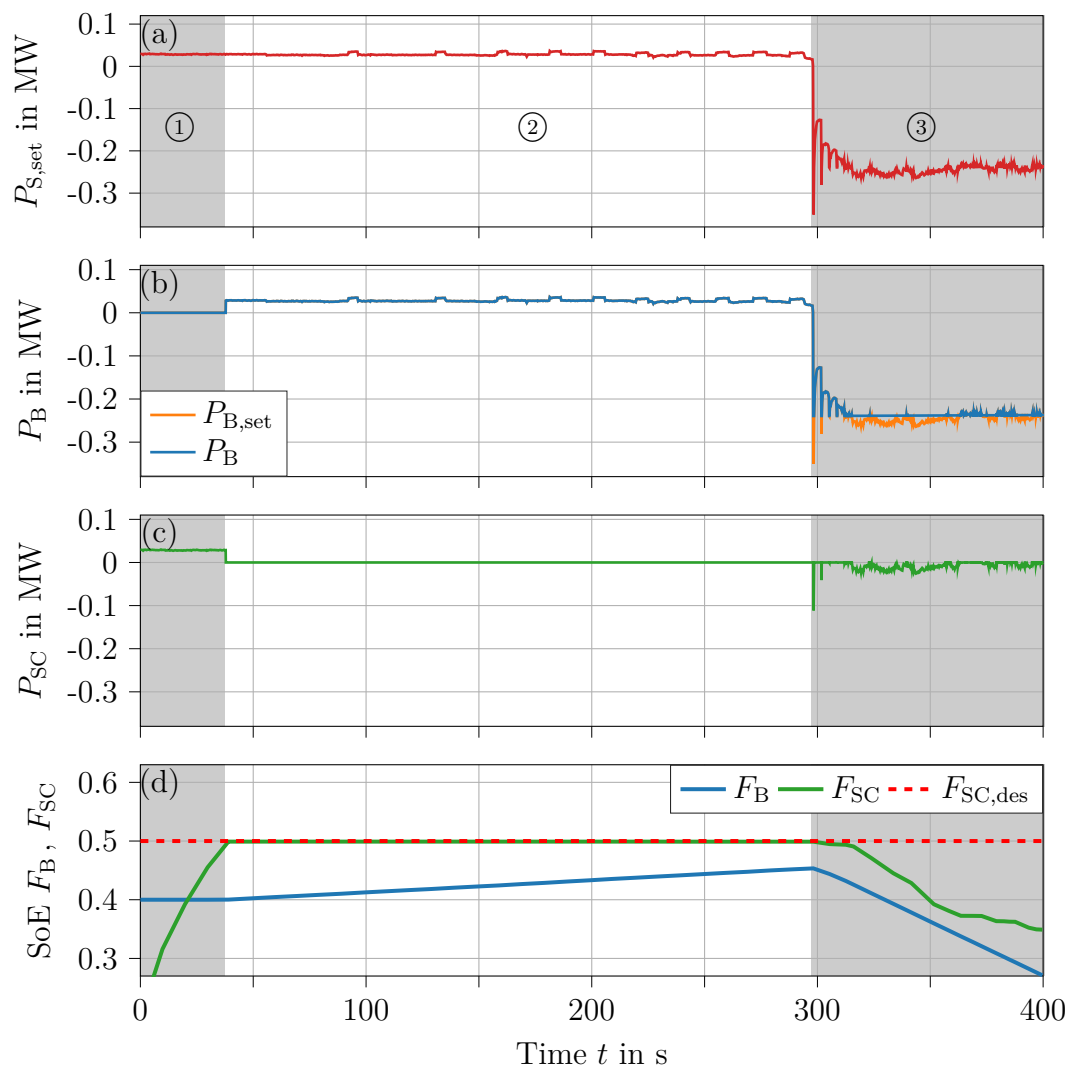


Fig. A.2: Total storage set power $P_{S,set}$, battery power P_B , supercap power P_{SC} , and states of energy F visualize the hybrid storage management: supercap charges until it reaches the standby SoE, excess power is received by battery, supercap and battery both discharge due to latter's power limitations.

A.2 Distributed SOFC-based Power System

Fuel Cell System Control Strategy – The four fuel-cell-related EMS priorities introduced in Section 5.4.2 are also displayed with the help of an example shown in Fig. A.3. Fig. A.3 (a) gives the total load demand and the cumulative SOFC power output, Fig. A.3 (b) shows the broken-down power output of three SOFC modules, and Fig. A.3 (c) depicts the average battery SoE resulting from the power delta between consumers and sources. The previously introduced four control strategy priorities are addressed and connected to the example case:

1. Successful load-following operation of the SOFCs is shown Fig. A.3 (a) for periods ① and ④, whereas a synchronization is restricted by the power gradient limitation in period ②.
2. Dynamic operation is allowed for a minimum amount of units required to keep synchronized, resulting in a cascading behavior shown in Fig. A.3 (b), period ①. Whenever a border of the desired corridor is reached, priority is switched to maintain preferred operating points. Periods ② and ④ also show that more than one unit is activated for modulation, if synchronization is not achieved within a defined time limit to accomplish priority 1.
3. Starting dynamic operation is not implemented in a fixed ranking but relies on the observation of local power deltas. This variable ranking can be observed Fig. A.3 (b) period ①, where the fuel cell module in fire zone $k = 1$ modulates first at $t = 0$, second at $t = 5.5$ min, first at $t = 10$ min etc.
4. The average SoE F_{\varnothing} should ideally stay within a corridor with the limits F_{high} and F_{low} . Whenever the SOFCs are not able to follow the load and the compensating battery reaches the SoE limits (Fig. A.3 ②→③), the SOFC set power value is maximized or minimized (cf. period ③) until the desired corridor is reached again. Only then, load-following operation is enabled. The indicator state Z_{FC} determines, if priority 1 or 4 is favored during operation.

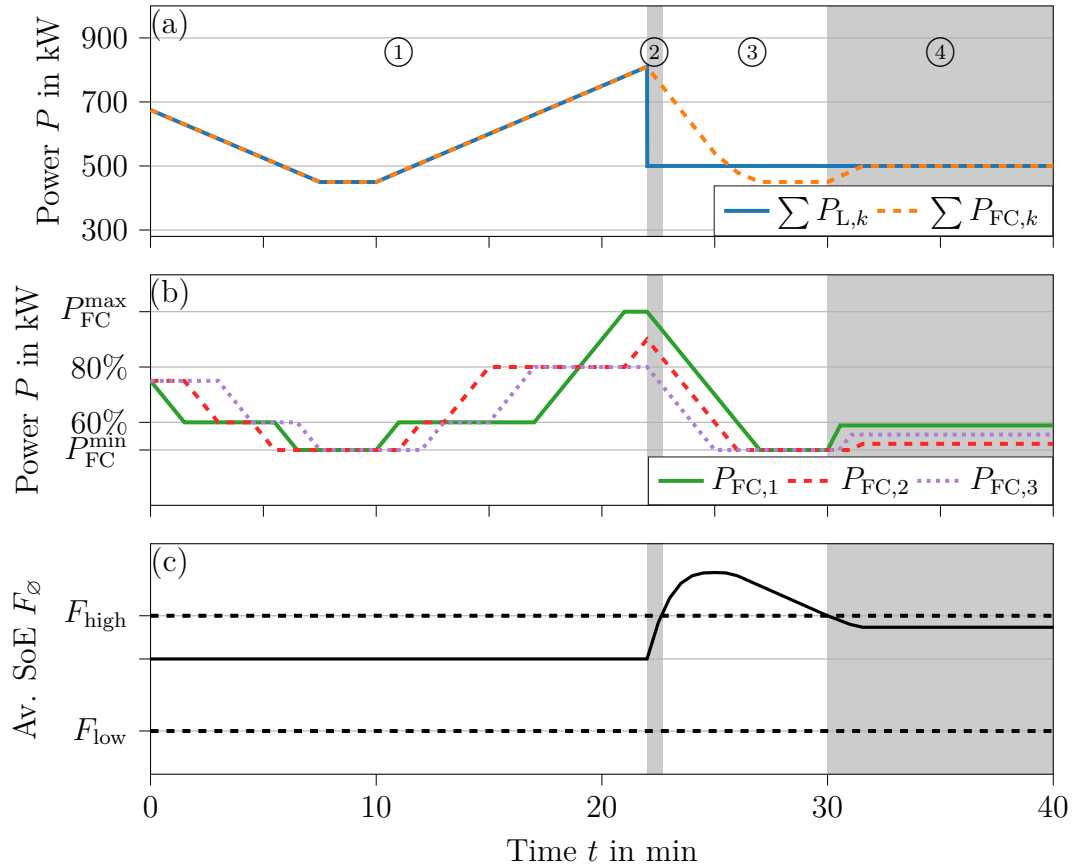


Fig. A.3: SOFC operation with one unit in each of three fire zones: ① average storage SoE within the desired range, load following in cascades depending on max. delta between local load and fuel cell operation; ② load drop, maximum power gradient to synchronize with load, storage is charging; ③ $F_{\varnothing} > F_{\text{high}}$, minimizing SOFC power to discharge storage; ④ batteries reach noncritical SoE, fuel cells synchronize with load

Storage Control Strategy – The three battery-related control strategy objectives described in Section 5.4.2 are further visualized in Fig. A.4. Fig. A.4 (a) displays a fluctuating load profile and the cumulative SOFC power. Fig. A.4 (b) depicts the derived distributed storage charge and discharge power. Fig. A.4 (c) displays the related states of energy. Fig. A.4 (d) shows the resulting power flow between the fire zones.

In this example the SOFCs cannot follow the load properly. Therefore, the storage units compensate the power delta. Hereby, the storage in fire zone 2 provides more power (cf. Fig. A.4 (b)) due to its double-sized energy capacity. While discharging, storage 1 provides a lower power output than storage 3 due to its lower SoE (cf. Fig. A.4 (c)). While charging, this behavior reverses. Consequently, the SoEs slowly converge. Fig. A.4 (d) demonstrates that transmission via the power

backbone is required, as the set value calculation does not consider component position, but degradation reduction at high priority.

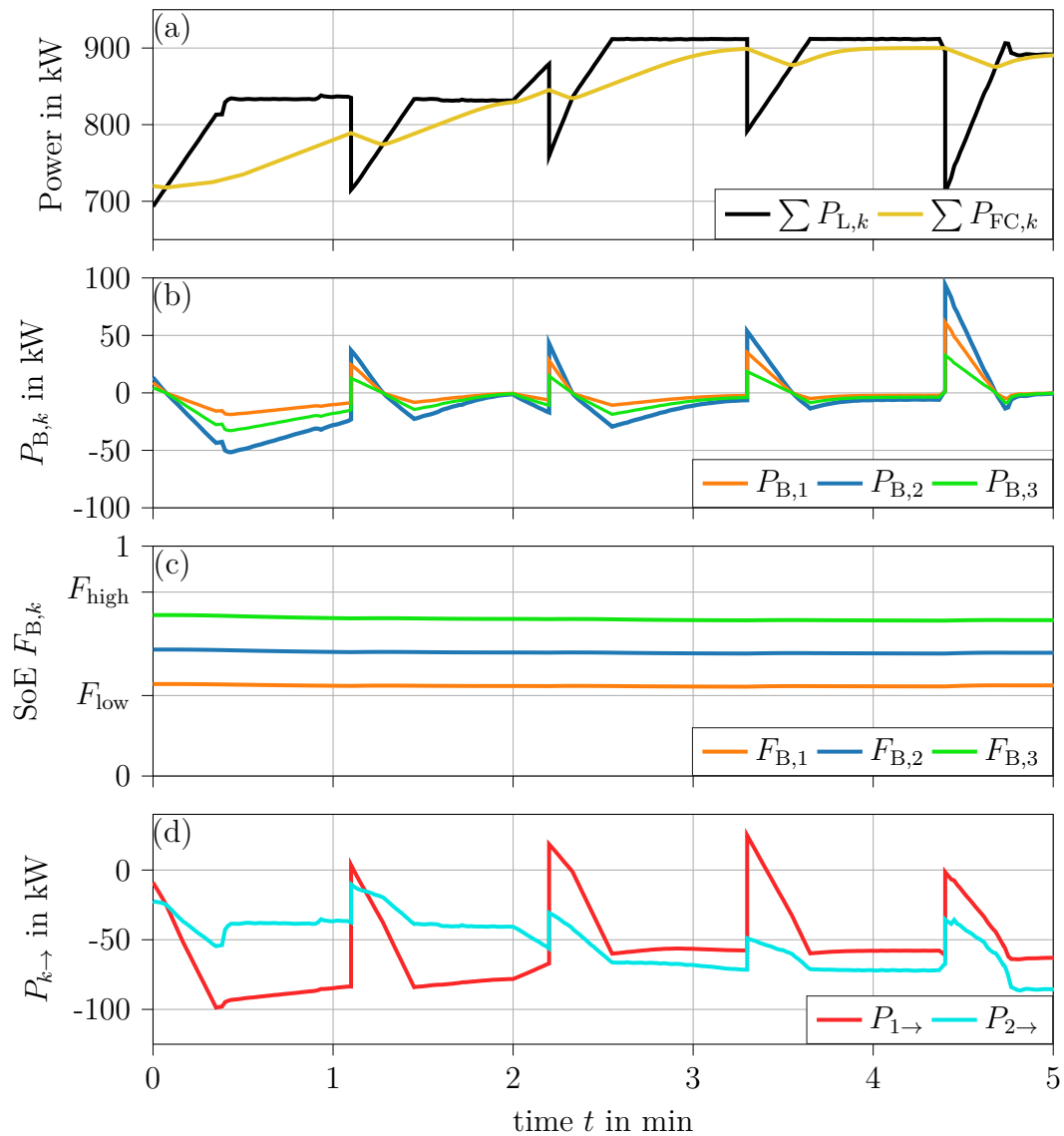


Fig. A.4: Exemplary storage operation; battery cell distribution: $N_{B,1} = N_{B,3} = 0.5 \cdot N_{B,2}$; storage powers vary in amplitude due to different SoE (cf. $P_{B,1}, P_{B,3}$) and rated capacity (cf. $P_{B,2}$); power distribution results in the usage of the transmission system

A.3 Universal System Control Strategy

An example for the universal EMS is given in Fig. A.5 for an NH₃-ICE genset containing two engines, since both the load shift limitations and genset controls can be visualized. Fig. A.5 (a) displays an exemplary load profile and the engines' total answer, Fig. A.5 (b) shows the battery power to compensate the resulting delta, and Fig. A.5 (c) depicts the derived battery state of energy.

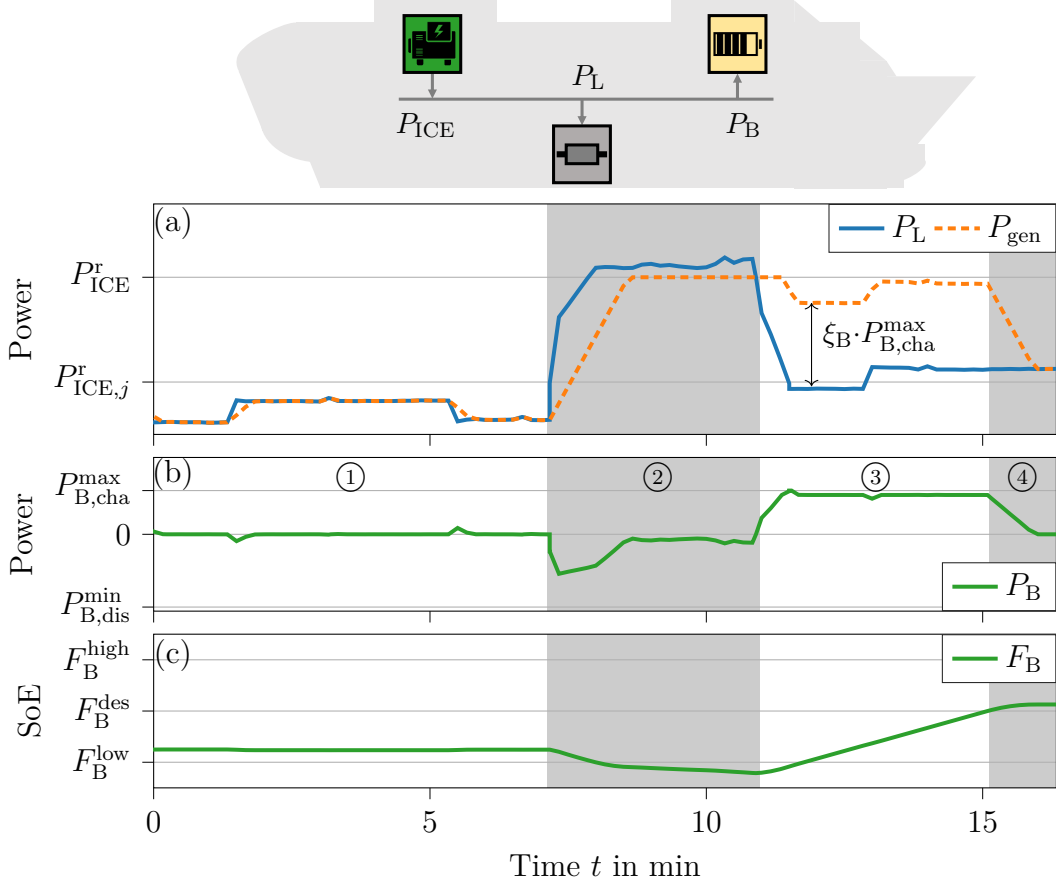


Fig. A.5: Control strategy example based on the NH₃-ICE approach: (a) load profile and generator power, (b) battery power, (c) battery state of energy. ① One of two generators operates in load-following mode with limited power gradient; ② second generator is turned on and maximum power is reached, battery compensates power delta and falls below the critical SoE F_{low} ; ③ generators operate above required power to recharge the battery until F_{des} is reached; ④ generators return to load-following operation.

While load-following operation is applicable in period ① with only one engine, the step increase of demand in period ② results in the activation of the second engine. However, load change limitations prohibit a rapid adjustment resulting in

a higher demand of battery power. As the battery is also deployed for load shaving, its SoE becomes lower and falls below the limit F_{low} . Therefore, in period ③ the generators operate on a higher power level than required by the load to recharge the battery (state machine: $Z_B = -1$). Since a high power factor ξ_B is chosen, the battery operates close to the unit's maximum charge power. When the desired SoE is reached in the beginning of period ④, the active engines decrease their power output simultaneously (state machine: $Z_B = 0$). No generator is switched off, since the power demand exceeds the rated power of one engine.

B Technology Performance Assumptions

B.1 Operation-specific Fuel Consumption

VLSFO-ICE: A characteristic curve according to [246] is used.

LNG-ICE: A curve describing lean-burn spark ignition engines is chosen [147].

FTD-ICE: No changes compared to conventional diesel ICEs are assumed.

SNG-ICE: No changes compared with state-of-the-art spark ICEs are assumed.

FTD-SOFC: A diesel pre-reforming SOFC system is modeled and validated in [165],[247]. Plausible arising efficiency and operating behavior changes for a scaled-up system are adjusted after a consultation of the accountable research group. An efficiency shift due to technological advances is included based on [248].

SNG-SOFC: Base results are obtained from [78] and include a prognosticated efficiency shift to 60% at full load until the year 2030 [248].

NH3-ICE: Technology reviews with ship context put ammonia combustion efficiencies on the same level as diesel (assumption in [50]) or natural gas combustion (qualitatively explained in [66]). In an experimental study including hydrogen admixture, efficiencies are around 2% worse compared to methane combustion [151].

NH3-SOFC: Fuel consumption is calculated for a plant with internal reforming and afterburner. Voltage-current curves and geometries are obtained from [172]. Predicted technology advances are adapted from [248]. Ammonia decomposition kinetics are quantified in [249]. System descriptions are found in [250],[251],[252].

MeOH-ICE: Peak efficiencies of 51% are reported for best operating conditions [154]. Qualitatively equal part-load behavior compared to diesel combustion is shown in [253]. Since most prototype plants are not scaled equally to ship engines, literature results are evaluated with regard to the engine size.

MeOH-PEM: PEMFC model assumptions are based on [254],[255],[256]. Voltage-current curves are obtained from [257] and adapted for predicted technology advances. Heat exchange between steam reformer and fuel cells is evaluated in [258]. Methanol steam reformer behavior is modeled with results from [174], [259], [260].

H2-PEM: The fuel consumption suitable for both LH2 and CGH2 is adopted from [261] and modified to display the 2030 goals from [197]. Fuel cells are operating

on close-to-ambient pressure levels. For LH2, autonomous fuel heating to ambient temperature and entire consumption of boil-off gases are assumed.

B.2 Operation-specific Emissions

VLSFO-ICE: Emissions from conventional diesel engines operated with fossil fuel entail black carbon [262], carbon monoxide [246], nitrogen oxides [211], and sulphur oxide emissions [142].

LNG-ICE: Emissions of a spark-ignition motor fueled with natural gas cause a methane slip [146], carbon monoxide [214], nitrogen oxides [214], as well as minuscule sulfur emissions [215].

FTD-ICE: The absence of aromatics in the synfuel and its higher cetane number lead to fewer emissions compared to fossil fuel combustion. CO, NO_x and BC emissions are adapted with the findings from [263] concerning gas-to-liquid fuel combustion. Also, sulfur oxide emissions are reduced to zero.

SNG-ICE: SNG contains smaller shares of impurities like nitrogen compared to natural gas. However, emission reduction effects are much smaller than for FTD and neglected here.

FTD-SOFC: With the assumed reformer operating range, carbon monoxide occurs in form of an intermediate product and mostly reacts in the water-gas-shift reaction. The remaining molecules are recirculated with other anode gases, reducing the leakage to a minimum.

SNG-SOFC: In analogy to FTD-SOFC, no operating emissions are assumed.

NH3-ICE: Nitrogen oxides: Even if a lower temperature is present in post flame zone and the premixing possibility also accounts for more homogeneous combustion [66], a higher amount of nitrogen in the combustion mixture increases the mass of emitted nitrogen oxides. Different exhaust analyses present NO_x values of 1200 ppm [264], around 1000 ppm [151], 1.9-5 g/kWh for compression ignition, and 0.5-7.7 g/kWh for spark ignition [66]. Data from [211] are used for part-load quantification, since similar effects influence the operation-dependent production. Certainly, emissions depend on combustion adjustments like spark timing [265]. While up to 8% in mass are reported without mixing in hydrogen [66], as low as 700 ppm are observed in [265] with the correct oxygen percentage. Similar results are obtained in [266]. The ammonia slip is derived for a lean combustion of a mixture with 20% hydrogen and air. Here, around 1% of the converted ammonia does not react. However, the hydrogen leakage is assumed to be negligibly small [66],[151],[264], as is the formation of nitrous oxides [264].

NH₃-SOFC: Neither for internal nor for external cracking, nitrogen oxides meaningfully occur in the exhaust gas but only as an intermediate product, since the subsequent nitrogen formation proceeds at a much faster rate than the ammonia decomposition [267]. However, nitrogen oxides occur during the off-gas combustion in the afterburner [268]. Maximal values of 0.18 g/kWh are reported for full load. Nitrous oxide emissions are below 2 ppm even for lower temperatures and therefore negligible.

MeOH-ICE: The absence of carbon-carbon bonds and aromatics results in fewer particulate matter emissions. Experiments from [269] indicate reduction potentials of up to 95% compared to conventional diesel engines. Experiments from [270] with partially premixed combustion engines also demonstrate NO_x emissions below 2 g/kWh independent from intake temperatures. For part load conditions, authors of the same research group present values from 0.3-1.4 g/kWh [253] for marine engines. In analogy, a 70% decrease of NO_x compared to diesel engines is reported in [154]. Carbon monoxide emissions of 2.5 g/kWh are reported in [270] for full load conditions, and a rapid increase from 2.7 to up to 22.7 g/kWh for part load conditions due to shorter ignition delay duration and resulting larger fuel-rich zones [253]. However, in [271] the possibility to reduce CO emissions down to 1.6 g/kWh by using an exhaust gas recirculation concept and an adapted air-fuel ratio is reported. By doing so, NO_x emissions stay low, while the engine efficiency is not affected negatively.

MeOH-PEM: The water-gas-shift reaction still is prevalent at lower operating temperatures reducing the intermediate product of the methanol decomposition. Residues of carbon monoxide are absorbed by a filter unit between reformer and fuel cells. Therefore, the methanol-fueled fuel cell approach is evaluated to not produce emissions during operation.

H₂-PEM: No relevant emissions occur during the electrochemical reaction. Anode off-gases are recirculated to maintain high efficiency.

C Publication Contributor Roles

Large parts of the present dissertation are adopted from four publications already released in or submitted to scientific journals. While the author of this dissertation is first author of all four articles, the intellectual properties are shared with several co-authors. For full disclosure, the ‘‘Contributor Roles Taxonomy’’ (CRediT) [272] is chosen to represent the roles played by the contributors of all published articles. This procedure is chosen to on the one hand give well-deserved recognition to all co-authors and on the other hand demonstrate that fundamental conceptual work, computational analysis, and writing were conducted by the author of this dissertation, Lukas Kistner. All contributor roles are listed in Tab. C.1.

Tab. C.1: CRediT [272] contributor roles of the underlying publications

Co-authors of [30]	Contributor roles
L. Kistner	Conceptualization, Methodology, Software, Investigation, Writing - Original Draft, Data Curation, Visualization
A. Bensmann	Validation, Resources, Writing - Review & Editing, Supervision, Project administration
R. Hanke-Rauschenbach	Validation, Writing - Review & Editing, Supervision, Funding acquisition
Co-authors of [38]	Contributor roles
L. Kistner	Conceptualization, Methodology, Software, Investigation, Writing - Original Draft, Data Curation, Visualization
F.L. Schubert	Software, Investigation, Data Curation
C. Minke	Validation, Resources, Writing - Review & Editing
A. Bensmann	Validation, Writing - Review & Editing, Supervision, Project administration
R. Hanke-Rauschenbach	Writing - Review & Editing, Supervision, Funding acquisition
Co-authors of [52]	Contributor roles
L. Kistner	Conceptualization, Methodology, Software, Investigation, Writing - Original Draft, Data Curation, Visualization
A. Bensmann	Validation, Resources, Writing - Review & Editing
R. Hanke-Rauschenbach	Writing - Review & Editing, Supervision, Funding acquisition
Co-authors of [61]	Contributor roles
L. Kistner	Conceptualization, Methodology, Software, Investigation, Writing - Original Draft, Data Curation, Visualization
A. Bensmann	Methodology, Validation, Writing - Review & Editing
C. Minke	Validation, Writing - Review & Editing
R. Hanke-Rauschenbach	Validation, Writing - Review&Editing, Supervision

D Curriculum Vitae

Tab. D.1: Professional Background & Education

12/2018 – 06/2023	Research assistant Institute of Electric Power Systems, Electric Energy Storage Systems Group, Leibniz Universität Hannover <ul style="list-style-type: none"> • Design of marine power systems in the <i>MultiSchIBZ</i> research project • Development of a software toolbox with program interfaces for model-based power system design optimization tasks
01/2019 – 04/2023	Ph.D. Electrical engineering , Leibniz Universität Hannover <ul style="list-style-type: none"> • Investigation of shipboard fuel cell technologies, internal combustion engines and synthetic fuels for marine applications • Design optimizations of hybrid energy systems as a basis for the preparation of economic and ecological assessments of energy technologies
10/2015 – 08/2018	M.Sc. Power engineering , Leibniz Universität Hannover <ul style="list-style-type: none"> • Project thesis: analysis of underwater energy storage concepts • Master thesis: efficiency calculation for the evaluation of electrolyzers
10/2011 – 07/2015	B.Sc. Power engineering , Leibniz Universität Hannover <ul style="list-style-type: none"> • Bachelor thesis: thermal simulation of an electric drive system

Tab. D.2: Scientific Publications

L. Kistner; A. Bensmann; R. Hanke-Rauschenbach, Optimal Design of Power Gradient Limited Solid Oxide Fuel Cell Systems with Hybrid Storage Support for Ship Applications, Energy Conversion and Management (2021)
L. Kistner; F.L. Schubert; C. Minke; A. Bensmann; R. Hanke-Rauschenbach, Techno-economic and Environmental Comparison of Internal Combustion Engines and Solid Oxide Fuel Cells for Ship Applications, Journal of Power Sources (2021)
L. Kistner; A. Bensmann; R. Hanke-Rauschenbach, Optimal Design of a Distributed Ship Power System with Solid Oxide Fuel Cells under the Consideration of Component Malfunctions, Applied Energy (2022)
L. Kistner; A. Bensmann; C. Minke; R. Hanke-Rauschenbach, Comprehensive techno-economic assessment of power technologies and synthetic fuels under discussion for ship applications, Renewable and Sustainable Energy Reviews (submitted)

Tab. D.3: Scientific Presentations

L. Kistner; A. Bensmann; R. Hanke-Rauschenbach, Model-based design of a decentralized ship energy system with fuel cell and energy storage units, Green Ship Technology Europe (2020)

L. Kistner; A. Bensmann; R. Hanke-Rauschenbach, Decentralized Ship Energy System with High Temperature Fuel Cells, Electric & Hybrid World Expo Virtual (01/2021)

L. Kistner; C. Minke; A. Bensmann; R. Hanke-Rauschenbach, Comprehensive Techno-economic and Environmental Assessment for Cruise Ship Energy Systems, Electric & Hybrid World Expo Virtual (09/2021)

List of Figures

1.1	Relevant aspects regarding the shipping industry’s defossilization challenge: economic and environmental key data, near-future legislations, and potentially utilizable sustainable technologies	2
3.1	Required elements for a system design optimization task: information input (degrees of freedom) and output (performance indicators) interfaces of a system model including power demand, active power system components, and a control strategy	17
3.2	Considered components and power flows of a ship energy system: electrical load (P_L), solid oxide fuel cell power output (P_{FC}), battery unit charge power (P_B), supercapacitor unit charge power (P_{SC}) . .	18
3.3	Schematic material flows, energy flows, and chemical reactions occurring in the SOFC module with external steam reforming chamber	19
3.4	General substructure of the developed four-parted system component models	22
3.5	(a) SOFC module’s operating-point-specific fuel consumption (SFC) including power electronics based on [78]; (b) equivalent efficiency calculated with LNG’s lower heating value (LHV), minor adaptations to display an upscaled system are included in consultation with the responsible research group	23
3.6	Power flow diagram for a rule-based ranking: the SOFC module cannot cover the load demand on its own either due to already reaching its maximum power output or its gradient limitations; the hybrid storage system covers the power delta with help of both battery and supercapacitor (load peak).	32
3.7	State machine for the SOFC system operation	33
3.8	State machine for comparing the supercap’s state of energy with the desired value	34
3.9	State machine for the unified storage model	36
3.10	Computational process workflow including input requirements, simulation framework, and optimization framework	38
4.1	Load profiles for (a) case study I; (b) case study II: ① bow thruster operation, ② open-sea operation.	40

4.2	Case study I: (a) total installed power, (b) rated battery capacity $C_{E,B}$, (c) specific power Π_B , and (d) annual system costs visualize the optimization results, \times marks the annual system cost minimum	42
4.3	Case study II: (a) total installed system power, (b) rated battery capacity $C_{E,B}$, (c) specific power Π_B , and (d) annual system costs visualize the optimization results, \times marks the annual system cost minimum	43
4.4	Case study II: (a) cost-optimal installed system power, (b) storage configuration, (c) annual system costs, (d) battery lifetime, discontinuities can be traced back to different times of EMS state change for fuel cell modulation	45
4.5	Equivalent circuit diagram of a Li-ion battery	47
4.6	State machine for Li-ion's voltage limitation control and CV phase initiation	48
4.7	Energy-power relations of one single battery cell, evaluated with the unified model and the technology-specific component description	50
4.8	SAFT Lithium-Ion Battery System BTR-0554V-VL30-SFP-012M (554 V / 15.5 kWh)	51
4.9	Circuit diagram of a two-layer capacitor [118]	52
4.10	State machine for the supercapacitor's voltage limitation control	54
4.11	Energy-power relations of one single supercapacitor cell, evaluated with the unified model and the technology-specific component description	55
4.12	Revision of case study I – detailed storage models: (a) number of battery cells N_B , (b) annual system costs, and (c) battery lifetime $t_{L,B}$, \bullet highlights the calculated cost optimum, \times marks the reference cost minimum declared with the basic storage model	57
4.13	Revision of case study II – detailed storage models: (a) number of supercapacitor cells N_{SC} , (b) annual system costs, (c) battery lifetime $t_{L,B}$, and (d) supercapacitor lifetime $t_{L,SC}$, \bullet highlights the calculated cost optimum, \times marks the reference cost minimum declared with the unified storage model	59
4.14	Revision of case study I – fuel cost consideration: (a) number of battery cells N_B , (b) battery lifetime $t_{L,B}$, (c) component costs, (d) fuel costs, and (e) annual system costs; \bullet highlights the calculated cost optimum considering fuel expenses, \times marks the reference cost minimum declared without fuel costs consideration	62

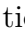
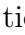
4.15	Revision of case study II – fuel cost consideration: (a) number of battery cells N_B , (b) battery lifetime $t_{L,B}$, (c) component costs, (d) fuel costs, and (e) annual system costs; • highlights the calculated cost optimum considering fuel expenses, × marks the reference cost minimum declared without fuel costs consideration	64
5.1	SOFC (orange), battery (yellow), electrical load (gray) in each of the ship's N_{FZ} fire zones, connected via power transformers (green) and a high-voltage power backbone	71
5.2	Nomenclature of power flow and fire zone connections: fuel cell power P_{FC} , consumer power P_L , battery power P_B , and power transmission P_{\rightarrow}	73
5.3	Different approaches to control a decentralized energy system with regard to the amount of information exchanged: black connectors represent the electrical grid, yellow connectors represent fire zone state information, red connectors represent set values calculated by the energy management system (EMS) and approved components' responses processed by the component management system (CMS).	81
5.4	State machine for the fuel cell system control to prevent fully charged or discharged battery units	83
5.5	Additional state machine for the fuel cell control if $Z_{FC} = 0$	84
5.6	(a) 72 h passage with total hotel load day-night rhythm and two harbor maneuvers, (b) second harbor maneuver load profile with separate and added up fire zone profiles.	87
5.7	Cost-optimal SOFC and battery unit distribution, resulting power transformer and cable design for a central and a distributed system without component failure consideration ($\zeta = 1$)	90
5.8	Average grid power flow $ P_{k\rightarrow} ^{av}$ and average transformer power transmission $ \Delta P_k ^{av}$ for a central and a distributed system without component failure consideration	91
5.9	(a) Annual costs for a central and a distributed system without component failure consideration; (b) detailed presentation of the power-distribution-related costs	92
5.10	Cost-optimal distribution of the central and distributed power system units and resulting power transmission component design when considering malfunction scenarios: shaded bars resembles the failing components for the two emergency scenarios ($\zeta = 2$ and $\zeta = 3$)	94
5.11	(a) Annual costs for systems with central and distributed components with failure consideration and comparison with previous design in parentheses (cf. Fig. 5.9); (b) detailed presentation of the power-distribution-related costs	95

6.1	Considered hybrid system configurations for the benchmark study (year 2020) and the future assessment (year 2030) – ship pictograms represent practical/investigated applications. The chosen color scheme is reused in the assessment.	100
6.2	Scope of the economic (yellow) and environmental (green) assessments, influenced by the production phase (cradle-to-gate, well-to-tank) and the system behavior (gate-to-grave, tank-to-wake), modeled in analogy to the concept introduced in Chapter 3.	104
6.3	(a) Operation-specific fuel consumption (SFC) of the investigated fuel-technology combinations, (b) resulting fuel efficiencies based on lower heating values.	105
6.4	Operating-point-dependent generator emissions displayed in g / kWh (electrical power)	115
6.5	State machine that monitors the battery state of energy F_B with help of the indicating state Z_B	118
6.6	72 h passage with day-night rhythm hotel load and two harbor maneuvers [138]	121
6.7	Considered system configurations for the benchmark assessment, including two design examples with configuration bias and two optimally designed hybrid configurations	122
6.8	State-of-the-art combustion engines in different configurations: (a) system designs, (b) resulting space requirements, (c) production and operating emissions with GWP, (d) non-CO ₂ operating emissions, (e) annual direct and indirect costs.	124
6.9	Fuel-generator configurations in the assessment for the year 2030, comparison with results from Section 6.5.1: (a) system designs, (b) resulting space requirements, (c) production and operating emissions with GWP, (d) non-CO ₂ emissions, (e) annual direct and indirect costs	128
6.10	Comparison of environmental costs resulting from emissions with negative local effects (LE) during fossil fuel and electrofuel operation.	129
6.11	Comparison of environmental costs resulting from emissions with global warming potential: conservative future scenario [223] and optimistic scenario [224].	130
6.12	Exemplary 192 h passage with seven open-sea days	131
6.13	(a) Annual direct system costs of the ten configurations as a function of the ship operating passage; (b) annual direct plus environmental costs	132

6.14	Annual direct power system costs for the different fuel price scenarios: (a) electricity price reduction, (b) additional production efficiency increase, (c) additional reduction of plant investment costs	135
6.15	Annual direct power system costs with varied volume opportunity costs: (a) 300% , (b) 500%, (c) 700% increased volume opportunity costs	136
6.16	Alternative load profiles: (a) 72 h cruise ship passage with linear scaling factor ϕ_L , (b) multi-purpose vessel, (c) general cargo ship	137
6.17	Annual system costs for a cruise ship with the investigated base load profile scaled with the factor $\phi_L = 0.5$ (cf. Fig. 6.16 (a))	139
6.18	Annual system costs for a ship with the multi-purpose vessel load profile (cf. Fig. 6.16 (b))	140
6.19	Annual system costs for a ship with the cargo vessel load profile (cf. Fig. 6.16 (c))	141
A.1	EMS strategy: fuel cells in full load operation (period ①) and part load operation after reaching the critical SoE (period ②).	151
A.2	Total storage set power $P_{S,set}$, battery power P_B , supercap power P_{SC} , and states of energy F visualize the hybrid storage management: supercap charges until it reaches the standby SoE, excess power is recieved by battery, supercap and battery both discharge due to latter's power limitations.	152
A.3	SOFC operation with one unit in each of three fire zones: ① average storage SoE within the desired range, load following in cascades depending on max. delta between local load and fuel cell operation; ② load drop, maximum power gradient to synchronize with load, storage is charging; ③ $F_\emptyset > F_{high}$, minimizing SOFC power to discharge storage; ④ batteries reach noncritical SoE, fuel cells synchronize with load	154
A.4	Exemplary storage operation; battery cell distribution: $N_{B,1} = N_{B,3} = 0.5 \cdot N_{B,2}$; storage powers vary in amplitude due to different SoE (cf. $P_{B,1}, P_{B,3}$) and rated capacity (cf. $P_{B,2}$); power distribution results in the usage of the transmission system	155

A.5 Control strategy example based on the NH3-ICE approach: (a) load profile and generator power, (b) battery power, (c) battery state of energy. ① One of two generators operates in load-following mode with limited power gradient; ② second generator is turned on and maximum power is reached, battery compensates power delta and falls below the critical SoE F_{low} ; ③ generators operate above required power to recharge the battery until F_{des} is reached; ④ generators return to load-following operation. 156

List of Tables

2.1	Literature overview: ship power technology and synthetic fuel discussions since the <i>IMO</i> released their climate reduction targets in 2018 [11]. Technology icons represent the study of internal combustion engines  and/or fuel cell systems  , colored boxes constitute considered fuels	13
3.1	SOFC system parameters	25
3.2	LFP and supercapacitor parameters for the nonspecific storage model; values are derived from internal manufacturer data sheets if not marked otherwise	27
3.3	Desired model attributes and programming requirements, resulting in a mixed-integer nonlinear programming (MINLP) problem	29
3.4	Potential numerical optimization methods applicable to (slightly) nonconvex equation systems	30
4.1	Battery cell operation parameters for the analyzed LFP battery . .	51
4.2	Simulation parameters for the 3000 F Maxwell supercapacitor [118], [119]	56
4.3	Parameters required to calculate annual occurring fuel costs of the investigated cases	61
5.1	Parameters for high-voltage cables and power transformers	76
5.2	Additional or altered parameters for one SOFC module	78
5.3	Additional or altered parameters for lithium iron phosphate batteries	79
5.4	Summary of the conducted assessments and their location in the following sections	88
6.1	Operating limitation parameters for the power generator-fuel-combinations (parameters without source are obtained by manufacturers or internal calculations)	106
6.2	Physical and economic simulation parameters for the investigated power technologies	108
6.3	Physical and economic simulation parameters for the considered fuels	110
6.4	General physical and economic parameters for the LFP battery unit	111

6.5	CO ₂ -equivalent emissions for supply of components and fuels including maintenance and stack replacements, carbon mass shares of the fossil fuels	113
6.6	GWP ₁₀₀ values and emission cost grading for the environmental investigation	116
6.7	Revised specific fuel prices based on three cost reduction scenarios, percentage values originate from [69]	134
C.1	CRediT [272] contributor roles of the underlying publications . . .	161
D.1	Professional Background & Education	162
D.2	Scientific Publications	162
D.3	Scientific Presentations	163

Bibliography

- [1] Bundeswehr, Fakten und Zahlen zur maritimen Abhängigkeit der Bundesrepublik Deutschland, MARINEKOMMANDO JAHRESBERICHT 2021 (2021).
- [2] statista, International seaborne trade carried by container ships from 1980 to 2020 , <https://www.statista.com/statistics/253987/international-seaborne-trade-carried-by-containers/>, accessed: 2022-09-10.
- [3] Grand View Research, Shipping Container Market Size, Share & Trends Analysis Report By Product (ISO, Non-standard), By Type (Dry, Reefer, Tank), By Size (20, 40, High Cube), By Flooring, By Application, By Region, And Segment Forecasts, 2020 - 2028, Market Analysis Report (2019).
- [4] Buhaug, O; et al., Second IMO Greenhouse Gas Study 2009, International Maritime Organization (2009).
- [5] International Energy Agency, International Shipping Tracking Report, <https://www.iea.org/reports/international-shipping>, accessed: 2022-09-10.
- [6] International Energy Agency, Global CO2 emissions in transport by mode in the Sustainable Development Scenario, 2000-2070, <https://www.iea.org/data-and-statistics/charts/global-co2-emissions-in-transport-by-mode-in-the-sustainable-development-scenario-2000-2070>, accessed: 2022-09-10.
- [7] International Maritime Organization, Fourth Greenhouse Gas Study 2020 (2020).
- [8] International Maritime Organization, MARPOL Annex VI regulation 14, International Convention for the Prevention of Pollution from ships (2020).
- [9] Tzannatos, E., Ship emissions and their externalities for Greece, Atmospheric Environment (2010).
- [10] NCE Maritime CleanTech, GHG emissions not on track, <https://maritimecleantech.no/2020/08/19/ghg-emissions-not-on-track/>, accessed: 2022-09-10.

- [11] International Maritime Organization, Adoption of the initial imo strategy on reduction of ghg emissions from ships and existing imo activity related to reducing ghg emissions in the shipping sector, UNFCCC Talanoa Dialogue (2018).
- [12] International Maritime Organization, Energy Efficiency Measures, <https://www.imo.org/en/OurWork/Environment/Pages/Technical-and-Operational-Measures.aspx>, accessed: 2022-01-10.
- [13] International Maritime Organization, IMO Environment Committee approves amendments to cut ship emissions, <https://www.imo.org/en/MediaCentre/PressBriefings/pages/42-MEPC-short-term-measure.aspx>, accessed: 2022-09-10.
- [14] Lloy’s List, Disappointment at slow pace of IMO green progress, <https://lloydslist.maritimeintelligence.informa.com/LL1134826/From-the-News-Desk-Disappointment-at-slow-pace-of-IMO-green-progress>, accessed: 2022-09-10.
- [15] International Maritime Organization, IMO 2020 – cutting sulphur oxide emissions, <https://www.imo.org/en/MediaCentre/HotTopics/Pages/Sulphur-2020.aspx>, accessed: 2022-09-10.
- [16] International Maritime Organization, Nitrogen Oxides (NOx) – Regulation 13, [https://www.imo.org/en/OurWork/Environment/Pages/Nitrogen-oxides-\(NOx\)-%E2%80%93-Regulation-13.aspx](https://www.imo.org/en/OurWork/Environment/Pages/Nitrogen-oxides-(NOx)-%E2%80%93-Regulation-13.aspx), accessed: 2022-09-10.
- [17] European Commission, REGULATION OF THE EUROPEAN PARLIAMENT AND OF THE COUNCIL on establishing the framework for achieving climate neutrality and amending Regulation (EU) 2018/1999 (European Climate Law), COM(2020) 563 final (2020).
- [18] European Commission, EU ETS Handbook, European Union (2015).
- [19] European Commission, DIRECTIVE OF THE EUROPEAN PARLIAMENT AND OF THE COUNCIL amending Directive 2003/87/EC establishing a system for greenhouse gas emission allowance trading within the Union, Decision (EU) 2015/1814 concerning the establishment and operation of a market stability reserve for the Union greenhouse gas emission trading scheme and Regulation (EU) 2015/757, COM(2021) 551 final (2021).
- [20] European Commission, REGULATION OF THE EUROPEAN PARLIAMENT AND OF THE COUNCIL on the use of renewable and low-carbon fuels in maritime transport and amending Directive 2009/16/EC, COM(2021) 562 final (2021).

- [21] International Maritime Organization, IMO’s work to cut GHG emissions from ships , <https://www.imo.org/en/MediaCentre/HotTopics/Pages/Cutting-GHG-emissions.aspx>, accessed: 2022-09-10.
- [22] Pereira, Newton N., A diagnostic of diesel-electric propulsion for ships, *Ship Science and Technology* 1.2 (2008) 27–42.
- [23] Dedes, Eleftherios K.; et al., Assessing the potential of hybrid energy technology to reduce exhaust emissions from global shipping, *Energy Policy* 40 (2012) 204–218.
- [24] Jang, J.; et al., Experimental investigation of frictional resistance reduction with air layer on the hull bottom of a ship, *International Journal of Naval Architecture and Ocean Engineering* (2014).
- [25] Offshore Energy, Neoline picks Solid Sail solution for its first sailing cargo ship, <https://www.offshore-energy.biz/neoline-picks-solid-sail-solution-for-its-first-sailing-cargo-ship/>, accessed: 2022-09-10.
- [26] Naaijen, P.; Koster, V., Performance of auxiliary wind propulsion for merchant ships using a kite, *2nd International Conference on Marine Research and Transportation* (2007).
- [27] Talluri, L.; et al., Techno economic and environmental assessment of flettner rotors for marine propulsion, *Ocean Engineering* (2018).
- [28] Offshore Energy, Industry firsts: Berge Bulk ship tests solar panels, <https://www.offshore-energy.biz/berge-bulk-ship-tests-solar-panels/>, accessed: 2022-09-10.
- [29] Lloyd’s register, Solas international convention for the safety of life at sea, *International Maritime Organisation* (2005).
- [30] Kistner, L.; Bensmann, A.; Hanke-Rauschenbach; R., Optimal Design of Power Gradient Limited Solid Oxide Fuel Cell Systems with Hybrid Storage Support for Ship Applications, *Energy Conversion and Management* (2021).
- [31] Marine Insight, What Are Hybrid Ships?, <https://www.marineinsight.com/types-of-ships/what-are-hybrid-ships/>, accessed: 2022-09-10.
- [32] Ship Technology, Hybrid vessels: here to stay, or fleeting trend?, <https://www.ship-technology.com/analysis/featurehybrid-vessels-here-to-stay-or-fleeting-trend-5769261/>, accessed: 2022-09-10.

- [33] Mashayekh, Salman; et al., Optimum sizing of energy storage for an electric ferry ship, *IEEE Power and Energy* (2012).
- [34] Lan, Hai; et al., Optimal sizing of hybrid pv/diesel/battery in ship power system, *Applied Energy* 158 (2015) 26–34.
- [35] Holsonback, Christopher; et al., System-level modeling and optimal design of an all-electric ship energy storage module, *Electric Machines Technology Symposium* (2006).
- [36] Boveri, A.; et al., Optimal Sizing of Energy Storage Systems for Shipboard Applications, *IEEE transactions on energy conversion*, VOL. 34 (2019).
- [37] Bassam, Ameen M.; et al., Sizing optimization of a fuel cell/battery hybrid system for a domestic ferry using a whole ship system simulator, *2016 ESARS-ITEC* (2016).
- [38] Kistner, L.; et al., Techno-economic and Environmental Comparison of Internal Combustion Engines and Solid Oxide Fuel Cells for Ship Applications, *Journal of Power Sources* (2021).
- [39] Hebner, Robert E.; et al., Technical cross-fertilization between terrestrial microgrids and ship power systems, *J. Mod. Power Syst. Clean Energy* (2016) 161–179.
- [40] MAN Energy Solutions, Batteries on board ocean-going vessels, *Future in the making* (2019).
- [41] van Biert, L.; et. al., A review of fuel cell systems for maritime applications, *Journal of Power Sources* (2016) 345–364.
- [42] Ros Chaos, S.; et al., Economies of scale in cruise shipping, *Maritime Economics & Logistics* (2020).
- [43] EMSA European Maritime Safety Agency, Study on the use of fuel cells in shipping, *DNVGL* (2017).
- [44] Wik, C.; Niemi, S., Low emission engine technologies for future tier 3 legislations - options and case studies, *Journal of Shipping and Trade* (2016).
- [45] van Biert, L.; et al., A comparison of steam reforming concepts in solid oxide fuel cell systems, *Applied Energy* (2020).
- [46] Leites, K.; et. al., Schibz - design of different diesel based fuel cell systems for seagoing vessels and their evaluation, *ECS Transactions* 42 (2012) 49–58.

- [47] Alkaner, S.; Zhou, P., A comparative study on life cycle analysis of molten carbon fuel cells and diesel engines for marine application, *Journal of Power Sources* (2006).
- [48] Strazza, C.; et al., Comparative LCA of methanol-fuelled SOFCs as auxiliary power systems on-board ships, *Applied Energy* (2010).
- [49] Baldi, F.; et al., The role of solid oxide fuel cells in future ship energy systems, *Energy* (2020).
- [50] Kim, K.; Roh, G.; Kim, W.; Chun, K., A Preliminary Study on an Alternative Ship Propulsion System Fueled by Ammonia: Environmental and Economic Assessments, *Journal of Marine Science and Engineering* (2020).
- [51] Haseltalab, A.; et al., Component sizing and energy management for SOFC-based ship power systems, *Energy Conversion and Management* (2021).
- [52] Kistner, L.; et al., Optimal Design of a Distributed Ship Power System with Solid Oxide Fuel Cells under the Consideration of Component Malfunctions, *Applied Energy* (2022).
- [53] Mariam , L.; et al., A review of existing microgrid architectures, Hindawi Publishing Corporation, *Journal of Engineering* (2013).
- [54] Hartono , B.S.; et al., Review of microgrid technology, 2013 International Conference on QiR (2013).
- [55] Sharma , S.; Sood Y.R., Microgrids: A review of status, technologies, software tools, and issues in indian power market, *IETE Technical Review* (2020).
- [56] Banerji , A.; et al., Microgrid: A review, 2013 IEEE Global Humanitarian Technology Conference: South Asia Satellite (2013).
- [57] Flore, G.; et al., Distributed energy resources on-board cruise ships: Integration into the ship design process, *Technology and Science for the Ships of the Future, Proceedings of NAV 2018* (2018).
- [58] Guerrero, J.M.; et al., Shipboard microgrids: Maritime islanded power systems technologies, *PCIM Asia 2016* (2016).
- [59] Boveri, A.; et al., Shipboard distributed energy resources: Motivations, challenges and possible solutions in the cruise ship arena, *International Shipbuilding Progress* 66, 2019 (2019).

- [60] Rivarolo, M.; et al., Best operative strategy for energy management of a cruise ship employing different distributed generation technologies, *International Journal of Hydrogen Energy* 43 (2018).
- [61] Kistner, L.; et al., Comprehensive techno-economic assessment of power technologies and synthetic fuels under discussion for ship applications, *Renewable and Sustainable Energy Reviews* ((submitted)).
- [62] Earl, T.; et al., Decarbonising European Shipping - Technological, operational, and legislative roadmap , *Transport and Environment* (2021).
- [63] Maersk Mc-Kinney Moller Center for Zero Carbon Shipping, We show the world it is possible - Industry Transition Strategy, (2021).
- [64] Hammer, L.S.; et al., Maritime Forecast to 2050, DNV (2021).
- [65] IRENA, A pathway to decarbonise the shipping sector by 2050, 2021 (International Renewable Energy Agency).
- [66] de Vries, N.; et al., Safe and effective application of ammonia as a marine fuel, Master thesis, Delft University of Technology (2019).
- [67] Horvath, S.; et al., Techno-economic analysis of a decarbonized shipping sector: Technology suggestions for a fleet in 2030 and 2040, *Energy Conversion and Management* (2018).
- [68] McKinlay, C.J.; et al., Route to zero emission shipping: Hydrogen, ammonia or methanol?, *International Journal of Hydrogen Energy* (2021).
- [69] Korberg, A.D.; et al., Techno-economic assessment of advanced fuels and propulsion systems in future fossil-free ships, *Renewable and Sustainable Energy Reviews* (2021).
- [70] van Biert, L.; et al., A comparison of steam reforming concepts in solid oxide fuel cell systems, *Applied Energy* (2020).
- [71] Besancon, B.M.; et al., Hydrogen quality from decarbonized fossil fuels to fuel cells, *International Journal of Hydrogen Energy* (2009).
- [72] Baschuk, J.J.; Li, Xianguo, Carbon monoxide poisoning of proton exchange membrane fuel cells, *International Journal of Energy Research* (2001) 695–713.
- [73] Baldi, F.; et al., The role of solid oxide fuel cells in future ship energy systems, *Energy* (2020).

- [74] Reurings, J.W.; Purushothaman Vellayani, A.; Stam, J., A modeling study to investigate performance of SOFC-ICE hybrid systems for marine applications, Master thesis, Delft University of Technology (2019).
- [75] Electric & hybrid marine technology, Corvus Energy enables emission-free sailing into World Heritage fjord, <https://www.electrichybridmarinetechnology.com/news/environmental/corvus-energy-enables-emission-free-sailing-into-world-heritage-fjord.html>, accessed: 2022-09-20.
- [76] Bundesamt für Seeschifffahrt und Hydrographie, Ship emissions, https://www.bsh.de/EN/TOPICS/Shipping/Environment_and_shipping/Ship_emissions/ship_emissions_node.html, accessed: 2022-09-10.
- [77] Chen, X.; et al., An overview of lithium-ion batteries for electric vehicles, 10th International Power and Energy Conference (IPEC) (2012).
- [78] Hollmann, J.; et al., System Simulation and Analysis of an LNG-Fueled SOFC System Using Additively Manufactured High Temperature Heat Exchangers, *Energies* (2022).
- [79] Weimar, M.R.; et al., Cost study for manufacturing of solid oxide fuel cell power systems, U.S. Department of Energy (2013).
- [80] Brandon, N. P.; et al., Solid oxide fuel cell lifetime and reliability, Elsevier (2017).
- [81] Rao, M.; et al., Durability of solid oxide electrolysis stack under dynamic load cycling for syngas production, *Journal of Power Sources* 451 (2020).
- [82] Nakajo, A.; et al., Modeling of thermal stresses and probability of survival of tubular sofc, *Journal of Power Sources* 451 (2020).
- [83] Anandakumar, G.; et al., Thermal stress and probability of failure analyses of functionally graded solidoxide fuel cells, *Journal of Power Sources* 195 (2010) 6659–6670.
- [84] Napoli, R.; et al., Economics evaluation of a 5 kW SOFC power system for residential use, *International Journal of Hydrogen Energy* 33 (2008) 3243–3247.
- [85] Santin, M.; Traverso, A.; Magistri, L., Liquid fuel utilization in sofc hybrid systems, *Applied Energy* 86 (2009) 2204–2212.

- [86] Ovrum, E.; Bergh T.F., Modelling lithium-ion battery hybrid ship crane operation, *Applied Energy* 152 (2015) 162–172.
- [87] Zhou, Z.; et al., A review of energy storage technologies for marine current energy systems, *Renewable and Sustainable Energy Reviews* 18 (2013) 390–400.
- [88] Mongird, K.; et al., Energy storage technology and cost characterization report, *Hydrowires* U.S. Department of Energy (2019).
- [89] Berthold, T., Heuristic algorithms in global MINLP solvers, Technische Universität Berlin (2014).
- [90] Boyd, S.; Vandenberghe, L., *Localization and Cutting-plane Methods*, Stanford University (2003).
- [91] Boyd, S.; Vandenberghe, L., *Convex Optimization*, Cambridge University Press (2004).
- [92] Yamashita, H.; Yabe, H., A primal-dual interior point method for nonlinear optimization over second order cones, *Optimization Methods & Software* (2009).
- [93] Clausen, C., *Branch and Bound Algorithms - Principles and Examples*, Department of Computer Science, University of Copenhagen (1999).
- [94] Dey, S.S., *Convexification in global optimization, Integer Programming and Combinatorial Optimization* (2020).
- [95] Hart, W.E.; et al., Pyomo: modeling and solving mathematical programs in Python, *Mathematical Programming Computation* 3 (2011).
- [96] Waechter, A.; et al., Ipopt Documentation, <https://coin-or.github.io/Ipopt/>, accessed: 2022-01-10.
- [97] Caspari, A.; et al., DyOS - A Framework for Optimization of Large-Scale Differential Algebraic Equation Systems, 29th European Symposium on Computer Aided Process Engineering (2019).
- [98] The Optimization Firm, BARON Solver, <https://minlp.com/baron-solver>, accessed: 2022-03-01.
- [99] GAMS, General Algebraic Modeling System, <https://www.gams.com/>, accessed: 2022-09-11.

- [100] Kronqvist, J., A review and comparison of solvers for convex MINLP, Optimization and Engineering (2019).
- [101] Tang, R.; et al., Optimal operation of hybrid energy system for intelligent ship: An ultrahigh-dimensional model and control method, Energy (2020).
- [102] Hou, J.; et al., Adaptive model predictive control with propulsion load estimation and prediction for all-electric ship energy management, Energy (2018).
- [103] Michalopoulos, P.; et al., A method for optimal operation of complex ship power systems employing shaft electric machines, IEEE Transactions on Transportation Electrification (2016).
- [104] Anvari-Moghaddam, A.; et al., Optimal planning and operation management of a ship electrical power system with energy storage system, Annual Conference of the IEEE Industrial Electronics Society (2016).
- [105] Rodriguez-Mier, P., A tutorial on Differential Evolution with Python, <https://pablormier.github.io/2017/09/05/a-tutorial-on-differential-evolution-with-python/>, accessed: 2022-10-12.
- [106] Bassam, Ameen M.; et al., Development of a multi-scheme energy management strategy for a hybrid fuel cell driven passenger ship, International Journal of Hydrogen Energy 42.1 (2017).
- [107] Zhu, Lisi; et al., Fuzzy logic based energy management strategy for a fuel cell/battery/ultra-capacitor hybrid ship, First International Conference on Green Energy ICGE (2014) 107–112.
- [108] Chen, Z.; et al., Energy Management for a Power-Split Plug-in Hybrid Electric Vehicle Based on Dynamic Programming and Neural Networks, IEEE Transactions on Vehicular Technology (2013).
- [109] Abdolrasol, M.G.M.; et al., Energy Management Scheduling for Microgrids in the Virtual Power Plant System Using Artificial Neural Networks, Energies (2021).
- [110] Open Source Modelica Consortium, Openmodelica homepage, <https://www.openmodelica.org/>, accessed: 2020-09-01.
- [111] Petzold, L.R., Description of DASSL: a differential/algebraic system solver, International mathematics and computers simulation congress on systems simulation and scientific computation (1982).

- [112] Sundials, IDA, <https://computing.llnl.gov/projects/sundials/ida>, accessed: 2022-10-12.
- [113] Biscani, F.; Izzo, D., pygmo Github, <https://esa.github.io/pygmo2/index.html>, Accessed: 2022-02-10.
- [114] Schlüter, M.; Gerds, M., The oracle penalty method, *Journal of Global Optimization* (2009).
- [115] Shepherd, C.M., Design of primary and secondary cells ii. an equation describing battery discharge, *Journal of the Electrochemical Society* (1965) 657–664.
- [116] Forman, J.C.; et al., Optimal experimental design for modeling battery degradation, *ASME 2012 5th Annual Dynamic Systems and Control Conference* (2012).
- [117] Fortenbacher, P.; Andersson, G., Battery degradation maps for power system optimization and as a benchmark reference, *2017 IEEE Manchester PowerTech* (2017).
- [118] Miller, John M., *Ultracapacitor applications*, Institution of Engineering and Technology (2011).
- [119] Kreczanik, J.C.; et al., Study of supercapacitor aging and lifetime estimation according to voltage, temperature, and rms current, *IEEE TRANSACTIONS ON INDUSTRIAL ELECTRONICS*, VOL. 61, NO. 9 (2014).
- [120] DNV GL, Current price development oil and gas, <https://www.dnvgl.com/maritime/lng/current-price-development-oil-and-gas.html>, Accessed: 2020-10-01.
- [121] Stenersen, D.; et al., D5-6 LNG supply chain feasibility study - overall report (2008).
- [122] Lin, C.-K.; et al., Mechanical durability of solid oxide fuel cell glass-ceramic sealant/steel interconnect joint under thermo-mechanical cycling, *Renewable Energy* (2019).
- [123] Jayasinghe, S.G.; et al., Review of ship microgrids: System architectures, storage technologies and power quality aspects, *MDPI Inventions* 2017 (2017).
- [124] DNV GL, *Guidance for safe return to port projects* (2016).

- [125] DNV GL, Dnvgl rules and standards pt. 1 ch. 1 general regulations (2020).
- [126] Siemens AG, Energy Management, Transformer selection according to utilisation profiles, Technical Series, Edition 16 (2016).
- [127] Lazaridis , L.P., Economic comparison of hvac and hvdc solutions for large offshore wind farms under special consideration of reliability, Master Thesis Royal Institute of Technology, Stockholm (2005).
- [128] Zhou, D.; et al., Power transformer lifetime modeling, Proceedings of the IEEE 2012 Prognostics and System Health Management Conference (2012).
- [129] I. E. Commission, Conductors of Insulated Cables, IEC 60228, IEC (2004).
- [130] DNV GL, Dnvgl rules and standards pt. 4 ch. 8 electrical installations (2020).
- [131] Whiston, M.M.; et al., Meeting U.S. Solid Oxide Fuel Cell Targets, Joule (2019).
- [132] Scataglini, R.; et al., A Total Cost of Ownership Model for Solid Oxide Fuel Cells in Combined Heat and Power and Power-Only Applications, Ernest Orlando Lawrence Berkeley National Laboratory (2015).
- [133] CrewCenter, Norwegian epic itineraries 2021, <http://crew-center.com/norwegian-epic-itinerary>, accessed: 2022-02-10.
- [134] D'Agostino, F.; et al., Control strategy and architecture for integrating distributed fuel cells on board large cruise ships, 2020 International Symposium on Power Electronics, Electrical Drives, Automation and Motion (SPEEDAM) (2020).
- [135] Li, Q.; et al., Agent-based decentralized control method for islanded microgrids, IEEE Transactions on Smart Grid (2015).
- [136] Su, W.; Wang, J., Energy management systems in microgrid operations, The Electricity Journal (2012).
- [137] Zia, M.F.; et al., Microgrids energy management systems: A critical review on methods, solutions, and prospects, Applied Energy (2018).
- [138] Marty, P.; et al., Modelling of energy flows and fuel consumption on board ships: application to a large modern cruise vessel and comparison with sea monitoring data, Proceedings of the 11th International Marine Design Conference, Glasgow, UK (2012).

- [139] Searle, S.; et al., What is the role for renewable methane in European decarbonization?, The International Council on Clean Transportation (2018).
- [140] Taljegard, M.; et al., Cost-Effective Choices of Marine Fuels in a Carbon-Constrained World: Results from a Global Energy Model, Environmental Science & Technology (2014).
- [141] McKinsey & Company, What shipowners, refiners, and traders should know about IMO 2020, <https://www.mckinsey.com/industries/oil-and-gas/our-insights/what-shipowners-refiners-and-traders-should-know-about-imo-2020>, Accessed: 2021-03-01.
- [142] Corbett, J.J.; et al., Emissions tradeoffs among alternative marine fuels: total fuel cycle analysis of residual oil, marine gas oil, and marine diesel oil, Journal of the Air & Waste Management Association (2008).
- [143] Schumacher, H., Einsatzgebiete der Dieselmotoren, Dieselmotor-Management im Überblick: einschließlich Abgastechnik (2010).
- [144] T. Cooper, D.; Gustafsson, Methodology for calculating emissions from ships. 1. update of emission factors (2004).
- [145] Schinas, O.; Butler, M., Feasibility and commercial considerations of LNG-fueled ships, Ocean Engineering (2016).
- [146] Ushakov, S.; et al., Methane slip from gas fuelled ships: a comprehensive summary based on measurement data, Journal of Marine Science and Technology (2019).
- [147] Altosole, M.; et al., Simulation and performance comparison between diesel and natural gas engines for marine applications, Proceedings of the Institution of Mechanical Engineers, Part M: Journal of Engineering for the Maritime Environment (2017).
- [148] SEA-LNG, The number of vessels using LNG as a marine fuel is growing rapidly, <https://sea-lng.org/why-lng/global-fleet/>, Accessed: 2021-04-07.
- [149] The Maritime Executive, Feeder Vessel Runs First Trial Voyage Using Synthetic Natural Gas, <https://www.maritime-executive.com/article/feeder-vessel-runs-first-trial-voyage-using-syntetic-natural-gas>, accessed: 2022-01-10.
- [150] Dimitriou, P.; Javaid, R., A review of ammonia as a compression ignition engine fuel, International Journal of Hydrogen Energy (2020).

- [151] Lhuillier, C.; et al., Combustion Characteristics of Ammonia in a Modern Spark-Ignition Engine, Conference on Sustainable Mobility (2019).
- [152] Wartsila, World's first full scale ammonia engine test - an important step towards carbon free shipping, <https://www.wartsila.com/media/news/30-06-2020-world-s-first-full-scale-ammonia-engine-test---an-important-step-towards-carbon-free-shipping-2737809>, accessed: 2022-01-10.
- [153] MAN Energy Solutions, Unlocking ammonia's potential for shipping, <https://www.man-es.com/discover/two-stroke-ammonia-engine>, accessed: 2022-01-10.
- [154] Tuner, M., Review and Benchmarking of Alternative Fuels in Conventional and Advanced Engine Concepts with Emphasis on Efficiency, CO₂, and Regulated Emissions, SAE International (2016).
- [155] Tuner, M.; et al., Sustainable Marine Methanol, SUMMETH - Sustainable Marine Methanol (2018).
- [156] Verhels, S.; et al., Methanol as a fuel for internal combustion engines, Progress in Energy and Combustion Science (2018).
- [157] Caterpillar, Caterpillar marine invests in methanol engines to promote sustainable future, https://www.cat.com/en_US/news/engine-press-releases/caterpillar-marine-invests-in-methanol-engines.html, accessed: 2022-03-01.
- [158] Methanex, Waterfront Shipping to Commission New Ships Built With Flex-Fuel Engines, <https://www.methanex.com/news/waterfront-shipping-commission-new-ships-built-flex-fuel-engines>, accessed: 2022-01-10.
- [159] Stenaline, SUPERGREEN mit Methanol, <https://www.stenaline.de/supergreen/treibstoff-der-zukunft>, accessed: 2022-01-10.
- [160] A.P. Moller - Maersk, A.P. Moller - Maersk accelerates fleet decarbonisation with 8 large ocean-going vessels to operate on carbon neutral methanol, <https://www.maersk.com/news/articles/2021/08/24/maersk-accelerates-fleet-decarbonisation>, accessed: 2022-01-10.
- [161] Shippingwatch, X-Press Feeders orders eight methanol-powered container vessels, <https://shippingwatch.com/carriers/Container/article13513981.ece>, accessed: 2022-01-10.

- [162] MAN ENergy Solutions, Designing the engines of the future, <https://www.man-es.com/discover/designing-the-engines-of-the-future>, accessed: 2022-03-01.
- [163] Boretti, A., Hydrogen internal combustion engines to 2030, *International Journal of Hydrogen Energy* (2020).
- [164] MAN Energy Solutions, H2 – key player in the Maritime Energy Transition, <https://www.man-es.com/marine/strategic-expertise/future-fuels/hydrogen>, accessed: 2022-01-10.
- [165] Valadez Huerta, G.; et al., Exergy analysis of the diesel pre-reforming solid oxide fuel cell system with anode off-gas recycling in the SchIBZ project. Part I: Modeling and validation, 2018 (*International Journal of Hydrogen Energy*).
- [166] e4ships, MultiSchIBZ, <https://www.e4ships.de/english/maritime-shipping/multischibz/>, accessed: 2022-01-10.
- [167] Nautilus, The Nautilus Project, <https://nautilus-project.eu/>, accessed: 2022-01-10.
- [168] Alma, EU-funded consortium aims to decarbonise cruise vessels, <https://almacleanpower.com/news/eu-funded-consortium-aims-to-decarbonise-cruise-vessels>, accessed: 2022-09-08.
- [169] Bloom Energy, Samsung Heavy Industries and Bloom Energy Advance Plans for Clean Power Ships with Joint Development Agreement, <https://www.bloomenergy.com/news/samsung-heavy-industries-and-bloom-energy-advance-plans-for-clean-power-ships-with-joint-development-agreement/>, accessed: 2022-01-10.
- [170] Rathore, S.S.; et al., Direct ammonia solid-oxide fuel cells: A review of progress and prospects, *International Journal of Hydrogen Energy* (2021).
- [171] Zhang, L.; et al., Dynamic modeling and analysis of a 5-kW solidoxide fuel cell system from the perspectives of cooperative control of thermal safety and high efficiency, *International Journal of Hydrogen Energy* (2015).
- [172] Stoeckl, B.; et al., Characterization and performance evaluation of ammonia as fuel for solid oxide fuel cells with Ni/YSZ anodes, *Electrochimica Acta* (2019).

- [173] Waterborne, Piloting Multi MW Ammonia Ship Fuel Cells, <https://www.waterborne.eu/projects/energy-efficiency-and-zero-emissions/shipfc>, accessed: 2022-01-10.
- [174] Iulianelli, A.; et al., Methanol steam reforming for hydrogen generation via conventional and membrane reactors: A review, *Renewable and Sustainable Energy Reviews* (2014).
- [175] CORDIS EU research results, Validation of renewable Methanol based Auxiliary Power System for commercial Vessels, <https://cordis.europa.eu/project/id/31414>, accessed: 2022-01-10.
- [176] ABB, ABB to become technology partner for world's first methanol-hydrogen fuel cell towboat, <https://new.abb.com/news/detail/85340/abb-to-become-technology-partner-for-worlds-first-methanol-hydrogen-fuel-cell-towboat>, accessed: 2022-03-01.
- [177] Alfa Laval, Successful testing of an HT-PEM fuel cell system using methanol paves the way for scale-up at the Alfa Laval Test & Training Centre, https://www.alfalaval.com/media/news/2022/fuel-cell-update-press-release/?utm_source=linkedin&utm_medium=social&utm_campaign=%5Bglobal%5D_lisoc_fuel-cell-pr&utm_content=300000336624580, accessed: 2022-09-08.
- [178] e4ships, Pa-X-cell 2, <https://www.e4ships.de/english/maritime-shipping/pa-x-cell-2/>, accessed: 2022-01-10.
- [179] e4ships, RiverCell2, <https://www.e4ships.de/deutsch/projekte-binnenschiffahrt/rivercell2/>, accessed: 2022-01-10.
- [180] Royal Caribbean Group, Trio of sustainable power sources to drive royal caribbean group's next class of ships into the future, <https://presscenter.rclcorporate.com/press-release/152/trio-of-sustainable-power-sources-to-drive-royal-caribbean-grouprsquos-next-class-of-ships-into-the-future/>, accessed: 2022-01-10.
- [181] MSC Cruises, MSC, Fincantieri and Snam to partner for world's first oceangoing hydrogen-powered cruise ship, <https://www.msccruises.com/en-gl/About-MS/News/First-Oceangoing-Hydrogen-Powered-Cruise-Ship.aspx>, accessed: 2022-01-10.
- [182] Proton Motor, 100 supplies Fincantieri with new fuel cell system "Hy-SHIP 72", <https://www.proton-motor.de/en/proton-motor-supplies->

- fincantieri-with-new-fuel-cell-system-hyship-72/, accessed: 2022-05-01.
- [183] Ballard, Marine Modules, <https://www.ballard.com/fuel-cell-solutions/fuel-cell-power-products/marine-modules>, accessed: 2022-04-01.
- [184] Offshore Energy, New ZeroCoaster study looks into hydrogen value chain for maritime, <https://www.offshore-energy.biz/new-zerocoaster-study-looks-into-hydrogen-value-chain-for-maritime/>, accessed: 2022-01-10.
- [185] FuelCellsWorks, Norse Group Announces Launch of MF Hydra, World's First LH2 Driven Ferry Boat, <https://fuelcellsworks.com/news/norse-group-announces-launch-of-mf-hydra-worlds-first-lh2-driven-ferry-boat/>, accessed: 2022-01-10.
- [186] Flagships, Raising the readiness of zero-emission waterborne transport, <https://flagships.eu/about/>, accessed: 2022-01-10.
- [187] HySeas III, The Project, <https://www.hyseas3.eu/the-project/>, accessed: 2022-01-10.
- [188] Gadducci, E.; et al., Experimental campaign and assessment of a complete 240-kW Proton Exchange Membrane Fuel Cell power system for maritime applications, *International Journal of Hydrogen Energy* (2022).
- [189] Menesy, A.S.; et al., Effective Parameter Extraction of Different Polymer Electrolyte Membrane Fuel Cell Stack Models Using a Modified Artificial Ecosystem Optimization Algorithm, *IEEE Access* (2020).
- [190] Fuel Cells and Hydrogen Joint Undertaking, State-of-the-art and future targets (kpis) as derived from the multi annual work plan: Fuel cell and hydrogen - transport applications, <https://www.fch.europa.eu/soa-and-targets>, accessed: 2021-11-26.
- [191] Whiston, M.M.; et al., Expert assessments of the cost and expected future performance of proton exchange membrane fuel cells for vehicles, *Proceedings of the National Academy of Sciences* (2019).
- [192] Papadias, D.; et al., Total cost of ownership (tco) analysis for hydrogen fuel cells in maritime applications preliminary results, <https://www.energy.gov/sites/prod/files/2019/10/f68/fcto-h2-at-ports-workshop-2019-viii5-ahluwalia.pdf>, accessed: 2021-11-26.

- [193] Advanced Propulsion Centre UK, Behind the scenes: The 2020 automotive fuel cell roadmap, <https://www.apcuk.co.uk/behind-the-scenes-the-2020-automotive-fuel-cell-roadmap/>, accessed: 2021-11-26.
- [194] Maritime Propulsion, Caterpillar MaK 16 M 43 C15200HP, <https://www.maritimepropulsion.com/directory/product/mak-16-m-43-c15200hp-500-110175>, Accessed: 2021-01-01.
- [195] Ballard, High Performance Fuel Cell Stack: Innovations in Proton Exchange Membrane Fuel Cell Stack Design, <https://fuelcellsworks.com/news/ballard-launches-industry-leading-high-power-density-fuel-cell-stack-for-vehicle-propulsion/> (2020).
- [196] Jiao, K.; et al., Designing the next generation of proton-exchange membrane fuel cells, *Nature* (2021).
- [197] United States Department of Energy, Hydrogen and Fuel Cell Technologies Office Multi-Year Research, Development, and Demonstration Plan, https://www.energy.gov/sites/default/files/2017/05/f34/fcto_myRDD_fuel_cells.pdf, accessed: 2021-11-26.
- [198] Wártsilá, Business White Paper - LNG as a marine fuel boosts profitability while ensuring compliance (2017).
- [199] DNV GL, LNG fuelled perfect, <https://www.dnvgl.de/publications/lng-fuelled-perfect--48498>, Accessed: 2020-09-01.
- [200] Barelli, L.; et al., Operation of a Solid Oxide Fuel Cell Based Power System with Ammonia as a Fuel: Experimental Test and System Design, *Energies* (2020).
- [201] Baldi, F.; et al., The cost of innovative and sustainable future ship energy systems, ECOS 2019 - THE 32ND INTERNATIONAL CONFERENCE ON EFFICIENCY, COST, OPTIMIZATION, SIMULATION AND ENVIRONMENTAL IMPACT OF ENERGY SYSTEMS, WROCLAW, POLAND (2019).
- [202] Gualeni, P; et. al., Life Cycle Performance Assessment Tool Development and Application with a Focus on Maintenance Aspects, *Journal of Marine Science and Engineering* (2019).
- [203] NCE Maritime CleanTech, Norwegian future value chains for liquid hydrogen (2019).

- [204] Parks, G.; et al., Hydrogen Station Compression, Storage, and Dispensing Technical Status and Costs, National Renewable Energy Laboratory (2014).
- [205] statista, Average monthly price of very low sulfur fuel oil (VLSFO) between January and March 2020, <https://www.statista.com/statistics/1109263/monthly-vlsfo-bunker-price-worldwide/>, Accessed: 2021-01-08.
- [206] Ship & Bunker, Integr8: VLSFO Caloric Value, Pour Point and Competitiveness with LSMGO, <https://shipandbunker.com/news/world/662089-integr8-vlsfo-calorific-value-pour-point-and-competitiveness-with-lsmgo>, accessed: 2022-10-01.
- [207] Sørheim, K.; et al., Characterization of Low Sulfur Fuel Oils (LSFO): A new generation of marine fuel oils.
- [208] International Gas Union, Natural-Gas-Conversion-Guide, <http://members.igu.org/old/IGU%20Events/wgc/wgc-2012/wgc-2012-proceedings/publications/igu-publications>, Accessed: 2021-03-01 (2012).
- [209] Aziz, M.; et al., Ammonia as Effective Hydrogen Storage: A Review on Production, Storage and Utilization, *Energies* (2020).
- [210] Persio, S.L., Tesla's Shift To Cobalt-Free Batteries Is Its Most Important Move Yet, <https://www.forbes.com/sites/jamesmorris/2020/07/11/teslas-shift-to-cobalt-free-batteries-is-its-most-important-move-yet/?sh=353734bf46b4>, accessed: 2021-11-26.
- [211] Wu, G.; et al., Emission Characteristics for Waste Cooking Oil Biodiesel Blend in a Marine Diesel Propulsion Engine, *Polish Journal of Environmental Studies* (2019).
- [212] The International Council on Clean Transportation, A policy-relevant summary of black carbon climate science and appropriate emission control strategies (2009).
- [213] Wurster, R.; et al., LNG als Alternativkraftstoff für den Antrieb von Schiffen und schweren Nutzfahrzeugen: Kurzstudie im Rahmen des Auftrags des Bundesministeriums für Verkehr und digitale Infrastruktur (BMVI) (2014).
- [214] Anderson, M.; et al., Particle- and Gaseous Emissions from an LNG Powered Ship, *Environmental science & technology* (2015).

- [215] Verbeek, R.; et al., Environmental and Economic aspects of using LNG as a fuel for shipping in the Netherlands, TNO report (2011).
- [216] Song, Su, Ship emissions inventory, social cost and eco-efficiency in Shanghai Yangshan port, Atmospheric Environment (2014).
- [217] Hassellóv, I.-M.; et al., Shipping contributes to ocean acidification, Geophysical Research Letters (2013).
- [218] Mauzerall, D.; et al., NO emissions from large point sources: variability in ozone production, resulting health damages and economic costs, Atmospheric Environment (2005).
- [219] Chen, T.-M.; et al., Outdoor Air Pollution: Nitrogen Dioxide, Sulfur Dioxide, and Carbon Monoxide Health Effects, The American Journal of the Medical Sciences (2007).
- [220] Huijbregts, M.A.J.; et al., Spatially Explicit Characterization of Acidifying and Eutrophying Air Pollution in Life-Cycle Assessment, Journal of Industrial Ecology (2000).
- [221] United States Environmental Protection Agency, Understanding Global Warming Potentials, <https://www.epa.gov/ghgemissions/understanding-global-warming-potentials>, Accessed: 2021-03-15.
- [222] Sternberg, A.; et al., Life Cycle Assessment of Power-to-Gas: Syngas vs Methane, ACS Sustainable Chemistry and Engineering (2016).
- [223] GaBi Software and database contents for Life Cycle Engineering, Electricity grid mix 1kV-60kV (2030) (significant improvements in sustainability policy) EU-28, PE INTERNATIONAL AG (2021).
- [224] Pehl, M.; et al., Understanding future emissions from low-carbon power systems by integration of life-cycle assessment and integrated energy modelling, Nature Energy (2017).
- [225] Avadi A.; et al., marine engine construction - GLO, Ecoinvent database 3.6 (2014).
- [226] Al-Khori, K.; et al., Life Cycle Assessment for Integration of Solid Oxide Fuel Cells into Gas Processing Operations, Energies (2021).
- [227] Stropnik, R.; et al., Critical materials in PEMFC systems and a LCA analysis for the potential reduction of environmental impacts with EoL strategies, Energy Science & Engineering (2019).

- [228] Le Varlet, T.; et al., Comparative life cycle assessment of lithium-ion battery chemistries for residential storage, *Journal of Energy Storage* (2020).
- [229] Thinkstep, Life Cycle GHG Emission Study on the Use of LNG as Marine Fuel: Final Report.
- [230] Akimoto, A.; Narita, H., Distribution of SO₂, NO_x and CO₂ Emissions from Fuel Combustion and Industrial Activities in Asia with 1x1 Resolution, *Atmospheric Environment Vol. 28* (1994).
- [231] Amoatey, P.; et al., Emissions and exposure assessments of SO_x, NO_x, PM_{10/2.5} and trace metals from oil industries: A review study (2000–2018), *Process Safety and Environmental Protection* (2019).
- [232] van den Bergh, J.C.J.M.; Botzen, W.J.W., Monetary valuation of the social cost of CO₂ emissions: A critical survey, *Ecological Economics* (2015).
- [233] IPCC, Climate Change 2013: The Physical Science Basis: Contribution of Working Group I to the Fifth Assessment Report of the Intergovernmental Panel on Climate Change (2013).
- [234] Bond, T.C.; Sun, H., Can reducing black carbon emissions counteract global warming?, *Environmental Science & Technology* (2005).
- [235] Ship Technology, Container shipping: is LNG the fuel of the future?, <https://www.ship-technology.com/analysis/featurecontainer-shipping-is-lng-the-fuel-of-the-future-4645479/>, accessed: 2022-09-10.
- [236] Safety 4 Sea, The case of LNG as a marine fuel: Latest developments, <https://safety4sea.com/cm-the-case-of-lng-as-a-marine-fuel-latest-developments/>, accessed: 2022-09-10.
- [237] NABU, LNG als Schiffstreibstoff: Besser für die Luft, schlecht fürs Klima, <https://www.nabu.de/umwelt-und-ressourcen/verkehr/schifffahrt/containerschifffahrt/20715.html>, accessed: 2022-09-10.
- [238] Greenpeace, LNG - sechs Mythen zu Flüssiggasterminals, <https://www.greenpeace.de/klimaschutz/energie/wende/gasausstieg/lng-sechs-mythen>, accessed: 2022-09-10.
- [239] Miola, A.; et al., Designing a climate change policy for the international maritime transport sector: Market-based measures and technological options for global and regional policy actions, *Energy Policy* (2011).

- [240] Moch, J.M.; et al., Carbon Capture, Utilization, and Storage: Technologies and Costs in the U.S. Context, <https://www.belfercenter.org/publication/carbon-capture-utilization-and-storage-technologies-and-costs-us-context>, accessed: 2022-09-10.
- [241] Roussanaly, S., Calculating CO₂ avoidance costs of Carbon Capture and Storage from industry, Carbon Management (2019).
- [242] International energy agency, Is carbon capture too expensive?, <https://www.iea.org/commentaries/is-carbon-capture-too-expensive>, accessed: 2022-10-12.
- [243] Panos, E.; Densing, M., The future developments of the electricity prices in view of the implementation of the Paris Agreements: Will the current trends prevail, or a reversal is ahead?, Energy Economics (2019).
- [244] Deutsch, M.; Maier, U., The Future Cost of Electricity-Based Synthetic Fuels, Agora Energiewende and Agora verkehrswende (2018).
- [245] Sorknaes, P.; et al., Quantifying the influence of wind power and photovoltaic on future electricity market prices, Energy Conversion and Management (2019).
- [246] Jalkanen, J.-P.; et al., Extension of an assessment model of ship traffic exhaust emissions for particulate matter and carbon monoxide, Atmospheric Chemistry and Physics (2012).
- [247] Valadez Huerta, G.; et al., Exergy analysis of the diesel pre-reforming SOFC-system with anode off-gas recycling in the SchIBZ project. Part II: System exergetic evaluation, 2018 (International Journal of Hydrogen Energy).
- [248] Birnbaum, K.U.; et al., Solid Oxide Fuel Cells, Sustainability Aspects, Fuel Cells (2013).
- [249] Kishimoto, M.; et al., Formulation of ammonia decomposition rate in Ni-YSZ anode of solid oxide fuel cells, International Journal of Hydrogen Energy (2017).
- [250] Cinti, G.; et al., SOFC operating with ammonia: Stack test and system analysis, International Journal of Hydrogen Energy (2016).
- [251] Farhad, S.; et al., Conceptual design of a novel ammonia-fuelled portable solid oxide fuel cell system, Journal of Power Sources (2010).

- [252] Dekker, N. J. J.; Rietveld, G., Highly Efficient Conversion of Ammonia in Electricity by Solid Oxide Fuel Cells, *Journal of Fuel Cell Science and Technology* (2006).
- [253] Zincir, B.; et al., Investigation of Environmental, Operational and Economic Performance of Methanol Partially Premixed Combustion at Slow Speed Operation of a Marine Engine, *Journal of Cleaner Production* (2019).
- [254] O'Hayre, R.; et al., *Fuel Cell Fundamentals*, John Wiley & Sons, Inc. (2016).
- [255] Wu, W.; et al., A novel distributed energy system using high-temperature proton exchange membrane fuel cell integrated with hybrid-energy heat pump, *Energy Conversion and Management* (2021).
- [256] Xu, B.; et al., Thermodynamic Optimization of a High Temperature Proton Exchange Membrane Fuel Cell for Fuel Cell Vehicle Applications, *Mathematics* (2021).
- [257] Zhang, J.; et al., Polybenzimidazole-membrane-based PEM fuel cell in the temperature range of 120–200°C, *Journal of Power Sources* (2007).
- [258] Schuller, G.; et al., Heat and fuel coupled operation of a high temperature polymer electrolyte fuel cell with a heat exchanger methanol steam reformer, *Journal of Power Sources* (2017).
- [259] Ribeirinha, P.; et al., Synergetic integration of a methanol steam reforming cell with a high temperature polymer electrolyte fuel cell, *International Journal of Hydrogen Energy* (2017).
- [260] Sankar, K.; et al., Sliding mode observer based nonlinear control of a PEMFC integrated with a methanol reformer, *Energy* (2017).
- [261] Kurzweil, P.; et al., *Brennstoffzellentechnik: Grundlagen, Materialien, Anwendungen*, Gaserzeugung, Springer Vieweg (2016).
- [262] Lack, D.; et al., Particulate emissions from commercial shipping: Chemical, physical, and optical properties, *Journal of Geophysical Research* (2009).
- [263] Wu, T.; et al., Physical and Chemical Properties of GTL-Diesel Fuel Blends and Their Effects on Performance and Emissions of a Multicylinder DICompression Ignition Engine, *Energy and Fuels* (2007).
- [264] Duynslaegher, C.; et al., Kinetics in Ammonia-Containing Premixed Flames and a Preliminary Investigation of Their Use as Fuel in Spark Ignition Engines, *Combustion Science and Technology* (2009).

- [265] Westlye, F.R.; et al., Experimental investigation of nitrogen based emissions from an ammonia fueled SI-engine, *Fuel* (2013).
- [266] Lhuillier, C.; et al., Performance and Emissions of an Ammonia-Fueled SI Engine with Hydrogen Enrichment, *International Conference on Engines & Vehicles* (2019).
- [267] Lan, R.; Tao, S., Ammonia as a suitable fuel for fuel cells, *Frontiers in Energy Research* (2014).
- [268] Weißenberger, T.; et al., Effect of the Active Metal on the Nox Formation During Catalytic Combustion of Ammonia Sofc Off-Gas, <https://ssrn.com/abstract=4113741>, accessed: 2022-05-31.
- [269] Shamun, S.; et al., Detailed characterization of particulate matter in alcohol exhaust emissions, *COMODIA 2017 - 9th International Conference on Modeling and Diagnostics for Advanced Engine Systems* (2017).
- [270] Zincir, B.; et al., Investigation of Effects of Intake Temperature on Low Load Limitations of Methanol Partially Premixed Combustion, *Energy Fuels* (2019).
- [271] Shamun, S.; et al., Experimental investigation of methanol compression ignition in a high compression ratio HD engine using a Box-Behnken design, *Fuel* (2017).
- [272] Contributor Roles Taxonomy, CRediT, <https://credit.niso.org/>, accessed: 2022-05-10.